Hybrid Surfactants with Fullerene as Functional Unit

Dissertation zur Erlangung des

akademischen Grades eines Doktors der

Naturwissenschaften (Dr.rer.nat.)

vorgelegt von

Marius Hendrik Andrea Kunkel

an der

Mathematisch-Naturwissenschaftliche Sektion

Fachbereich Chemie

Konstanz, 2020

Tag der mündlichen Prüfung: 05.02.2021

1. Referent: Prof. Dr. Sebastian Polarz
2. Referent: Prof. Dr. Helmut Cölfen
3. Referent: Prof. Dr. Valentin Wittmann

Scientists should provide solutions to social problems and dreams for people.

Eiichi Nakamura

Danksagung

Zuerst möchte ich dir danken Sebastian für dein Vertrauen in mich, bei der Bearbeitung meines Themas und für die vielen Freiheiten die du mir gelassen hast, um eigene Ideen umzusetzen und neue Wege zu gehen, auch wenn dich nicht alles von Anfang an überzeugt hat. Ich danke dir für die wissenschaftliche Zusammenarbeit, bei der du immer versucht hast das Beste aus einem herauszulocken und die vielen Erfahrungen die ich in der AG sammeln konnte.

Vielen Dank dir Helmut für die Mitbetreuung meiner Arbeit und die Übernahme des Zweitgutachtens. Danke für dein positives Feedback und deinen Input.

Ein großer Dank geht an die ganze AG Polarz für vier spannende Jahre. Mit euch wurde es bei der Arbeit nie langweilig. Aber auch abseits der Arbeit hatte ich viel Spaß und eine gute Zeit mit euch, egal ob auf den zahlreichen AG-Hütten, den Ausflügen oder auch einfach beim gemeinsamen Zusammensein nach der Arbeit. Ich freue mich sehr, dass aus dieser Zeit Freundschaften entstanden sind. Ich danke euch für eure Unterstützung mit wissenschaftlichen Diskussionen, Messungen und Dateninterpretation. Auch in schwierigen Zeiten wart ihr immer da und habt mich unterstützt. Vielen Dank vor allem auch an Stephan, der mich bei vielen Projekten mit Rat und Tat unterstützt hat. Besonderer Dank geht an Alex der „Schuld“ daran ist, dass ich mich für die AG Polarz entschieden habe. Angefangen mit einem Mitarbeiterpraktikum, gefolgt von der Zusammenarbeit mit dir im Team Self-assembly, konnte ich sehr viel von dir lernen und Erfahrungen sammeln die meine Arbeit bis zum Schluss geprägt haben. Mit deiner positiven Art standest du nicht nur mir immer zu Seite, wenn es ein Problem gab.

Tausend Dank geht auch an meinen Laborpartner Dennis. Wir hatten eine sehr gute Zeit im Labor und immer viel Spaß. Du hast immer mein Chaos ertragen und mich immer gut unterhalten. In diesem Zusammenhang möchte ich auch besonders der L11-Crew danken. Mit euch war es immer sehr unterhaltsam.

Ich danke meinen Studenten, Veit, Lukas, Alexander, Marc, Frank die mich bei meiner Arbeit unterstützt und einen Beitrag zu meiner Forschung geleistet haben. Vor allem danke ich Frank der in unzähligen Stunden den Fulleren Reaktor mit mir zum Laufen gebracht hat und einen wichtigen Beitrag zu meiner vierten Publikation geleistet hat.

Des Weiteren geht ein großer Dank an meine Co-Autoren, Stefan Schildknecht, David Schleheck, Klaus Boldt, Lukas Zeyffert, Marcel Leist, Sebastian Sutter, Stefan Bitter, Frank Sailer die mir mit Rat und Tat zur Seite standen. Besonderer Dank gilt hierbei Rainer Winter, für seine Mithilfe bei meiner vierten Publikation. Danke, dass ich über viele Wochen das Equipment ihrer AG nutzen durfte und für ihren Input zu meiner Arbeit.

Weiterhin danke ich Anke und Uli für die vielen Stunden der gemeinsamen NMR Messungen, die oft komplizierter waren als erwartet. Auch wenn nach sieben Tagen Messzeit nur eine Baseline zu erkennen war, habt ihr nicht aufgegeben und hattet immer noch eine weitere Idee. Danke euch auch für die Gespräche abseits der Forschung. Auch geht mein Dank an Marina für die cryo-TEM Messungen sowie an Malin und Silke für eure Unterstützung bei Masse Messungen.

Meinen Freunden aus Konstanz, Basti, Max, Rapha, Theissi, Hannah, Conny, Lisa, Ilona, Chris, Wurmi, Hannah, Andi und Hannes, euch danke ich für die gemeinsame Zeit hier in Konstanz. Ihr seid eine super Truppe und es war eine unvergessliche Zeit mit euch. Auch wenn sich die Wege mit der Zeit trennen werden, hoffe ich, dass wir alle weiter so in Kontakt bleiben.

Meiner Familie danke dafür, dass ihr das Alles möglich gemacht habt. Ihr habt mich immer unterstützt und steht immer zu mir. Auch wenn es durch die Entfernung manchmal schwierig ist habt ihr mich immer bestärkt meinen Weg zu gehen. Ich bin sehr glücklich, dass wir uns so gut verstehen und freue mich immer über gegenseitige Besuche. Ich habe immer großen Spaß gehabt euch von meiner Arbeit zu erzählen, an der ihr immer großes Interesse hattet, auch wenn ihr wahrscheinlich nicht immer wusstet worum es genau geht.

Lena, dir danke ich für so vieles, dass ich gar nicht weiß wo ich anfangen soll. Du hast mich durch mein Studium und die Promotion begleitet und mich immer unterstützt. Du erträgst meine Eigenheiten und bist immer für mich da. Ohne dich wäre das Alles wahrscheinlich nicht möglich gewesen. Ich freue mich sehr auf unsere gemeinsame Zukunft.

1 Publication List

Included in the thesis

Kunkel, M., Schildknecht, S., Boldt, K., Zeyffert, L., Schleheck, D., Leist, M., & Polarz, S. Increasing the Resistance of Living Cells against Oxidative Stress by Nonnatural Surfactants as Membrane Guards.

ACS applied materials & interfaces, *2018*. DOI:10.1021/acsami.8b07032

Kunkel, M., & Polarz, S. Easy, efficient and versatile one-pot synthesis of Janus-type-substituted fullerenols.

Beilstein journal of organic chemistry, 2019. DOI:10.3762/bjoc.15.87

Kunkel, M., Sutter, S., & Polarz, S. Molecular Semiconductor Surfactants with Fullerenol Heads and Colored Tails for Carbon Dioxide Photoconversion.

Angewandte Chemie International Edition, 2019. DOI:10.1002/anie.201905410

Kunkel, M., Bitter, S., Sailer, F., Winter, R. F., & Polarz, S. Aggregation-Induced Improvement of Catalytic Activity by Inner-Aggregate Electronic Communication of Metal-Fullerene-Based Surfactants.

ChemCatChem., 2020. DOI:10.1002/cctc.202000412

Not included in the thesis

Voggel, M., Meinusch, R. M., Siewert, V., **Kunkel, M**., Wittmann, V., & Polarz, S. Sweet surfactants: packing parameter-invariant amphiphiles as emulsifiers and capping agents for morphology control of inorganic particles.

Soft matter, 2018. DOI:10.1039/C8SM01091A

Bitter, S., **Kunkel, M**., Burkart, L., Mang, A., Winter, R. F., & Polarz, S. Organometallic, Nonclassical Surfactant with Gemini Design Comprising π-Conjugated Constituents Ready for Modification.

ACS omega, 2018. DOI:10.1021/acsomega.8b01405

Polarz, S., **Kunkel, M**., Donner, A., & Schlötter, M. Added-Value Surfactants.

Chemistry–A European Journal, 2018. DOI:10.1002/chem.201802279

Bronner, H., Holzer, A. K., Finke, A., **Kunkel, M**., Marx, A., Leist, M., & Polarz, S. The influence of structural gradients in large pore organosilica materials on the capabilities for hosting cellular communities

RSC Advances, DOI:10.1039/D0RA00927J

Table of Contents

2 General Introduction

Soap – more than meets the eye; this could be the motto of this thesis. Soap, in principle, is a high-tech nanomaterial that is also part of our everyday's life as detergents, emulsifiers, wetting agents, foaming agents and even as part of our body. So, what is soap? In general, the non-scientific word soap describes amphiphilic molecules that consist of a hydrophilic, water attracting part and a hydrophobic or lipophilic, water repelling part. This very molecular structure is, for example, the basis of the working principle of detergents. The hydrophobic part sticks to contaminants whereas, the hydrophilic part sticks to the water to enable the removal of the contaminants. This is also the principle how emulsions like milk or cosmetics work. To put it simply, an emulsion consists of water and oil that can be combined with the help of amphiphilic molecules. In our body amphiphiles have a different duty to fulfill. A body's cells are mainly built up by amphiphiles, namely phospholipids, that form the structure of the cell membrane due to its differently polarized components. The phospholipids assemble hydrophilic part adjacent to hydrophilic part and hydrophobic part adjacent to hydrophobic part forming a stable layer. Especially with these properties of amphiphiles a bridge to nanomaterials can be forged. As a nanomaterial they possess several physical properties that are the basis of these various features. At first, the influence on surface tension needs to be mentioned. Adding amphiphilic molecules to an aqueous solution, the molecules adsorb at the surface of the solution with the hydrophilic part pointing towards the solution and the hydrophobic part pointing away from it. The cohesive forces between the water molecules are very strong resulting in a high surface tension. As amphiphiles adsorb, they break these interactions. The intermolecular forces between surfactant and water molecule are much weaker than between two water molecules and thus surface tension decreases. The decrease of the interfacial tension becomes stronger the more molecules are adsorbed at the interface. This property also leads to the name surfactants which basically means surface active agent. At a certain, compound dependent, concentration the interface is fully occupied by surfactant molecules and the so called critical micelle concentration is reached, which leads to another property of surfactants – the ability of forming aggregates like micelles. The minimization of the unfavorable contact between non-polar surfactant chains and the polar solvent compensates the loss of entropy by

micelle formation. The ability to form micelles is a result of the hydrophobic effect which competes with the electrostatic or steric repulsion between the head groups. Additionally, other effects depending on the head group's charge, its counter ion, pH value and temperature play a role. The appearance of the formed aggregates can be further controlled by adapting the molecule's shape. Among other parameters the packing parameter, defined by Israelachvili *et al.*,[1] can give a suggestion of the aggregates' shape depending on the molecule's proportions. The resulting aggregate structures are of various shape and kind. Most prominent are spherical micelles, cylindrical micelles or bilayered (or multilayered) structures like vesicles. This controllable structuration in nanoscale regime is also an important part in nanotechnology. Nanoscale structures can be built up by two general approaches, the bottom-up method and the top-down method. In a top-down approach the nanostructures are produced from macrostructures by e.g. lithography, while the bottom-up method starts with molecular building block producing nanostructures. The commonly used top-down method starts to reach its limits, especially for very small structures. For a bottom-up approach small molecules that form superstructures, that self-assemble controllably into defined aggregates, surfactants seem to be a suitable source. Using surfactants as building blocks for nanomaterials and not only as a templating system is a promising approach because of the controllable superstructures and the easy way to introduce functionalities by just adapting the surfactant molecule. Next generation surfactants are able to respond to external triggers changing their properties depending on e.g. temperature, pH value or irradiation. It is further possible to introduce e.g. catalytic properties.[2, 3] This can lead to future high-tech materials.

This attempt of tailoring surfactant molecules to obtain functional superstructures is one of the fundamental pillars of the research in the group of Sebastian Polarz. Previous systems were built up by amphiphilic polyoxometalates, rare earth metal head groups or NHC-containing head groups, showing various features in addition to surfactant properties.[4-7] This repertoire of inorganic-organic hybrid surfactants is now to be extended by fullerene based surfactants. This compound class shows versatile electronic and optoelectronic properties in addition to unique self-assembly behavior being a promising system for further research in this group.

3 Structure of the Thesis

The following topics are discussed in the presented thesis:

- **Overview over fullerenes**
- **Fullerenes in solution**
- **Amphiphilic fullerenes and their self-assembly**
- **Applications of fullerene amphiphiles**

In **chapter 4**, the above mentioned topics are discussed under state of the art. The findings and progresses are highlighted and sorted into a greater context. **Chapter 5** 'challenges and objectives' displays the resulting scientific challenges for this thesis. **Chapter 6** describes the scientific contribution of the thesis in this context. **Chapter 7** shows the references from **chapter 1-6**.

In **chapter 8**, the scientific results of the thesis are presented. **8.1** deals with the synthesis, characterization and self-assembly behavior of a new class of amphiphilic fullerenes. Furthermore, their application as potent membrane guard against oxidative stress in biological systems is evaluated. An easy and versatile synthesis method for more complex derivatives of the compound, introduced in **chapter 8.1**, is presented in **8.2**. With this synthesis protocol it was possible to generate an amphiphilic molecular semiconductor. This system was not only investigated regarding its electronic properties but also regarding the influence of self-assembly on these properties, thereby a new kind of artificial leaf could be generated that is based on the inner and inter aggregate energy and electron transfer. This system is presented in **chapter 8.3**. In **chapter 8.4**, a new prototype system was developed to further investigate the phenomenon of a beneficial effect of inter and inner aggregate energy and electron transfer on catalytic reactions. With electro catalytic water splitting as test reaction, it could be shown that the catalytic activity of amphiphilic fullerenes is tremendously enhanced during self-assembly into supramolecular structures fighting the paradigm of aggregation being a disadvantage for catalytic reactions.

The thesis closes with **chapter 9** and **10** with ‘conclusion and outlook’ and ‘Zusammenfassung und Ausblick’. The key results are highlighted and explained and future perspectives for this very research area are presented.

4 State of the Art

When Richard Smalley, Robert F. Curl Jr. and Sir Harold W. Kroto synthesized and characterized fullerenes in the 80ies,[8] which they were granted the Nobel prize in chemistry for in 1996, none of them could ever imagine that they set the stage for a new field of chemistry with a molecule Eiji Osawa had theoretically described years before.[9] As Smalley said, after discovering the fullerenes, that "(..) scientists are excited by buckyballs for their own sake, and if they turn out to have practical application, such much the better", not yet knowing the potential of this new fullerenes.[10] The newly discovered family of molecules obtained an artificial name – Buckminster fullerenes or short fullerenes, named after the most abundant member of the fullerenes, C_{60}, which reminded its finders of the geodesic constructs built by the architect Richard Buckminster Fuller. This trivial name for this class of compounds, fullerenes, was in the beginning not accepted by the international union of pure and applied chemistry (IUPAC), who develops standards for the naming of chemical compounds. Its rational name was:

Hentriacontacyclo[29.29.0.$0^{2,14}$.$0^{3,12}$.$0^{4,59}$.$0^{5,10}$.$0^{6,58}$.$0^{7,55}$.$0^{8,53}$.$0^{9,21}$.$0^{11,20}$.$0^{13,18}$.$0^{15,30}$.$0^{16,28}$.$0^{17,25}$.$0^{19,24}$.$0^{22,52}$.$0^{23.50}$.$0^{26,49}$.$0^{27,47}$.$0^{29,45}$.$0^{32,44}$.$0^{33,60}$.$0^{34,57}$.$0^{35,43}$.$0^{36,56}$.$0^{37,41}$.$0^{38,54}$.$0^{39,51}$.$0^{40,48}$.$0^{42,46}$]hexaconta, 3,5(10),6,8,11,13(18),14,16,19,21,23,25,27,29(45),30,32(44),33,35(43),36,38(54),39(51),40(48), 41,46,49,52,55,57,59-triaconten.

In 1997, IUPAC published a guideline for the naming of fullerene compounds, officially introducing the word fullerene. Fullerenes shall be named as such, the number of carbons in the molecule being indicated in square brackets before the word "fullerene", followed by the point group symmetry. Thus for Buckminsterfullerene, a full description is: [60-I_h]Fullerene.[11] This was then later updated to include also all discovered derivatives.[12]

The beginning of the success story of the fullerenes is their accidental synthesis in 1985 when Kroto Heath, O'Brian, Curl and Smalley discovered traces of carbon clusters in the soot generated by vaporizing carbon in helium during their attempt to synthesize carbon chain molecules.[8] Four years later Fostipropoulos, Krätschmer und Huffman applied a suitable synthesis for this new molecule to achieve synthesis on a preparative scale. This method made the field of fullerene

chemistry possible on a big scale.[13] Nowadays, several methods exist to produce fullerenes like resistive heating of graphite, inductive heating of carbon, pyrolysis of hydrocarbons, total synthesis and the arc heating method used by Krätschmer.[14, 15] During the arc heating method graphite is vaporized in an electric arc, in a so called Krätschmer reactor under reduced helium atmosphere.[16, 17] Under these conditions the graphite evaporates and carbon clusters form in the gas phase by colliding with the gas molecules, eventually forming fullerenes. The underlying mechanism may be rather complex but two general proposals for the mechanism exist in literature. One mechanism is the pentagon route during which the evaporating carbon forms a network of small carbon radicals, serving as precursors for the addition of further radicals. It is assumed that the lowest-energy form of any small graphitic fragment is only made up of hexagons and pentagons, including as many pentagons as possible, and none of the pentagons are adjacent. For carbon clusters which have more than 20-30 atoms, but are too small to make a closed fullerene with isolated pentagons, open graphitic structures are lower in energy than any other structure. Annealing allows the carbon clusters to find the structures with minimum energy. Thus, thermochemical stability dictates the formation of these graphitic structures in preference to other possible structures, and kinetic reactivity determines that they continue to grow toward fullerenes. Eventually, the networks form a closed shell due to thermodynamics.[18, 19] The other mechanism is called fullerene route which proposes that small cage-like intermediates are formed during evaporation that can grow to yield in fullerenes. As with the pentagon route mechanism, the fullerene route requires a large concentration of C_2 and C_3, even at the later stages of cluster growth. The advantage of this mechanism is that it is based on the most abundant, and thermodynamically most stable, species in the 50-60-atom size range.[18, 19]

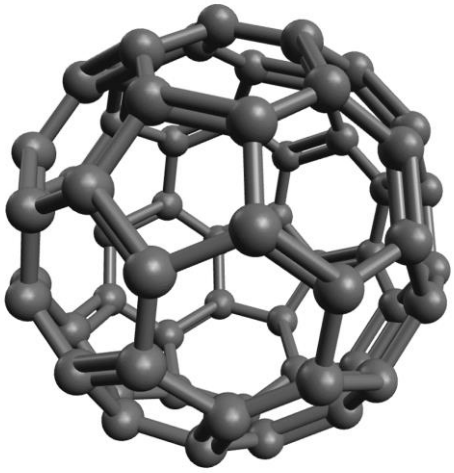

Figure 1: Schematic structure of [60-I_h]-fullerene.

The family of fullerenes has a lot of members, since the number of carbon atoms in the cluster range from about 30 to 100 and more. But they all share a common structure motif. All of them possess 12 five-membered rings and a number of six-membered rings depending on the cage size, following Euler's Rule, which relates the number of vertices, edges and faces. Another commonality is the isolated pentagon rule which states that five membered rings are not allowed

to connect whereas, ongoing research showed several exceptions to this rule. These two 'rules' are a prerequisite for the stability of the fullerene. By following these rules, while forming in the gas phase, the strain in the molecule is reduced and the closed cage structure is possible.[14, 20] The members of the fullerene family can not only be distinguished by number of carbon atoms but also by isomers. Whereas, smaller fullerenes up to C_{74} only have one isomer, higher fullerenes have an increasing number of isomers with larger cage size. C_{84}, for example has 24 isomers. In fact, the most abundant representative, C_{60}, could theoretically have 1812 isomers, if there were no rules for the formation of fullerenes.[21] But the only isomer of C_{60} (**Figure 1**), which has the symmetry of an icosahedron (I_h), even is the most symmetrical molecule with 120 possible symmetrical operations. Its appearance can be seen as molecular nanoparticle with a diameter of 700 pm and with a Van-der-Waals diameter of 1000 pm.[8]

And it is this very structure, a closed cage made from five-membered and six- membered rings that is the reason for the chemical and physical behavior of the fullerene C_{60}, which will be in focus in the following. Having a closer look at the structure, it can be described as a mixture of [5]radialene and cyclohexatriene. All double bonds are located at a connection of two adjacent hexagons, resulting in shorter bonds for a hexagon-hexagon junction (138 pm) than for a hexagon-pentagon junction (145 pm). This motif leads to a behavior similar to an electron deficient olefin system but different from an aromatic system.[22, 23] Nevertheless, there are 60 π-electrons in the system whereas, 72 would be required for a totally delocalized π-system. This results in a high electron affinity of the fullerene, combined with low lying frontier molecular orbitals of -6.3 eV (HOMO) and -4.1 eV (LUMO).[24] These features directly lead to the chemical behavior and reactivity of the fullerene. The general driving force for reactions at a fullerene is the relief of ring strain within the carbon cage derived from the highly pyramidalized sp^2 carbon atoms and therefore, reactions take place at the 6-6 ring junction, having a higher electron density. The list of possible reactions is long but will be discussed shortly due to the versatility of C_{60},[22, 23, 25-27] but with focus on exohedral modifications, modifications that take place at the outside of the carbon cage (**Figure 2**).

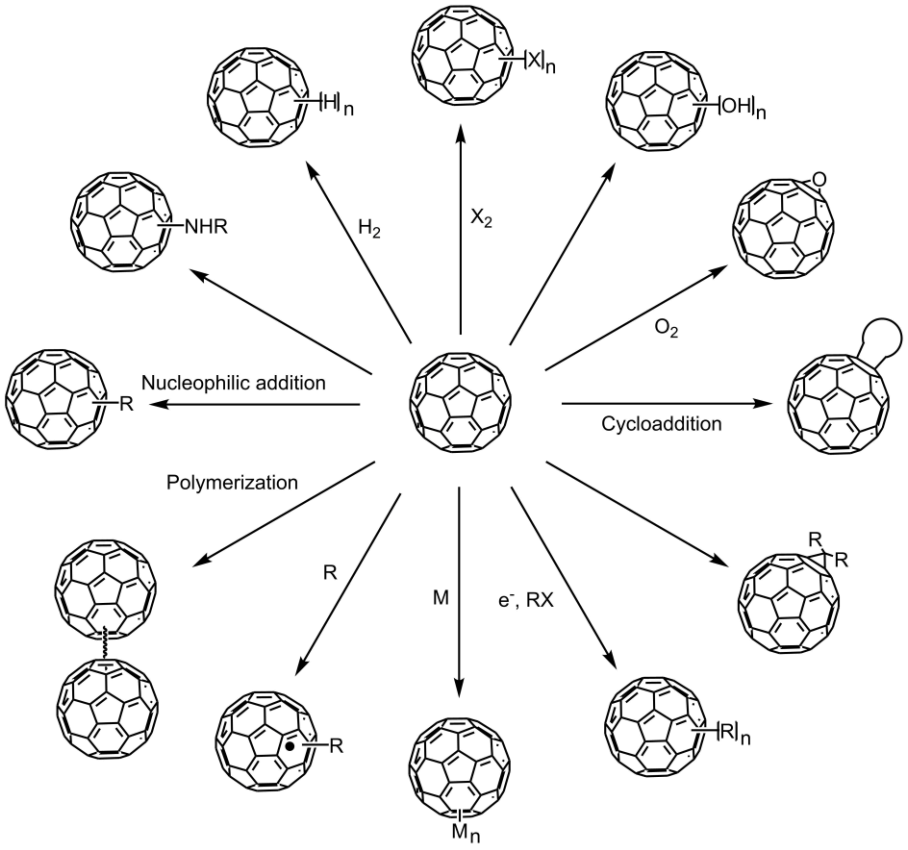

Figure 2: Schematic overview over different reactions that can take place at a fullerene.

Fullerenes react in nucleophilic addition reactions under the formation of a carbanion that can be reacted with an electrophile. One popular example would be the Bingel reaction which is a cyclopropanation reaction with malonate derivatives.[28, 29] The deprotonated malonate reacts at a 6-6 ring junction double bond whereas, the resulting carbanion reacts with the malonate under release of a leaving group, forming a cyclopropane unit. A further example would be the Friedel-Crafts alkylation type reaction under the formation of 1,2-adducts.[30, 31] In pericyclic reactions, the 6-6 ring junctions can act as diens as well as dienophiles in reactions like Diels-Alder reactions.[32] Similar to aromates or alkynes fullerenes can react in hydrogenation, ozonylation and halogenation reactions. In this reactions the fullerene acts as nucleophile. Depending on the reaction conditions C_{60} can be halogenated up to 60 times ($C_{60}F_{60}$).[33, 34] For bromine and chlorine stable compounds with up to 24 halogens are reported.[35] A very interesting feature of fullerene reactions is the selectivity. In nucleophilic or electrophilic reactions like halogenations or Grignard reactions it is possible to selectively derivatize one hemisphere, one pentagonal side, of the fullerene.[36] The reaction starts at on 6-6 ring bond and in a cascade like fashion continues around a pentagon

eventually leading to hexa-substituted fullerene with a cyclopentadiene unit. This reaction distorts the cage in a manner that the reaction stops afterwards. Especially, for addition reactions the regiochemistry and possible isomers are of interest (**Figure 3**).[37] After the first functionalization the remaining 6-6 bonds of the C_{60} are not equal and, in principal, eight different regioisomers can be formed. Usually these isomers cannot be separated. Different procedures for functionalization drive certain modifications in the regioadduct distribution but e and trans-3 position are preferred. Taking addition reactions as an example, the addition can lead to [1,6] isomers or [1,4] isomers. This is often determined by the reaction mechanism since the sterical demand of the molecules which attack at the fullerene plays a crucial role.[38]

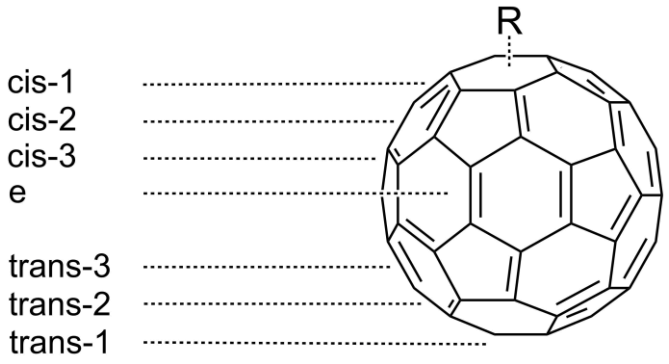

Figure 3: Possible region-isomers of [60-I_h]-fullerene in multi-functionalization.

The resulting diversity of fullerene derivatives find application in a broad field of research areas ranging from material science to biological science or medicine. An excerpt of these applications is discussed in the following. In material science, undoubtedly, photovoltaics is the field of research in which the fullerene is most abundant. This includes organic photovoltaics and perovskite solar cells (**Figure 4**). There, the fullerene shines as electron transfer material due to its physical properties described earlier.[39-41] The general working principle of an organic photovoltaic system is that light is absorbed by an electron donor unit that generates an exciton upon irradiation, followed by the migration of the exciton to the donor-acceptor interface. The donor-acceptor interface can be seen as p-n junction in which the positive and the negative charge of the exciton can migrate. Then the charge is transported to the electrode. This process, the dissociation of the exciton requires that the orbital energy of the donor and the acceptor show a suitable difference as well as that the charge transport properties of the material to avoid recombination.[42] A huge combination variety for such systems exists but the combination of a polymer as donor unit and fullerene derivatives as acceptors proved to be very efficient.[43] The most widely used fullerene derivative in this case is $PC_{61}BM$ which is a phenyl-C_{61}-butyric acid methyl ester. The $PC_{61}BM$ was utilized as a role model and reference acceptor for all kinds of fullerene acceptors, because of easy preparation, good solubility, electron mobility, low lying LUMO energy levels, and stability

compared to the pristine fullerenes.[39, 44, 45] The phenyl moiety enables π-π-stacking of the molecules, resulting in efficient electronic communication within the system. Different variations of this compound have emerged in research over the years, optimizing the solubility, the π-π-interaction or even adding absorption properties.[44] Nowadays, the research community slowly turns its back on fullerenes as materials for organic photovoltaics and the trend goes towards non-fullerene small molecules.[46, 47] The second type of photovoltaics in which fullerenes are used is the perovskite solar cells which consist of an organic-inorganic hybrid material. One component consists of an organic cation, a metal and a halide that crystalize in the perovskite structure to obtain a light harvesting, charge generating material. The second component is a charge transfer material for which TiO_2 is widely used.[41, 48] Here the fullerene comes into play to replace TiO_2. In 2013, fullerene C_{60}, and among others, its derivative $PC_{61}BM$ were introduced into perovskite solar cells for the first time by Jeng *et al.*[48] It has been widely demonstrated that the use of fullerenes either as electron transfer material, interface modification of the electron transfer material or as additives in the perovskite layer can play an important role in passivating the charge traps at the surfaces and grain boundaries of the thin films, which significantly reduces the hysteresis and leads to higher device performances. Additionally, fullerenes can also act as a barrier for moisture, thus enhancing long-term stability, as well as a template for perovskite crystal growth and to decrease or even completely avoid ion migration. Beyond the morphological considerations of the fullerene/perovskite layers, fullerene functionalization can also have a remarkable effect on device performance and therefore, more and more derivatives are used to increase the system's performance.[49-51]

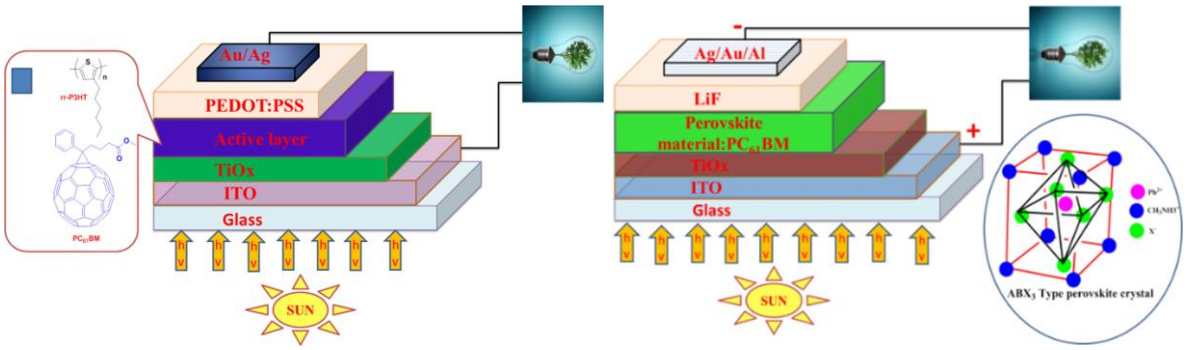

Figure 4: Left: Inverted OSCs schematic diagram. Right: Lead halide Perovskite solar cell schematic diagram. Reproduced from ref. 40 with permission from Elsevier.

The fullerenes' ability to accept and to donate as well as to mediate electrons lies also at the heart of biological applications of fullerenes in which they act for example as antioxidants (**Figure 5**).[52-

[56] Oxidative stress is a major issue in a wide number of pathologies (neurodegenerative, cardiovascular, immune diseases and cancer). Relevant oxidants for biological systems are $O_2^{\bullet-}$ (superoxide), •OH (hydroxyl) radicals and H_2O_2 molecules. These reactive oxygen species can be brought into the organism by external factors and triggers but can as well be sideproducts during metabolism. Water soluble, and with that biocompatible, fullerene derivatives are capable of catalytically scavenging harmful oxidants and further free radicals similar to naturally occurring superoxide dismutase. Therefore, they are also called radical sponges. Common examples for such studies are fullerenols and C_{60} tris(malonic)acid which are not only water soluble but also able to cross the cell membrane. Inside the cell they can also reduce the cellular oxygen radicals produced by the mitochondria.[57] Even though fullerene derivatives proofed to be potent antioxidants outperforming other antioxidants in *in vitro* and *in vivo* studies the detailed mechanism and the dependence of the antioxidant properties on the exact chemical structure remain still unclear and further effort needs to be taken to fully understand this system. As mentioned above, fullerene derivatives can not only accept electrons but also donate electrons which is being used in phototherapy. Phototherapy is a treatment for multiple diseases and is based on the targeted generation of reactive oxygen species by a photosensitizer. Fullerene derivatives as photosensitizer can be excited to S_1 state under irradiation. This state is readily transferred to long-lived T_1 via intersystem crossing. In the presence of molecular oxygen, T_1 can react with oxygen, generating a non-excited S_0 and singlet oxygen which is known to be a cytotoxic species. In addition, the high-energy species $^1C_{60}$ and $^3C_{60}$ are excellent electron acceptors and in the presence of a donor can easily be reduced to $C_{60}^{\bullet-}$ by electron transfer. Again, in the presence of oxygen, the fullerene radical anion can transfer one electron, producing a superoxide anion radical $O_2^{\bullet-}$ and hydroxyl radical •OH. Singlet oxygen and superoxide radical anions are well known reactive species towards DNA. Biocompatible fullerenes also find application in another field – drug delivery. Using nanoparticle systems can drastically improve the pharmacokinetics of a drug. Transferring bioactive elements like proteins, DNAs, and also various small molecules through the membrane into cells has got considerable attention due to its essential role in medicine and drug delivery and reaching the inner cell nucleus is even more challenging.[58] Due to their size and modifiability fullerenes can shine over other nanomaterials. The geometry, size and surface of the fullerene cage perfectly fits the requirements for biological systems, considering its diameter in the range of 1 nm. Despite the hydrophobicity of the fullerene, it can be functionalized with hydrophilic moieties achieving water-solubility and biocompatibility. The main positive point in fullerene-based drug

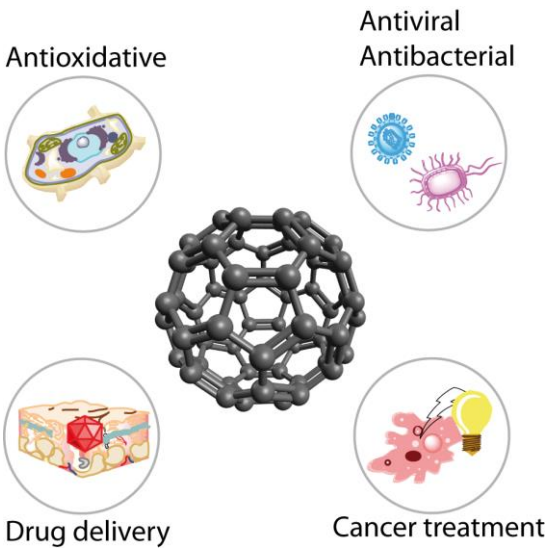

Figure 5: Overview over biomedical applications of fullerene derivatives.

delivery systems is their ability to carry multiple drug payloads. This approach is of great benefit in cancer treatment, since cancer cells can readily develop drug-resistance and effective treatment often needs combination of more than one type of drug to overcome the resistance mechanism.[58, 59]

Besides the presented applications for biologically active fullerenes there is a huge number of further areas in which research is going on from antiviral and antibacterial activity to the treatment of neuro disease.

Fullerenes in aqueous solution

Most of the applications mentioned in the previous paragraph are based on dissolved fullerenes or dissolving the compound during the process. The best solvents to dissolve pristine fullerenes are non-polar aromatic solvents and carbon disulfide.[60] More polar solvents are drastically weaker but can be used in mixtures with non-polar solvents. In these mixtures fullerenes form colloidal aggregates with sizes ranging from some to hundreds nanometers,[61] whereas, solutions of fullerenes in toluene, benzene, chlorobenzene, etc. are considered as molecular solutions. Especially, for their application in biological context, the solvent of choice is water. As well as in other polar solvents, fullerenes mostly form spherical clusters, whereas, the aggregation in aqueous solution for biological applications is directly related to its *in vitro* toxicity.[62, 63] On first sight water soluble fullerene derivatives, like the easy to obtain polyhydroxylated fullerene, the fullerenol, might be a better choice here. Interestingly, these compounds behave like a nanoparticle in solution, forming bigger aggregates, similar to pristine C_{60}. The properties of the fullerenol can be adapted during its synthesis by adapting the number and nature of its polyhydroxylation moieties. Since this very molecule is of further relevance for this thesis, its properties are discussed in more detail. A fullerenol can be described with a general formula of $C_{60}(OH)_{n\ 2<n<42}$ or $C_{60}H_zO_x(OH)_y$. The solubility of this compound is directly related to the number of introduced hydroxyl groups. A low

degree of hydroxylation ($C_{60}(OH)_{10-12}$) results in fullerenols that are soluble in less polar solvents compared to water like tetrahydrofuran, dimethyl formamide and dimethyl sulfoxide. Fullerenols with a higher degree in hydroxylation, $C_{60}(OH)_{16}$ and $C_{60}(OH)_{20-24}$, are also water soluble. The specific behavior of fullerenols is a consequence of their structural flexibility, the rotation of the OH groups, and the distribution of these groups across different carbon sites of the fullerene surface.[64] The water soluble representatives form a molecular solution at low concentration whereas, at higher concentrations aggregation occurs and nanoclusters of fullerenol are formed. These clusters range in size of some to 100 nanometers.[65] Depending on the number of hydroxyl groups per C_{60} molecule, the pH values and concentration stable nanoclusters range from 10 to 250 nm. Since the protonation state of polyhydroxylated C_{60} is pH dependent, in aqueous solutions, depending on the pH value, they are more or less deprotonated and exist in the form of stable polyanionic nanoparticles.

For the synthesis of fullerenol several methods are commonly used depending on the desired degree of hydroxylation. In 1993 Li *et al*. synthesized fullerenols with 24 to 26 hydroxyl groups directly by the reaction of fullerene C_{60} with aqueous NaOH in the presence of tetrabutylammonium hydroxide.[66] Under cyclosulfonation followed by hydrolysis of C_{60} different kinds of moieties can be introduced. With this method the fullerenol contains hemiketals with vinyl ether linkages in addition to hydroxyl moieties.[67] A further common method is the synthesis starting from halogenated fullerenes leading mostly to polyhydroxylated polyanion derivatives $C_{60}(OH)_{24-n}O_nNa_n$, by complete substitution of the bromine atoms from $C_{60}Br_{24}$. A workup with an ion exchange column enables the isolation of a single fullerenol species $C_{60}(OH)_{24}$.[68] For the synthesis of derivatives with more than 24 hydroxyl groups different strategies are needed. One example is the use of $C_{60}(OH)_{12}$ as precursor.[69] The precursor is reacted with excess hydrogen peroxide to obtain $C_{60}(OH)_{36}$. Kokubo *et al.* synthesized fullerenol $C_{60}(OH)_{44}$ in a facile one-step reaction starting from a C_{60} solution in toluene. Hydroxylation was achieved with hydrogen peroxide in the presence of a phase-transfer catalyst, tetrabutylammonium hydroxide (TBAH).[70] This fullerenol exhibited a significantly higher water solubility of up 65 mg/mL compared to fullerenol with a lower degree of hydroxylation. This might be related to the fact that these very fullerenols possess a very narrow distribution of particle size (1.46 +/- 0.4) indicating that the fullerenol is highly dispersed. The usual aggregation to clusters was not prevalent. The reason for this is a stable water layer surrounding the fullerenol core due to its high number of hydroxyl moieties. Nevertheless, a high degree of hydroxylation does not only have advantages. Calculations suggest that, in terms of

thermodynamics, fullerenols with less hydroxyl groups are more stable.[69, 71] Fullerenols with more than 24 hydroxyl groups have a tendency to open and destabilize cages. Characteristic functional groups that may appear in an open cage structure include hydroxyls, epoxies, carbonyls and hemiacetals.[72] In any case the structure of fullerenols that are not synthesized by substitution is rather complex and is only formally described as hydroxylated. In fact, not only fullerenols with a high degree of hydroxylation share a great variety of moieties but also samples with a low degree of hydroxylation. The nature of these moieties vastly depends on synthesis method and mostly results in a complex pattern. Wang *et al.* presented a structural model for fullerenols that fit electronic, IR and NMR spectroscopic properties and also a mechanisms for the instability of highly hydroxylated compounds (**Figure 6**).[71]

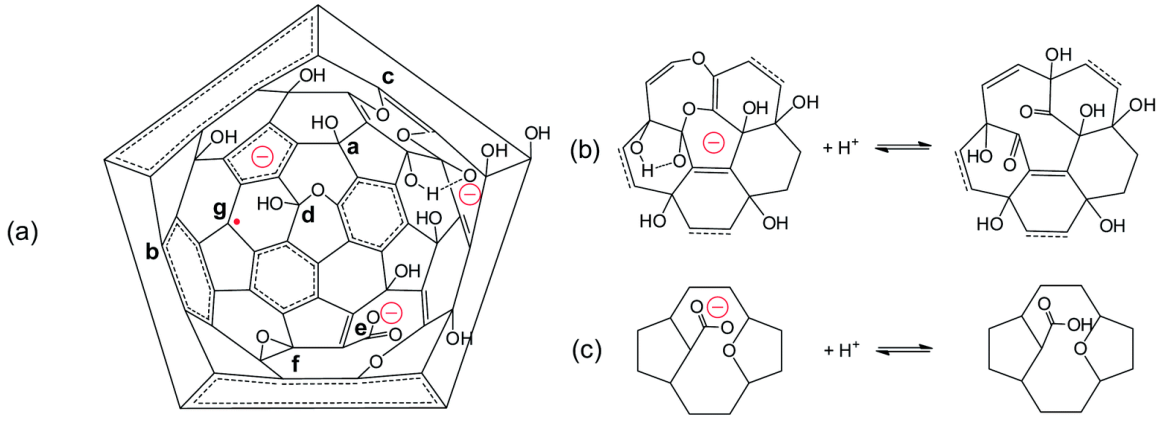

Figure 6: A structural model for C_{60} fullerenols (a) and reactions of partial structures in the model to interpret the pH-dependent transformations of C═O (b and c). Adapted and reproduced from ref. 71 with permission from The Royal Society of Chemistry.

Regardless which kind of fullerenol, the aggregation behavior is not controllable and far away from defined self-assembly. A first step towards a controlled self-assembly with this compound was made by Zhou, Shengju, *et al.*[73, 74] They could show, that mixing positively charged surfactants with anionic fullerenols led to the formation of supramolecular structures. The superstructures change their appearance with increasing concentration of surfactant. In a fullerenol rich mixture the surfaces of the fullerenol are partially covered with hydrophobic alkyl chains which then equals a giant surfactant that forms vesicular structures. Increasing the surfactant concentration leads to precipitation of the mixture since the fullerenol is then covered with alkyl chains and not water soluble anymore. In a surfactant rich mixture cylindrical micelles are formed. With a large excess of surfactants huge micelles are formed in which the fullerenol is embedded in the core of the aggregate (**Figure 7**).

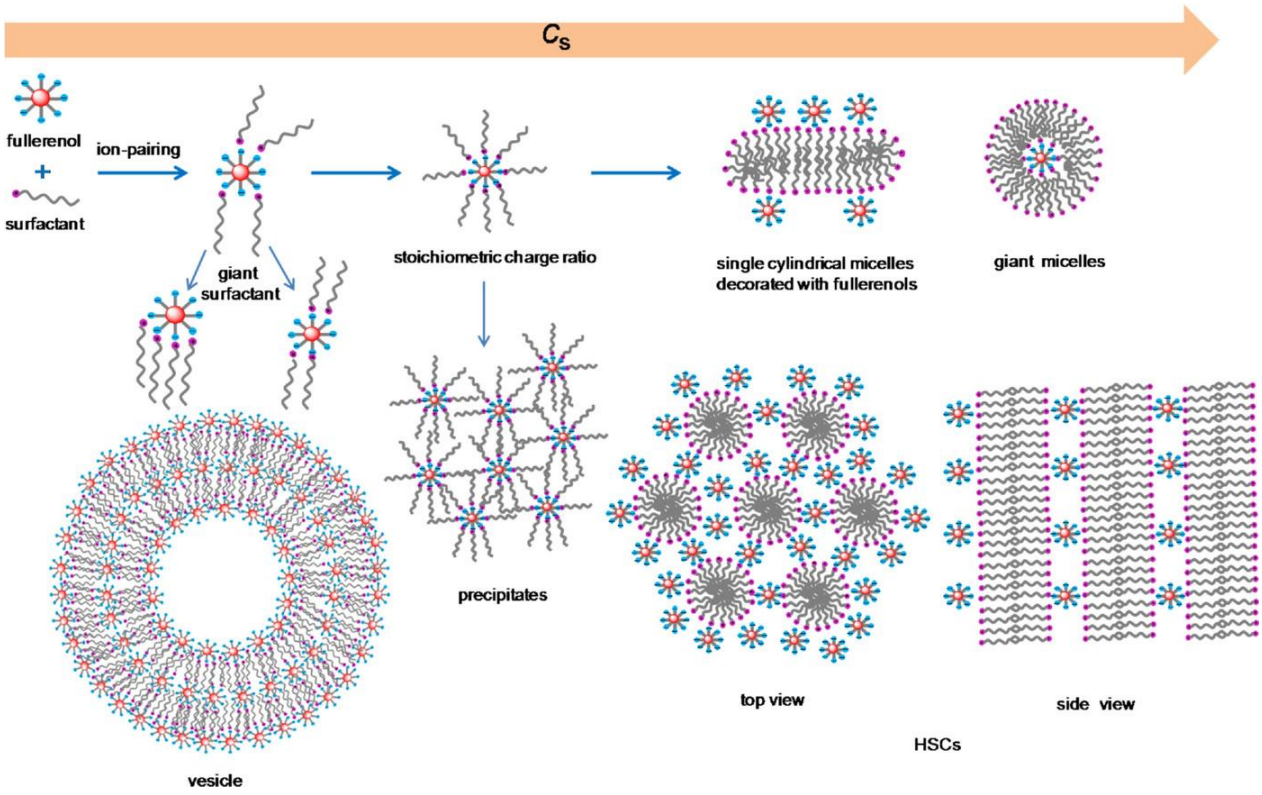

Figure 7: Illustration of the self-assembly of fullerenols induced by the oppositely charged surfactant. Reproduced with permission from ref 73. Copyright (2018), Wiley VCH.

Of course, in these examples defined self-assembly does not derive from the fullerenol itself but from the formed synergistic amphiphilic compound. Therefore, the next logical step towards a defined fullerene self-assembly is the synthesis of an amphiphilic fullerene with a janus-type structure. Liu *et al.*[75] presented $C_{60}(OH)_8$ which truly consists of only hydroxyl moieties that are located at one hemisphere of the fullerene. The system acts as amphiphilic nanoparticles in solution and $C_{60}(OH)_8$ has a strong tendency to form aggregates. When deposited on the surface, $C_{60}(OH)_8$ assembles into a spherical structure or a single layered fiber on the hydrophilic surface, but it forms a toroidal structure with concentric rings on the hydrophobic surface.

Amphiphilic fullerenes and their self-assembly in water

Amphiphilic fullerenes are very rarely spread in the wide range of fullerene derivatives even though, an amphiphilic structure is easy to achieve. The most obvious strategy is to attach a polar and water soluble moiety to the hydrophobic fullerene core by one of the manifold derivatisation methods. Nevertheless, for a long time in fullerene research there was no need for such a compound

class due to the lack of potential benefits compared to small molecule compounds. A pioneer of fullerene research, Eiichi Nakamura, and his group changed the situation. They developed a new structural motif for amphiphilic fullerenes which blazed the way for a new field of fullerene research with compounds showing properties that had not been observed before. The new structural motif was called conical fullerene amphiphiles. These compounds are built up by a fullerene core as hydrophobic unit with added structural features on one hemisphere of the core to make the system water soluble. The janus-type design leads to the formation into superstructures in aqueous solution. The aggregates of these amphiphiles differ from the aggregates formed by non-amphiphilic compounds discussed in the previous paragraph. In general, amphiphilic fullerenes form unilamellar micelles and vesicles at a very low critical aggregation concentration showing only little interfacial activity. Preferring aggregation over monolayer formation is a rather unique feature under non-polymeric compounds.[76] The following examples of these conical fullerene amphiphiles are mostly part of the work of the group of Eiichi Nakamura, and will display the features of the conical motif and its self-assembly. Nakamure *et al.* used a synthesis protocol that allows to selectively add five substituents to one hemisphere of the fullerene core to yield penta(aryl)C_{60} (**Figure 8**).[36] In this reaction a strong nucleophile, an organo copper reagent is used to add substituents to the fullerene core. The reaction follows a special mechanism only observed for fullerenes. The first addition of one organo copper reagent generates a monosubsituted fullerene anion. This anion can be oxidized by copper(I) to obtain the radical compound which can undergo a further addition reaction. This process is repeated once to produce the fulvene. The fifth substituent adds to the fulvene to produce a cyclopentadienide.[36]

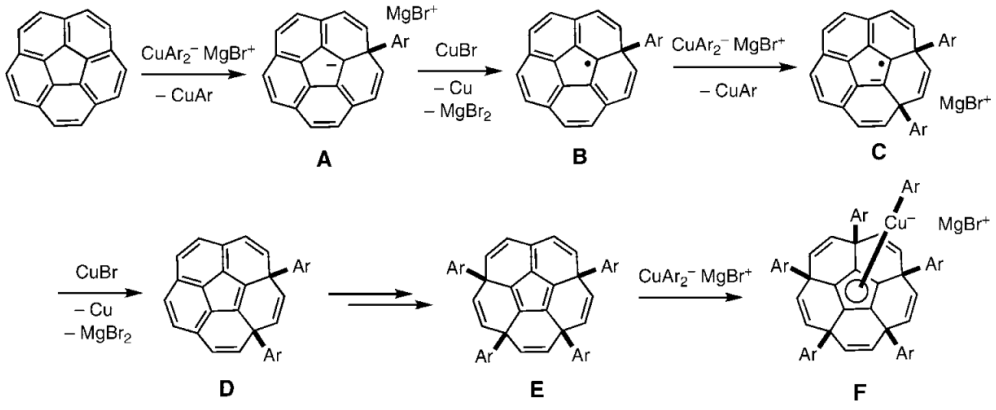

Figure 8: Plausible Reaction Mechanism for the Penta-Addition of Five Phenyl Groups onto [60]Fullerene. Reprinted with permission from ref 36. Copyright (2008) American Chemical Society.

The aryl groups attached to the fullerene created a conical shape. This compound and its derivatives already formed interesting superstructures in the crystal[77] but was far from being a water soluble amphiphile. In their further work the group synthesized two systems of conical fullerene amphiphiles, one that bears five sets of hydrophilic groups and the other comprises a cyclopentadienyl fullerene anion surrounded by five substituents. These amphiphiles have a strong tendency to form aggregates in solution due to their large size and their rigidity. Furthermore, they are resistant to crystallization because of the quasi-5-fold symmetry (**Figure 9**).[76]

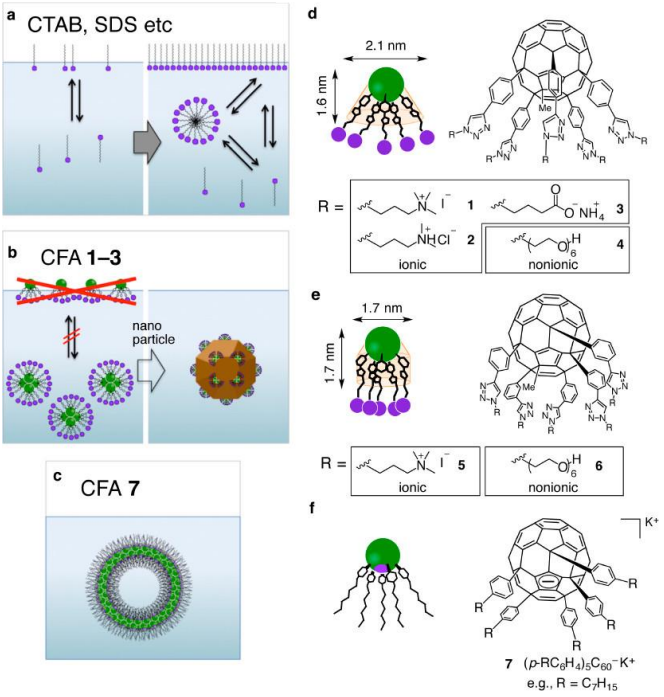

Figure 9: Overview over conical fullerene amphiphiles and related properties. Reprinted with permission from ref 78. Copyright (2008) American Chemical Society.

Interestingly, some of these compounds lack one feature that is normally typical for amphiphiles. Upon dissolving a conventional surfactant in water, it will first form a Gibbs monolayer at the air–water interface and when the air–water interface is saturated by the surfactant monolayer, it will form micelles. Hence, the critical micelle concentration value coincides with the concentration where the surface tension starts to plateau. This was not found to be the case for conical fullerene amphiphiles, in particular, with ionic derivatives. Conical fullerene amphiphiles lack air-water interfacial activity despite the strong property to form micelles and bilayer vesicles in water.[78] Self-assembling amphiphiles lacking surface activity have been recorded only for polymers, polymeric bola-amphiphiles and hydrophobic ionic polymers.[76] As a result, the compounds possess neither foaming nor emulsification properties. On the other hand, they form micelles at micromolar concentration and disperse nanoparticles and nanocarbon materials through hemimicelle formation. The required concentration is more than 100 times lower than those required for conventional small molecule dispersants. The preference to form micelles over a Gibb's monolayer results from the high charge repulsion of the five substituents that would destabilize the Gibbs

monolayer. This phenomenon is also the case for the monoanionic compound in which the charge is located at the fullerene core.[78]

As already mentioned, the conical fullerene amphiphiles mostly form stable vesicles. The mono-anionic derivatives have a nonpolar-polar-nonpolar structure whereas the penta-anionic compounds have a nonpolar head group represented by the fullerene. In 2001 Nakamura *et al.* presented the first detailed evaluation of the aggregates formed by conical fullerene amphiphiles (**Figure 10**). A monoanionic representative of this compound class, pentaphenyl[60]fullerene monoanion (Ph_5C_{60}–K^+, PhK), forms a bilayer vesicle with a diameter of approximately 30 nm with unimodal size distribution,[79] similar to an example with fluorinated chains.[80] For the above mentioned compound these aggregates have a zeta potential of approximately -40 mV, indicating that the vesicles form a solvent-separated ion pair. The vesicle's solutions are stable upon heating to 90 °C or exposure to air for more than one year, as well as on a solid substrate in air or in vacuum, maintaining their spherical form. The vesicle membrane consists of an interdigitated bilayer of the amphiphile molecules, in which the fullerene is inside and the substituents are exposed to water.[76] Furthermore, the vesicles show only low permeability to water being rather watertight compared to vesicles formed by lipids. Water permeation through the conical fullerene membrane shows a negative activation entropy as well as a negative activation enthalpy. Nakamura *et al.* suggested that this is due to hydrogen binding of water molecules to the anionic fullerene core being in the "middle" of a bilayer. This behavior is contrary to a lipid membrane, in which water permeation is regulated largely by a positive activation enthalpy.[76, 81, 82]

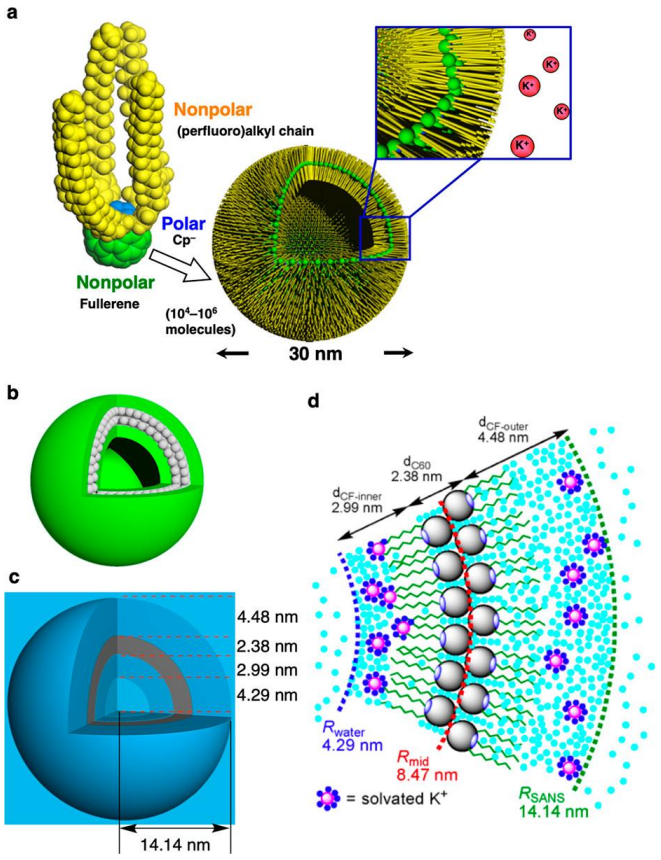

Figure 10: Structure and formation of bilayer vesicles of a conical fullerene amphiphile. Reprinted with permission from ref 79. Copyright (2019) American Chemical Society.

Hirsch *et al.* followed another approach generating an amphiphilic fullerene system.[83-85] This system is, based on a C_{60} core, containing both hydrophobic and hydrophilic moieties and self-assembles into multiple shapes of aggregates dependent on several factors. One representative consists of a fullerene cage to which a Newkome-like dendrimer unit is connected via amine linker and ten lipophilic C_{12} chains positioned octahedrally to the dendrimer are attached. This fullerene amphiphile has a low critical micelle concentration and the polar dendrimer head group contains multiple carboxylic acid groups, resulting in pH sensitive assembly. In neutral water (pH 7.2), it aggregates into cylinders with a diameter of ca. 65 nm as revealed by cryogenic TEM studies. Increasing the pH value to approximately 9.2, the formation of defined micelles with a diameter of 8.5 nm was observed. The pH-dependent aggregation behavior was attributed to the different degree of protonation that altered the repulsion and the size of hydration shell. When the amine linker is replaced by esters the aggregation behavior changes. The compound now forms vesicular aggregates similar to the aggregates reported by Nakamura *et al*. These aggregates are rarely referred to as "buckysomes". An explanation for this is that the dendritic amide moieties have more pronounced rigidity that favors aggregation with a high degree of curvature rather than a planar alignment.[83, 85] The structure formation of these globular fullerene amphiphiles was further investigates with a [3:3]-hexakis C_{60} adduct as model system. Unlike the previous compounds this derivative carries three hydrophilic dendrons. Although the number of hydrophilic moieties is the same for both systems, in the new derivative the hydrophilic units are more spread over the fullerene cage. It was found that these compounds only form small nanospheres with a diameter of approximately 5 nm. 3D reconstruction based on molecular modeling and TEM imaging indicated that these spherical micelles were made of three identical S-shaped motifs in the D 3 symmetry.[86, 87]

Besides the above discussed examples further scattered examples of fullerene amphiphiles can be found in literature. A structural motif that is used by many groups is to tether a highly polar and water-soluble group such as ammonium to the C_{60} via a e.g. alkyl chains. These compounds form aggregates of various size and shape which are more or less evaluated in detail. In general, the supramolecular assembling of chain-like C_{60} amphiphiles seems to be more simple since it is basically dominated by two major forces. These are π-stacking and ionic interaction, the π-stacking acts attracting, whereas the ionic interaction acts repelling. The balance between these factors determines the aggregate's size.[88] It is evident that functionalization of C_{60} with rationally designed pendant groups offers an effective approach to avert the random aggregation inherent in spherical

C_{60} cage and hence, delivers controllability over the microstructure of self-assembly and organization.

Application of fullerene amphiphiles

For amphiphilic fullerenes various applications derive from their self-assembly and their molecular structure. Nevertheless, due to lack of variety in amphiphilic fullerenes the presented applications are limited. In most cases the investigation of new systems in this field ends with the evaluation of its self-assembly. The class of conical fullerene amphiphiles reported by Nakamura *et al.* are obviously investigated in more detail than others. In the following three examples for the use of this compound class are presented. Ionic conical fullerene amphiphiles show powerful dispersant properties for nanomaterial that are too large for small molecule surfactants. Compared to common dispersants like SDS or CTAB, that require millimolar concentration to disperse magnetite nanoparticles or carbon nanotubes the presented fullerene amphiphiles only require micromolar concentrations with long term stability. These compounds disperse materials via hemimicelle formation on the solid surface.[78] Another application of this compound class that is related to its self-assembly is the use of the formed bilayer membrane as nanosized chemical reactor. Previous studies by Nakamura *et al.* not only showed the stability of the formed aggregates in solution but also that the integrity of the aggregates stays intact under implementing small molecules into the bilayer membrane. A Hoveyda-Grubbs catalyst loaded into different types of conical fullerene amphiphile vesicles together with a suitable monomer yielded different results. The reaction in the fluorinated vesicle, presented in the chapter before, yielded unisize polymer particles. Performing the polymerization in a vesicle containing conical fullerene amphiphiles with short chain length yielded a hollow polymer capsule in the size of the vesicle.[89, 90] Furthermore, lot of applications are related to drug delivery. Min-Song presented a system, structurally similar to these of Nakamura, that forms special vesicles for delayed drug release (**Figure 11**).[91] The biocompatible vesicles formed by $C_{60}R_5Cl$ (R = methyl ester of 4-aminobutyric/glutamic acid or phenylalanine) can be used as delayed-release carriers of anti-cancer drugs such as cyclophosphamide and cisplatin, with the time of release from drug-containing vesicles exceeding that of non-encapsulated forms by a factor of three. A different structural motif was used by Adeli *et al.* A fullerene-polyglycerol amphiphile that was synthesized *via* a grafting method was used as nanocarrier with controlled transport properties.[92] Size and transport properties of those amphiphiles in aqueous

solution can be controlled via photocrosslinking of their hydrophobic fullerene segments. *In vivo* studies of the use of fullerene nanocarriers are reported by Partha *et al.*[93] They used the dendritic compound, presented by Hirsch *et al.* for their studies and prepared vesicular structures with a diameter of 100 to 200 nm. Due to the structure of the fullerene amphiphile the aggregates contained big hydrophobic areas in between the layers to incorporate hydrophobic substances. Pratha *et al.* incorporated the highly hydrophobic anti-cancer drug Paclitaxel as a model system with promising results.

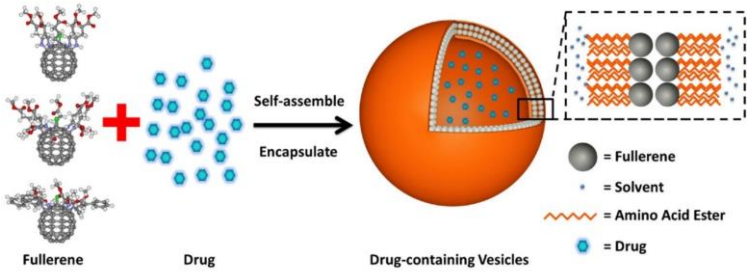

Figure 11: Fullerene-based amino acid ester chlorides self-assembled as spherical nano-vesicles for drug delayed release. Reproduced from Ref. 91 with permission from Elsevier.

In summary, fullerenes and their derivatives proofed to be tremendously versatile compounds. This is not only due to their modifiability but also due to their electronic and optoelectronic properties derived from their structure. This modifiability enables them to be used in different research areas in which they are able to outperform standard small organic molecules. They are also found to possess special self-assembly properties when modified as amphiphile, whereas this self-assembly can be used to build up complex systems. Nevertheless, in all the reported systems the intrinsic properties of fullerenes are neglected and they were only used as scaffold in amphiphilic systems. Only little is known about the self-assembly properties and related abilities of amphiphilic fullerenes and there are only rare examples of their use. The potential of this compound class has only been evaluated by few researchers so far. The most obvious challenge is to combine a fullerenes' properties with the controllable self-assembly of fullerene amphiphiles to obtain a further new class of compounds in which the intrinsic properties benefit from its self-assembly. Hence, after all the years in fullerene research amphiphilic fullerenes are still a promising chapter for future years of research with lots of possibilities to be explored.

5 Challenges and Objectives

Fullerenes of all kind are allrounders and were promising top choice as molecular scaffold for further modifications. Due to their functionality they have found their way into a broad variety of research areas as described before. Even the use of fullerene derivatives in supramolecular structures showed potential. Nevertheless, after 30 years of fullerene research the state of the art in supramolecular fullerene chemistry is, that the fullerene is a suitable building block for myriads of structures achieved by derivatisation, combination or synthesis and preparation methods. A versatile building block, that is what the fullerene is only used for. And with that limitation to just being a building block the huge potential of fullerenes, regarding their electronic and optoelectronic properties is neglected. Even though amphiphiles in general are capable of much more than only being building blocks for superstructures. Decades of research on amphiphilic compounds, surfactants, often times based on polymer structures, revealed that this class of compounds can possess properties as versatile as fullerenes. Nowadays, surfactants are much more than simple molecules to build up superstructures. They can be tuned to respond to external triggers like temperature, pH value, magnetic field and much more to change their properties.[2] Even catalytically active surfactants are known in literature, combining amphiphilic character, resulting in controllable self-assembly, with further functionalities like catalyzing reactions. They turned out to be real functional materials. These very functional surfactants are a research topic in the group of Sebastian Polarz. Our group is specialized in combining the defined and controllable self-assembly properties of amphiphilic compounds with a functionality of the head groups that benefits from its self-assembly. Especially, in the field of polyoxometalate (POM) organic-inorganic hybrid surfactants pioneer work was done. Different systems of this class with its redox active POM head group were evaluated.[6, 94-97] Also, surfactants containing NHC-ligand based head groups were presented for polymerization and interfacial catalysis.[4, 98] Obviously, it comes to mind that the functionality of fullerenes should be combined with controlled and defined self-assembly to achieve a functional fullerene surfactant that benefits from its self-assembly. Although this seems not to be possible with existing fullerene amphiphiles that, in general, contain the fullerene as hydrophobic part and organic moieties as hydrophilic part, neglecting the fullerenes properties, but only being amphiphilic for its purpose. The focus of this thesis is set on synthesizing a new class of fullerene based surfactants that possess additional functional properties that benefit from its self-

assembly, which has to be evaluated as well. Therefore, the key objectives of this thesis are as follows:

- **Synthesis of a new class of fullerene based surfactants**
- **Evaluate functionalities that benefit from self-assembly**
- **Tune self-assembly beneficial properties in a more complex system**
- **Investigate the origins of beneficial effects of self-assembly**

For the realization of these tasks a new molecular fullerene building block needs to be developed. Referring to the systems of Nakamura a conical structure motif seems to guarantee controllable and defined self-assembly but compared to the work of Nakamura the polarity within the systems needs to be inverted. To benefit from the fullerenes' intrinsic properties, it seems to be best if the fullerene is the hydrophilic part of the structure guaranteeing the fullerene is exposed to the outside of the formed aggregates. This shall be realized by derivatize the fullerene in a janus-type fashion. A promising derivatisation might be a janus-type fullerenol compound since fullerenols are known to be water soluble and possess properties like antioxidative effects by catalytically reacting with oxygen. Is it possible to combine this feature with controlled self-assembly and can a beneficial effect of the aggregation be observed? No similar systems are described in literature so far. With such a new system in hand one could also think about more complex derivatives with not only simple alkyl chains attached to the fullerene but more complex moieties that exhibit further features. The fullerene itself, can not only act as an electron acceptor like it does in the reaction with oxygen, but it can also serve as an electron mediator. This could be the basis to achieve more complex systems that benefit from the self-assembly. The self-assembly itself plays a crucial role in these systems. Its' specific self-assembly needs to be understood and possible beneficial effects need to be evaluated. The challenges can be concluded as follows: can a system be generated whose intrinsic properties benefit from self-assembly.

6 Scientific Contribution of the Thesis

The presented thesis contributes to the research in the field of functionalized surfactants in particular fullerene surfactants, and the impact of self-assembly to improve catalytic properties with the following key achievements:

- **Lipid-like self-assembly behavior of fullerene surfactants with catalytically active head group**
- **Janus-type design for molecular semiconductors in vesicular systems**
- **Self-assembly as crucial factor in fullerene centered catalytic reactions**

Hereafter, the key achievements of the thesis are highlighted and classified into the context of the research area.

Lipid-like self-assembly behavior of fullerene surfactants with catalytically active head group

Due to its easy modifiability the molecular nanoparticle fullerene C_{60} finds application in lots of research areas ranging from material science to biochemical science. For many applications, solubility, precisely water solubility is a crucial factor for the usability of fullerene-based compounds. As mentioned earlier there are several examples of water soluble and even amphiphilic fullerene compounds. These water soluble compounds tend to ill-definably aggregate in solution like nanoparticles can do. Also, most of the amphiphilic compounds that avoid ill-defined self-assembly have one drawback. In most of these compounds the fullerene itself, serves as the hydrophobic component and with that, during aggregation in aqueous solution, is located in the inside of the aggregate and is not accessible to further reactions anymore. Aggregation and solubility are both important issues especially for biological applications. A fullerenol, a polyhydroxylized, and with that water soluble, fullerene derivative is widely used in biological and chemical biology studies since this compound enables the utilization of a crucial property of the fullerene. This property is that the fullerene can act as a radical sponge and can further react with reactive oxygen species (ROS). Fullerenes and fullerenols are able to catalytically scavenge ROS which make them promising candidates for anti-tumor or cancer-preventing research. Nevertheless, these rather simple compounds have some major drawbacks, regarding their not fully

understood features. The metabolism of this compounds, the distribution, the molecular behavior of the compound in biological systems and its solubility properties in regard of aggregation behavior in biological media. In this context, especially the solubility, aggregation behavior and with that the distribution of the compound in biological media shall be addressed. Fullerenols, as molecular nanoparticles, tend to aggregates in solution to more or less ill-defined clusters of various sizes influencing its solubility, and behavior in biological systems. In 2018, we presented an attempt to overcome these problematics by using an amphiphilic fullerenol compound, combining the biological activity of the fullerenol and the controllable aggregation, defined self-assembly, of the amphiphilic structure. The fullerenol surfactants show controllable and stable self-assembly and proved its biocompatibility as well as its ROS scavenging properties in biological systems with prokaryotic and eukaryotic cells in which it is expected to be incorporated into the cell membrane. The two presented surfactant systems with an acidic and a basic fullerenol head group form defined hollow aggregates in solution, similar to lipids e.g. phospholipids in the cell membrane. Furthermore, it could be shown that the amphiphilic compounds outperform standard ROS scavengers like quercetin or the non-amphiphilic equivalent compound for O_2^-, $ONOO^-$, OH and H_2O_2 scavenging. It is proposed that this is mostly due to the, reactive side of the compound which is exposed by self-assembly and on the change in the (electronic) structure of the compound due to janus-type modification. With the in detail evaluated lipid like self-assembly properties and the *ex vivo* ROS scavenging studies we eventually could show the impact of the surfactant behavior in biological systems. With the compound proven to be nontoxic to prokaryotic and eukaryotic cells it was further shown that the cells do actually integrate the surfactants. The lipid-like character and the high activity in ROS scavenging in the cells indicate that the cells implement the fullerenol surfactants into their cellular membranes as kind of membrane guards.

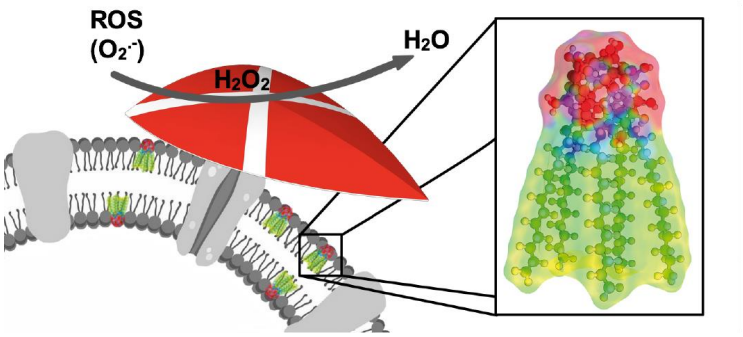

Figure 12: TOC figure of publication 1. Reproduced from ref. 99 with permission. Copyright (2018) American Chemical Society.

Janus-type design for molecular semiconductors in vesicular systems

In the next part of the project we aimed to go one step further building on the knowledge already obtained from the system. The effect of intrinsic property improvement through self-assembly should further be evaluated. The fullerenol head group presented in publication 1 is not only capable of scavenging reactive oxygen species, by catalytically accepting electrons but also of producing reactive oxygen species, by donating electrons under irradiation, which is an indicator for being a reductive photocatalyst. To achieve the efficient photocatalytic activity, the general molecular design was adapted without changing the basic structure motif. The former alkyl chains have been replaced with linear dye molecules, acridine derivatives. A new synthesis strategy needed to be developed, since the former presented protocol reached its limits due to the insolubility of the intermediates. The synthesis to achieve the new compounds was presented in publication 2. It could be shown that almost any motif of a janus-type fullerenol surfactant with five substituents of various kind can be synthesized in a one-pot reaction. It combines the polyhydroxylation and the penta-substitution of the fullerene core in one step via phase transfer reaction followed by an easy workup. Aliphatic and aromatic primary amines, even with further functional groups, showed to be very reactive in this reaction and led to yields of up to 90 % for the surfactant compound. For workup a hydrophilic interaction liquid chromatography was established. Furthermore, several ways to characterize these compounds were presented, since the characterization of these highly functionalized, water soluble, aggregating fullerene derivatives turned out to be challenging and was not well documented in literature. With this method in hand, it was eventually possible to synthesize janus-type fullerenol surfactants with five dye molecules attached.

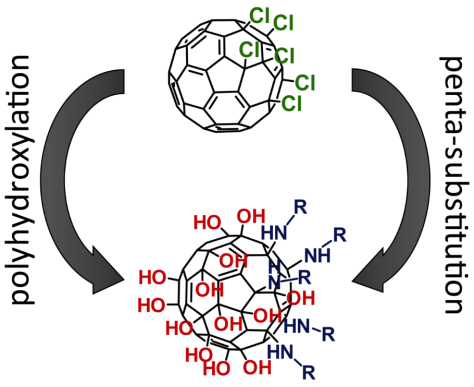

Figure 13: TOC figure of publication 2. Reproduced under the Creative Commons Attribution License.

Their properties were presented in publication 3. Inspired by the research of fullerene dyads, which are basically donor-acceptor systems with the fullerene being the electron acceptor, we described a molecular semiconductor system which generates a charge separation upon irradiation with visible light. Nowadays, most of these dyads lack a proper application due to their low solubility in water and their non-evaluated aggregation behavior. These drawbacks are overcome by our fullerenol surfactant system with defined and controllable self-assembly. Depending on the polarity of the attached dye molecules the compounds self-assembled in stable spherical aggregates in a size range from 50 nm to 100 nm. We could show that the system acts as molecular semiconductor in aqueous solution. The absorbance spectrum of the fullerenol dyes showed an absorption edge similar to regular semiconductors. DFT calculations confirmed that under irradiation a charge separation takes place. The HOMOs of the molecules are located on the dyes whereas, the LUMO is located on the fullerenol head group. We demonstrated that the chemical energy of the charge separated state can be used for further reactions in water which was evaluated by reducing oxygen, being an efficient oxidant. Interestingly, it was observed that the aggregation of the system enables the electronic communication within the aggregates. Electron transfer processes in the vesicles from one surfactant to another have been observed. In a prototype reaction we could further show that the chemical energy of the charge separated state can be used to reduce chemicals like carbon dioxide. With these findings we basically developed a new system of a so called artificial leaf in whose properties emerge due to self-assembly to vesicular structures.

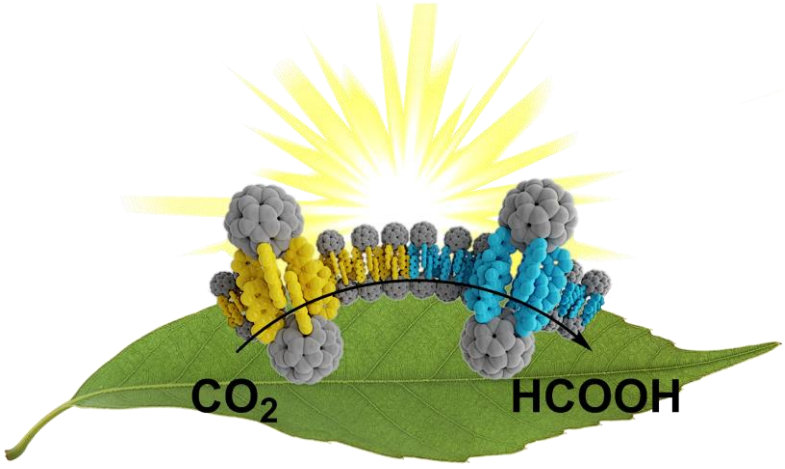

Figure 14: TOC figure of publication 3. Reproduced under the Creative Commons Attribution License.

Self-assembly as crucial factor in fullerene centered catalytic reactions

Having shown the beneficial effect of self-assembly on fullerene centered reactions we eventually, in the fourth publication, took a closer look at the effect of an inner and inter aggregates electron transfer by choosing a well observable catalytic process - the electrocatalytic water splitting reaction in aqueous solution. These evaluations are presented in publication 4 which was published in 2020. A new fullerene surfactant was used as model systems. The fullerenol head group was exchanged with a metal complex. A cobalt diethylenetriamine complex was coordinated to the fullerene, since cobalt complexes are known to undergo water splitting reaction. This compound showed activity in electrochemical oxygen evolving reaction (OER) and hydrogen evolving reaction (HER). The OER was located at the metal center and the system showed medium activity regarding the overpotential and TOF, below and above the critical aggregation concentration. Nevertheless, this is a totally different case for the HER. In this system the fullerene is a non-innocent ligand and serves as electron reservoir for the reaction. It was observed that this process heavily depends on the self-assembly of the system. Whereas, the catalytic activity below the cac is rather low regarding the overpotential, the current and the TOF, the compound becomes drastically more active above the cac. Reaching the cac, not only the overpotential shifts but also the TOF is increased by 1300 %. It was suggested that this tremendous increase in performance is related to the spatial closeness of the fullerene head groups that enables an inter molecular electron transfer easing the reduction reaction. This effect was confirmed by diluting the reactive compound in the aggregates with a co-surfactant which diminished the observed improvements.

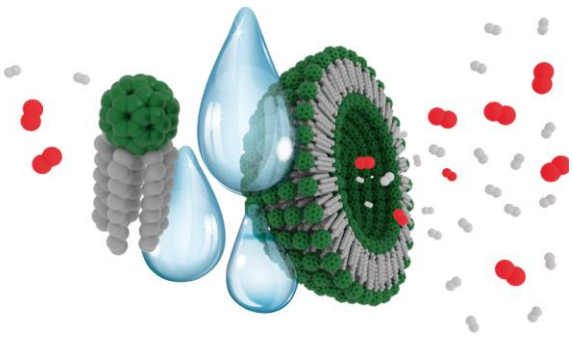

Figure 15: TOC figure of publication 4. Reproduced under the Creative Commons Attribution License.

Within this thesis not only a new class of fullerene and fullerenol surfactants was defined, but it was also clearly shown that self-assembly is an underestimated tool to improve a system's properties or even enable new properties and applications. In aggregates formed by fullerene amphiphiles a strong communication within and in between the aggregates is present, resulting in a change in the overall electronic situation. These findings can not only be applied to fullerene based systems but to all self-assembling compounds bearing a catalytically active head group.

7 References of Chapter 1-6

1. Israelachvili, J. N., *Intermolecular and surface forces*. Academic press: **2011**.
2. Polarz, S.; Kunkel, M.; Donner, A.; Schlotter, M., *Chemistry–A European Journal* **2018**, *24*, 18842-18856.
3. Brown, P.; Butts, C. P.; Eastoe, J., *Soft Matter* **2013**, *9*, 2365-2374.
4. Donner, A.; Hagedorn, K.; Mattes, L.; Drechsler, M.; Polarz, S., *Chemistry–A European Journal* **2017**, *23*, 18129-18133.
5. Hermann, S.; Wessig, M.; Kollofrath, D.; Gerigk, M.; Hagedorn, K.; Odendal, J. A.; Hagner, M.; Drechsler, M.; Erler, P.; Fonin, M., *Angewandte Chemie International Edition* **2017**, *129*, 5567-5571.
6. Klaiber, A.; Kollek, T.; Cardinal, S.; Hug, N.; Drechsler, M.; Polarz, S., *Advanced Materials Interfaces* **2018**, *5*, 1701430.
7. Sutter, S.; Trepka, B.; Siroky, S.; Hagedorn, K.; Theiss, S.; Baum, P.; Polarz, S., *ACS Applied Material Interfaces* **2019**, *11*, 15936-15944.
8. Smalley, R. E.; Kroto, H.; Heath, J., *Nature* **1985**, *318*, 162-163.
9. Osawa, E. J. K., **1970**, *25*, 854-863.
10. Browne, M., The New York Times: **1991**.
11. Godly, E.; Taylor, R., *Fullerenes, Nanotubes, Carbon Nanostructures* **1997**, *5*, 1667-1708.
12. Powell, W.; Cozzi, F.; Moss, G.; Thilgen, C.; Hwu, R.-R.; Yerin, A., *Pure applied chemistry* **2002**, *74*, 629-695.
13. Krätschmer, W.; Lamb, L. D.; Fostiropoulos, K.; Huffman, D. R., *Nature* **1990**, *347*, 354.
14. Shanbogh, P. P.; Sundaram, N. G., *Resonance* **2015**, *20*, 123-135.
15. Boorum, M. M.; Vasil'ev, Y. V.; Drewello, T.; Scott, L. T., *Science* **2001**, *294*, 828-31.
16. Anderson, T.; Dyer, P.; Dykes, J.; Klavins, P.; Anderson, P.; Liu, J.; Shelton, R., *Review of scientific instruments* **1994**, *65*, 3820-3822.
17. Krestinin, A.; Moravsky, A., *Chemical physics letters* **1998**, *286*, 479-484.
18. Goroff, N. S., *Accounts of chemical research* **1996**, *29*, 77-83.
19. Churilov, G.; Novikov, P.; Tarabanko, V.; Lopatin, V.; Vnukova, N.; Bulina, N., *Carbon* **2002**, *40*, 891-896.
20. Pierson, H. O., *Handbook of carbon, graphite, diamonds and fullerenes: processing, properties and applications*. William Andrew: **2012**.
21. Schein, S.; Sands-Kidner, M.; Friedrich, T., *Biophysical journal* **2008**, *94*, 938-957.
22. Hirsch, A., *Synthesis* **1995**, *1995*, 895-913.
23. Prato, M., *Journal of Materials Chemistry* **1997**, *7*, 1097-1109.
24. Schulz, G. L.; Urdanpilleta, M.; Fitzner, R.; Brier, E.; Mena-Osteritz, E.; Reinold, E.; Bäuerle, P., *Beilstein journal of nanotechnology* **2013**, *4*, 680-689.
25. Campbell, E. E.; Rohmund, F., *Reports on Progress in Physics* **2000**, *63*, 1061.
26. Diederich, F.; Thilgen, C., *Science* **1996**, *271*, 317-324.
27. Tajima, Y.; Takeshi, K.; Shigemitsu, Y.; Numata, Y., *Molecules* **2012**, *17*, 6395-414.
28. Bingel, C., *Chemische Berichte* **1993**, *126*, 1957-1959.

29. Ball, G. E.; Burley, G. A.; Chaker, L.; Hawkins, B. C.; Williams, J. R.; Keller, P. A.; Pyne, S. G., *Journal of Organic Chemistry* **2005**, *70*, 8572-4.
30. Olah, G. A., *Friedel-crafts and Related Reactions: Alkylation and Related Reactions*. Interscience: **1964**.
31. Olah, G. A.; Bucsi, I.; Ha, D. S.; Aniszfeld, R.; Lee, C. S.; Prakash, G. S., *Fullerenes, Nanotubes, Carbon Nanostructures* **1997**, *5*, 389-405.
32. Śliwa, W., *Fullerenes, Nanotubes, Carbon Nanostructures* **1997**, *5*, 1133-1175.
33. Selig, H.; Lifshitz, C.; Peres, T.; Fischer, J.; McGhie, A.; Romanow, W.; McCauley Jr, J.; Smith III, A., *Journal of the American Chemical Society* **1991**, *113*, 5475-5476.
34. Ala'a, K., *Journal of the Chemical Society, Perkin Transactions 2* **1995**, 981-985.
35. Troshin, P. A.; Kolesnikov, D.; Burtsev, A. V.; Lubovskaya, R. N.; Denisenko, N. I.; Popov, A. A.; Troyanov, S. I.; Boltalina, O. V., *Fullerenes, Nanotubes Carbon Nanostructures* **2003**, *11*, 47-60.
36. Matsuo, Y.; Nakamura, E., *Chemical Reviews* **2008**, *108*, 3016-28.
37. Langa, F.; Nierengarten, J., Fullerenes Principles and Applications. 2007. Cambridge: The Royal Society of Chemistry.
38. Buhl, M.; Hirsch, A., *Chemical Reviews* **2001**, *101*, 1153-83.
39. Collavini, S.; Delgado, J. L.; *Sustainable Energy Fuels* **2018**, *2*, 2480-2493.
40. Ganesamoorthy, R.; Sathiyan, G.; Sakthivel, P., *Solar Energy Materials Solar Cells* **2017**, *161*, 102-148.
41. Castro, E.; Murillo, J.; Fernandez-Delgado, O.; Echegoyen, L., *Journal of Materials Chemistry C* **2018**, *6*, 2635-2651.
42. Xue, J., *Polymer Reviews* **2010**, *50*, 411-419.
43. Dennler, G.; Scharber, M. C.; Brabec, C. J., *Advanced Materials Interfaces* **2009**, *21*, 1323-1338.
44. Troshin, P. A.; Hoppe, H.; Renz, J.; Egginger, M.; Mayorova, J. Y.; Goryachev, A. E.; Peregudov, A. S.; Lyubovskaya, R. N.; Gobsch, G.; Sariciftci, N. S., *Advanced Functional Materials* **2009**, *19*, 779-788.
45. Yu, G.; Gao, J.; Hummelen, J. C.; Wudl, F.; Heeger, A. J., *Science* **1995**, *270*, 1789-1791.
46. Xu, Y.; Yao, H.; Hou, J., *Chinese Journal of Chemistry* **2019**, *37*, 207-215.
47. Ans, M.; Ayub, K.; Muhammad, S.; Iqbal, J., *Computational Theoretical Chemistry* **2019**, *1161*, 26-38.
48. Jeng, J. Y.; Chiang, Y. F.; Lee, M. H.; Peng, S. R.; Guo, T. F.; Chen, P.; Wen, T. C., *Advanced Materials* **2013**, *25*, 3727-32.
49. Wojciechowski, K.; Stranks, S. D.; Abate, A.; Sadoughi, G.; Sadhanala, A.; Kopidakis, N.; Rumbles, G.; Li, C. Z.; Friend, R. H.; Jen, A. K.; Snaith, H. J., *ACS Nano* **2014**, *8*, 12701-9.
50. Liu, X.; Lin, F.; Chueh, C.-C.; Chen, Q.; Zhao, T.; Liang, P.-W.; Zhu, Z.; Sun, Y.; Jen, A. K.-Y., *Nano energy* **2016**, *30*, 417-425.
51. Zhang, F.; Shi, W.; Luo, J.; Pellet, N.; Yi, C.; Li, X.; Zhao, X.; Dennis, T. J. S.; Li, X.; Wang, S.; Xiao, Y.; Zakeeruddin, S. M.; Bi, D.; Gratzel, M., *Advanced Materials* **2017**, *29*, 1606806.
52. Djordjevic, A.; Srdjenovic, B.; Seke, M.; Petrovic, D.; Injac, R.; Mrdjanovic, J., *Journal of Nanomaterials* **2015**, *2015*.
53. Thakral, S.; Mehta, R., *Indian journal of pharmaceutical sciences* **2006**, *68*, 13.
54. Jensen, A. W.; Wilson, S. R.; Schuster, D. I., *Bioorganic & Medicinal Chemistry* **1996**, *4*, 767-79.

55. Bakry, R.; Vallant, R. M.; Najam-ul-Haq, M.; Rainer, M.; Szabo, Z.; Huck, C. W.; Bonn, G. K., *International Journal of Nanomedicine* **2007**, *2*, 639-49.
56. Semenov, K.; Charykov, N.; Postnov, V.; Sharoyko, V.; Vorotyntsev, I.; Galagudza, M.; Murin, I., *Progress in Solid State Chemistry* **2016**, *44*, 59-74.
57. Sergeeva, V.; Kraevaya, O.; Ershova, E.; Kameneva, L.; Malinovskaya, E.; Dolgikh, O.; Konkova, M.; Voronov, I.; Zhilenkov, A.; Veiko, N., *Oxidative medicine cellular longevity* **2019**, *2019*.
58. Goodarzi, S.; Da Ros, T.; Conde, J.; Sefat, F.; Mozafari, M., *Materials Today* **2017**.
59. Kazemzadeh, H.; Mozafari, M., *Drug Discovery Today* **2019**, *24*, 898-905.
60. Semenov, K. N.; Charykov, N. A.; Keskinov, V. A.; Piartman, A. K.; Blokhin, A. A.; Kopyrin, A. A., *Journal of Chemical Engineering Data* **2009**, *55*, 13-36.
61. Beck, M. T., *Pure applied chemistry* **1998**, *70*, 1881-1887.
62. Lyon, D. Y.; Adams, L. K.; Falkner, J. C.; Alvarezt, P. J., *Environ Sci Technol* **2006**, *40*, 4360-6.
63. Lyon, D. Y.; Brunet, L.; Hinkal, G. W.; Wiesner, M. R.; Alvarez, P. J., *Nano letters* **2008**, *8*, 1539-1543.
64. Fileti, E. E.; Rivelino, R.; Brito Mota, F.; Malaspina, T., *Nanotechnology* **2008**, *19*, 365703.
65. Piatek, A.; Dawid, A.; Gburski, Z., *Spectrochimica Acta A: Molecular and Biomolecular Spectroscopy* **2011**, *79*, 819-23.
66. Li, J.; Takeuchi, A.; Ozawa, M.; Li, X.; Saigo, K.; Kitazawa, K., *Chemical Communications* **1993**, 1784-1785.
67. Chiang, L. Y.; Upasani, R. B.; Swirczewski, J. W.; Soled, S., *Journal of the American Chemical Society* **1993**, *115*, 5453-5457.
68. Mirkov, S. M.; Djordjevic, A. N.; Andric, N. L.; Andric, S. A.; Kostic, T. S.; Bogdanovic, G. M.; Vojinovic-Miloradov, M. B.; Kovacevic, R. Z., *Nitric Oxide* **2004**, *11*, 201-7.
69. Chiang, L. Y.; Wang, L.-Y. Swirczewski, J. W.; Soled, S.; Cameron, S., *The Journal of Organic Chemistry* **1994**, *59*, 3960-3968.
70. Kokubo, K.; Shirakawa, S.; Kobayashi, N.; Aoshima, H.; Oshima, T., *Nano Research* **2011**, *4*, 204-215.
71. Wang, Z.; Chang, X.; Lu, Z.; Gu, M.; Zhao, Y.; Gao, X., *Chemical Science* **2014**, *5*, 2940-2948.
72. Rodriguez-Zavala, J. G.; Guirado-Lopez, R. A., *Journal Physical Chemistry A* **2006**, *110*, 9459-68.
73. Zhou, S.; Zhang, L.; Feng, Y.; Li, H.; Chen, M.; Pan, W.; Hao, J., *Chemistry–A European Journal* **2018**, *24*, 16609-16619.
74. Sun, X.; Zhang, Q.; Yin, K.; Zhou, S.; Li, H., *Chemical Communications* **2016**, *52*, 12024-12027.
75. Liu, Y.; Zhang, G.; Niu, L.; Gan, L.; Liang, D., *Journal of Materials Chemistry* **2011**, *21*, 14864-14868.
76. Harano, K.; Nakamura, E., *Account of Chemical Ressearch* **2019**, *52*, 2090-2100.
77. Sawamura, M.; Kawai, K.; Matsuo, Y.; Kanie, K.; Kato, T.; Nakamura, E., *Nature* **2002**, *419*, 702.
78. Nitta, H.; Harano, K.; Isomura, M.; Backus, E. H. G.; Bonn, M.; Nakamura, E., *Journal of American Chemical Society* **2017**, *139*, 7677-7680.
79. Zhou, S.; Burger, C.; Chu, B.; Sawamura, M.; Nagahama, N.; Toganoh, M.; Hackler, U. E.; Isobe, H.; Nakamura, E., *Science* **2001**, *291*, 1944-7.
80. Homma, T.; Harano, K.; Isobe, H.; Nakamura, E., *Angewewandte Chemie International Edition* **2010**, *49*, 1665-8.

81. Isobe, H.; Homma, T.; Nakamura, E., *Proceedings of the National Academy of Sciences* **2007**, *104*, 14895-14898.
82. Homma, T.; Harano, K.; Isobe, H.; Nakamura, E., *Journal of the American Chemical Society* **2011**, *133*, 6364-6370.
83. Burghardt, S.; Hirsch, A.; Schade, B.; Ludwig, K.; Bottcher, C., *Angewwandte Chemie International Edition* **2005**, *44*, 2976-9.
84. Maierhofer, A. P.; Brettreich, M.; Burghardt, S.; Vostrowsky, O.; Hirsch, A.; Langridge, S.; Bayerl, T. M., *Langmuir* **2000**, *16*, 8884-8891.
85. Brettreich, M.; Burghardt, S.; Böttcher, C.; Bayerl, T.; Bayerl, S.; Hirsch, A., *Angewandte Chemie International Edition* **2000**, *39*, 1845-1848.
86. Schade, B.; Ludwig, K.; Bottcher, C.; Hartnagel, U.; Hirsch, A., *Angewandte Chemie International Edition* **2007**, *46*, 4393-6.
87. Hirsch, A., *Pure Applied Chemistry* **2008**, *80*, 571-587.
88. Zhao, Y.; Chen, G., *Fullerenes and Other Carbon-rich Nanostructures*, Springer: **2013**; pp 23-53.
89. Gorgoll, R. M.; Harano, K.; Nakamura, E., *Journal of the American Chemical Society* **2016**, *138*, 9675-81.
90. Harano, K.; Gorgoll, R. M.; Nakamura, E., *Chemical Communications* **2013**, *49*, 7629-31.
91. Lin, M.-S.; Chen, R.-T.; Yu, N.-Y.; Sun, L.-C.; Liu, Y.; Cui, C.-H.; Xie, S.-Y.; Huang, R.-B.; Zheng, L.-S., *Colloids Surfaces B: Biointerfaces* **2017**, *159*, 613-619.
92. Donskyi, I.; Achazi, K.; Wycisk, V.; Böttcher, C.; Adeli, M., *Chemical Communications* **2016**, *52*, 4373-4376.
93. Partha, R.; Mitchell, L. R.; Lyon, J. L.; Joshi, P. P.; Conyers, J. L., *ACS Nano* **2008**, *2*, 1950-8.
94. Klaiber, A.; Polarz, S., *ACS nano* **2016**, *10*, 10041-10048.
95. Klaiber, A.; Landsmann, S.; Löffler, T.; Polarz, S., *New Journal of Chemistry* **2016**, *40*, 919-922.
96. Polarz, S.; Landsmann, S.; Klaiber, A., *Angewwandte Chemie International Edition* **2014**, *53*, 946-54.
97. Landsmann, S.; Luka, M.; Polarz, S., *Nature communications* **2012**, *3*, 1-6.
98. Donner, A.; Trepka, B.; Theiss, S.; Immler, F.; Traber, J.; Polarz, S., *Langmuir* **2019**, *35*, 16514-16520.
99. Kunkel, M.; Schildknecht, S.; Boldt, K.; Zeyffert, L.; Schleheck, D.; Leist, M.; Polarz, S., *ACS Applied Materials & Interfaces* **2018**, *10*, 23638-23646.

8 Publications and Contribution

8.1 Publication I:

Increasing the Resistance of Living Cells against Oxidative Stress by Nonnatural Surfactants as Membrane Guards,

ACS Appl. Mater. Interfaces 2018

Marius Kunkel, Stefan Schildknecht, Klaus Boldt, Lukas Zeyffert, David Schleheck, Marcel Leist and Sebastian Polarz*

ABSTRACT: *The importation of construction principles or even constituents from biology into materials science is a prevailing concept. Vice versa, the cellular level modification of living systems with nonnatural components is much more difficult to achieve. It has been done for analytical purposes, for example, imaging, to learn something about intracellular processes. Cases describing the improvement of a biological function by the integration of a nonnatural (nano)constituent are extremely rare. Because biological membranes contain some kind of a surfactant, for example, phospholipids, our idea is to modify cells with a newly synthesized surfactant. However, this surfactant is intended to possess an additional functionality, which is the reduction of oxidative stress. We report the synthesis of a surfactant with Janus-type head group architecture, a fullerene C_{60} modified by five alkyl chains on one side and an average of 20 oxygen species on the other hemisphere. It is demonstrated that the amphiphilic properties of the fullerenol surfactant are similar to that of lipids. Not only quenching of reactive oxygen species (superoxide, hydroxyl radicals, peroxynitrite, and hydrogen peroxide) was successful, but also the fullerenol surfactant exceeds benchmark antioxidant agents such as quercetin. The surfactant was then brought into contact with different cell types, and the viability even of delicate cells such as human liver cells (HepG2) and human dopaminergic neurons (LUHMES) has proven to be extraordinarily*

high. We could show further that the cells take up the fullerenol surfactant, and as a consequence, they are protected much better against oxidative stress.

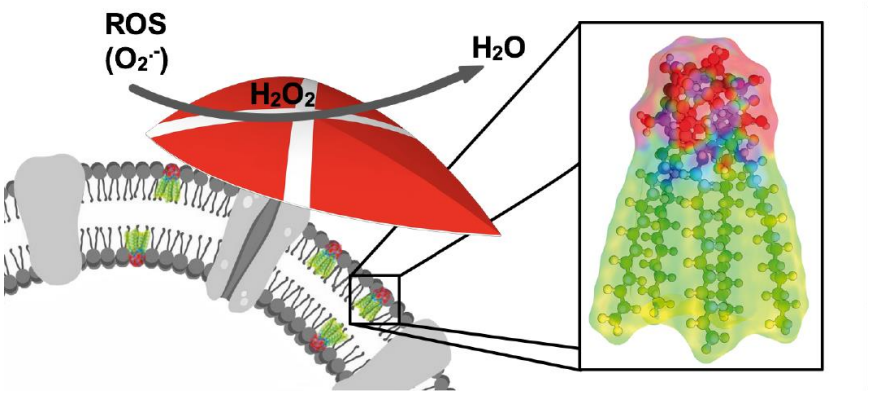

TOC figure of publication 4. Reproduced. Reproduced under the Creative Commons Attribution License. Reproduced with permission from ref. 99. Copyright (2018) American Chemical Society.

8.1.1 Record of Contribution

Material synthesis, characterization, further chemical experiments and interpretation were performed by M. Kunkel if not stated differently. S. Schildknecht designed, performed and interpreted the experiments with eukaryotic cells. K. Boldt assisted M. Kunkel with the interpretation. L. Zeyffert performed preliminary experiments on ROS quenching under the supervision of M. Kunkel. D. Schleheck and M. Leist designed the biological experiments. M. Kunkel and S. Polarz designed the research and S. Polarz wrote the manuscript. All authors have given approval to the final version of the manuscript.

8.1.2 Introduction

Because of the exponentially growing global population, we will have to provide more commodities than have ever been produced before. In addition to the extension and improvement of the capacities of chemical industry as we know, a seminal approach is to use microbes in chemical factories.[100, 101] One of the problems involved in realizing this goal is that many cells, prokaryotes as well as eukaryotes, are sensitive to oxidative stress.[102] Reactive oxygen species (ROS) are in any case major reasons for cellular damages and aging processes. Anaerobic microorganisms are of course even more sensitive to an oxygen-rich environment. In particular, in

an aqueous dispersion and in contact to daylight, there is an inevitable level of ROS such as the superoxide anion, hydroxyl radicals, or singlet oxygen. Evolution has countered this problem by the development of cellular mechanisms for self-protection against those species by scavenging enzymes such as superoxide dismutase.[103] However, if the oxidative stress level becomes too high or occurs very fast, the biological protection alone is not sufficient anymore, which then results in damages and diseases associated with oxidative stress.[104] Therefore, it would be highly interesting to aid cells and to increase their resistance against ROS.

Fullerene derivatives have been evaluated for biomedical use for quite some time. Depending on their modification, they have shown promising results as antiviral, antibacterial, or antioxidative compounds. However, a huge disadvantage of most fullerene derivatives is their poor solubility in water, which is of course pivotal for most biomedical usage. One approach for making them more suitable for applications in biotechnology is the formation of hybrids with phospholipids, the so-called fullerene liposomes. The encapsulation of fullerene derivatives in liposomes or the direct interaction with cell membranes can lower the compound's toxicity and enhance its bioavailability. Another approach is the use of water-soluble derivatives such as polyhydroxylated fullerenes, the so-called fullerenols.[105, 106] It has been reported that these compounds can reliably quench ROS in aqueous systems.[106-109] Fullerenols can even penetrate the cellular membranes and accumulate inside the cell, where they possibly aggregate. Unfortunately, it was found that the presence of fullerenols in the internal regions of the cell is harmful and can even lead to necrosis. Besides ill-defined accumulation, there are also other reasons for the toxicity of fullerene derivatives in cellular systems. The solubility of the compound, functional groups, and the degree of derivatization influence the compound's toxicity.[109, 110] Because of the argument given above, one has to effectively suppress the undesired aggregation of fullerenols. Further, they would ideally remain as guards against oxidative stress integrated in the cellular membrane instead of entering the cell. The importance of the exact positioning of the fullerenol entities was also discussed by Nakamura et al. in a theoretical study in 2017.[111] Because cellular membranes mainly consist of phospholipids, our idea is to generate a new surfactant showing lipid-like behavior and a fullerenol head group as the entity capable of protection against oxidative stress via catalytic conversion of ROS into less harmful compounds. A great body of work exists on amphiphiles containing fullerenes.[112, 113] Amphiphilic fullerenes are known for forming bi- or multilayered vesicular aggregates in solution.[82, 114-116] They have also been explored for biochemical applications.[93, 112, 117] The work of Hirsch *et al*. needs to be mentioned in this context, who synthesized membrane-forming hexa-

adducts of C_{60}.[85] These compounds can, for example, be used as nanocarriers for drug delivery systems.[93, 118] The vesicular self-assembly of amphiphilic fullerenes was also investigated by Nakamura et al. They showed that different kinds of fullerene amphiphiles aggregate in a membrane-like structure.[78, 82, 114] However, the fullerene is part of the hydrophobic moiety in most cases. True surfactants, in which the fullerene represents the hydrophilic head group, are rare.[83, 92, 119, 120] In this paper, we report the synthesis and characterization of a surfactant (**see Figure 1**) comprising a fullerenol head group. After characterization of its surfactant and self-assembly properties, we will test the ROS deactivation features. Finally, the biocompatibility of the surfactant will be explored, and the protection of cells against oxidative stress will be tested.

8.1.3 Results and Discussion

Surfactant Preparation. We achieved the synthesis of the Janus-type target molecule (**4**) as follows (**Figure 1a,b**).

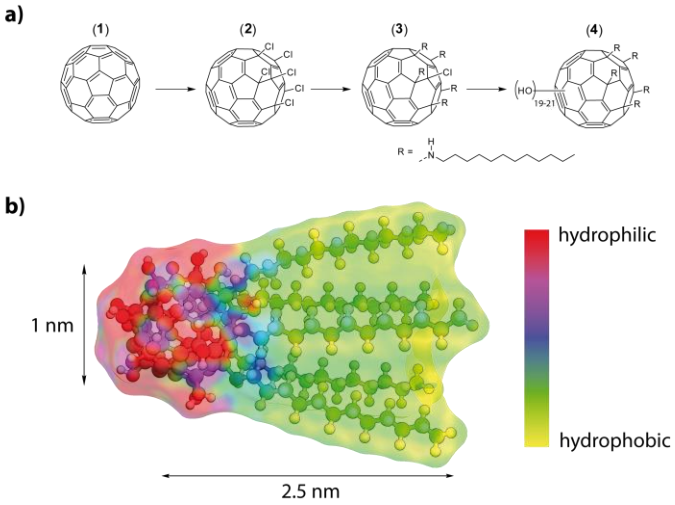

Figure 1. (a) Synthesis sequence to derive surfactants with a fullerenol head group. (b) Optimized molecular structure of surfactant (4) with dimensions and electrostatic potential map.

The method published by Kuvychko et al. was applied to obtain hexa-chlorination selectively on only one side of C_{60} (**2**).[121] Penta-alkylation with dodecyl amine was achieved by adapting a protocol published by Kornev et al.[122] to obtain the precursor molecule (**3**). ^{1}H-NMR, ^{13}C-NMR, and matrix-assisted laser desorption ionization mass spectrometry (MALDI-MS) could confirm the penta-alkylation. This can clearly be seen in the ^{1}H-NMR. Besides the signals for the alkyl chains, it shows the signals of the secondary amines bound to the fullerene core as five triplets centered at

3.22 ppm (see the Supporting Information, **Figure S1**). Also, the ^{13}C-NMR shows distinct signals for the sp^3-hybridized carbons of the fullerene core at which the chains are attached at 66, 68.2, and 69.4 ppm. Three signals can be observed because of the 2:2:1 symmetry (see the Supporting Information, **Figure S2**). The MALDI-MS reveals the M − HCl peak at m/z = 1641.6 (1641.3). In the last step, the hydroxyl moieties are introduced to the precursor using NaOH and H_2O_2 (see also the experimental part). The fullerenol surfactant (**4**) was characterized by a combination of methods. Fourier transform infrared (FT-IR) spectroscopy confirms the polyhydroxylation of precursor (**3**). The observed spectrum is in agreement with the characteristics compared to fullerenols found in the literature.[70, 123, 124] Signals at 3365, 1410, and 1032 cm−1 can be assigned to the hydroxyl moieties. Weak signals at 2971 and 2942 cm−1 fit to the attached alkyl chains. Furthermore, a strong signal at 1645 cm−1 indicates the presence of hemiketal moieties which include the hydroxyl groups (shown in the Supporting Information, **Figure S3**).[67, 125] The ^{13}C NMR spectrum (see the Supporting Information, **Figure S4**) is also in full agreement with the proposed structure and confirms that the scaffold of the precursor is still intact. The alkyl chains are located between 13 and 40 ppm. Signals at 52.4, 57.2, and 57.3 ppm fit the carbons of the fullerene at which the alkyl amines are attached to. Three signals are observed because they have a 2:2:1 symmetry. Because the hydroxyl groups are not introduced by substitution of, for example, halogens but directly to the fullerene core, one needs to determine the degree of poly-hydroxylation and the kind of the attached oxygen species. Therefore, thermogravimetric analysis (TGA) was performed among others (shown in the Supporting Information, **Figure S5**). We assign the mass loss below 200 °C to the removal of water loosely bound to the head group via hydrogen bonding. The mass loss at a higher temperature (Δm = −17.05%) fits to the elimination of hydroxyl groups and vinyl ethers (hemiketals).[126] The latter mass loss corresponds to an average number of ≈20 ± 1 oxygen species attached to C_{60} in (**4**). The penta-alkylated fullerene remains after the loss of the oxygen species. The successful synthesis and structure of the surfactant could be confirmed conclusively by MALDI-MS (shown in the Supporting Information, **Figure S6**). All signals of the complex fragmentation pattern could also be assigned by comparison with fullerenol compounds known in the literature.[127, 128] Every signal belongs to a singly charged species and can be assigned with the following formula: [M − (v − 1)H − w(OH) − xH2O − yNH − zC12H25]+. Like for other fullerenols, the hydroxyl groups are released as water, generating an oxygen radical species or hydroxyl radicals. Furthermore, the chains can be released with or without the amine linker. A maximum of five chains can be detected, which fits the findings from the NMR. As a result of these

decomposition mechanisms, no molecular ion peak can be observed. Though MALDI-MS reveals a mixture of different oxygen species, a maximum number of 21 oxygen species could be detected, which is in agreement with the results from the TGA. Further information about the degree of poly-hydroxylation and the kind of oxygen species can be obtained from the ^{13}C NMR spectrum of the compound. It reveals 11 signals between 61 and 77 ppm which correspond to the sp^3-hybridized carbons of the fullerene core, where the hydroxyl groups are attached to, and 5 signals between 110 and 130 ppm which correspond to the vinyl ether species. To ensure the identity and purity of the compound, liquid chromatography was performed. It shows three very narrow signals with a similar retention time (shown in the Supporting Information, **Figure S7**). These signals represent the different number of oxygen species and confirm that no broad distribution nor a mixture of other compounds but a narrow distribution of oxygen species is present. It is also confirmed that no species with different chain numbers exist. Conclusively, one can say that precursor (**3**) was successfully polyhydroxylated with about 10 hemiketal moieties (which consist of a hydroxyl group and a vinyl ether group), resulting in an average of 20 oxygen species in total.

It can be concluded that because of the inevitable characteristics of the polyhydroxylation chemistry of fullerenes (see, for instance, the overview given by Wang et al.),[129] we are not dealing with a monomolecular species but rather with a system. In addition, the occurrence of regioisomers cannot be excluded. However, from all we can say is that there is a narrow distribution among the compounds and that their behavior is very similar. It is important to note one further twist in the chemistry of fullerenols. It has been shown in the literature that the addition of acids leads to the conversion of hemiketals to ketones and hydroxyl groups accompanied by partial ring opening.[67, 125] These reactions can be transferred successfully to our fullerenol surfactant, leading to the open-cage (oc) compound (**4oc**) (see the schematic Schlegel diagram shown in the Supporting Information, **Figure S8**). The FT-IR of (**4oc**) no longer shows the hemiketal signal but a strong ketone signal at 1720 cm^{-1} and 10 new ^{13}C NMR signals between 170 and 175 ppm, which are also characteristic for the presence of carbonyl units (see the Supporting Information, **Figures S9 and S10**). The number of ketone moieties perfectly fits the results obtained for the number of hemiketals in (**4cc**). Also, because of the complexity of the ring-opening processes (see also **Figure S8**), it is important to note that (**4oc**) does not represent a single molecular species but rather a range of compounds. In agreement with the literature, we also observed that the process is entirely reversible. The reformation of the molecule with its closed cage head group (**4cc**) can be achieved by the addition of diluted sodium hydroxide solution to (**4oc**).

Interfacial Properties and Self-Assembly. A first indication for the surfactant properties of (**4**) is that it forms strong foams at the air/water interface even at a low concentration (**Figure 2**). Further information can be obtained from concentration-dependent surface tension (γ) measurements shown in **Figure 2**.

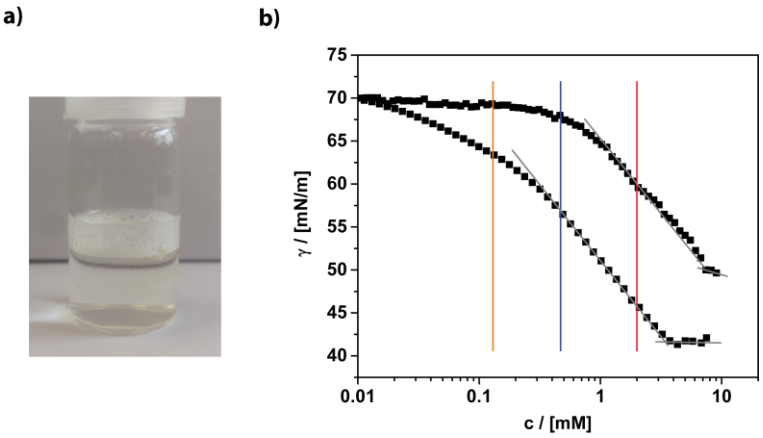

Figure 2. (a) Photograph of a diluted solution of the fullerenol surfactant indicating its foaming abilities. **(b)** Concentration-dependent surface tension measurements of (**4cc**) ≅ circles and (**4oc**) ≅ squares in water. The vertical bars indicate the concentrations whose particle size distribution curves are shown in **Figure 3**.

Compound (**4**) is obviously surface-active, but compared to classical nonionic surfactants such as Brij or Tween, there are differences. The behavior is more comparable to lipids.[130, 131] The surface tension γ drops more slowly and does not reach such low values as for classical surfactants ($\gamma_{c=sat}$(Brij) ≈ 32 mN/m), and the concentration, at which γ begins to saturate, is roughly 1 magnitude higher [c_s(Brij 35) = 0.09 mM]. A possible explanation for the latter could be a less dense coverage of the air/water interface because of the large size of the head group in (4). This assumption can be confirmed by the calculation of the surface excess Γ and the minimum area per molecule at the air/water interface (Am ≈ 60 Å^2), which represents a rather large value. The corresponding radius r = 0.44 nm fits very well to the cross section of the surfactant molecule (**Figure 1b**). One can also see that the chemical structure of the head has a marked influence on the surfactant properties. The overall performance of the (**4oc**) system seems to be better; the surfactant is more soluble and occupies the air/water interface at a lower concentration compared to (**4cc**). Micelles are usually formed above the critical micelle concentration (cmc), which is reached as soon as the air/ water interface is fully occupied. Therefore, at none of the three concentrations marked in **Figure 2**, one should expect to find aggregates in solution. We checked this by dynamic light scattering (DLS) shown in **Figure 3a**.

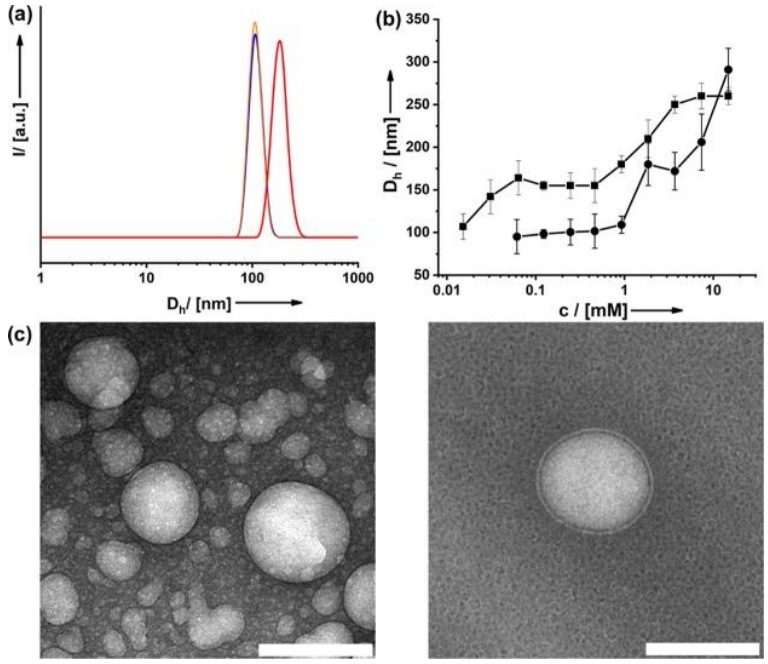

Figure 3. (a) Particle size distribution functions derived from DLS for the three concentrations of (**4cc**) given in **Figure 2**. (b) Aggregate size in water at different surfactant concentrations of (**4cc**) ≅ circles and (**4oc**) ≅ squares. (c) Cryo-TEM micrographs of aggregates in solution; scale bar = 100 nm.

However, already at c ≈ 0.1 mM, one observes large aggregates, although γ has just begun to drop, and thus, the air/water interface is covered only partially. The absence of a classic cmc was confirmed by independent methods (concentration-dependent viscosity and ionic conductivity measurements; see the Supporting Information, **Figure S11**). We suppose that the packing of (**4**) at the air/water interface is so ineffective that it is thermodynamically more favorable to form aggregates even at very low concentration. Interestingly, Nakamura and co-workers observed that for an alternative amphiphilic fullerene system, aggregate formation is possible without interaction with the air/water interface.[78] Even at much lower concentration, we never saw the formation of micelles but large aggregates with (DH ≈ 100 nm) even at ≈ 20 μM. The concentration of the aggregates becomes lower, until they vanish. The particle size (DH ≈ 100/150 nm) remains unchanged in the concentration range 0.1 − 2 mM and then raises until the solution is saturated (**Figure 2b**). As a consequence, the optical appearance of the dispersions has become turbid (see also the Supporting Information, **Figure S12**). The mentioned aggregates are obviously much larger than the ordinary micelles, which are typically only twice the length of the surfactant. Because the packing parameter of (**4**) is close to 1, one can expect a tendency for the formation of bilayered or vesicle-like structures. Other researchers working on amphiphilic fullerenes could also observe vesicle-like structures.[82, 114, 118, 132] Investigations using cryogenic transmission electron

microscopy (cryo-TEM) confirm this (**Figure 3c**). The size of the hollow aggregates is in agreement with the DLS data. One has to bear in mind that DLS is an averaging technique, and one preferentially sees only the strongest light scatters, for example, the larger aggregates. Actually, the size of the vesicles is not monodisperse at all (**Figure 3c**). Additional TEM data are given in the Supporting Information (**Figure S12**). It can also be seen that with higher concentration, more and more vesicles form, and they seem to be fusing together, which is the reason for the increasing aggregate size observed in DLS. Similar processes have also been reported in the literature for other surfactant systems, for example, cetyltrimethylammonium bromide.[133, 134] The TEM data reveal that the vesicles contain a single shell. The thickness of this shell (~4.8 nm) is compliant with the double dimension of the fullerenol surfactant (**Figure 1b**) and, thus, fits a double-layer structure. Although both surfactant types (**4cc**) and (**4oc**) form vesicles, one can see that the chemical conformation of the head groups has an influence on the average size of the aggregates (**Figure 3b**). At higher concentration, liquid crystalline phases can be observed. Optical microscopy under crossed polarizers shows phases with intense birefringence and marked textures (see the Supporting Information, **Figure S13**). Depending on the surfactant concentration, one observes columnar droplets with the characteristic Maltese cross or smectic phases. *Ex vivo* ROS Quenching. The antioxidative properties and the influence of the amphiphilic character are investigated next. Quenching of superoxide monitored by a nitroblue tetrazolium assay (see the Supporting Information, **Figure S14**)[135] was used to evaluate the efficiency of the fullerenol surfactants at different concentrations (**Figure 4**).

The results were compared to two reference systems: a non-amphiphilic fullerenol compound, synthesized by hydroxylation of $C_{60}Br_{24}$,[136] and the flavonoid quercetin which was employed as a benchmark because it is a commercially available and well understood antioxidant.[106, 108, 109, 124, 137] The non-amphiphilic fullerenol is active in superoxide quenching, as described in the literature. The quenching efficiency depends almost linearly on the concentration of (**4cc**) (**Figure 4**). A substantial amount of superoxide (>60%) remains in solution even at a relatively high concentration of fullerenol. The 50% inhibitory concentration (IC_{50}) of this reference is not reached during our experiment.

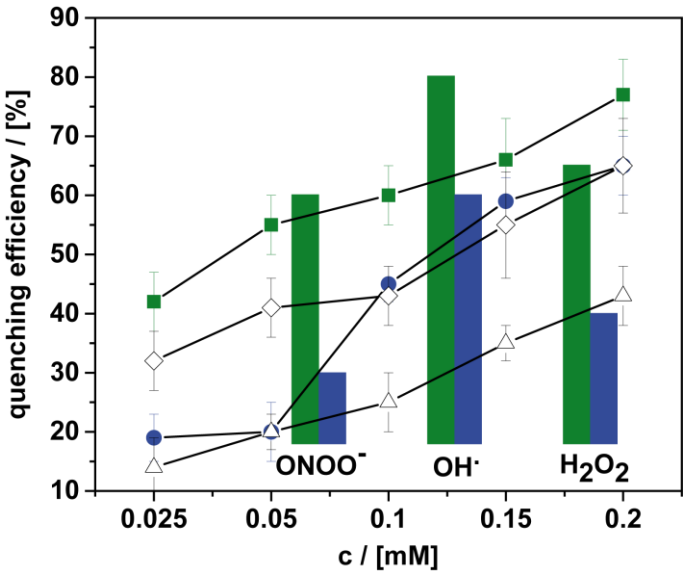

Figure 4. Concentration-dependent superoxide quenching efficiency of different compounds: (**4cc**) ≅ blue circles, (4oc) ≅ green squares, non-amphiphilic fullerenol (open triangles), and quercetin (open hashes). The bars give an overview over the ROS quenching capabilities of (4cc) (blue) and (**4oc**) (green) for ONOO−, OH •, and H_2O_2 as the alternative ROS (see the Supporting Information for method details).

The surfactant containing fullerenol as a head group (**4cc**) clearly shows an improved performance. The IC_{50} of (**4cc**) is 0.15 mM. One sees that there is a jump in the quenching efficiency between 0.05 and 0.1 mM surfactant concentration. Because this is the same region, where the (**4cc**) vesicles are formed (**see Figure 3a**), the step can be seen as an indication; the presence of the vesicles is very important. The fraction of the fullerenol entities exposed to the aqueous interface is obviously maximized for the vesicles, and therefore, the superoxide quenching ability is much better. The vesicles containing (**4cc**) are just as efficient as the benchmark quercetin (**Figure 4**) but unfortunately not better. Because (**4oc**) forms vesicles at much lower concentration (**Figure 3a**), we hoped that it could exhibit higher quenching efficiency in particular at those low concentrations. This is indeed the case as can be seen from **Figure 4**. Compound (**4oc**) does outperform (**4cc**) and, more importantly, quercetin. Since this is also the case for higher concentrations, one can assume that more than the tendency to form vesicles is a relevant factor. Because the vesicles of (**4oc**) are larger than those formed by (**4cc**) (**Figure 3**), the explanation cannot be due to an improved surface-to-volume ratio, which could result in an increased catalytic conversion rate of superoxide. Therefore, the chemical structure of the head group in (**4oc**) must be relevant; in particular, the ketone moieties play a crucial role regarding the ROS deactivation mechanism (see the Supporting Information, **Figure S15**). Besides the superoxide ion ($O_2^{\bullet-}$), other ROS were investigated as well, such as peroxynitrite ($ONOO^-$), hydroxyl radicals ($OH^\bullet$), and hydrogen peroxide (H_2O_2).[138] For the other ROS, the surfactants also quenched the radical species reliably (**Figure S16**), and (**4oc**) was in all cases superior than (**4cc**). The activity regarding the catalytic conversion of H_2O_2 is a positive result. According to the literature, H_2O_2 is the main product of the deactivation process of superoxide.[124] Of course, H_2O_2 is still quite reactive and a strong oxidant. Because the surfactants

(**4**) lead to a decrease in H_2O_2 concentration, we expect an even more significant improvement in the oxidative stress level.

Biocompatibility and *in vitro* ROS Quenching. Before a beneficial biological function of (**4**) can be explored, it is pivotal to scrutinize any potential toxicity factors. Although nonnatural surfactants are in general not very toxic, they can be harmful, in particular, when they come in contact with more sensitive cells.[139-141] Therefore, we investigated the viability and morphology of a range of prokaryotic and eukaryotic cell types in contact to (**4**). *Pseudomonas aeruginosa* and *Escherichia coli* were chosen as prokaryotic model organisms. In comparison, the eukaryotic model systems human liver cells (HepG2) and human dopaminergic neurons (LUHMES) represent much more delicate systems. The intrinsic toxicity of the surfactants was tested in a range of 1−125 μM, according to standard procedures (see also the Supporting Information). For *E. coli*, as well as for *P. aeruginosa* (not shown), the presence of the surfactant had no negative effects neither on their growth (see the Supporting Information, **Figure S17**) nor on their viability (**Figure 5a**). The viability of both, LUHMES and HepG2, is also not influenced at a low concentration (32 μM) of the surfactant (**Figure 5b,c**). There is a minor effect at a higher concentration (125 μM), if compound (**4cc**) is used. Interestingly, the toxicity of (**4oc**) is so low; we cannot see any changes at the same concentration. The extraordinary biocompatibility of the surfactants was confirmed further by lactate dehydrogenase (LDH) release assay and resazurin metabolization assay (**Figures S18−S21**). Obviously, our fullerenol surfactants are harmless to both prokaryotic and eukaryotic cells in biologically relevant concentrations. Therefore, we can test now the possible

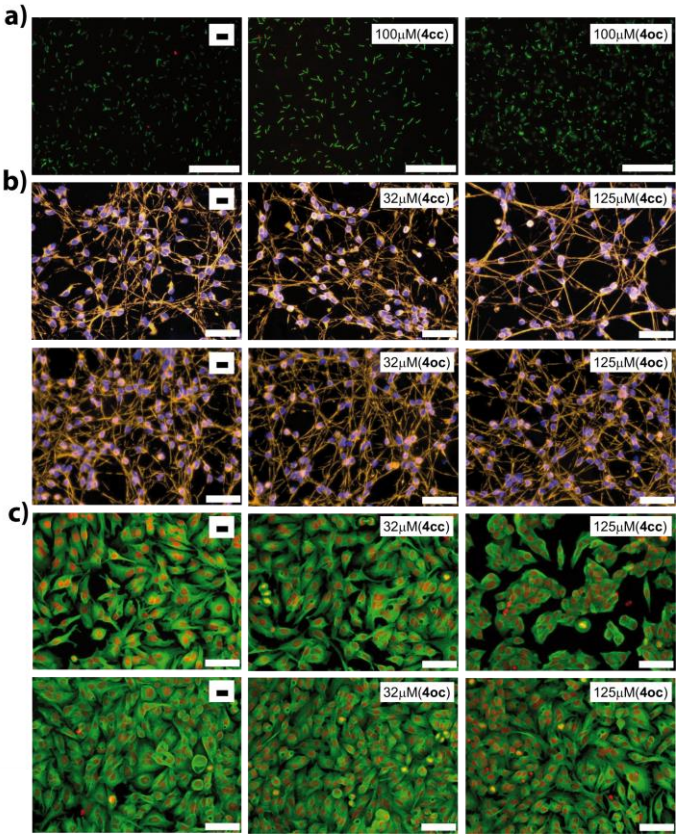

Figure 5. Live/dead stain images or morphology of different cells treated with (**4**). Blank experiments in the absence of any surfactant are always shown on the left. The concentration of the surfactant and the head group form is given in the white boxes. *E. coli* (a; scale bar = 20 μm), LUHMES neurons (b; scale bar = 100 μm), and HepG2 hepatoma cells (c; scale bar = 100

antioxidative properties of the compounds in a cellular system (LUHMES). The cells were treated with the neurotoxicant 1-methyl-4-phenyl pyridinium (MPP+).[142] As expected, the viability of the cells is drastically reduced caused by MPP+ (**Figure 6**). The situation changed when the surfactant was present. Even low concentrations of (**4**) had a positive effect, and at 25 µM, the viability of the cells has increased significantly. The viability of the cells was again confirmed by LDH release assay and resazurin metabolization assay (Supporting Information, **Figure S22**).

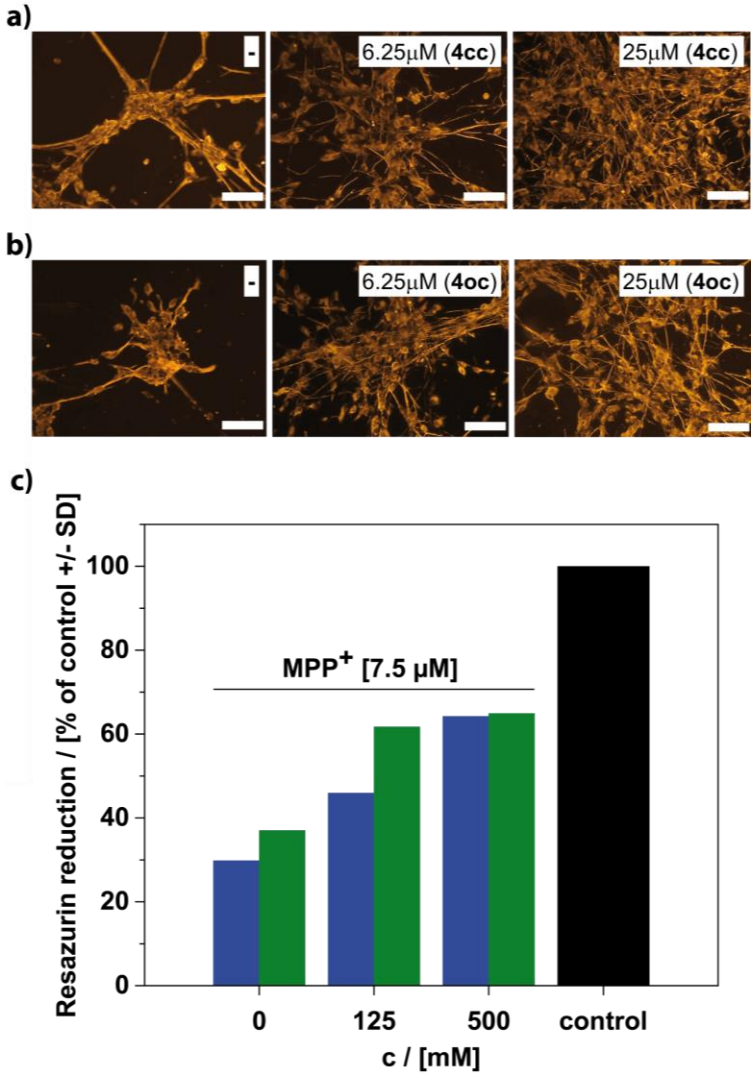

Figure 6. (a,b; scale bar = 100 µm) Morphology of eukaryotic LUHMES cell line treated with MPP+ (7.5 µM) and surfactant (**4**). Blank experiments in the absence of any surfactant are always shown on the left. The concentration of the surfactant and the head group form is given in the white boxes. **(c)** Viability of LUHMES after the cells were loaded with the surfactant in the concentrations as indicated for a period of 3 h. Following the removal of the compounds in the supernatant by medium exchange, the toxicant MPP+ (7.5 µM) was added for 60 h. Control cells received neither MPP+ nor surfactant. Compound (**4cc**) blue bars and compound (**4oc**) green bars

There are only minor differences comparing (**4cc**) and (**4oc**). The final question remaining is that if the protection against oxidative stress is due to surfactants and their vesicle present in the outer medium or if the cells do actually include the surfactants into their cell membrane. The treatment of cells with the surfactant is a standard procedure in cell biology. We have followed similar protocols (see Methods section), but the surfactant concentration was low enough to avoid lysis. Furthermore, we have exposed LUHMES to a surfactant solution containing different concentrations of (**4**) only for 3 h. This short time was sufficient; a notable decrease of concentration in the mother liquor could be detected. The cells were then separated from the supernatant solvent and washed. It was made sure that there is no surfactant anymore in the external medium. Finally, the cells were then treated with MPP+ for 60 h. If the surfactant had just been present in the external medium, we should not expect any protection anymore and in particular no concentration dependence. **Figure 6c** shows the results of the assessment of resazurin reduction assay; there still remains significant protection, which scales with the concentration of the surfactant used in the original solution. This allows only one conclusion. LUHMES cells have integrated with the fullerenol surfactant, and this way, they could decrease the stress level significantly. It is important to mention that the interaction of the surfactants with cells has already been studied multiple times by others in the past.[143-145] It could be proven that certain amphiphiles do interact with cellular membranes and become incorporated. Therefore, we have followed similar protocols. Therefore, it is not surprising that the fullerenol surfactant behaves similar.

8.1.4 Conclusion

On the basis of the encouraging findings about potential biotechnological applications of fullerene derivatives in the literature, we prepared a defined surfactant species containing a polyhydroxylated C_{60}, a fullerenol, as the hydrophilic head group. The necessary Janus-type modification of the fullerene was accomplished by attaching five alkyl chains on one side of C_{60} first, followed by modification with an average of 20 oxygen species consisting of hemiketals for compound **4cc** and ketones and hydroxyl groups for compound **4oc** on the other side. Caused by the packing parameter close to 1, the surfactant showed features similar to natural surfactants (lipids). There is a high tendency for the formation of vesicle-like structures in water, and at higher concentration lyotropic liquid crystals with lamellar characteristics have been observed. Because of the fullerenol head group, the surfactant obtained an added functionality, the catalytic deactivation of ROS-like

superoxide, peroxynitrite, hydroxyl radicals, and even hydrogen peroxide. Because the surfactants are fully biocompatible and benign even against delicate cells such as human liver cells (HepG2) and human dopaminergic neurons (LUHMES), we could explore the in vivo application for the reduction of oxidative stress. It was shown that the cells do actually integrate the surfactants. The lipid-like character and the high activity in ROS quenching in the cells indicate that the cells implement the fullerenol surfactants into their cellular membranes. We have also seen that the fullerenol head group can exist in two alternative forms, which can be reversibly converted into each other by acid/base treatment. The form of the head group had a marked effect on all surfactant properties, including self-assembly and ROS quenching behavior. The surfactant containing the open-cluster form (**4oc**) seems to be superior overall.

8.1.5 Methods

General Information. The synthesis that acquired inert gas atmosphere was performed using general Schlenk techniques under argon atmosphere. The solvents were dried according to the standard literature and stored under argon. Water was deionized with Millipore Milli-Q. All starting materials used for the synthesis were purchased from commercial sources unless stated differently. The fullerene C_{60} (pur. 99.9%) was purchased from SES research.

Synthesis of Hexachlorofullerene ($C_{60}Cl_6$) (2). C_{60} (0.28 mmol) was dissolved in chlorobenzene (11 mL) and sonicated for 5 min. Iodine monochloride (6.95 mmol) was added in one shot, and the solvent was evaporated at 35 °C. The crude product was further purified by column chromatography (silica gel, eluent: toluene). $C_{60}Cl_6$ is obtained as a red solid (0.2 mmol, 70%). Synthesis of Penta-Alkylated Fullerene ($C_{60}R_5Cl$) (**3**). $C_{60}Cl_6$ (0.28 mmol) was dissolved in dry toluene (30 mL) and vigorously stirred. Dodecylamine (2.52 mmol) and potassium carbonate (1 g) were added. The mixture was stirred for 12 h. The solvent was evaporated under reduced pressure. The obtained solid was suspended in methanol, filtrated, and washed three times with methanol. The crude product was obtained by washing with ethyl acetate. The solvent was evaporated, and the crude product was further purified by column chromatography (silica gel, eluent: toluene/EE). The title compound is obtained as a red solid (0.17 mmol, 60%). IR (powder): 3285, 2920, 2851, 1770, 1658, 1570, 1466, 1316, 1115 cm−1; 1H NMR (400 MHz, CDCl3): δ 0.89 (t, 3J = 7.2 Hz, 15H), 1.27 (m, 90H), 1.45 (m, 10H), 1.67 (m, 10H), 3.22 (m, 5H); 13C NMR (100 MHz, CDCl3): δ 22.56, 27.57, 27.67, 29.56, 29.58, 29.91, 29.93, 30.95, 31.02, 32.11, 47.36, 47.87, 47.88, 66.02,

68.21, 69.35, 143.24, 143.31, 143.71, 143.81, 143.83, 143.84, 143.84, 143.88, 144.02, 144.08, 144.31, 144.47, 144.51, 144.53, 144.91, 145.43, 147.16, 147.21, 147.23, 147.29, 147.62, 148.02, 148.21, 148.33, 148.57, 148.71, 149.12, 150.81, 153.88, 155.31; MS (MALDI): 1641.6 [M − HCl]$^-$, 1506.2 [M − $C_{12}H_{26}$]$^-$, 1457.1 [M − $C_{12}H_{25}$ − Cl]$^-$, 1337.9 [M − $C_{24}H_{51}$]$^-$, 1307.0 [M − $N_2C_{24}H_{54}$]$^-$, 1272.8, 1307.0 [M − $N_2C_{24}H_{54}$ − Cl]$^-$, 1167.6 [M − $C_{36}H_{76}$]$^-$, 1152.5 [M − $NC_{36}H_{77}$]$^-$, 1137.5 [M − $N_2C_{36}H_{78}$]$^-$, 1122.5 [M − $N_3C_{36}H_{79}$]$^-$, 1087.3 [M − $N_3C_{36}H_{79}$ − Cl]$^-$.

Synthesis of the Polyhydroxylated Penta-Alkylated Fullerene Surfactant (4cc). $C_{60}Cl(HNC_{12}H_{25})_5$ (0.15 mmol) was dissolved in tetrahydrofuran (THF) (8 mL) and sonicated for 10 min. Solid NaOH (0.3 g) was added, and H_2O_2 (15 mL) was added under vigorous stirring. The mixture was heated to reflux for 4 h until a yellow solution is formed. THF was evaporated under reduced pressure, and the mixture was filtrated to remove nonwater-soluble compounds. Afterward, the volume of the solution was reduced to about 3 mL, and the reaction was cooled to room temperature. Methanol was added, and the product was precipitated. The precipitate was stirred in diluted NaOH for 5 min, and the solvent was evaporated. The crude product was washed five times with methanol to remove the remaining NaOH. The product is obtained as a light yellow-brown solid with an average number of 20 oxygen species (0.075 mmol, 50%). For characterization data, see the Supporting Information.

Conversion to the Open-Cage Compound (4oc). Compound (**4**) was dissolved in diluted hydrochloric acid and stirred for 10 min. The solvent was evaporated, and the product was obtained as a yellow oily solid. For characterization data, see the Supporting Information.

Biological Experiments. Treatment of Cells with the Surfactant. In a first step, the cells were grown under standard conditions as described in **Figure S18**. The cell culture plates were coated with 50 poly-L-ornithine and fibronectin overnight at 37 °C and washed two times with water. Cells were propagated in advanced Dulbecco's modified Eagle's medium (DMEM)/F12, 1× N2 supplement, 2 mM L-glutamine (Gibco), and 40 ng/mL recombinant bFGF (R + D Systems; Minneapolis, MN). The differentiation process was initiated by the addition of differentiation medium consisting of advanced DMEM/F12, 1× N2 supplement, 2 mM L-glutamine, 1 mM dibutyryl-cAMP, 1 μg/mL tetracycline, and 2 ng/mL recombinant human GDNF (R + D Systems). After 2 days, cells were trypsinized and collected in advanced DMEM/F12 medium. Cells were seeded onto 96-well plates at a density of 35000 cells/well. The differentiation process was continued for additional 3 days. After the growing and differentiation process, the cells were treated

with different surfactant concentrations for 3 h. During this time, the surfactant molecules could interact with the cell membranes. After that process, the medium was changed and washed several times, so all remaining surfactant molecules that are not incorporated into the cell wall are removed from the system. With these prepared cells, the experiments were performed. These cells were then treated with MPP+. After an incubation time of 60 h, resazurin metabolization assay and LDH release assay have been performed. Live/Dead Stain *E. coli* treated with the Surfactant. Live/dead staining is performed by following the manufacturer's instructions (LIVE/DEAD BacLight Bacterial Viability Kit, Thermofisher); it stains cells with membrane damage in red, against viable cells stained in green. The stained cells were placed on agar-coated microscopic slides and observed under a fluorescence microscope at 400-fold magnification. Morphology of LUHMES Treated with the Surfactant. For visualization of cell morphology, the cells were fixed with 4% paraformaldehyde for 20 min at room temperature (RT), permeabilized with 0.2% Triton X-100, washed, and blocked with 1% bovine serum albumin (BSA; Calbiochem, San Diego, CA) in phosphate-buffered saline (PBS) for 1 h. LUHMES were stained with an anti-β-III-tubulin antibody (rabbit, Sigma, 1:1000) in 1% BSA/ PBS at 4 °C overnight. After washing, the secondary antibodies were added for 1 h, and nuclei were stained by Hoechst H-33342 (1 μg/ mL) for 20 min. For quantitative evaluation of the neurite area, live staining of LUHMES was conducted with calcein-AM (1 μM) and Hoechst H-33342 (1 μg/mL) for 30 min. Images were collected by an automated microplate-reading microscope (Array-Scan II HCS Reader, Cellomics, Pittsburgh, PA) equipped with a Hamamatsu ORCA-ER camera (resolution 1024 × 1024; run at 2 × 2 binning) in two different fluorescence channels. Nuclei were identified as objects according to their intensity, size, area, and shape. A virtual area corresponding to the cell soma was defined around each nucleus. The total calcein pixel area per field minus the soma areas in that field was defined as the neurite mass. In addition, viability was analyzed by the detection of the percentage of those cells positive for calcein and for H-33342. Morphology of HepG2 Treated with the Surfactant. For visualization of cell morphology, the cells were fixed with 4% paraformaldehyde for 20 min at RT, permeabilized with 0.2% Triton X-100, washed, and blocked with 1% BSA (Calbiochem, San Diego, CA) in PBS for 1 h. HepG2 cells were stained with a monoclonal antiα-tubulin antibody (Sigma; 1:1000). Resazurin Metabolization Assay and LDH Release Assay. Resazurin metabolization assay: Resazurin (Sigma) was added to the cell culture medium in a final concentration of 5 μg/mL and fluorescence was measured after 60 min (λex = 530 nm; λem = 590 nm). LDH release assay: The LDH activity was detected separately in the supernatant and cell

lysate. Following the separation of the supernatants, the cells were lysed in PBS/0.5% Triton X-100 for >60 min. The percentage of LDH released was calculated as 100 × LDHsupernatant/LDHsupernatant+lysate. For the enzymatic assay, 20 μL of the sample was combined with 180 μL of the reaction buffer containing NADH (100 μM) and sodium pyruvate (600 μM) in sodium phosphate buffer adjusted to pH 7.4 by titration with K2HPO4 (40 mM) and KH2PO4 (10 mM). Absorption at 340 nm was detected at 37 °C in 1 min intervals over a period of 20 min, and the enzyme activity was calculated from the respective slopes.

Analytical Methods. NMR measurements (1H, 13C) were performed on a Varian INOVA 400 MHz spectrometer. MALDIMS measurements were performed using a Bruker Microflex MALDITOF. The samples were prepared in a cyano-4-hydroxycinnamic acid matrix or a trans-2-[3-(4-tert-butylphenyl)-2-methyl-2propenylidene]malononitrile matrix. Attenuated total reflection− infrared (ATR−IR) spectra were measured with a Perkin Elmer 100 Spectrum spectrometer including an ATR unit. TGA was measured at Netzsch Jupiter STA 449 F3. Liquid chromatography was measured with Thermo Fisher Scientific Dionex 3000. As the column, Agilent Poroshell 120 EC-C18 (2.1 × 100 mm, 2.7 μm) was used. MeCN (5%) as eluent A and 95% water as eluent B with 0.1% formic acid were used. A linear gradient of 5% A to 100% A was applied with a flow rate of 0.3 mL/min. The DLS measurements were done by using a Malvern Zen5600. Liquid-crystal pictures were taken with an Olympus CX41 light microscope. The high-resolution TEM observations were carried out using JEOL JEM-2200FS, and the TEM observations were carried out using Zeiss Libra120. The surface tension measurements were performed using Krüss K100.

8.1.6 Supporting Information

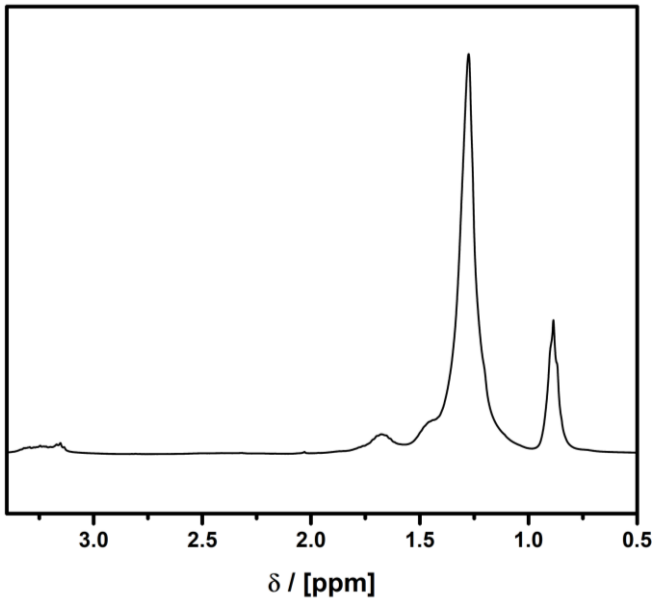

Fig. S1. ^{1}H NMR for compound (**3**) in $CDCl_3$. ^{1}H NMR (400 MHz, $CDCl_3$): δ(ppm) = 0.89 (t, 3J = 7.2 Hz, 15 H), 1.27 (m, 90 H), 1.45 (m, 10 H), 1.67 (m, 10 H), 3.22 (m, 5 H)

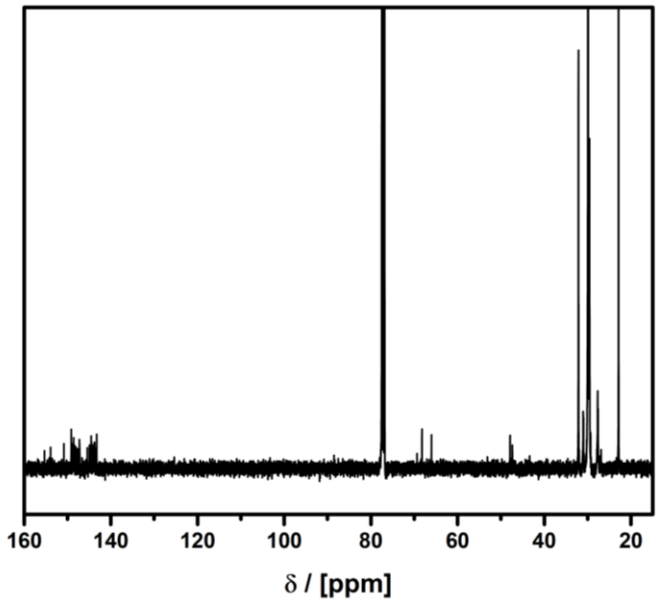

Fig. S2. ^{13}C NMR for compound (**3**) in $CDCl_3$. ^{13}C NMR (100 MHz, $CDCl_3$): δ(ppm) = 22.56, 27.57, 27.67, 29.56, 29.58, 29.91, 29.93, 30.95, 31.02, 32.11, 47.36, 47.87, 47.88, 66.02, 68.21, 69.35, 143.24, 143.31, 143.71, 143.81, 143.83, 143.84, 143.84, 143.88, 144.02, 144.08, 144.31,

144.47, 144.51, 144.53, 144.91, 145.43, 147.16, 147.21, 147.23, 147.29, 147.62, 148.02, 148.21, 148.33, 148.57, 148.71, 149.12, 150.81, 153.88, 155.31

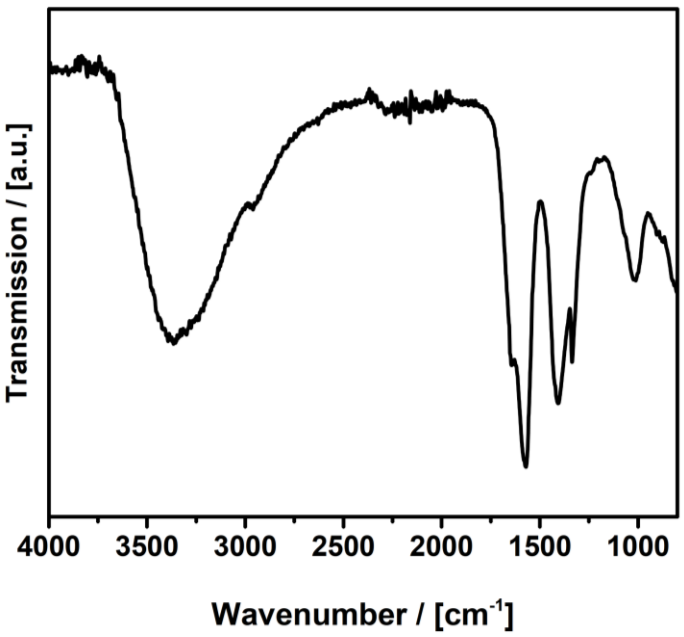

Fig. S3. FT-IR for compound (**4cc**). ATR-IR: ν (cm^{-1}) = 3365, 2942, 2971, 1645, 1574, 1409, 1325, 1032.

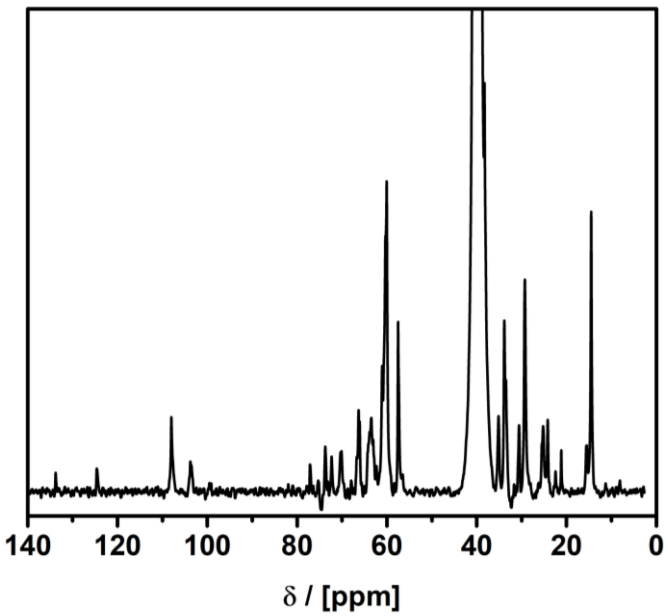

Fig. S4. ^{13}C NMR for compound (**4cc**) in D_2O. ^{13}C NMR (100 MHz, D2O): δ(ppm) = 13.26, 16.81, 20.39, 20.53, 23.23, 23.34, 27.93, 28.77, 30.35, 30.65, 33.24, 33.33, 36.722, 36.84. 36.85, 52.42, 57.26, 57.28, 60.52, 60.59, 60.76, 60.84, 61.73, 64.45, 174.16, 174.48.

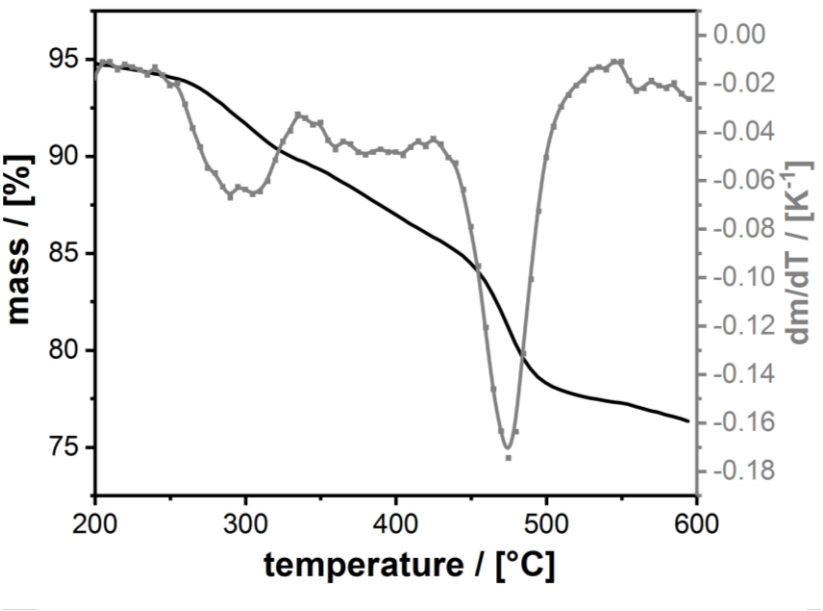

Fig. S5. TGA for compound (**4cc**) under inert conditions (N_2 atmosphere). step: 5.91 %, 2. step: 17.05 %. The number of OH-groups was among others determined by TGA (N_2, 1 K/min).

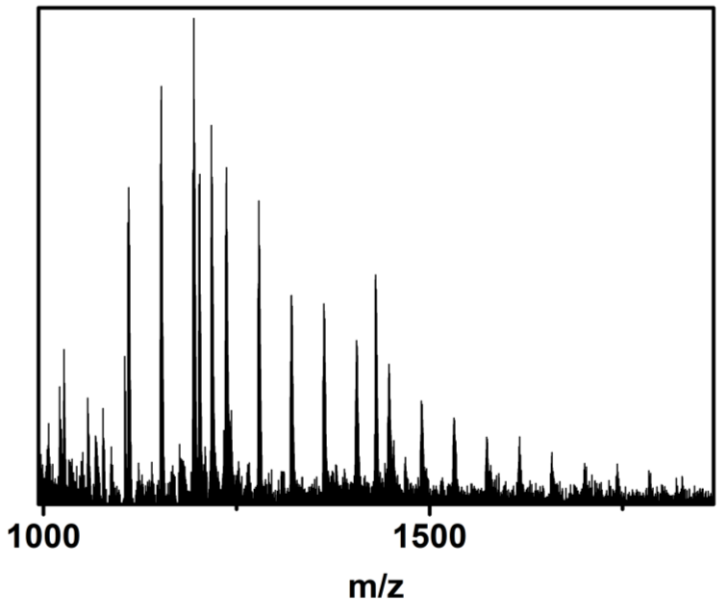

Fig. S6. MALDI-MS for compound (**4cc**). 1615 $[HC_{60}(HNC_{12}H_{25})_3(OH)_{20}]^+$,1827.1 $[HC_{60}(HNC_{12}H_{25})_5(OH)_8(O)_3]^+$, 1741,7 $[HC_{60}(HNC_{12}H_{25})_4(OH)_{12}(O)_4(NH)]^+$, 1656.8 $[HC_{60}(HNC_{12}H_{25})_4(OH)_7(O)_4NH]^+$, 1615 $[HC_{60}(HNC_{12}H_{25})_3(OH)_{20}]^+$, 1573.6 $[HC_{60}(HNC_{12}H_{25})_3(HN)_2(OH)_{13}(O)_3]^+$, 1529.6 $[HC_{60}(HNC_{12}H_{25})_3(OH)_{15}]^+$, 1488.6 $[HC_{60}(HNC_{12}H_{25})_3(NH)(OH)_7(O)_5]^+$, 1446.9 $[HC_{60}(HNC_{12}H_{25})_2(OH)_{21}]^+$, 1429.8 $[HC_{60}(HNC12H25)_2(OH)_{20}]^+$, 1404.2 $[HC_{60}(HNC_{12}H_{25})_2(HN)_2(OH)_{13}(O)_4]^+$, 1361.5

$[HC_{60}(HNC12H25)_2(OH)_{16}]^+$, 1319.9 $[HC_{60}(HNC12H25)_2(HN)_3(OH)_9(O)_2]^+$, 1277.8 $[HC_{60}(HNC_{12}H_{25})_2(OH)_{11}]^+$, 1235.8 $[HC_{60}(HNC_{12}H_{25})_1(HN)_3(OH)_{13}O_4]^+$, 1217.3 $[HC_{60}(HNC_{12}H_{25})_1(HN)_3(OH)_{11}O_5]^+$, 1201.3 $[HC_{60}(HNC_{12}H_{25})_1(HN)_3(OH)_{11}O_4]^+$, 1193.7 $[HC_{60}(HNC_{12}H_{25})_1(OH)_{16}O]^+$, 1151.5 $[HC_{60}(HNC_{12}H_{25})_1(HN)_2(OH)_8(O)_5]^+$, 1109.4 $[HC_{60}(HNC_{12}H_{25})_1(OH)_{12}]^+$**,** 1026.3 $[HC_{60}(OH)_{17}(O)]^+$

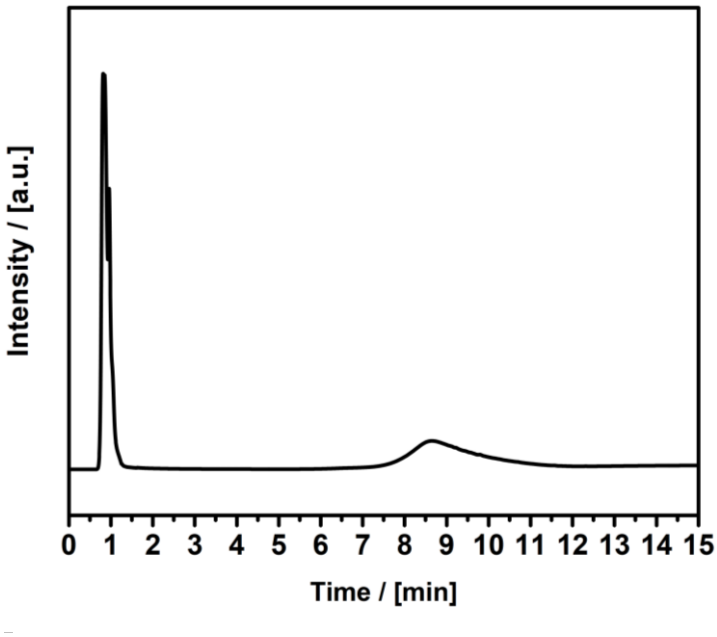

Fig. S7. Chromatogram of (**4cc**). 5% MeCN as eluent A and 95% water as eluent B with 0.1 % formic acid. A linear gradient of 5% A to 100% A was applied with a flow rate of 0.3 mL/min.

The broad signal from 8 to 11 min derives from a decomposition of the compound on the column. This was ensured by repetitively collecting the first signal in a measurement and processing the measurement again.

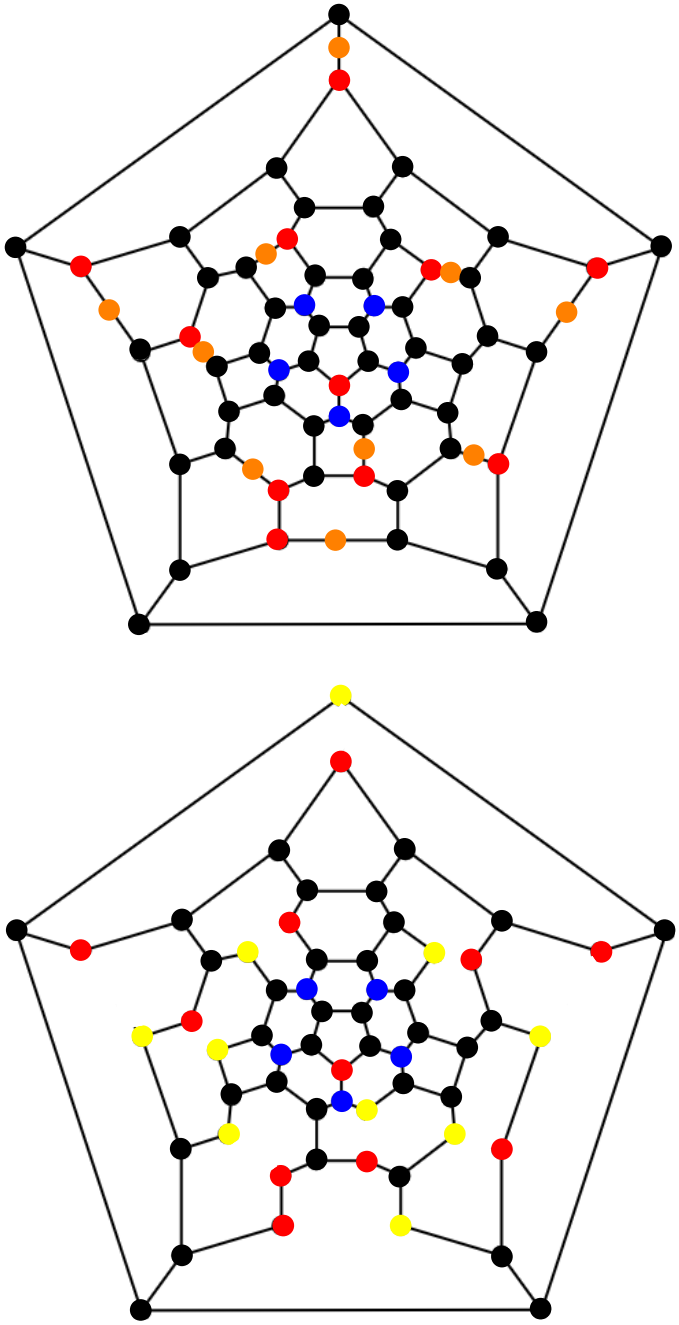

Fig. S8. Schematic Schlegel diagrams of possible structures of the fullerenol surfactant. Top hemiketal structure (**4cc**), bottom ketone enriched structure (**4oc**). Red: C-OH, orange: -O-, yellow: C=O, blue: C-NHR.

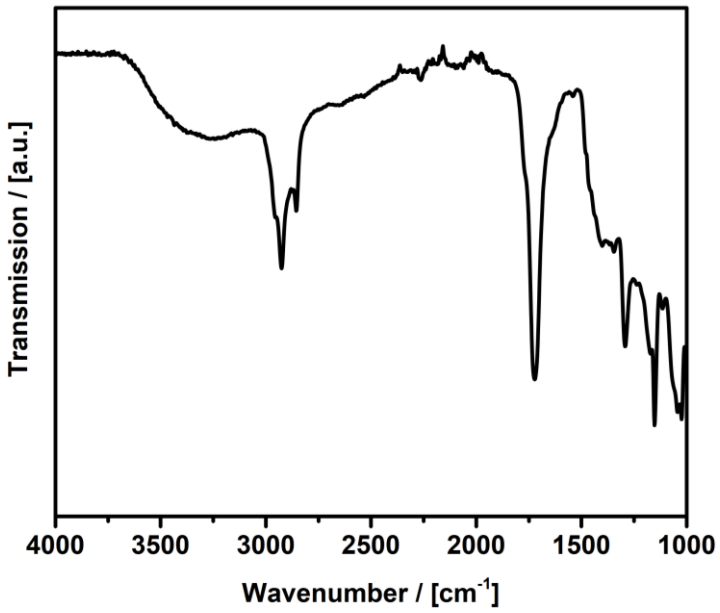

Fig. S9. Conversion of (**4cc**) to (**4oc**). ATR-IR: ν (cm^{-1}) = 3600-2364, 2971, 2942, 1720, 1623, 1396, 1155, 1023.

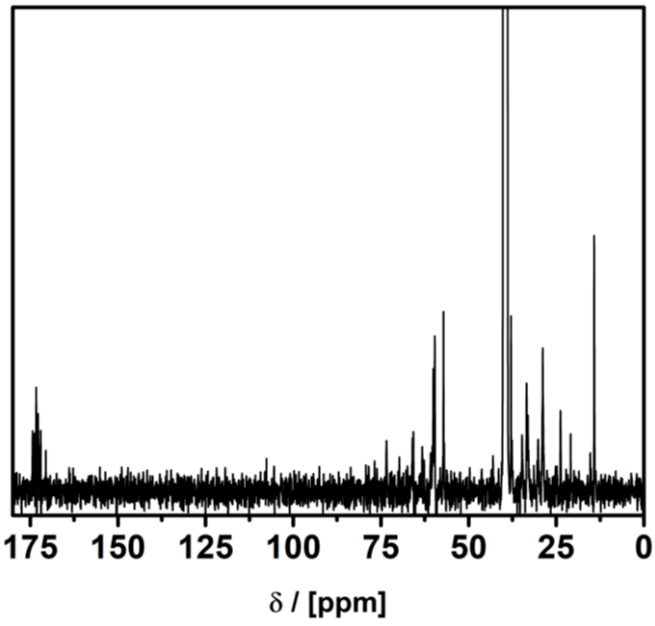

Fig. S10. ^{13}C NMR compound open cage (**4oc**) in DMSO-d_6. ^{13}C NMR (100 MHz, DMSO): δ(ppm) = 14.18, 20.89, 23.78, 28.84, 28.89, 30.18, 32.88, 33.07, 33.45, 34.74, 37.63, 37.89. 37.91, 60.31, 60.78, 62.65, 63.21, 65.72, 65.77, 65.98, 69.73, 73.39, 114.32, 170.54, 172.02, 172.27, 172.62, 172.76, 173.27, 173.52, 173.73, 174.29, 174.33.

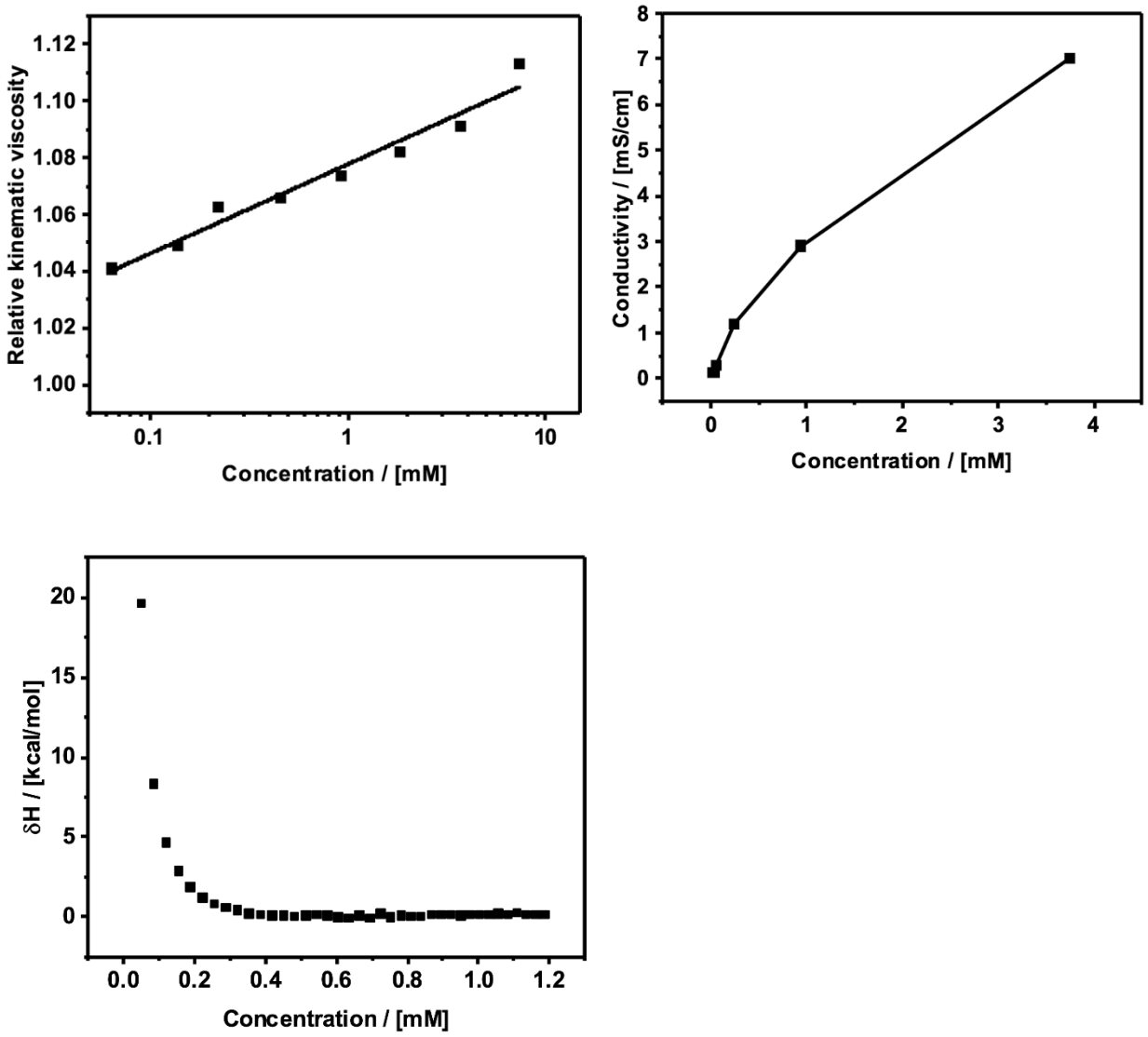

Fig. S11. Top left: Relative viscosity measurement of (**4cc**) in Milli-Q at rt. Top right: Conductivity (ionic) of (**4**) in Milli-Q at rt. Bottom: Isothermal titration calorimetry (ITC) of (**4**) in Milli-Q. A discontinuous relation between concentration and the observable parameter (viscosity, conductivity, or ITC signal) would indicate a change in the aggregation state of the system, respectively the occurrence of aggregation/ micellization. Obviously, all curves are continuous. A classic cmc cannot be identified.

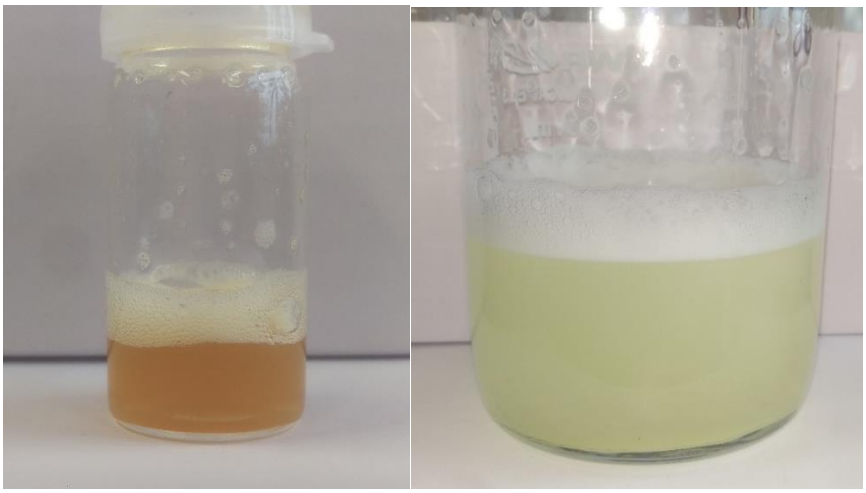

Fig. S12. Dispersions of (**4cc**; left) and (**4oc**; right) in water at oversaturated concentration.

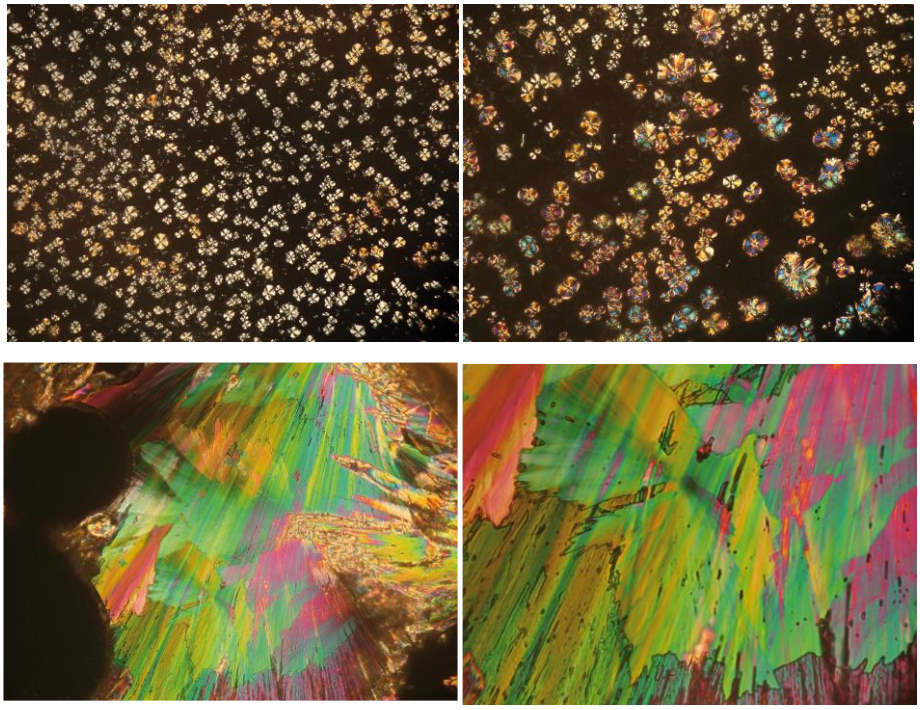

Fig. S13. Optical polarization microscopy image of columnar super structures of (**4cc**) with characteristic Maltese crosses (top) and smectic phase of (**4cc**) (bottom). In dependence of the surfactant concentration and grow time, one observes columnar droplets and extended birefringent areas. The columnar droplets show the classic Maltese cross pattern indicating a 360 ° rotation in optic axis orientation. The extended birefringent areas imply lamellar packing.[146, 147]

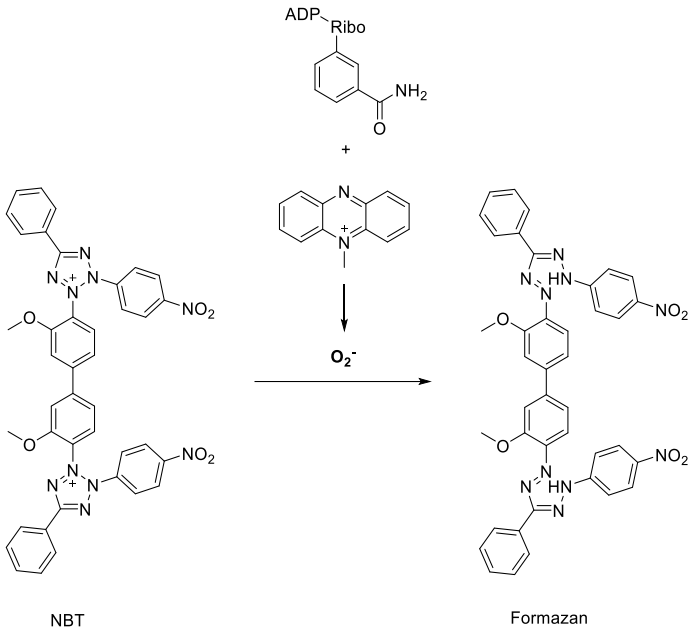

Fig. S14. Nitroblue tetrazolium assay.[135] The NBT-assay was performed after a standard procedure. 1 mL reaction mixture contained phosphate buffer (20 mM, pH 7.4), NADH (146 µM), NBT (100 µM), PMS (30 µM) and various concentrations of sample solution. After incubation for 5 min at ambient temperature, the absorbance was taken at 560 nm against an appropriate blank solution. All tests were performed at least 3 times. For the quercetin experiment methanolic solutions were used.

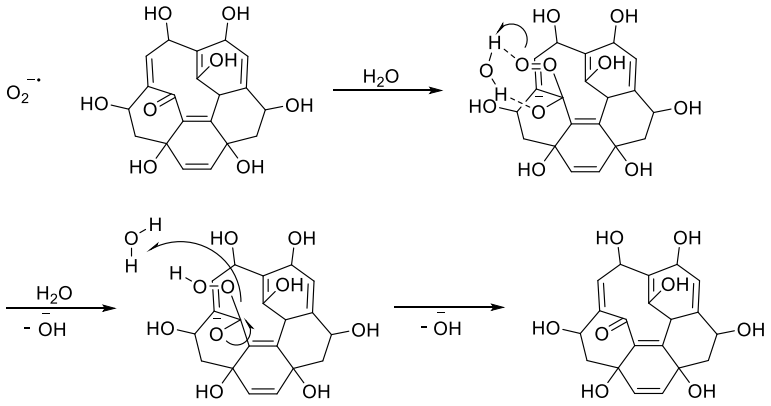

Fig. S15. Molecular mechanism for the improved ROS quenching activity of the open form. Additionally, to the classic superoxide quenching mechanism of fullerenol, in which the superoxide coordinates to the remaining double bonds, one can assume a mechanism in which the superoxide directly reacts with a ketone moiety. This mechanism might be reversible.

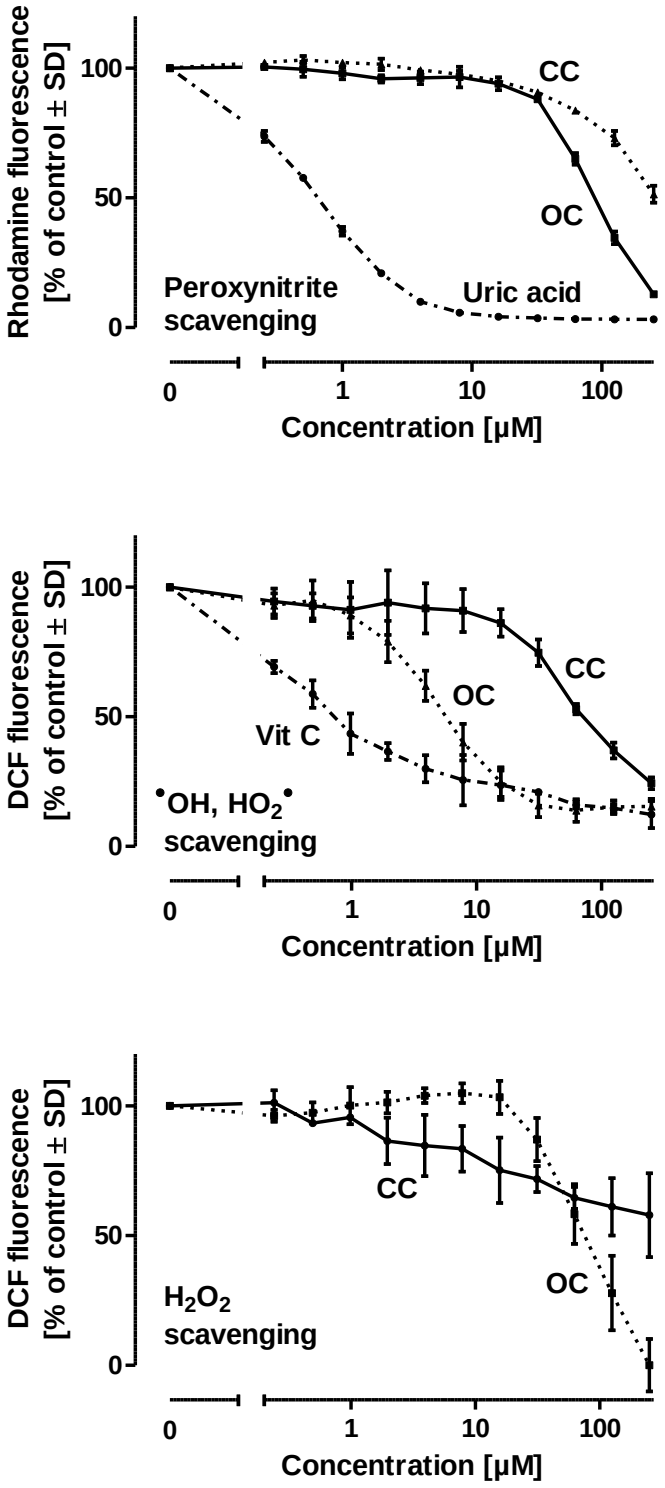

Fig. S16. ROS quenching assays for peroxynitrite, hydroxyl radicals and hydrogen peroxide[138]

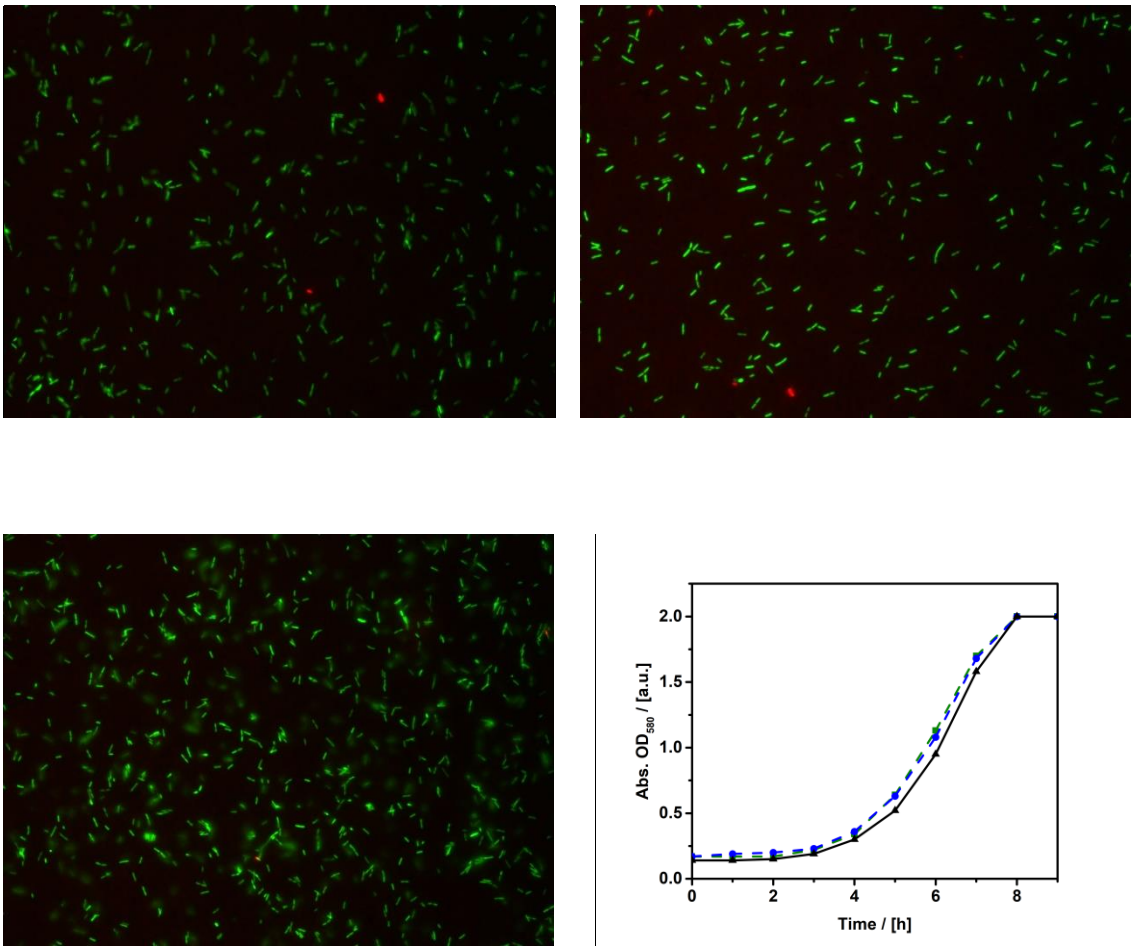

Fig. S17. Live-Dead stain and growth for *E.coli* treated with surfactant . Top left control, top right, in the presence of 100 µM of (**4cc**), bottom left, in the presence of 100 µM of (**4oc**), bottom right growth curves with the control culture indicated in blue, the culture with (**4**) green, and the culture with the open cage isomer of (**4**) in black.

E.coli K-12 as well as *P. aeruginosa* PAO1 (data not shown) were inoculated from precultures into 3 mL LB-medium (10 g tryptone, 5 g yeast extract, 5 g NaCl per liter) and incubated at 30 °C. The surfactant was tested from 1 µM up to 100 µM. The growth of the cultures was followed by measuring the optical density (OD 580 nm), and during the growth and in the stationary phase, samples were taken. For live-dead staining when following the manufacturer's instructions (LIVE/DEAD BacLight Bacterial Viability Kit, Thermofisher), it stains cells with membrane damage in red, against viable cells stained in green. The stained cells were placed on agar-coated microscope slides and observed under a fluorescence microscope at 400-fold magnification.

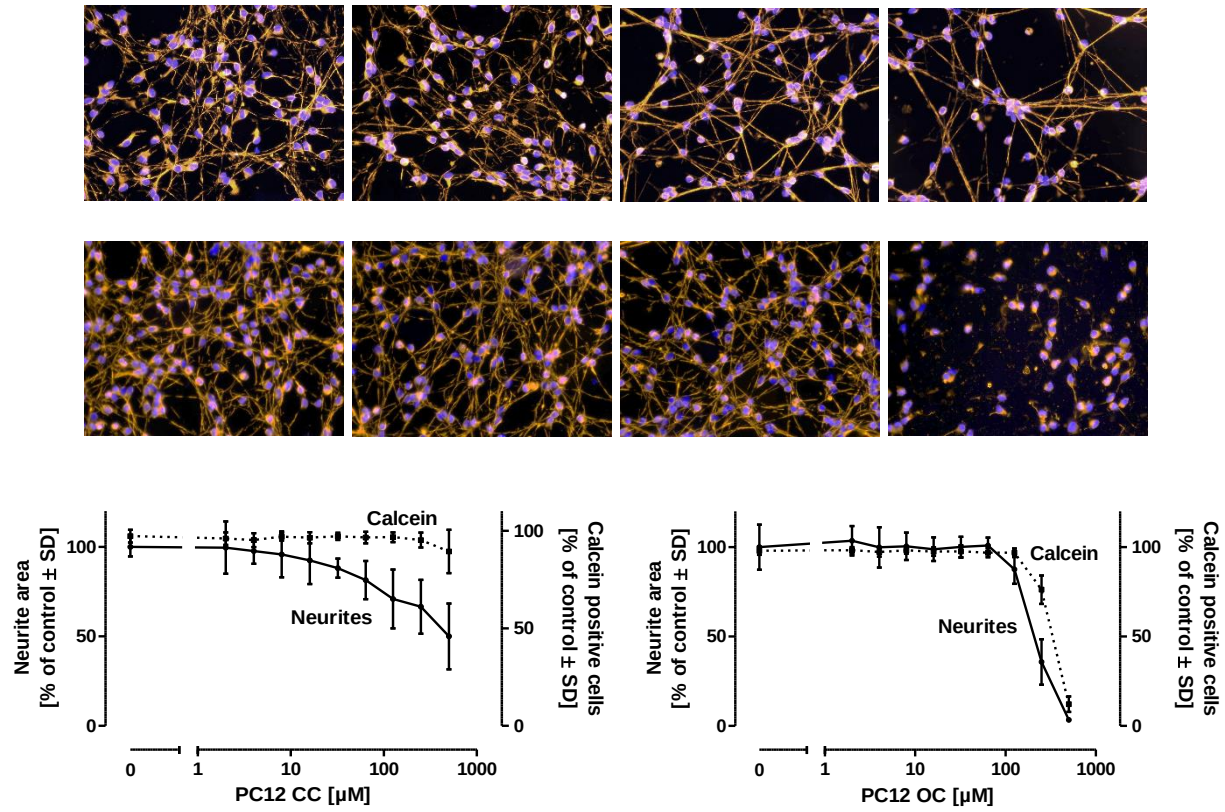

Fig. S18. Morphology of LUHMES treated with (**4cc**) (top), with (**4oc**) (mid) and quantification of the assay (bot) (0 µM, 32 µM, 125 µM, 500 µM). ***Cell culture:*** LUHMES cells are conditionally immortalized human fetal ventral mesencephalic neuronal precursor cells with a distinct dopaminergic phenotype, described in detail previously.[142, 148] Cell culture plates (Sarstedt) were coated with 50 µg/mL poly-L-ornithine (PLO) and 1 µg/mL fibronectin overnight at 37°C and washed 2 times with water. Cells were propagated in Advanced DMEM/F12 (Gibco/Invitrogen, Darmstadt, Germany), 1x N2 supplement (Invitrogen), 2 mM L-glutamine (Gibco), and 40 ng/mL recombinant bFGF (R+D Systems; Minneapolis, MN). The differentiation process was initiated by addition of differentiation medium consisting of advanced DMEM/F12, 1x N2 supplement, 2 mM L-glutamine, 1 mM dibutyryl-cAMP (Sigma), 1 µg/mL tetracycline (Sigma), and 2 ng/mL recombinant human GDNF (R+D Systems). After 2 days, cells were trypsinized and collected in Advanced DMEM/F12 medium. Cells were seeded onto 96-well plates at a density of 35.000 cells/well. The differentiation process was continued for additional 3 days, the cells were then treated with the respective compounds for an additional period of 48 h. For visualization of cell morphology, cells were fixed with 4% paraformaldehyde for 20 min at RT, permeabilized with 0.2% Triton X-100, washed, and blocked with 1% BSA (Calbiochem, San Diego, CA) in PBS for

1 h. LUHMES were stained with an anti-β-III-tubulin antibody (rabbit, Sigma, 1:1000) in 1% BSA/PBS at 4°C over night. After washing, the secondary antibodies were added for 1 h, nuclei were stained by Hoechst H-33342 (1 µg/mL) for 20 min. For quantitative evaluation of the neurite area, live staining of LUHMES was conducted with Calcein-AM (1 µM) and Hoechst H-33342 (1 µg/mL) for 30 min. Images were collected by an automated microplate-reading microscope (Array-Scan II® HCS Reader, Cellomics, Pittsburgh, PA) equipped with a Hamamatsu ORCA-ER camera (resolutuion 1024 x 1024; run at 2 x 2 binning) in two different fluorescence channels. Nuclei were identified as objects according to their intensity, size, area and shape. A virtual area corresponding to the cell soma was defined around each nucleus. The total Calcein pixel area per field minus the soma areas in that field was defined as neurite mass. In addition, viability was analyzed by the detection of the percentage of those cells positive for Calcein and for H-33342.

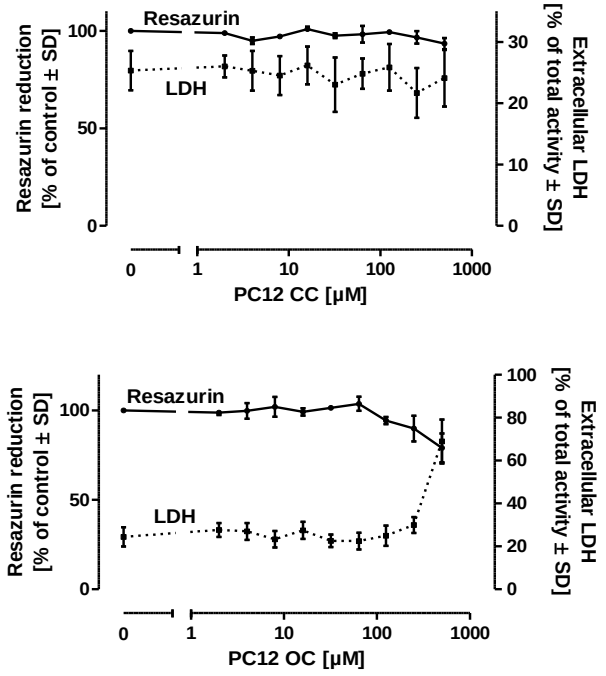

Fig. S19. Resazurin metabolization assay and Lactate dehydrogenase (LDH) release assay for the treatment of LUHMES with (**4cc**) (left) and (**4oc**) (right).

Resazurin metabolization assay: Resazurin (Sigma) was added to the cell culture medium in a final concentration of 5 µg/mL, fluorescence was measured after 60 min (λ_{ex}=530 nm; λ_{em}=590 nm). Lactate dehydrogenase (LDH) release assay: LDH activity was detected separately in the supernatant and cell lysate. Following separation of the supernatants, cells were lysed in PBS /

0.5% Triton X-100 for > 60 min. The percentage of LDH released was calculated as 100 x LDH $_{supernatant}$ / LDH $_{supernat + lysate}$. For the enzymatic assay, 20 µl of sample was combined with 180 µl of reaction buffer containing NADH (100 µM) and sodium pyruvate (600 µM) in sodium phosphate buffer adjusted to pH 7.4 by titration with K_2HPO_4 (40 mM) and KH_2PO_4 (10 mM). Absorption at 340 nm was detected at 37°C in 1 min intervals over a period of 20 min, enzyme activity was calculated from the respective slopes.

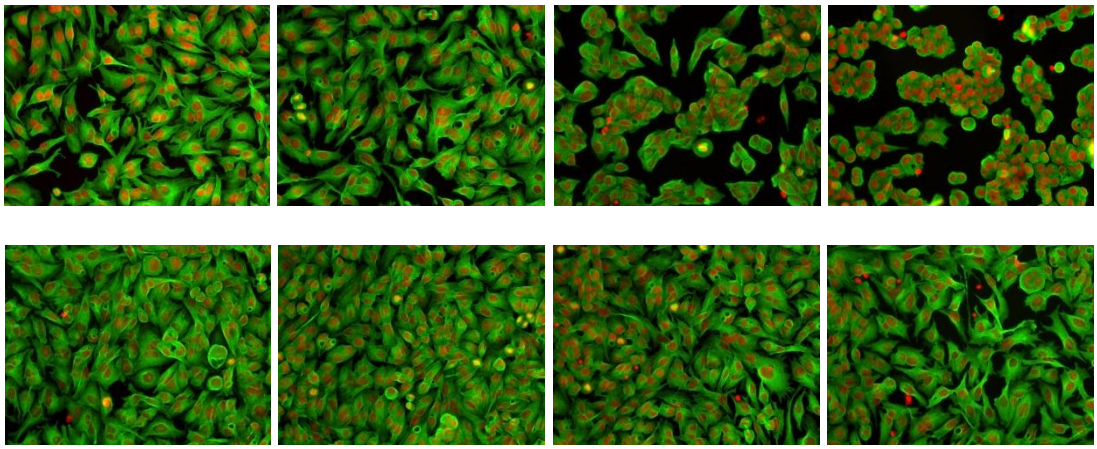

Fig. S20. Morphology of HepG2 treated with (**4cc**) (top), with (**4oc**) (mid) and quantification of the assay (bot) (0 µM, 32 µM, 125 µM, 500 µM). Human hepatoma HepG2 cells were propagated and maintained in DMEM (high glucose), supplemented with 10 % FBS, 25 U/mL penicillin and 25 µg/mL streptomycin. 96-well plates were coated with 50 µg/mL poly-L-ornithine (PLO) and 1 µg/mL fibronectin over night at 37°C. Following a washing step of the coated plates with water, 30.000 cells/well were seeded and grown for 1 day. Then, the cells were treated with the respective compounds for additional 48 h. For visualization of cell morphology, cells were fixed with 4% paraformaldehyde for 20 min at RT, permeabilized with 0.2% Triton X-100, washed, and blocked with 1% BSA (Calbiochem, San Diego, CA) in PBS for 1 h. HepG2 were stained with a monoclonal anti-α-tubulin antibody (Sigma; 1:1000)

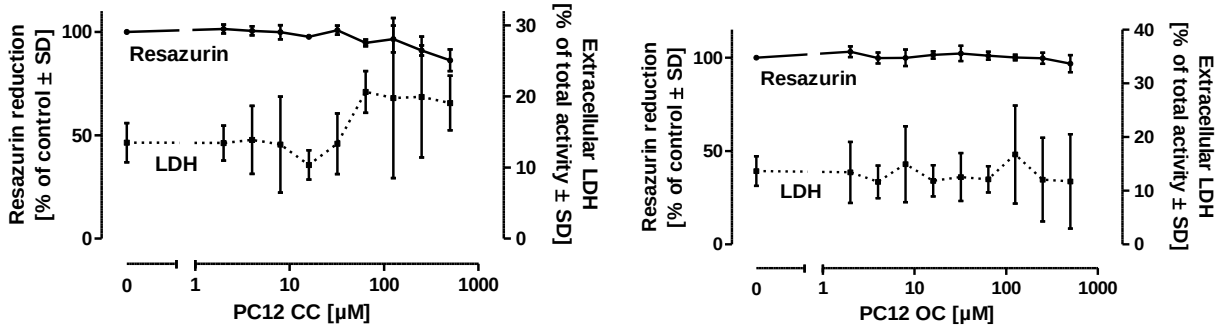

Fig. S21. Resazurin metabolization assay and Lactate dehydrogenase (LDH) release assay for the treatment of HepG2 with (**4cc**) (left) and (**4oc**) (right).

Resazurin metabolization assay: Resazurin (Sigma) was added to the cell culture medium in a final concentration of 5 µg/mL, fluorescence was measured after 60 min (λ_{ex}=530 nm; λ_{em}=590 nm). Lactate dehydrogenase (LDH) release assay: LDH activity was detected separately in the supernatant and cell lysate. Following separation of the supernatants, cells were lysed in PBS / 0.5% Triton X-100 for > 60 min. The percentage of LDH released was calculated as 100 x LDH $_{supernatant}$ / LDH $_{supernat + lysate}$. For the enzymatic assay, 20 µL of sample was combined with 180 µl of reaction buffer containing NADH (100 µM) and sodium pyruvate (600 µM) in sodium phosphate buffer adjusted to pH 7.4 by titration with K_2HPO_4 (40 mM) and KH_2PO_4 (10 mM). Absorption at 340 nm was detected at 37°C in 1 min intervals over a period of 20 min, enzyme activity was calculated from the respective slopes.

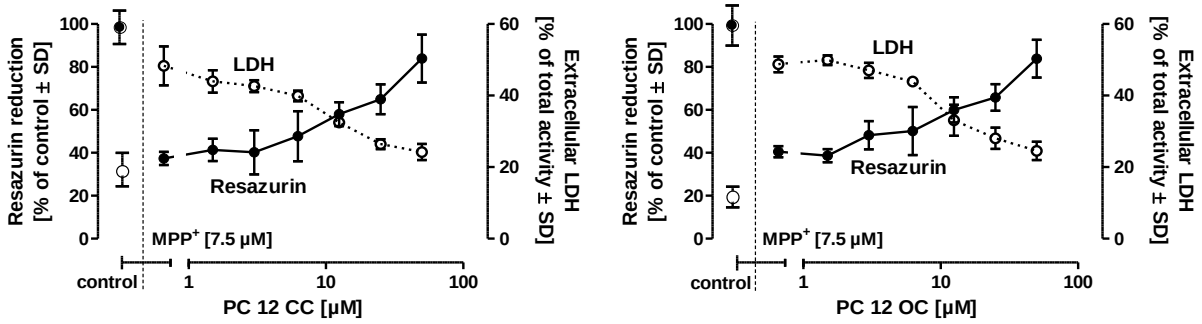

Fig. S22. Resazurin metabolization assay and Lactate dehydrogenase (LDH) release assay for the treatment of LUHMES with (**4cc**) and partially open cage compound (**4oc**) and MPP+.[142, 148]

8.2 Publication II:

Easy, efficient and versatile one-pot synthesis of Janus-type-substituted fullerenols,

Beilstein J. Org. Chem. 2019

Marius Kunkel and Sebastian Polarz*

Abstract: *An efficient one-pot synthesis for Janus-type fullerenol derivatives and how to characterize them is reported. This synthesis provides access to asymmetrically substituted fullerenol with five substituents on one pole of the fullerene and polyhydroxylation moieties, mostly ether and hydroxy groups, on the rest of the fullerene core. As substituents a broad variety of primary amines can be used to obtain Janus-type amphiphilic fullerenols in good to excellent yield. These fullerenol amphiphiles can serve as suitable precursors for further reactions resulting in new applications for fullerenols.*

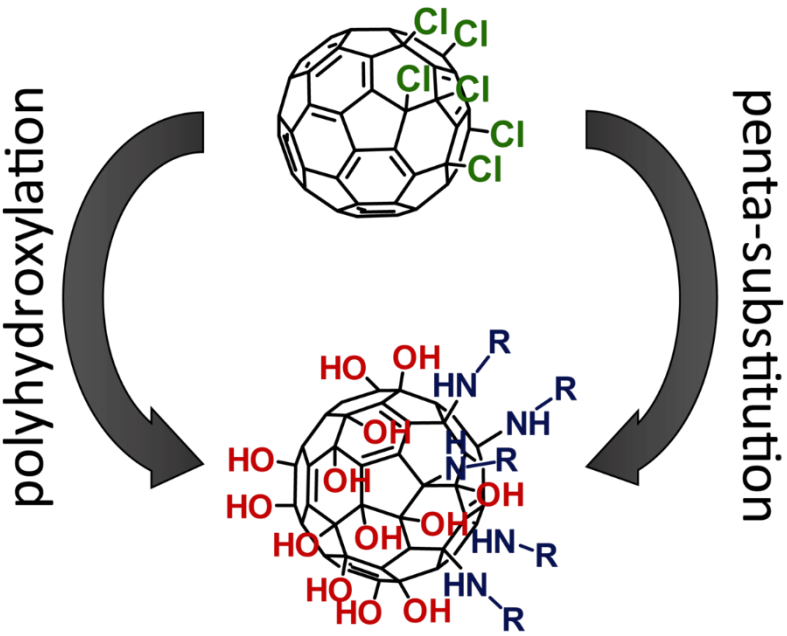

TOC figure of publication 2. Reproduced. Reproduced under the Creative Commons Attribution License.

8.2.1 Record of Contribution

Material synthesis, characterization and data interpretation were performed by M. Kunkel. M. Kunkel and S. Polarz designed the research. M. Kunkel and S. Polarz wrote the manuscript. All authors have given approval to the final version of the manuscript.

8.2.2 Introduction

The roman god Janus, who is typically depicted with two faces, metaphorically stands for duality in one person or object. Consequently, nanoparticles characterized by two different hemispheres have been named Janus-type nanoparticles as well, and have attracted major attention due to their special properties.[150, 151] The term 'Janus' is much less used in molecular chemistry, presumably because there are not many spherical molecules known. Examples are the giant polyoxometalates reported by Müller *et al.*[152] and, more importantly for the current paper, fullerene C_{60}. Because of the high symmetry of those compounds asymmetric modification is tedious with multiple synthesis and purification steps involved. Fullerene derivatives are of great interest in numerous research areas such as biological sciences and materials sciences.[23, 58, 109, 153-155]

A vast amount of synthetic protocols have been developed over the years to modify fullerenes.[26, 156-158] A particular task was to provide fullerenes with solubility in water. Thus, one important class of fullerene derivatives are the hydroxylated and polyhydroxylated compounds, so called fullerenols ($C_{60}(OH)_n$).[159] The degree of hydroxylation and with that the solubility of these compounds can be tuned by using different synthetic approaches making it possible to obtain water soluble fullerenols as well as fullerenols that are still soluble in organic solvents.[69, 70, 160-162] The maximum number of OH groups, which could be attached to C_{60} is $n = 44$.[70] Further derivatizations, where all hydroxyl moieties of the compound have been modified, are well known in the literature. These reactions can be achieved by esterification or etherification.[163-165] However, partial modifications are rare, especially when it comes to asymmetric substitutions.[166, 167] Although, janus-type fullerenols at which only a part of the fullerene core is hydroxylated are known,[168, 169] literature lacks fullerenol compounds with Janus-type substitution. The advantage of those special molecular species, e.g., amphiphilic behavior, was demonstrated in a paper published by our group in 2018.[99] A fullerenol derivative with a maximum of 21 OH groups on one hemisphere and 5 alkyl chains on the other was reported. The synthesis of this species was elaborate and tedious with

relatively low yield, we also failed to introduce more complex substituents than alkyl chains, for instance. The success of the used, multistep synthetic pathway drastically depends on the reactants that are used. One may obtain insoluble or unreactive intermediates, which then prevent the synthesis of the final compound in good yield or to obtain the final compound at all.

For future exploration of the potential of Janus-type fullerenols it is pivotal to establish new synthetic pathways, which allow to introduce a broader variety of substituents and better yield. We report an easy and efficient one-pot approach using $C_{60}Cl_6$ as a precursor. The attachment of substituents, in our case primary amines, and the polyhydroxylation of the fullerene core are performed simultaneously by using a common phase transfer reaction which enables even the combination of water-soluble substituents with the precursor $C_{60}Cl_6$. High yields of Janus fullerenol derivatives bearing five defined substituents on one pole of the C_{60} core combined with in average 19 (+/−3) oxygen containing moieties on the other pole are obtained.

8.2.3 Results and Discussion

The general procedure for the one-pot preparation of asymmetrically substituted fullerenols is depicted in **Scheme 1**, and experimental details are presented in the following.

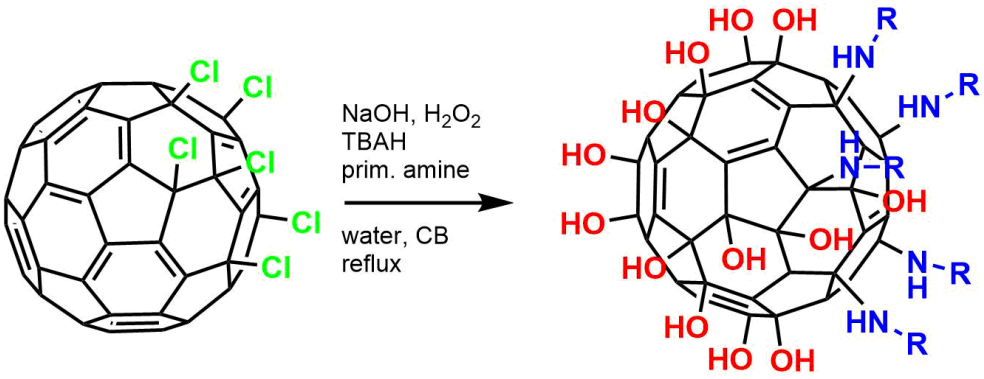

Scheme 1: Reaction scheme for the one-pot reaction of $C_{60}Cl_6$ to produce Janus-type fullerenols $(OH)_{19+/-3}C_{60}(HNR)_5$.

The starting material for all syntheses is $C_{60}Cl_6$ which was synthesized according to procedure reported by Kuvychko *et al.* and adapted by our group.[99, 121, 170] Though, several compounds are known to undergo the penta-substitution reaction with $C_{60}Cl_6$, like amines, thiols or alcohols,[122, 171, 172] it has been observed that primary amines show a high reactivity under these conditions and form stable intermediates during this reaction that can further react. In a general procedure, $C_{60}Cl_6$

(200 mg, 0.21 mmol) and the primary amine of choice (8 equiv) are dissolved in a chlorobenzene/water mixture (8 mL/40 mL). The mixture is combined with the phase transfer agent tetrabutylammonium hydroxide (0.5 mL of a 30% solution in H_2O). The reactants for the polyhydroxylation are added, H_2O_2 (1.5 mL of a 30% solution) and NaOH (0.7 g). The mixture is heated to reflux until the chlorobenzene phase decolorizes. The reaction is completed after 2 h of reflux. The aqueous phase is separated and poured in methanol to precipitate the crude product. The obtained brown solid is washed with methanol to remove remaining TBAH and NaOH to obtain the sodium salt of the compound. The sodium salt compound can be ion exchanged (amberlite 120) prior to hydrophilic interaction liquid chromatography (silica gel 60, gradient acetonitrile/water 90:10 to 70:30) for purification.

In a first attempt a methyl-protected aminocatechol, namely dimethoxyaniline, was reacted under these conditions. After purification the product was obtained in a good yield of 88%. The compound was characterized as follows.

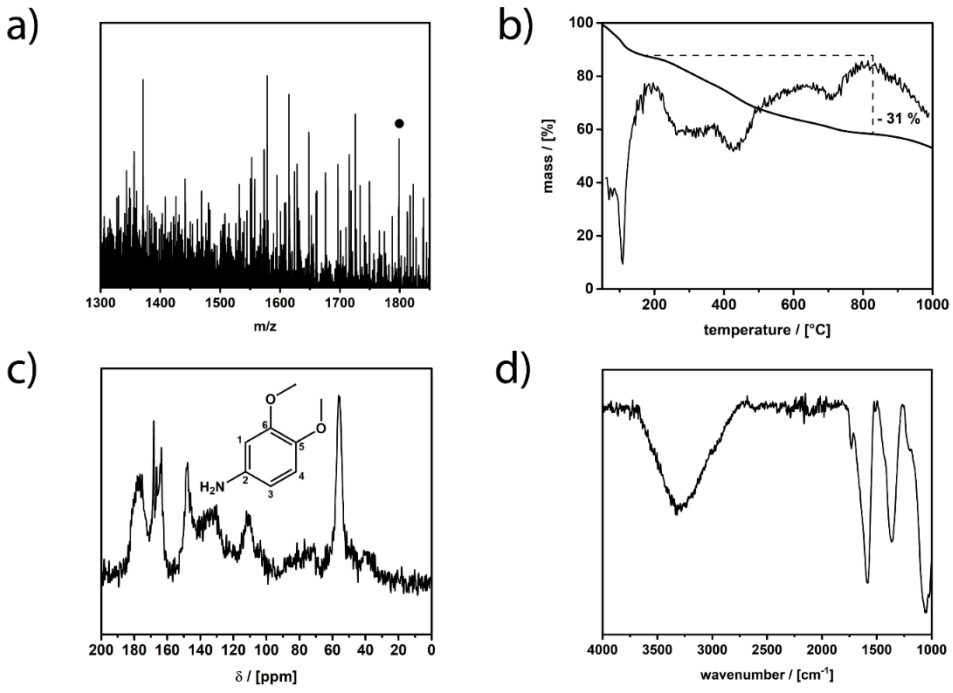

Figure 1: Characterization of fullerenol amphiphile with substituent 1. a) ESIMS in positive mode, molecular ion peak marked with circle, b) TGA under nitrogen with 5 K/min, c) MAS-NMR (^{1}H-^{13}C-CP) with structure of substituent, d) ATR–IR.

For the characterization of Janus-type fullerenol amphiphiles more than one method is needed to perfectly identify the compounds. Polyhydroxylation reaction of the fullerene can lead to a mixture of several oxygen moieties like hydroxyl groups, diols, ketones, hemiketals, epoxides and ethers. The general formula of the compound is identified by electrospray ionization mass spectrometry (ESIMS). The degree of polyhydroxylation and the number of substituents is determined and confirmed with thermogravimetric analysis (TGA) and the nature of oxygen moieties as well as the substituents attached are evaluated via a ^{13}C magic angle spinning nuclear magnetic resonance spectroscopy (MAS NMR) ^{1}H-^{13}C-CP experiment. An overall information of the compound is obtained by attenuated total reflection infrared spectroscopy (ATR-IR). **Figure 1** shows the results of the characterization exemplarily for the fullerenol amphiphile with dimethoxyaniline as substituent (all characterization data can be found in Supporting Information File 1). ESIMS (**Figure 1a**) shows a rather complex fragmentation pattern similar to unsubstituted fullerenol compounds known in the literature.[173] The general complexity of the spectrum derives from the isomerization and fragmentation of the oxygen species in addition to the fragmentation of the substituents. The signals can be assigned with a general formula $[M - xH_2O - yH - zO - v(HNR)]^{a-/+}$. The molecular ion peak of the janus fullerenol with 1 as substituent can be identified at m/z 1798.6 (1798.6) which corresponds to $(H)_{13}(O)_{19}C_{60}(HNR)_5^+$ and with that fits 19 oxygen species. As already mentioned there are several oxygen species present in the compound which are further identified later on with MAS NMR. The formula of the compound indicates that there are 12 hydroxy groups present and 7 other oxygen species. The TGA (**Figure 1b**) is another method to confirm the number of attached oxygen species and substituents. The first step up to 180 °C fits the release of secondary and tertiary bound water. The measurement shows that 12 H_2O molecules are bound to the fullerene. The second step up to around 800 °C can be assigned to the release of the different oxygen species, which also explains the little steps which correspond to different oxygen types. In addition to the oxygen species attached to the fullerene core, the methoxy moieties of the substituent are also released. The average number of oxygen species can be calculated to 19.5, which fits the data obtained from ESIMS. Above 800 °C the decomposition of the core structure and the substituents starts. After that step only amorphous carbon remains and the compound is completely decomposed. Finally, the MAS-NMR (**Figure 1c**) confirms the attachment of the substituents and that the structure of substituents is unchanged. Furthermore, it provides evidence to determine the kind of the oxygen species.[71, 174] At 175 ppm the signals of C=C–O groups are located. These signals are rather intense which gives evidence that the most

prominent oxygen structure motive besides hydroxyl groups are ethers. This may result from the reaction conditions since it was already shown that the reaction conditions influence the obtained oxygen moieties. The signal at 163 ppm can be assigned to carbon atoms 5 and 6 of the substituent. Carbon atom 2 of the substituent is located at 148 ppm. Remaining sp^2-hybridized carbons of the fullerene core are located between 142 and 120 ppm. At 110 ppm the remaining carbons of the substituent are located. The sp^3-hybridized carbons of the fullerene core at which the hydroxyl groups are attached are located between 80 and 60 ppm. Finally, the carbon atoms of the methoxy moieties can be found at 55 ppm. **Figure 1d** displays the ATR–IR spectrum of the compound which confirms the results from the other analytical methods. Most prominent in the spectrum are the signals of the polyhydroxylation moieties. Signals at 3293, 1579, 1358, 1200 and 1049 cm^{-1} can be assigned to the O–H, C–O–C, C–O and C–OH vibrations.

The scope of the reaction was further tested with other primary amines, aliphatic as well as aromatic (**Table 1**). The aliphatic amines **2** and **3** react in good yields over 70%. For these compounds the reaction needs about 2 h to be finished. The reaction with compound **2** leads to a little amount of insoluble byproduct which might be double reacted amine although an excess of amine was used. The loss of yield for the reaction with **3** results mainly from byproducts that are not penta-substituted. The aromatic compound **4** reacts the fastest and the reaction was completed after 20 min. Strong foaming indicates the completion of the reaction. Almost no byproduct could be isolated here.

Of special interest for this reaction are compounds with additional functional groups like alkynes or bromides that can be reacted with other compounds in further

Table 1: Scope of the reaction and isolated yields.

Entry	Reactant	Yield[a]
1	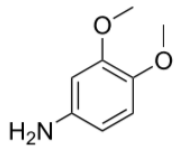 **1**	88%
2	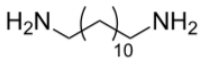 **2**	70%
3	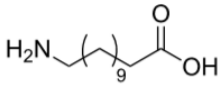 **3**	75%
4	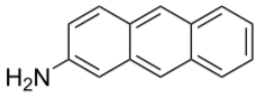 **4**	90%
5	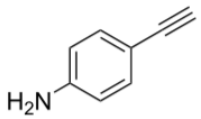 **5**	82%
6	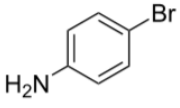 **6**	80%

[a]Yield after purification.

reactions, e.g., click reactions or Sonogashira coupling. Systems for such reactions are tested with compounds **5** and **6**. These compounds react in high yields up to 90%. The additional functional groups, which must of course be not base-labile survive the reaction conditions with no harm. The attached moieties, no matter if electron withdrawing or donating, do not seem to influence the reaction. Moreover, neither the degree of polyhydroxylation nor the kind of attached oxygen species seem to be influenced by the attached substituents. For all compounds the average degree of polyhydroxylation is 19(+/−3). Noteworthy, neither the degree of polyhydroxylation could be increased nor the nature of oxygen species could be varied by extending the reaction time.

8.2.4 Conclusion

In summary, we have established a new and easy one-pot method for the synthesis of Janus-type fullerenol amphiphiles. The reaction includes a wide range of primary amines reaching from aliphatic amines over aromatic amines to further functionalized amines. All resulting compounds have the general formula $(OH)_{19+/-3}C_{60}(HNR)_5$, whereas, mainly hydroxyl and ether moieties are included. They have been characterized with ESIMS, TGA and MAS NMR. These compounds can serve as precursors for further modified fullerenols or as true surfactants.

8.2.5 Supporting Information

General Methods

Synthesis that acquired inert gas atmosphere were performed using general Schlenk techniques under argon atmosphere. The solvents were dried according to standard literature and stored under argon. Water was deionized with Millipore Milli-Q. All starting materials used for synthesis were purchased from commercial sources unless stated differently. The fullerene C_{60} (pur. 99.9 %) was purchased from Research & Production Company “Modern Synthesis Technology”.

Analytical Methods

Mass spectra were measured on Bruker amazon SL in pos. or neg. mode via direct inject from a methanolic solution. For assignment of signals work of Silion, Mihaela, *et al*. was used as reference.[175] Assignment was done as follows: $[M - xH_2O - yH - zO - v(HNR)]^{a-/+}$. Molecular ion peak is identified in combination with results from TGA and NMR. TGA was measured on Netzsch Jupiter STA 449 F3. All measurements were performed under nitrogen atmosphere with 80 mL/min

flowrate and with heating rate of 5 K/min. NMR measurements were performed on Bruker Avance II 400 solid-state NMR at 295 or 350 K and with 10k Hz rotational speed. Number of scans 5k – 10k with D1 = 10 to 100 sec. Attenuated total reflection−infrared (ATR−IR) spectra were measured with a Perkin Elmer100 Spectrum spectrometer including an ATR unit.

Characterization data

Entry 1

Substituent

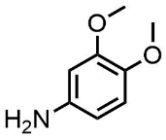

ESI-MS

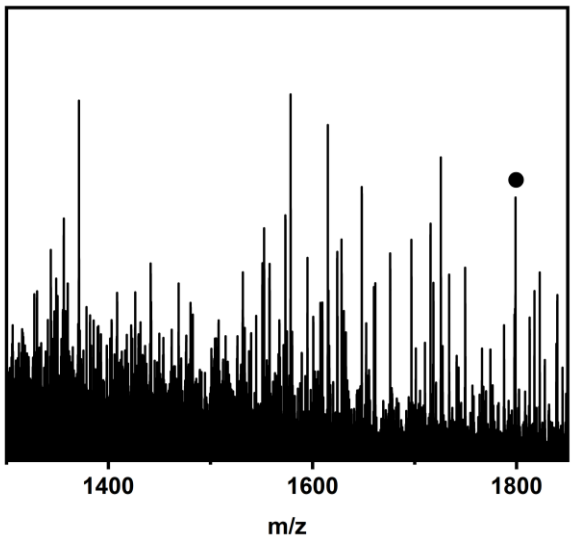

$[H_{13}O_{19}C_{60}(NC_8H_{10}O_2)]^+$ m/z = 1798.7 (1798.6)

MAS NMR

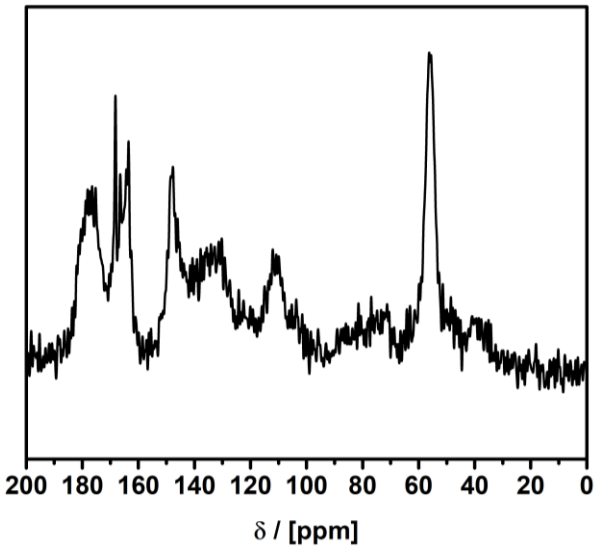

^{1}H-^{13}C-CP MAS-NMR (100 MHz): δ (ppm): 175 C=C-O, 163 160 C(sp^2)-N, 148 ppm C sp^2, 142-120 ppm C sp^2, 110 ppm C sp^2, 80-60 ppm C-OH, 55 ppm O-CH_3

TGA

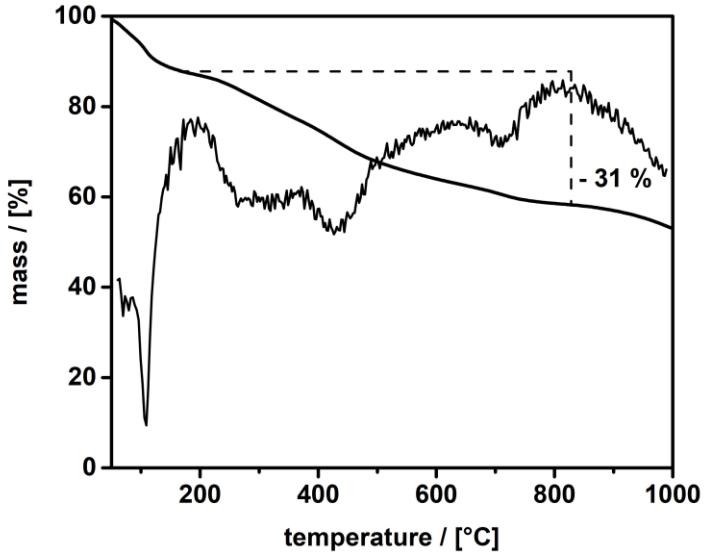

Step 50 °C – 180 °C 13 %

180 °C – 800 °C 31 % → 19.5 oxygen species

>800 °C 56 %

ATR-IR

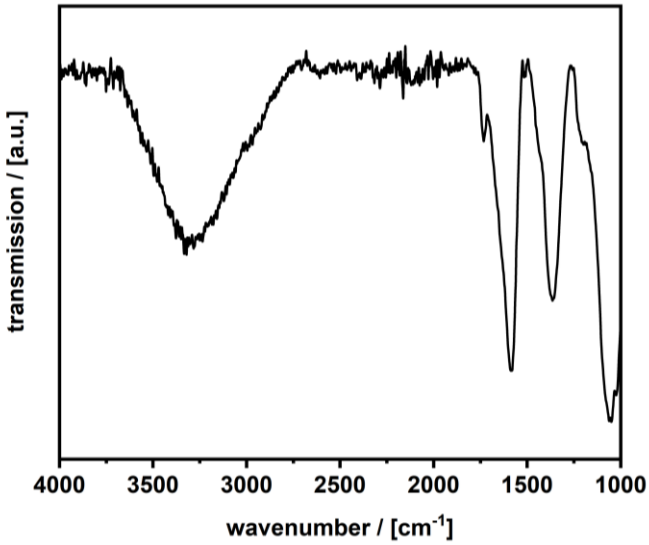

IR (powder): 3293, 3000, 2971, 1579, 1440, 1358, 1200, 1049 cm^{-1}

Entry 2

Substituent

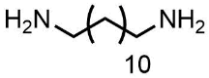

ESI-MS

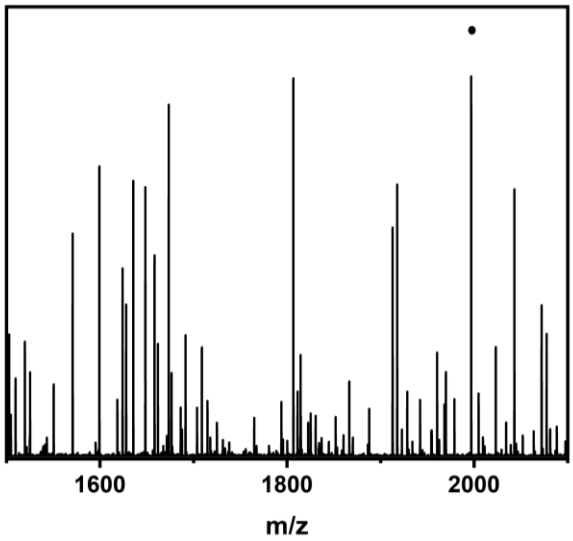

$[H_7O_{17}C_{60}(N_2C_{12}H_{27})]^-$ m/z = 1996.9 (1996.5)

MAS-NMR

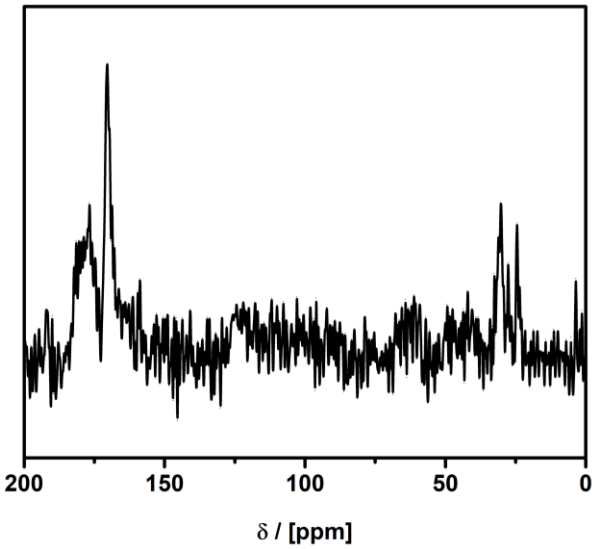

^{1}H-^{13}C-CP MAS-NMR (100 MHz): δ (ppm) 177 C=C-O, 150 C sp^2 (fullerene), 60 - 40 C-OH, 42 C-N-, 29 C sp^3 (chain)

TGA

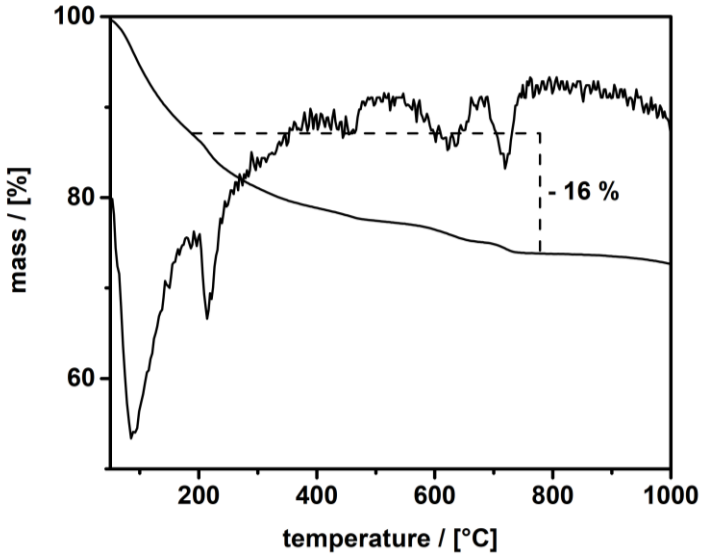

Step 50 °C – 190 °C 13 %

190 °C – 775 °C 16 % → 18 oxygen species + amine endgroups

>775 °C 71 %

ATR-IR

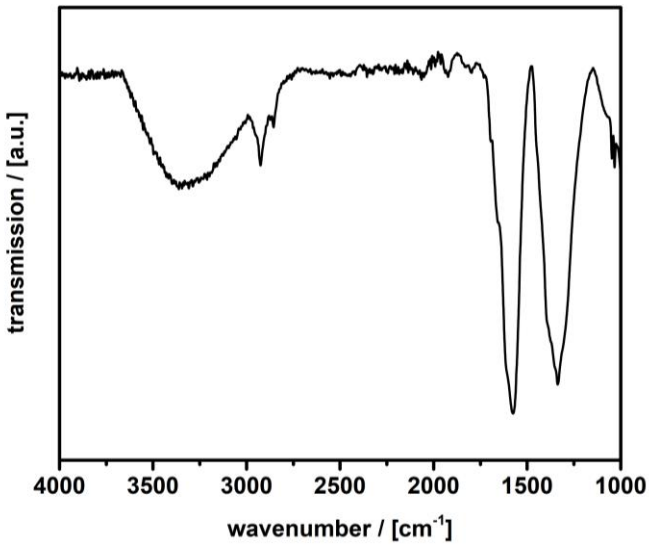

IR (powder): 3320, 2923, 2852, 1655, 1574, 1393, 1327 cm^{-1}

Entry 3

Substituent

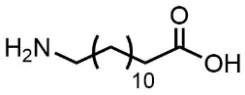

ESI-MS

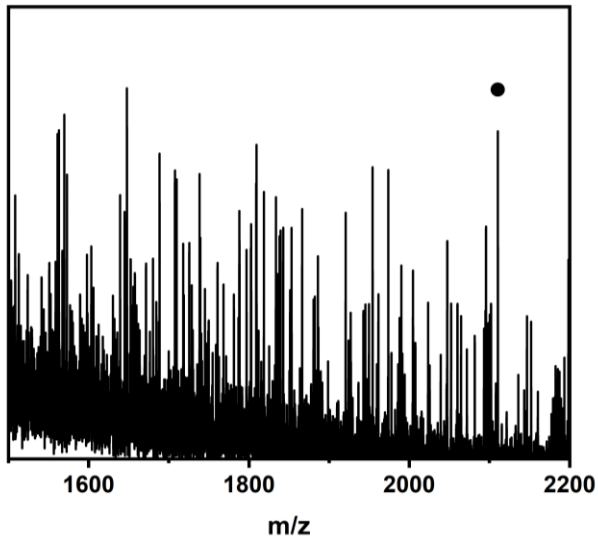

$[H_{14}O_{19}C_{60}(NO_2C_{12}H_{24})]^+$ m/z = 2110.2 (2110.4)

MAS-NMR

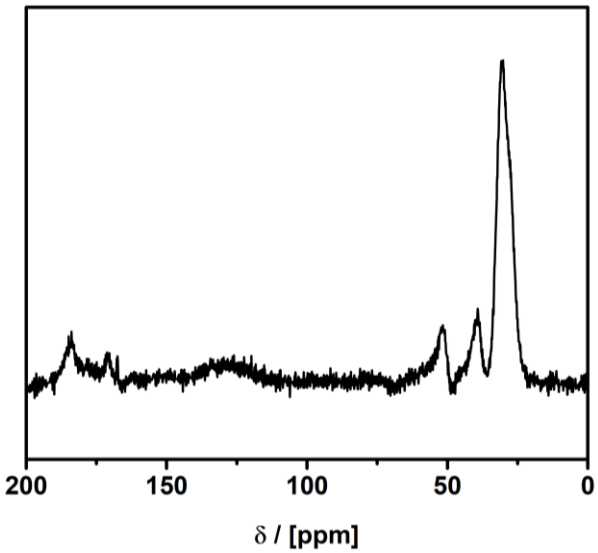

^{1}H-^{13}C-CP MAS-NMR (100 MHz): δ (ppm) 184 COOH, 170 C=C-O, 160 C sp^2 (fullerene), 75-50 C-OH, 51 C-N, 39 C-COOH, 29 C sp^3 (chain)

TGA

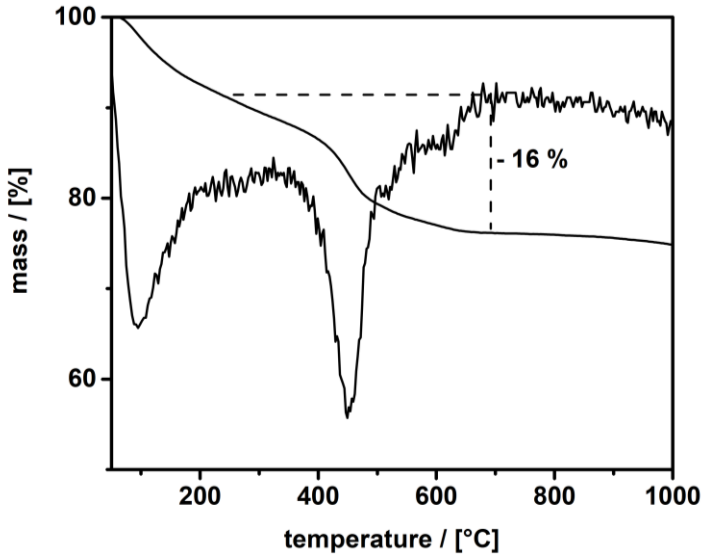

Step 50 °C – 190 °C 9 %

190 °C – 775 °C 16 % → 21 oxygen species

>775 °C 75 %

ATR-IR

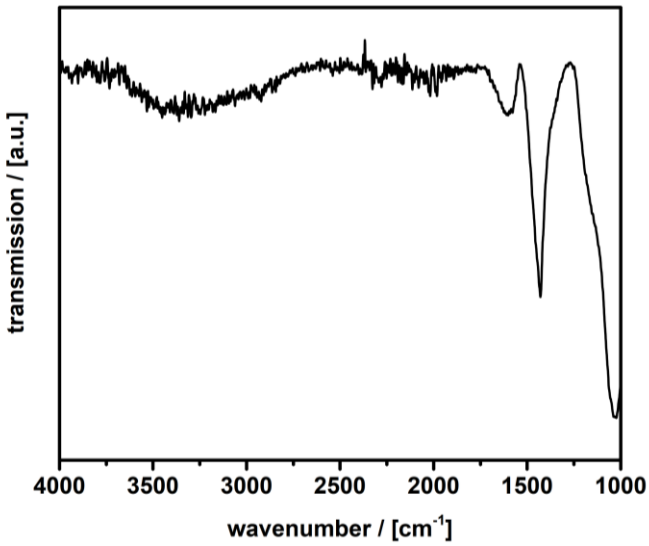

IR (powder): 3340, 2923, 2841, 2300, 1599, 1431, 1158, 1028 cm^{-1}

Entry 4

Substituent

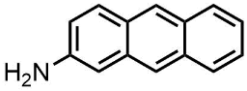

ESI-MS

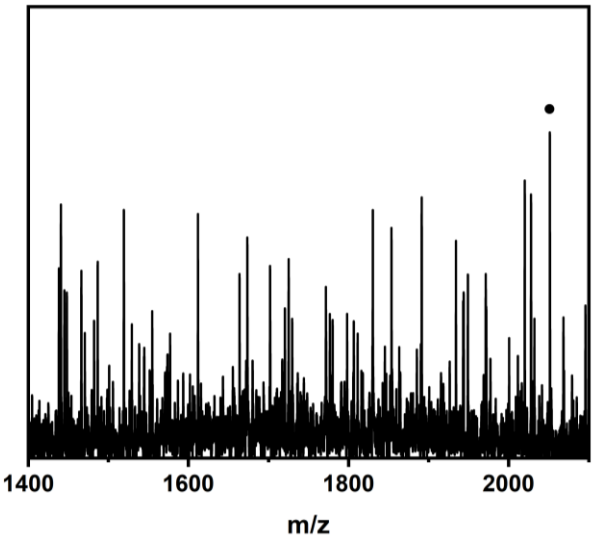

$[H_{17}O_{21}C_{60}(NC_{14}H_{10})]^-$ m/z = 2051.1 (2051.0)

MAS NMR

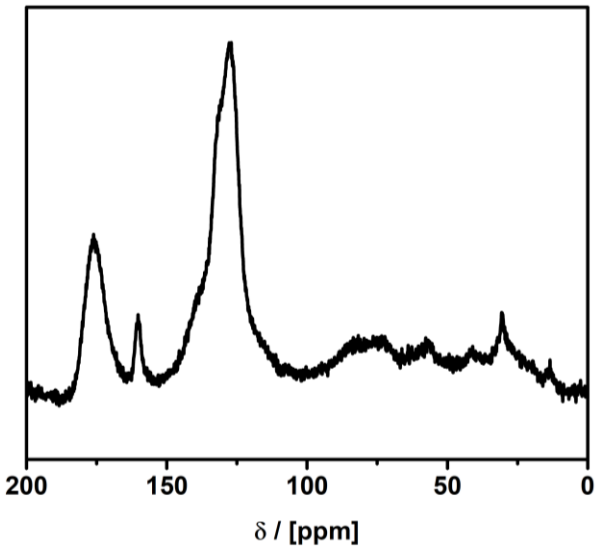

^{1}H-^{13}C-CP MAS-NMR (100 MHz): δ (ppm) 175 C=C-O, 160 C(sp^2)-N, 127 C sp^2, 75-50 C-OH, 29 SSB

TGA

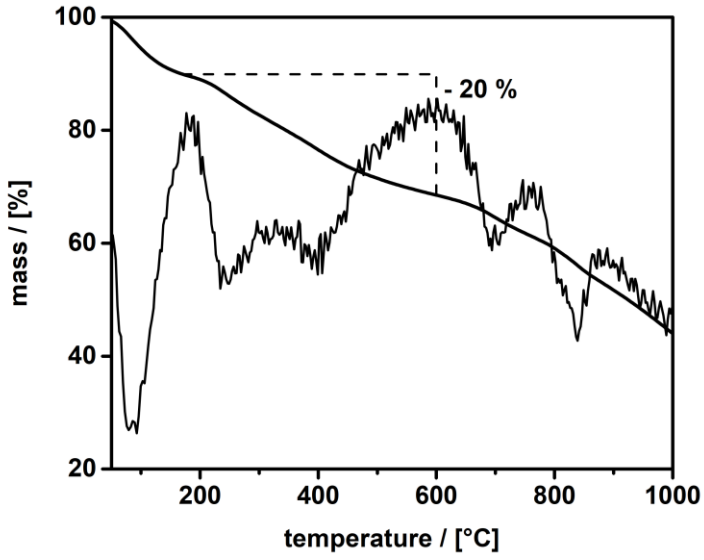

Step 50 °C – 180 °C 12 %

180 °C – 600 °C 20 % → 22 oxygen species

>600 °C 68 %

ATR-IR

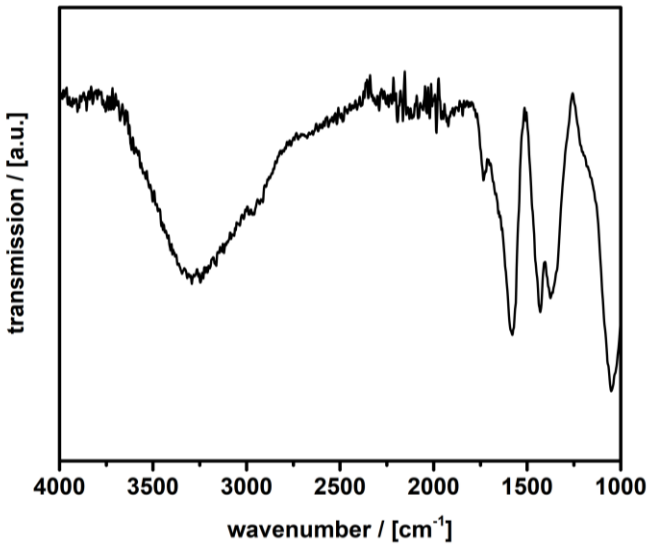

IR (powder): 3270, 2970, 2910, 1732, 1577, 1433, 1361, 1058 cm^{-1}

Entry 5

Substituent

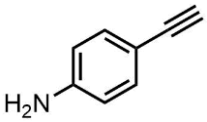

ESI-MS

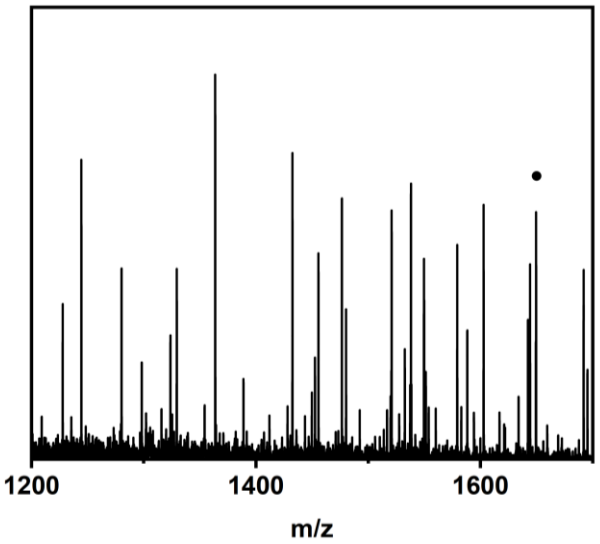

$[H_{12}O_{21}C_{60}(NC_8H_6)]^-$ m/z = 1649.5 (1649.5)

MAS-NMR

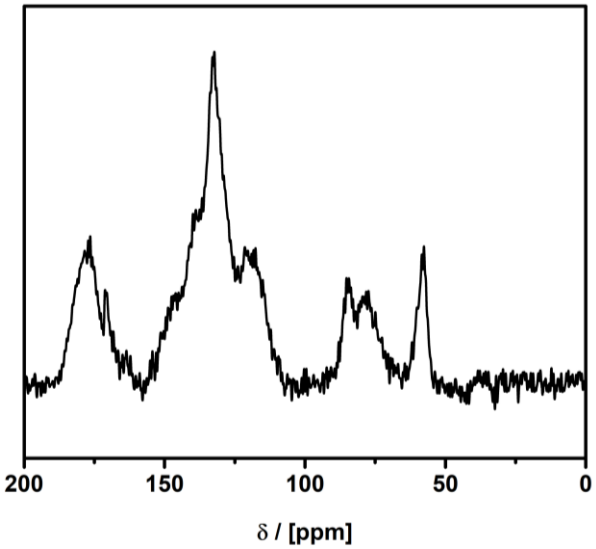

^{1}H-^{13}C-CP MAS-NMR (100 MHz): δ (ppm) 175 C=C-O, 132 C sp^2, 120 C sp^2, 84 C sp, 77 C sp, 60-40 C-OH

TGA

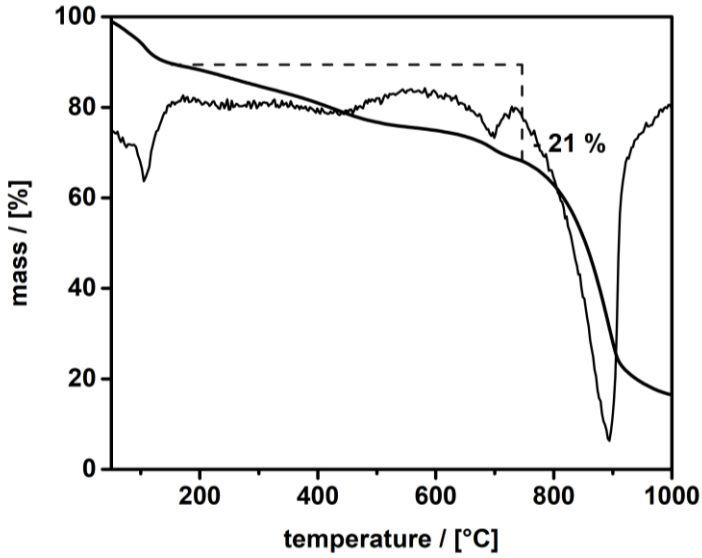

Step 50 °C – 150 °C 11 %

190 °C – 750 °C 21 % → 22 oxygen species

>750 °C 68 %

ATR-IR

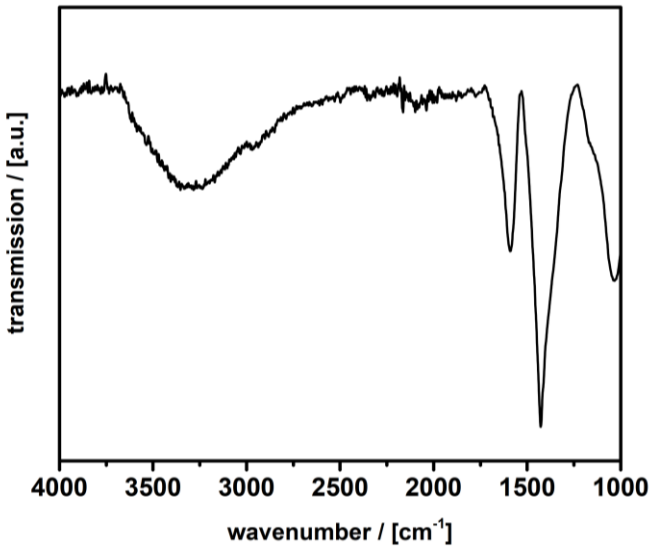

IR (powder): 3280, 2983, 2926, 1593, 1422, 1166, 1033 cm^{-1}

Entry 6

Substituent

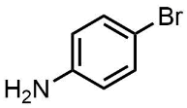

ESI-MS

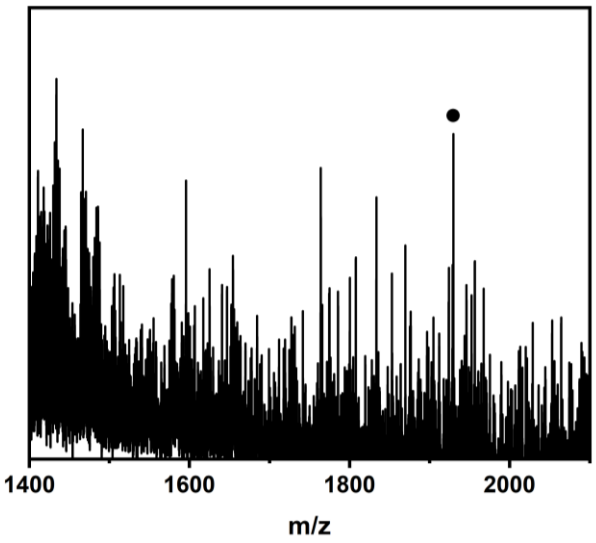

$[H_{18}O_{21}C_{60}(NC_8H_5Br)_5]^+$ m/z = 1929.7 (1929.9)

MAS-NMR

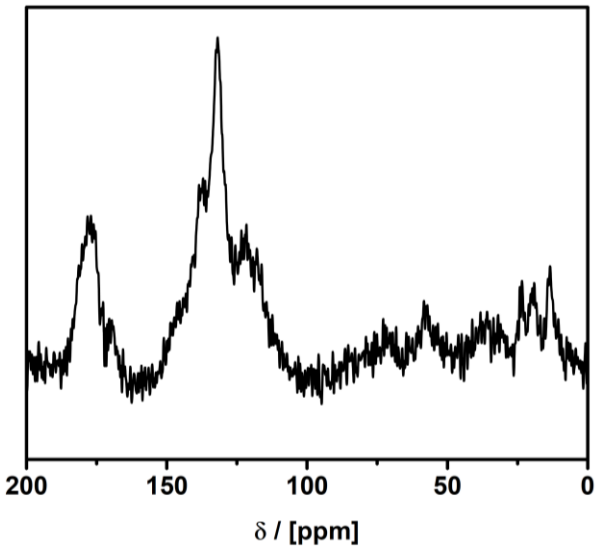

^{1}H-^{13}C-CP MAS-NMR (100 MHz): δ (ppm) 175 C=C-O, 140 C(sp^2)-N, 130 C sp^2, 118 C sp^2, 65-40 C-OH, 17 SSB

TGA

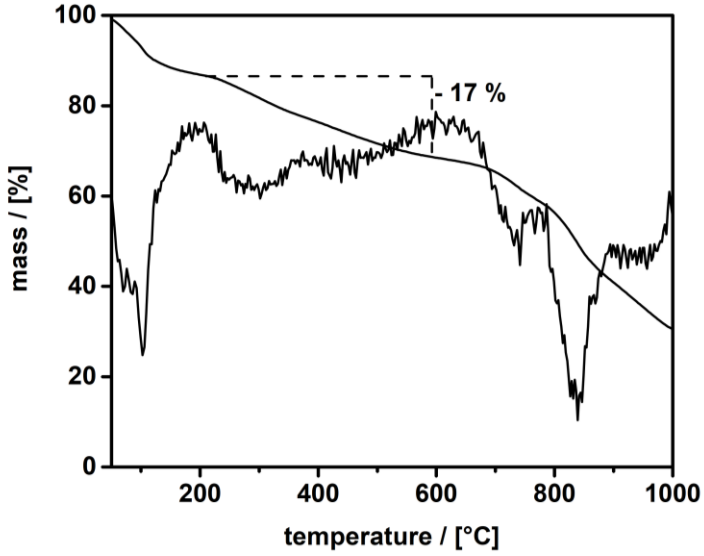

Step 50 °C – 200 °C 15 %

200 °C – 600 °C 17 % → 21.5 oxygen species

>600 °C 68 %

ATR-IR

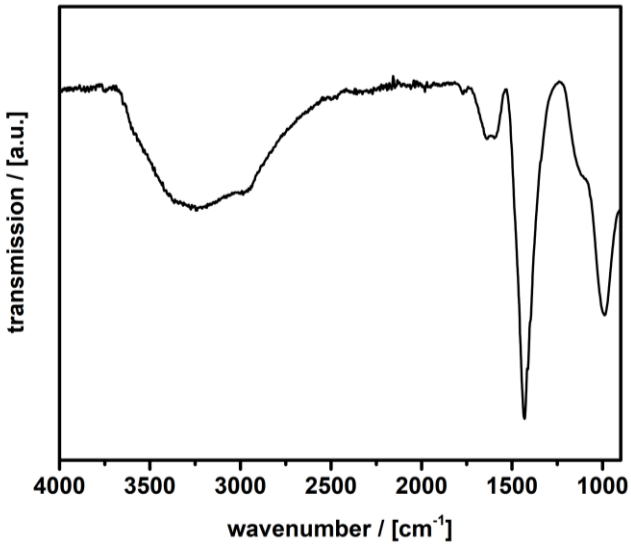

IR (powder): 3240, 2982, 2942, 1639, 1588, 1429, 1117 cm^{-1}

8.3 Publication III:

Molecular Semiconductor Surfactants with Fullerenol Heads and Colored Tails for Carbon Dioxide Photoconversion,

Angew. Chem. Int. Ed. 2019

Marius Kunkel, Sebastian Sutter and Sebastian Polarz*

Abstract: *The leaf is a prime example of a material converting waste (CO_2) into value with maximum sustainability. As the most important constituent, it contains the coupled photosystems II and I, which are imbedded in the cellular membrane of the chloroplasts. Can key functions of the leaf be packed into soap? We present next-generation surfactants that self-assemble into bilayer vesicles (similar to the cellular membrane), are able to absorb photons of two different visible wavelengths, and exchange excited charge carriers (similar to the photosystems), followed by conversion of CO_2 (in analogy to the leaf). The amphiphiles contain five dye molecules as the hydrophobic entity attached exclusively to one hemisphere of a polyhydroxylated fullerene (Janus-type). We herein report on their surfactant, optical, electronic, and catalytic properties. Photons absorbed by the dyes are transferred to the fullerenol head, where they can react with different species such as CO_2 to give formic acid.*

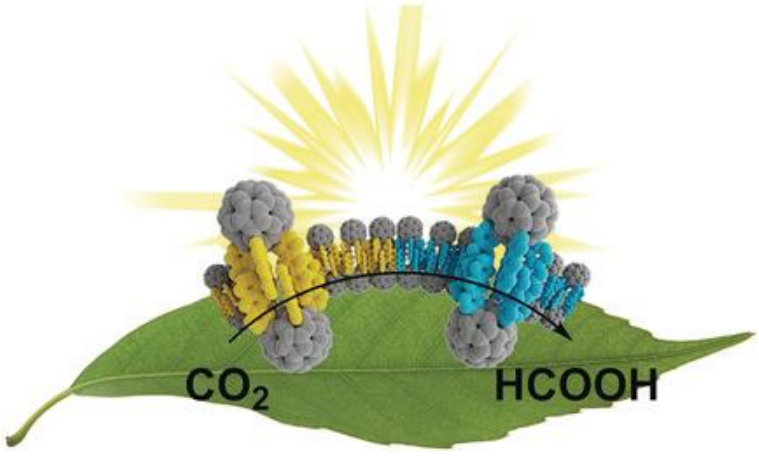

TOC figure of publication 3. Reproduced. Reproduced under the Creative Commons Attribution License.

8.3.1 Record of Contribution

Material synthesis, characterization and data interpretation were performed by M. Kunkel. S. Sutter performed the DFT calculations. M. Kunkel and S. Polarz designed the research and M. Kunkel and S. Polarz wrote the manuscript. All authors have given approval to the final version of the manuscript.

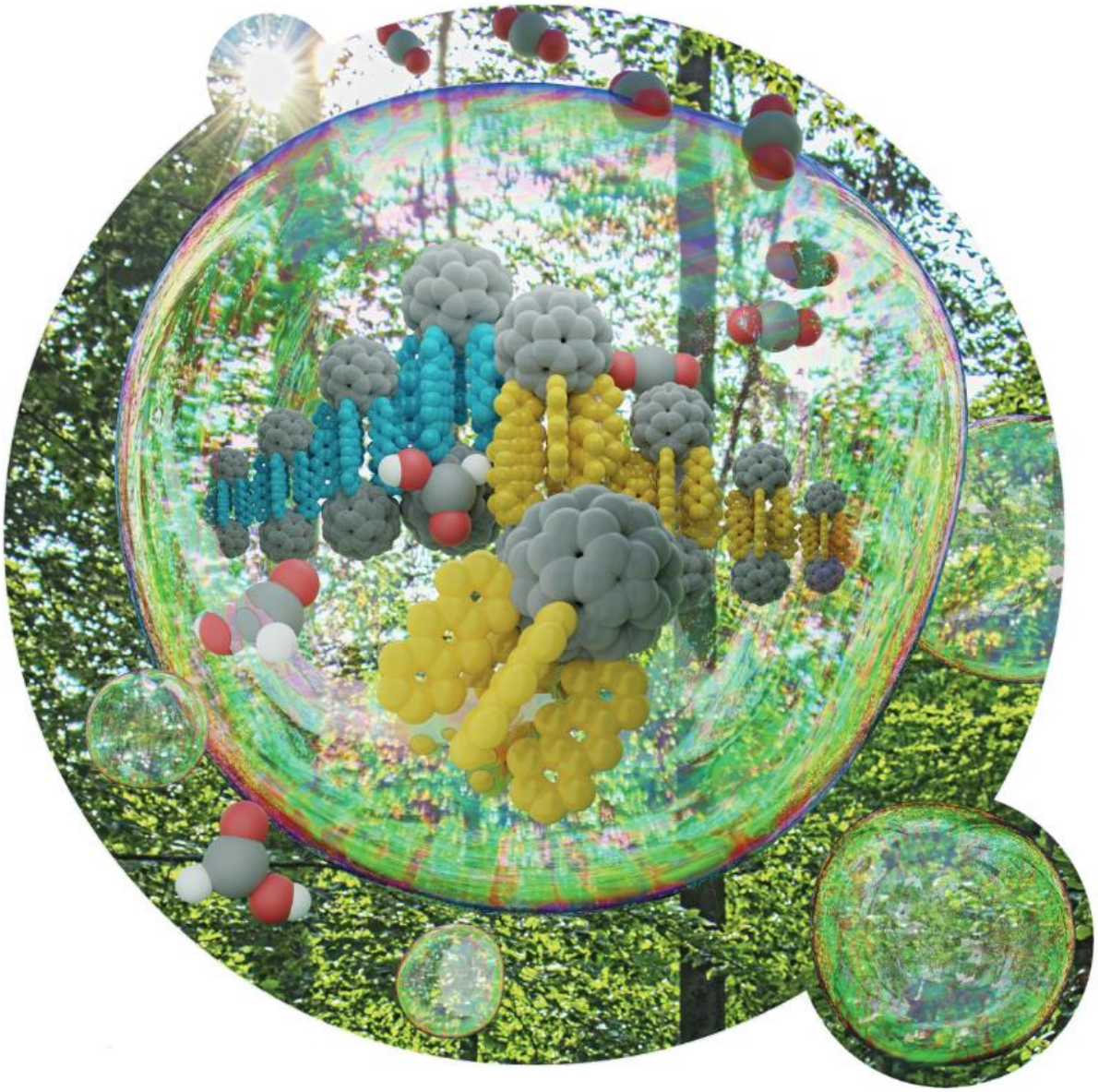

Frontispiece of ref. 176. Reproduced under the Creative Commons Attribution License. The graphic was generated in cooperation with Stephan Siroky.

8.3.2 Introduction

Nature has found a unique way to exploit sunlight for driving biological processes: photosynthesis. The most important constituents of chloroplasts are the photosystems II and I, which convert light into chemical energy. As photosynthesis consumes the greenhouse gas CO_2, major research efforts have been devoted to the identification of synthetic mimics. The "artificial leaf" is an illustrative expression for this field of research.[177] Impressive success has been achieved for photocatalytic water splitting using semiconductor nanoparticles.[178] The absorption of light leads to the formation of electron–hole pairs, which are separated and, in an ideal case, induce photo-reduction and-oxidation in one system. Numerous systems have been evaluated for the photo reduction of CO_2, which are mostly based on inorganic semiconductors combined with suitable photosensitizers.[179-182] However, as the customizability of inorganic semiconductors is restricted, it has also been considered to let molecular systems do the job.[181, 183] Fullerene derivatives have proven to be valuable compounds in optoelectronic or photocatalytic applications.[40, 43, 184-187] Fullerenes in general have a high electron affinity, which makes them suitable for donor–acceptor systems. A common example are fullerene dyads.[188-193] Fullerene dyads belong to the fascinating class of so-called small molecule semiconductors,[194] which became of interest in bulk heterojunction solar cells as strong optical absorbents and electron mediators.[195-197] A donor unit is attached to the fullerene, which can be excited by absorbing light and then transfers an electron in a process accompanied by charge separation. During this process, a fullerene radical anion is produced, which can further transfer the electron.[193, 198, 199] Studies have also shown that fullerene dyads can produce significant amounts of reactive oxygen species (ROS).[200-203] Unfortunately, the use of fullerene dyads in aqueous systems is difficult because of their hydrophobic character. This problem could be addressed by a small-molecule, fullerene-based semiconductor with surfactant properties. Surfactants are functional molecules composed of a hydrophobic chain (typically alkyl groups) and a hydrophilic head group that are attached to each other in a dipolar fashion. The two important features of surfactants are their abilities to stabilize interfaces and to self-assemble into higher organized structures such as micelles, vesicles, or lyotropic phases depending on concentration, temperature, and, last but not least, molecular shape. The advantage of a self-organized superstructure formed by a molecular semiconductor surfactant is that it could come close to a new type of an artificial leaf (**see Figure 1**). It undergoes multi-wavelength light triggered charge generation and separation to compartments at the two sides of an interface, followed by

coupling to chemical conversion of reagents such as CO_2 or others into different, more valuable products.[179, 204]

8.3.3 Results and Discussion

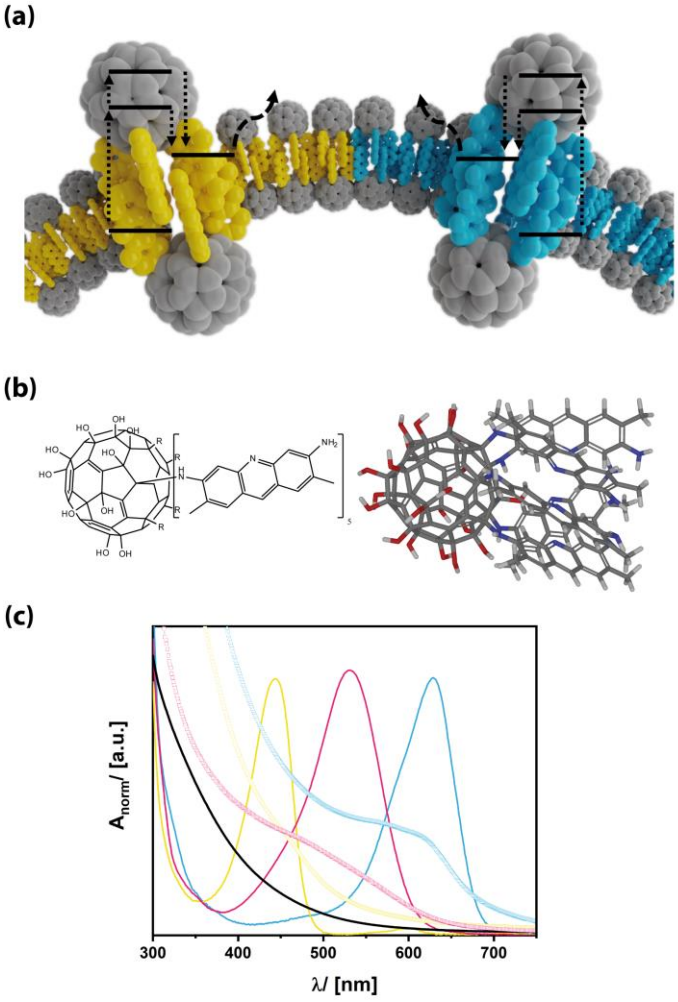

Figure 1. a) Fullerenol dyads as surfactant semiconductors with lipidlike properties and associated photochemical processes. **b)** Schematic structure (left) and calculated structure of **FuDy-Y**. C gray, H white, N blue, O red. **c)** UV/Vis absorption spectra of the dyes (lines) and the fullerenol dyads (symbols) according to the color of the dye. yellow-G: yellow, neutral red: red, toluidine blue: blue, reference fullerenol: black.

To realize such surfactant properties, we chose a so-called fullerenol as the head group as they are known to show similar electronic behavior as unmodified fullerenes and to be water soluble.[205-207] We have recently presented surfactants with fullerenol head groups and alkyl tails and tested their biocompatibility.[99] In Ref.[149],we presented anew and efficient one-pot approach for the preparation of arbitrary Janus-type substituted fullerenols.[149] Whereas Ref.[149] focused on synthetic details and molecular characterization of the compounds, any special, functional properties of those fascinating compounds have been omitted, and are the subject of the current paper. We focused on compounds with one hemisphere of the fullerenol modified by five dye molecules (**see Figure 1a,b** and **Figure S1** in the Supporting Information). These dyes are acridine yellow-G (λ_{max} = 445 nm; **FuDy-Y**), neutral red (λ_{max} = 530 nm; **FuDy-R**), and toluidine blue O (λ_{max} = 629 nm; **FuDy-B**). The dyes were selected to cover almost the entire visible range (**Figure 1b**).

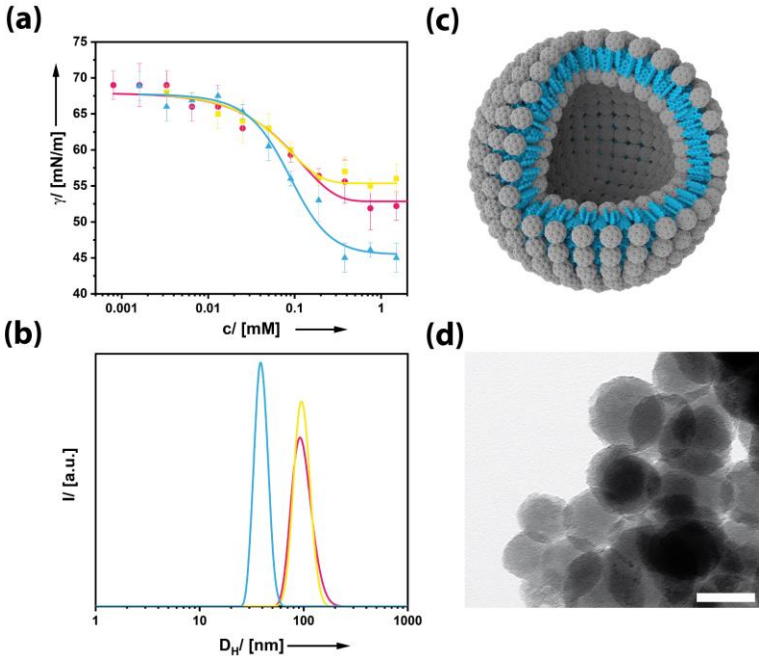

Figure 2. a) Concentration-dependent surface tension measurements and **b)** aggregate size distribution functions derived from DLS at c = 0.4 mm for the three different **FuDy** surfactants. **FuDy-B**: blue, **FuDy-Y**: yellow, **FuDy-R**: red. **c)** Schematic structure of the vesicular aggregates formed in solution. **d)** TEM image of a dried sample of a colloidal solution of **FuDy-Y** aggregates; scale bar:100 nm.

Because of their amphiphilic structure, the presented compounds are designated for possessing amphiphilic properties. Surface activity was probed by concentration-dependent surface-tension γ measurements (**Figure 2a**). The curves show a shape characteristic for surfactants. Above a certain concentration, aggregates form. The size of those aggregates is around 100 nm for **FuDyY** according to dynamic light scattering (DLS; **Figure 2b**). Considering the fact that the diameter of a single surfactant molecule is only about 1.5 nm, the aggregate size cannot correspond to spherical micelles, which are expected to have double the surfactant length. The latter could be confirmed by transmission electron microscopy (TEM), also under cryogenic conditions, as shown in **Figure 2d** (see also **Figure S2**). Spherical objects with diameters corresponding well to the DLS results were observed. Thus we concluded that vesicles rather than micelles had been formed with acritical aggregation concentration of $c_{cac} \approx 0.4$ mM. Because of the relatively large packing parameter of the surfactants (see **Figure S1**), they behave rather similar to lipids and prefer structures of lower curvature. This observation is in line with our previous findings for fullerenol surfactants with simple alkyl chains as hydrophobic tails.[99] Although the sizes, shapes, and polarities of the three compounds are similar according to molecular geometry optimization (**Figure S1**), **FuDy-B** gave a lower γ value at saturation of the interface (c > 0.5 mM) than **FuDyY**

and **FuDy-R**. The aggregates of the latter two compounds are also larger with a hydrodynamic diameter D_H of about 90 – 100 nm. The different substituents in the hydrophobic, conjugated p-system obviously have an effect on the so-called hydrophilic–lipophilic balance (HLB). Having shown that the **FuDy**s motifs have surfactant properties, we investigated whether they are molecular semiconductors. Therefore, a thorough photophysical characterization was necessary. Optical absorption spectra of reference compounds (the unmodified dyes and $C_{60}(OH)_{24}$)[136] are compared to each other in **Figure 1b** (see also **Figure S3**). The absorption spectra of the different **FuDy** compounds are not simple superposition of the spectra of their constituents.[193, 198] Instead of distinct absorption bands, an absorption edge has emerged, which is rather typical for semiconductors.

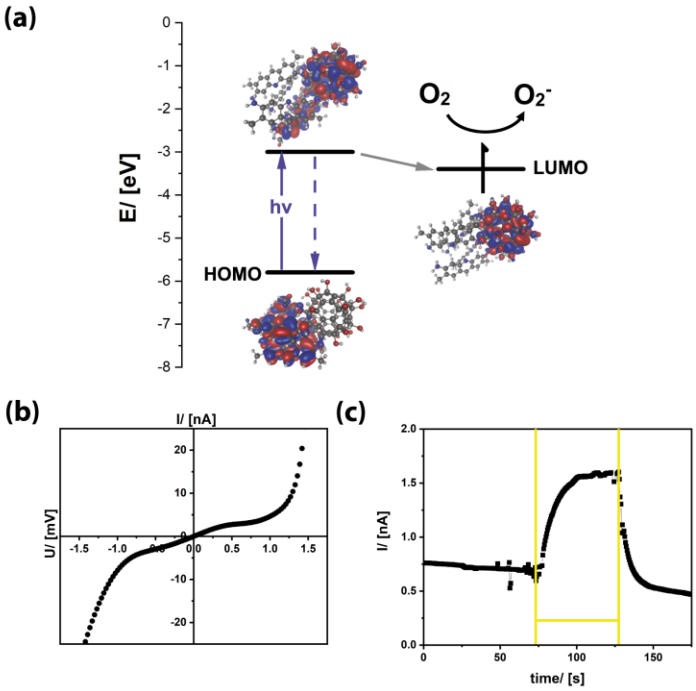

Figure 3. a) Frontier orbitals of **FuDy-Y** deduced from DFT calculations and PESA measurements (HOMO: combined HOMO to HOMO-4). **b)** I/V measurement (measurement in the dark with 20 mVs^{-1}) and **c)** photocurrent measurement of **FuDy-Y** (the yellow lines mark the irradiation time with white light; 1 mV was applied).

The shift of the energy of the absorption edge compared to λ_{max} of the dyes indicates that there is electronic communication between the surfactant's head and tail. The fact that the dyes are not electronically isolated was confirmed by DFT calculations (**Figure 3a**). The highest occupied molecular orbital (HOMO) is located exclusively on the dye molecules. The absolute energy of the HOMO of **FuDy-Y**, for instance, is -5.8 eV according to photoelectron spectroscopy on air (PESA;

Figure S3). The first unoccupied orbital with sufficient orbital overlap between head and tail is located at ca. -2.8 eV, and corresponds well to the optical transition (**Figure 3a**). However, the DFT calculations show that the lowest unoccupied molecular orbital (LUMO) is located at -3.4 eV and consists only of fullerenol orbitals. Therefore, after electronic excitation, the charge carriers are quickly transferred to the LUMO. This was confirmed by photoluminescence (PL) measurements (**Figure S3**). The red-shift in the PL maximum points to an extended conjugation length of the p-system. However, the PL intensity is reduced by almost 90%. Considering that fullerenols exhibit no fluorescence in the relevant spectral region (**Figure S2**), the decrease in the PL intensity can be interpreted as a sign for the transfer of photo generated charges to the head group. These findings are in agreement with literature on standard fullerene dyads.[188-193] Our conclusions were further confirmed by fluorescence lifetime τ_{PL} measurements (**Figure S3**).The τ_{PL} of **FuDy** (1.7 ns) is tremendously reduced compared to that of the free dye (τ_{PL} = 6 ns) in solution. Furthermore, the fluorescence decay of **FuDy** is not mono-exponential anymore, which indicates that relaxation processes have become more complex upon attachment to the fullerenol residue. Further confirmation of a true semiconductor nature was obtained by current–voltage (IV) measurements of **FuDy-Y** (**Figure 3b**). The material obviously shows macroscopic charge transport, but the behavior is non-ohmic, which is consistent with a semiconducting electronic system. Light absorption should increase the number of mobile charge carriers in a semiconductor material, and accordingly, also **FuDy-Y** displays a signal when used as a photoconductor (**Figure 3c**). After the light is switched off, the photocurrent decreases again, as expected. We now expected that the charge-separated state with the high-energy electron depicted in **Figure 3** can act as a donor state for initialization of further reactions.

Thus we selected a reagent with high electro negativity, and thus energetically low-lying acceptor orbitals, first: molecular oxygen O_2. For quantification of the resulting superoxide, a nitrotetrazolium blue essay (NBT) was applied.[203, 208] To exclude unintentional and direct excitation of the fullerenol head group (by absorption in the UV range), tests were performed with light-emitting diodes (LEDs) as the light source with wavelengths strictly above 400 nm (**Figure S4**). As only the absorption edges of **FuDy-Y** and **FuDy-B** correlate well with the LED, **FuDy-R** will not be considered in the following. As a reference and for further confirmation, anon-substituted fullerenol $C_{60}(OH)_{24}$[136] was used. All systems containing fullerenols produced superoxide over time (**Figure 4a**), but at the same concentration of the photocatalyst (c_{cat}), both **FuDy** species produce up to 700% more than the reference system. This result clearly demonstrates

the importance of the dye entities attached to the fullerene head and the charge separation process depicted in **Figure 3**. Higher superoxide production can, of course, be managed by increasing the concentration of the photocatalyst (**Figure 4b**). An interesting question is how a system behaves that contains two different photosystems/dyes like a leaf. Therefore, we combined **FuDy-B** and **FuDy-Y** under otherwise constant conditions. It does not make a difference if one uses a mixture of **FuDy-B** and **FuDy-Y** directly or combines aggregates of the two prepared in two separate vials. This can be understood by realizing that surfactant aggregates are highly dynamic systems in which molecules are rapidly exchanged.[209] If the two photosystems act independently from each other, one would not expect a significant change in superoxide production efficiency because the previous experiments have shown **FuDy-B** and **FuDy-Y** are almost equally effective (**Figure 4a,b**).

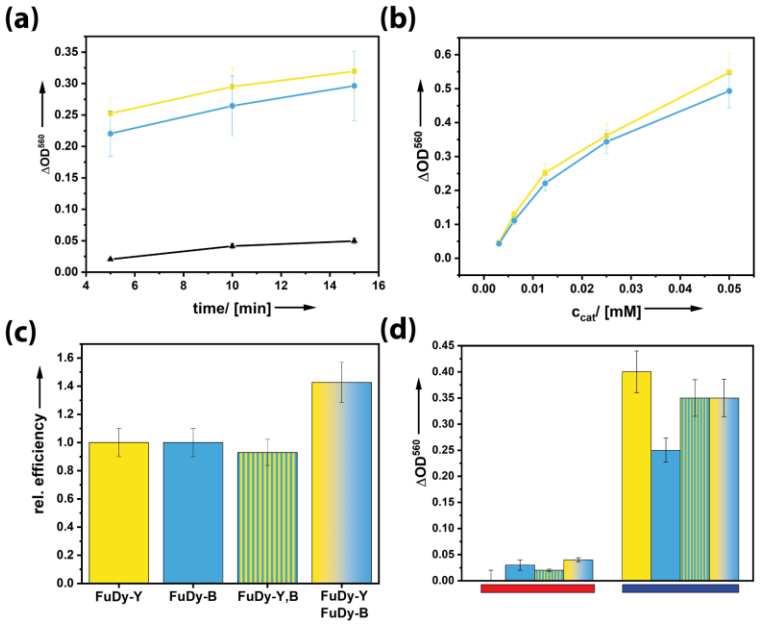

Figure 4. a–c) Results of the NBT assay for investigating the superoxide formation efficiency of different **FuDy** systems; $C_{60}(OH)_{24}$ (reference system): black; **FuDy-Y**: yellow; **FuDy-B**: blue, under white light irradiation. **a)** Superoxide formation over time for c_{cat}= 0.0125 mM. **b)** Concentration dependence; t = 5min. **c)** Comparison of the relative photocatalytic efficiencies of systems comprising only one type of dye with a mixture of **FuDy-B,Y** (gradient color) and a **FuDy** compound containing two dyes in one molecule, c_{cat}= 0.05 mM. **d)** Wavelength-dependent superoxide efficiency for irradiation with monochromatic light (red:630 nm, blue:450 nm) for c_{cat} = 0.05 mm.

However, we measured an efficiency increase of 40% (**Figure 4c**). To make sure that this increase is really due to an intermolecular, cooperative effect (as in the natural leaf), we prepared a new **FuDy** with two types of dye (yellow and toluidine blue) attached to the fullerenol head group in one molecule (**FuDy-B,Y**). The efficiency of this system is slightly lower than that of the pure **FuDy** (**Figure 4c**), but within the measurement error. We interpret our findings as follows. The

fullerenol head group can only host one electron transferred from one of the dye molecules attached to it, followed by superoxide formation. Therefore, attaching different types of dyes to one fullerenol head does not provide any advantages. However, it seems that the **FuDy** molecules can, in their self-assembled structures, transfer the photo excited electron to neighboring surfactants, which then leads to an overall increase in efficiency. Furthermore, the efficiency of superoxide production at different wavelengths was evaluated. **Figure 4d** shows that the **FuDy** systems, the combined as well as the mixed dyes, only produce little superoxide under irradiation at longer wavelengths whereas the efficiency tremendously increased under irradiation with blue light. As it was ensured that the fullerenol head group does not absorb in this region, this effect only derives from the absorption of the attached dyes into higher LUMOs, which then populate the charge-separated state. These findings indicate that all absorbed wavelengths take part in the generation of superoxide whereby especially the absorption of higher-energy photons leads to the charge-separated state. Again, the effect of an intermolecular electron transfer can be observed. The final, exciting question is whether the acceptor orbitals of CO_2 are also low enough in energy for undergoing the described photo reduction process. Thus the experiments were repeated with CO_2 instead of O_2. The results were evaluated by ^{1}H NMR spectroscopy (**Figure 5a**) and GC-MS. We clearly observed the generation of formic acid when **FuDy-B/FuDy-Y** was used as the photo catalyst. Formic acid can be formed by a two-electron two-proton reaction, which is likely to happen directly at the **FuDy's** head groups. **Figure 5b,c** shows a proposed mechanism for this process.[210] We assume that the general mechanism is similar to that of photo catalyzed superoxide production of fullerenes and fullerenols, in which the fullerenol is likely to transfer electrons.[108, 201, 203, 205] The reducibility of the fullerenol compound strongly depends on the degree of polyhydroxylation and the type of polyhydroxylation moieties and can vary between a slightly negative or a slightly positive potential, whereas a stronger reducibility derives from a larger p-electron stabilization.[71] An intramolecular charge transfer results in a reduction of the head group, whereas the charge is located at the C_{60} core as oxygen has a weak ability to accommodate radical electrons.[71] This fullerenol anion, according to the known literature mentioned above, can reduce, for example, carbon dioxide in a fast process to again enable the reduction of the fullerenol.

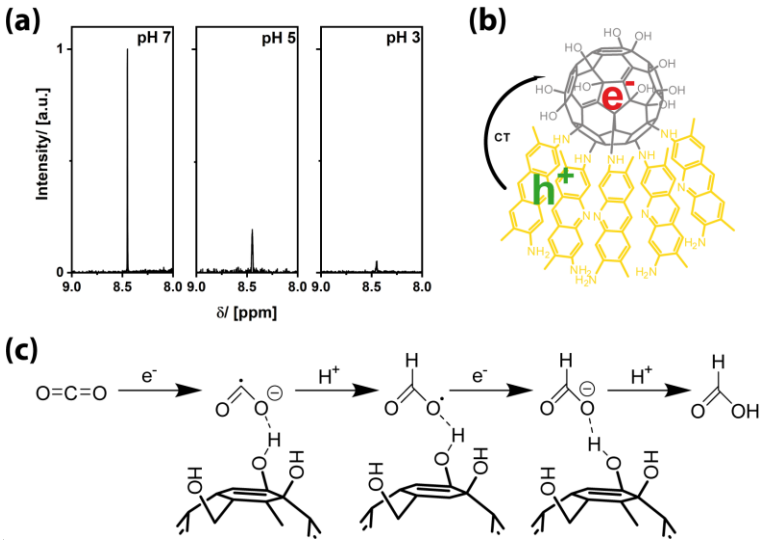

Figure 5. Photo reduction of carbon dioxide with a mixture of **FuDy-Y** and **FuDy-B** in aqueous solution. **a)** Excerpts of ^{1}-HNMR spectra for formic acid production from CO_2 at different pH values. **b)** Overall scheme for the **FuDy**-catalyzed reaction. **c)** Proposed mechanism for the photo reduction of CO_2 by the **FuDy** system (water molecules not shown).

The fullerenol head group is predestined for the coordination of, for example, carbon dioxide because of the multiple hydrogen binding sites. In a first step, carbon dioxide is reduced to yield the carbon dioxide radical anion. After protonation at the carbon atom, a fast second electron transfer has to take place, which emphasizes the importance of the intermolecular exciton transfer described before. Final protonation yields formic acid. No further reduction occurs according to GC-MS. Performing the reaction at different pH values shows that the highest yield of formic acid was achieved at pH 7, with decreasing efficiency with decreasing pH value. The yield of formic acid at pH 5 is only about 18 % of the value at pH 7, whereas at more acidic pH values, almost no formic acid is produced. At pH 7, the predominant species is HCO_3^-, which can obviously interact very well with the fullerenol surfactants.

8.3.4 Conclusion

The leaf is an unparalleled example for the “green” conversion of energy in the form of light into valuable products. Therefore, numerous attempts have been made in materials science to create systems with similar functionality. We have presented a new approach based on multifunctional surfactants. Inspired by literature on fullerene dyads and our own work on amphiphiles with fullerenol head groups, we have discussed surfactants with semiconductor properties. The compounds self-assemble into bilayer vesicle structures in solution and exhibit properties such as

charge separation of photo generated excitons. Intermolecular electron transfer takes place between surfactant fullerenol dyads covering different regions of the electromagnetic spectrum, thus fulfilling one key criterion of an artificial leaf. The chemical energy of the charge-separated states could be exploited to produce superoxide from oxygen and formic acid from carbon dioxide by irradiation with visible light in aqueous solution. The dependence of the efficiency on different parameters was evaluated, and a mechanism was proposed. Therefore, also the second criterion of an artificial leaf, the conversion of less valuable compounds (CO_2) into better products, has been realized. The current work extends not only the horizon of functional fullerene-based materials but also that of surfactant chemistry in general.

8.3.5 Supporting Information

Experimental part

The synthesis was performed according to a protocol by Kunkel *et al.*[149] For the synthesis of FuDy-Y,B a mixture of acridine yellow and toluidine blue was used instead of only one dye. This result is a statistic mixture. Additionally, to the protocol the compounds have been purified by HPLC (see Analytical methods).

The yield of the compounds is: FuDy-Y 60 %, FuDy-R 69 %, FuDy-B 45 %, FuDy-Y,B 38 %.

Characterization

FuDy-Y

^{1}H-^{13}C- CP MAS-NMR (100 MHz): δ (ppm) 176, 160, 133, 77, 56, 39, 15

ATR-IR: ν (cm^{-1}) = 3200, 2927, 2874, 2607, 1564, 1372, 1244, 989, 818

TGA: 40-192 °C 11 %; 192-550 °C 17 %; 550 °C+ 72 % → 20 +/- 2 OH

ESIMS: $[(OH)_8O_{12}C_{60}(C_{15}H_{14}N_3)_5]^+$ m/z = 2230.2 (2230.2); $[(OH)_4O_{17}C_{60}(C_{15}H_{14}N_3)_5]^-$ m/z = 2242.2 (2242.2)

FuDy-R

^{1}H-^{13}C- CP MAS-NMR (100 MHz): δ (ppm) 177, 160, 150, 137, 129, 101, 74, 57, 39, 18

ATR-IR: ν (cm^{-1}) = 3177, 2957, 2858, 1580, 1443, 1359, 1002

TGA: 40-180 °C 11 %; 180-575 °C 22 %; 575 °C+ 67 % → 21 +/-3 OH

ESIMS: $[(OH)_{17}O_4C_{60}(C_{15}H_{15}N_4)_5]^+$ m/z = 2330.3 (2330.3); $[(OH)_{17}O_3C_{60}(C_{15}H_{15}N_4)_5]^-$ m/z = 2314.3 (2314.3)

FuDy-B

^1H-^{13}C- CP MAS-NMR (100 MHz): δ (ppm) 176, 160, 133, 79, 57, 39, 15

ATR-IR: ν (cm^{-1}) = 3200, 2927, 2874, 1564, 1361, 1010

TGA: 40 – 200 °C 10%; 200-570 °C 21 %; 570 °C+ 69% → 20+/-3 OH

ESIMS: $[(OH)_{10}O_{11}C_{60}(C_{15}H_{16}N_3S)_5]^+$ m/z = 2418.6 (2418.6); $[(OH)_{16}O_4C_{60}(C_{15}H_{16}N_3S)_5]^-$ m/z = 2408.6 (2408.6)

FuDy-Y,B

ATR-IR: ν (cm^{-1}) = 3231, 2943, 2893, 1560, 1342, 1169, 1011

ESIMS: $[(OH)_{14}O_8C_{60}(C_{15}H_{14}N_4)_2(C_{15}H_{16}N_3S)_3]^+$ m/z = 2370.5 (2370.5)

Methods

General Methods

Synthesis that acquired inert gas atmosphere were performed using general Schlenk techniques under argon atmosphere. The solvents were dried according to standard literature and stored under argon. Water was deionized with Millipore Milli-Q. All starting materials used for synthesis were purchased from commercial sources unless stated differently. The fullerene C_{60} (pur. 99.9 %) was purchased from Research & Production Company "Modern Synthesis Technology".

Analytical Methods

Liquid chromatography was measured with Thermo Fisher Scientific Dionex 3000. As the column, Agilent Poroshell 120 EC-C18 (2.1×100 mm, 2.7µm) was used. MeCN (5%) as eluent A and 95% water as eluent B with 0.1% formic acid were used. A linear gradient of 5% A to 100% A was applied a flow rate of 0.3 mL/min. Mass spectra were measured on Bruker amazon SL respectively on Bruker microtof II system in pos. or neg. mode via direct inject from a methanolic solution. Assignment of peaks was done as follows: $[M - xH_2O - yH - zO - v(HNR)]^{a-/+}$. Molecular ion peak is identified in combination with results from TGA and NMR.

TGA was measured on Netzsch Jupiter STA 449 F3. All measurements were performed under nitrogen atmosphere with 80 mL/min flowrate and with heating rate of 5 K/min. MAS-NMR measurements were performed on Bruker Avance II 400 solid-state NMR at 295 or 350 K and with 10k Hz rotational speed. Number of scans 5k – 10k with D1 = 10 to 100 sec. NMR measurements (^{1}H, ^{13}C) were performed on a Varian INOVA 400 MHz spectrometer. Attenuated total reflection−infrared (ATR−IR) spectra were measured with a Perkin Elmer100 Spectrum spectrometer including an ATR unit. DLS measurements were done by using a Malvern Zen5600. Transmission electron microscopy (TEM) observations were carried out using Zeiss Libra120. For cryo transmission electron microscopy studies, a sample droplet of 2ul was put on a lacey carbon filmed copper grid (Science Services, Muenchen), which was hydrophilized by air plasma glow discharge unit (30s with 50W, Solarus 950, Gatan, Muenchen, Germany). Subsequently, most of the liquid was removed with blotting paper in a Leica EM GP (Wetzlar, Germany) grid plunge device, leaving a thin film stretched over the lace holes in the saturated water atmosphere of the environmental chamber. The specimens were instantly shock frozen by rapid immersion into liquid ethane cooled to approximately 97K by liquid nitrogen in the temperature-controlled freezing unit of the Leica EM GP. The temperature was monitored and kept constant in the chamber during all the sample preparation steps. The specimen was inserted into a cryotransfer holder (CT3500, Gatan, Muenchen, Germany) and transferred. Surface tension measurements were performed at Krüss K100.

Photosensor measurements were performed on 3 mm×3 mm sensor substrates from Umweltsensortechnik and measured with a Zahner IM6 potentiostat. Measurements in solution were performed in a folded capillary cell. UV/Vis absorption spectra were acquired using an Agilent Cary 60 spectrometer. PL spectra were obtained from a PicoQuant FluoTime-300 spectrometer. Geometry optimization and frontier orbital calculation was performed using Density-Functional Theory (DFT) with the TURBOMOLE Program Package for ab initio Electronic Structure Calculations using B3LYP/def2-TZVP level of theory. TURBOMOLE V7.1, a development of University of Karlsruhe and Forschungszentrum Karlsruhe GmbH, 1989-2007, TURBOMOLE GmbH, since 2007; available from http://www.turbomole.com.

NBT assay

0.5 mM NBT and 0.05/0.025/0.0125/0.0061 mM FuDy in Milli-Q were irradiated for 5/10/15 min with 100 W white LED (see Fig. S3). The difference in absorbance was measured at 560 nm versus blank sample.

CO_2 conversion

5mM aqueous solution (pH 7, pH 5 and pH 3) of FuDy-Y,B has been saturated with 100% CO_2 gas. The vessel was sealed and irradiated with 100 W white LED (see Fig. S3). Formic acid was detected with ^{1}H-NMR. 0.1 M solution of ascorbate was added as electron donor.

Figure S1. Molecular structure of FuDy-compounds.

(a) Lewis-structures.

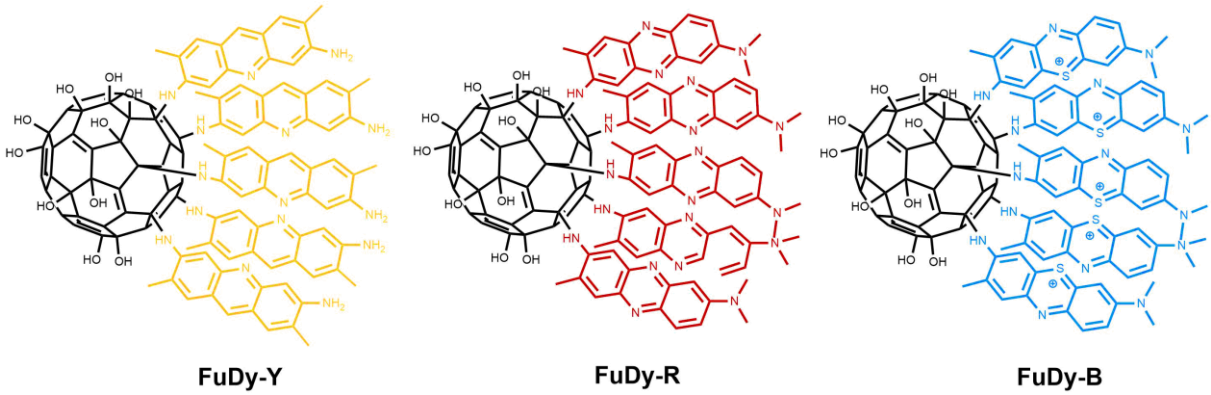

(b) Calculated molecular geometry and electrostatic potential maps.

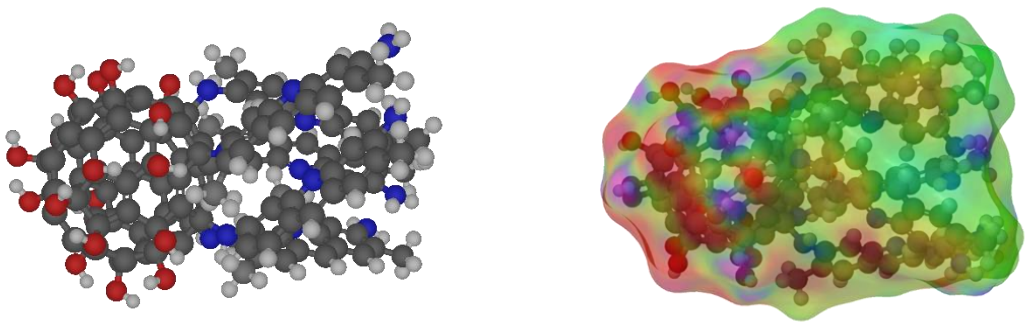

FuDy-Y

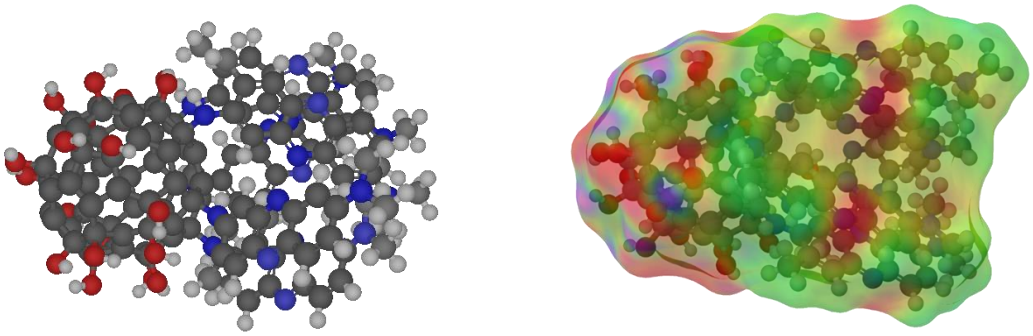

FuDy-R

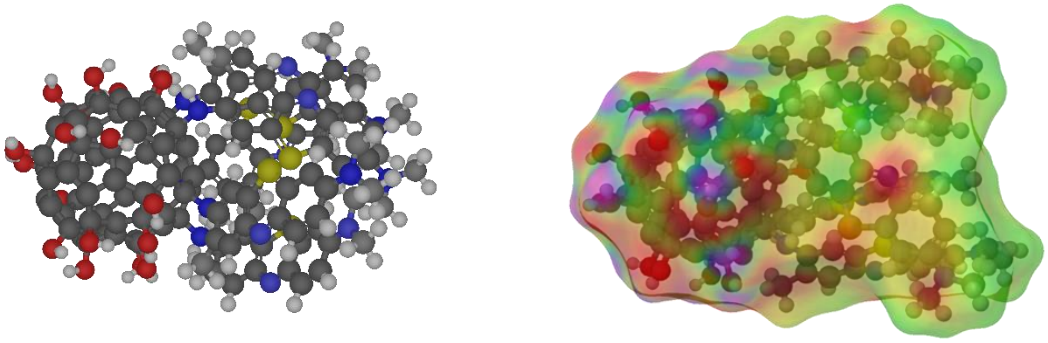

FUDY-B

Figure S2. Cryo-TEM investigation of FuDy-Y aggregates in solution.

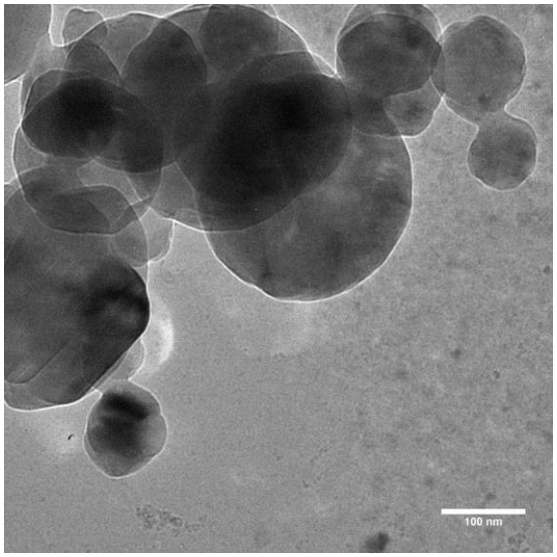

Figure S3. Photophysical characterization of **FuDy** compounds.

(a) Quantitative adsorption spectra.

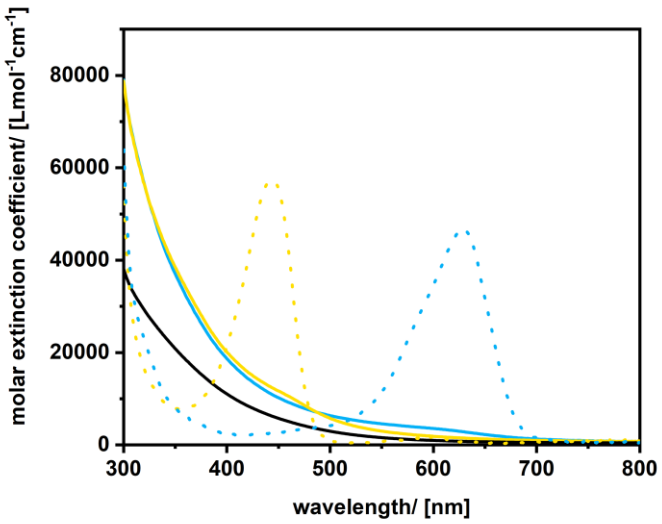

yellow dotted = yellow-G, blue dotted = toluidine blue, black = $C_{60}(OH)_{24}$, yellow line = **FuDy-Y**, blue line = **FuDy-B**.

(b) PL spectra.

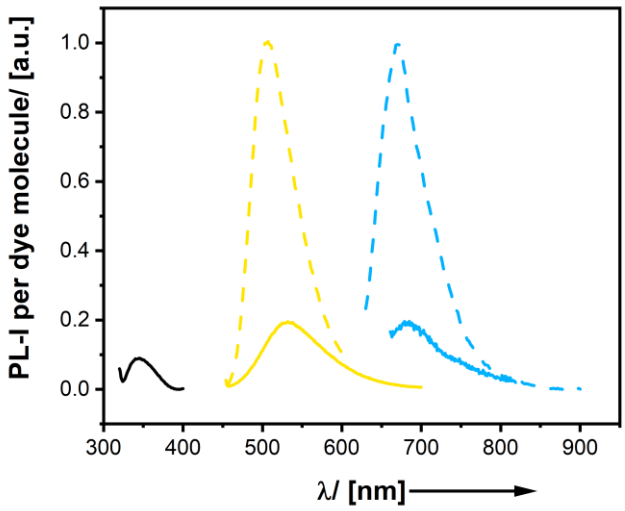

yellow dashed = yellow-G, blue dashed = toluidine blue, black = $C_{60}(OH)_{24}$, yellow line = **FuDy-Y**, blue line = **FuDy-B**.

(c) PESA

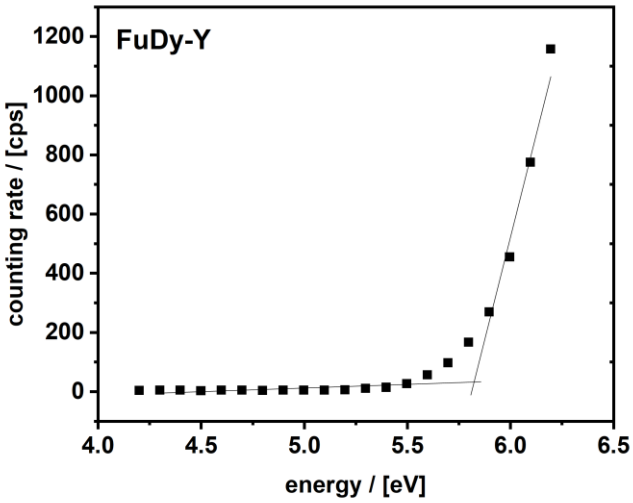
FuDy-Y
counting rate / [cps]
energy / [eV]
1200
1000
800
600
400
200
0
4.0
4.5
5.0
5.5
6.0
6.5

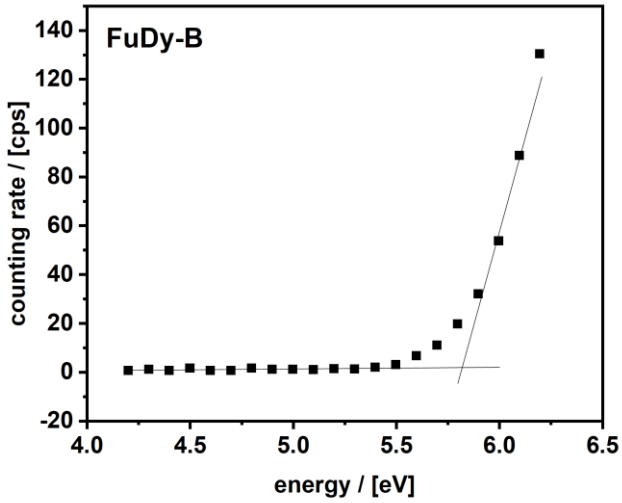
FuDy-B
counting rate / [cps]
energy / [eV]
140
120
100
80
60
40
20
0
-20
4.0
4.5
5.0
5.5
6.0
6.5

(d) fluorescence lifetime

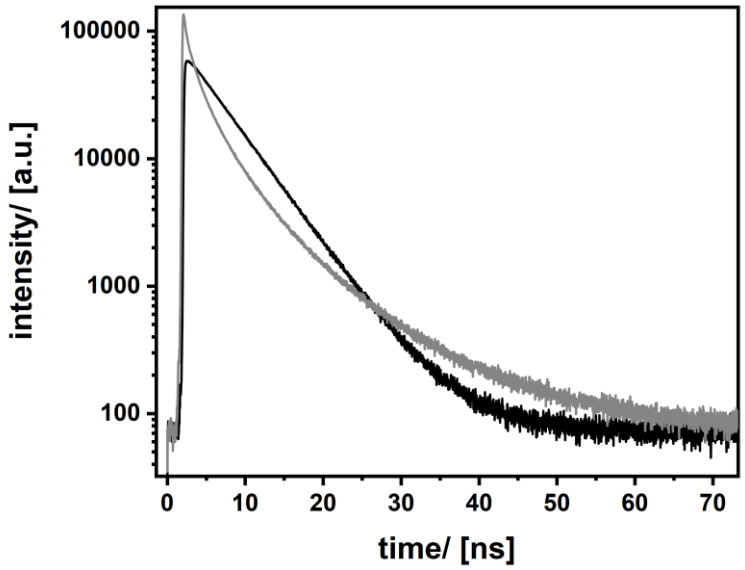

Figure S4. Spectrum of the white LED used for the photochemical reactions.

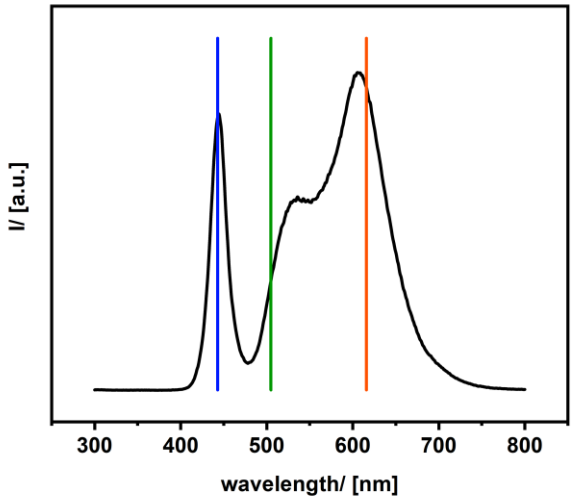

The vertical bars show the position of the absorption maxima of the dyes used in the current study.

8.4 Publication IV:

Aggregation-Induced Improvement of Catalytic Activity by Inner-Aggregate Electronic Communication of Metal-Fullerene-Based Surfactants,
ChemCatChem 2020

Marius Kunkel, Stefan Bitter, Frank Sailer, Rainer F. Winter and Sebastian Polarz*

Abstract: *A paradigm for active constituents in (homogeneous) catalysis is that optimum performance requires maximum dispersion. Generally, aggregation results in a decline. This is a different case in supramolecular catalysis. A new concept based on surfactants equipped with functional heads is presented, which becomes a more active catalyst itself upon aggregation. The head group of the surfactants is composed of a diethylenetriamine-functionalized fullerene capable of coordinating to catalytically active metals like* Co^{II}*. The improvement of catalytic properties upon aggregation is demonstrated via electrocatalytic water-splitting reaction as a model system. Detailed electrochemistry studies were performed at concentrations below and above the critical aggregation concentration (cac). While isolated surfactant molecules represent only moderately active catalysts, drastic improvement of efficiency in the hydrogen evolution (HER) as well as in the oxygen evolution reactions (OER) were detected, once vesicular structures have formed. Self-organization of the surfactants leads to an increase in turnover frequencies of up to 1300% (HER). The strongly beneficial effect of aggregation arises from the favorable alignment of individual molecules, thus, facilitating intermolecular charge transfer processes in the vesicles.*

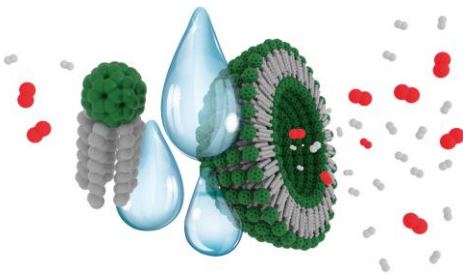

TOC figure of publication 4. Reproduced. Reproduced under the Creative Commons Attribution License.

8.4.1 Record of Contribution

Material synthesis, characterization and data interpretation was performed by M. Kunkel. S. Bitter and Rainer F. Winter assisted M. Kunkel with the electrochemical measurements. F. Sailer developed the syntheses under the supervision of M. Kunkel. M. Kunkel designed the research and M. Kunkel and S. Polarz wrote the manuscript. All authors have given approval to the final version of the manuscript.

8.4.2 Introduction

In many cases, aggregation is seen as a major drawback for catalytic reactions since upon aggregation the number of accessible reactive centers is reduced and a maximum of dispersion, especially for heterogeneous systems was the goal to achieve. Research perspective changed and systems have been developed in which aggregation comes hand in hand with beneficial effects. The field of self-assembled compounds, the supramolecular chemistry gives rise to supramolecular catalysis. In micellar catalysis, the formation of aggregates is used to perform reactions at their interface with compounds that would otherwise not be combinable. It is also possible to use solvents that would normally not be suitable for such reaction. These aggregates can be formed by supporting compounds that do not take place in the reaction themselves or by the catalyst molecule.[4, 98, 211] The phrase supramolecular catalysis is manly known from reactions with enzymatic systems which can catalyze reaction via weak interactions within their structural motif. Furthermore, this field describes the assembly of small-molecule organic catalysts.[212, 213] This very assembly of the catalyst influences the reactants in a way that reactive moieties are exposed and activated, intermediates or transition states are stabilized or that the reactivity is enhanced by increasing the local concentration of the reactants.[214-216] In this work, we present a new concept of supramolecular catalysis that does not influence the reactant's properties but the catalyst itself. This is achieved by a catalytically active surfactant. Surfactants are molecular compounds with amphiphilic properties, which form well-defined aggregates. Depending on concentration, individual surfactant molecules self-assemble into micelles, vesicles or liquid crystals. Recently, more and more papers describe advanced surfactants with properties beyond simple amphiphilic properties.[2, 217] Our group has specialized in the synthesis of surfactants equipped with functional, metal-containing head groups,[5, 94, 97, 218] and several examples of catalytically active surfactants have already been published by us.[4, 98] Important preliminary work of relevance to the current work

is centered on fullerene-based surfactants that evaluated their self-assembly behavior and the related beneficial effect of self-assembly on their properties.[99, 149, 176] For our supramolecular catalyst system electrocatalytic water splitting was chosen as a model system as a rather simple electron transfer reaction regarding intermediates and transition state species that is well observable. For water splitting, huge efforts during the last decades were taken in exploring and developing different realizations of the water splitting reaction, resulting in H2 (hydrogen evolution reaction; HER) and O_2 (oxygen evolution reaction; OER).[219-221] A lot of heterogeneous and homogeneous systems have been evaluated. In the field of homogeneous systems mostly rare earth and transition metal complexes are used and groups have developed and tailored the systems to achieve low over potentials and high turnover frequencies (TOF).[222-228] The turnover frequency, one factor that defines the efficiency of a catalytic system ranges from several to several thousand per second for reported systems. A special challenge for such systems is the performance in pure aqueous system being stable as well as active. Catalytic systems of different facets with nickel, cobalt, copper and more are known to literature.[229-235] Although we do not want to compete with established systems we chose to combine a water soluble surfactant system with controlled self-assembly to enhance its catalytically activity via aggregation presenting a new way of improving such systems.

8.4.3 Results and Discussion

In the current work, we aim at developing a system, which is equipped with moieties that are capable of effecting electrocatalytic water splitting,[229, 236] but with a fullerene-based surfactant design. Particular focus is on the role of self-assembly on catalytic activity.

The major synthesis steps leading to our target system are depicted in **Figure 1a**. The asymmetrical, pentachlorinated C_{60} (**1**)[121] is reacted with dodecylamine to obtain the penta-alkylated compound (**2**). Diethylenetriamine is then attached to the remaining hemisphere to obtain the ligand modified species (3). It is used as a ligand for complexation of cobalt(II)chloride to obtain the final product (4) (see Supporting Information for detailed synthesis procedure and characterization, Figure S1). Figure 1b,c shows the characteristic signals for the organic ligand before (3) and after coordination to cobalt (4) in electrospray ionization time of flight mass spectrometry (ESI-TOF MS) data of characteristic signals for the organic ligand before (3) and after coordination to cobalt (4). Successful coordination of Co(II) ions was also proven by UV/Vis spectroscopy, which, in addition

to the absorption of the fullerene core, showed the d-d transition band of a Co(II) triamine chelate with a maximum at 480 nm (**Figure S1**).

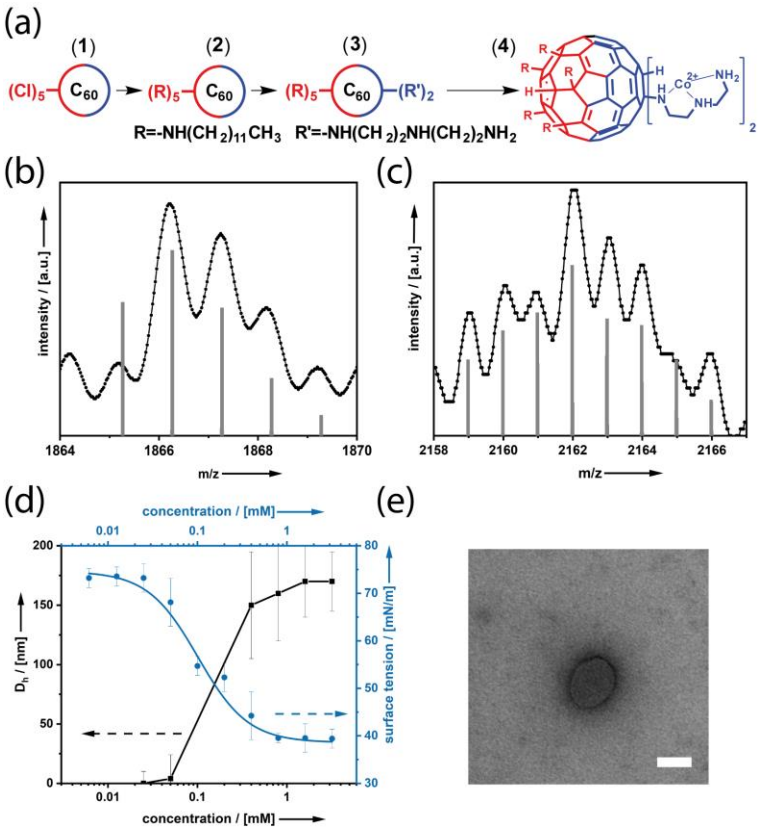

Figure 1. (a) Synthesis scheme for amphiphilic metal-fullerene-based catalyst (**4**). (b) ESI-TOF MS data of the organic ligand (**3**; black dots) and simulation of the molecular ion peak [M]-(H^+)+(H_2O) = 1866.23 g/mol (grey bars) and (c) of the surfactant (**4**; black dots) and simulation of the molecular ion peak [M]+(Cl^-)+(H_2O) = 2161.98 g/mol (grey bars). (d) Concentration-dependent aggregate size (black) and surface tension (blue). (e) TEM micrograph of a vesicle formed by (**4**) above the *cac*; scalebar = 100 nm.

The amphiphilic properties of (**4**) were investigated by recording concentration dependent surface tension γ(c). The corresponding plot shows a shape, (see **Figure 1d**), which is typical for surfactants. The minimal surface tension reached is about 39 mN/m. The position of the kink in the γ(c) curve indicates that aggregation commences at a concentration *cac* of approximately 0.2 mM. Aggregation has also been confirmed by dynamic light scattering (DLS). The aggregate sizes determined from DLS are shown in **Figure 1d**. There were no aggregates found at low concentration, and above *cac* aggregates with a hydrodynamic diameter D_H = 150 nm (**Figure S2)** appear. Analysis of these aggregates using transmission electron microscopy (TEM; **Figure 1e**) confirms that surfactant (**4**) forms hollow, bilayer vesicular structures rather than micelles. In these

aggregates the polar metal-fullerene complex, which serves as head group to the surfactant, align side by side at the outside of the bilayer. This general structuration was reported before for fullerene-based surfactants.[99, 176] That this alignment is indeed the case a zetapotential measurement was performed. The measurement shows a high positive potential of +60 mV confirming this circumstance. As a prototype reaction, electrocatalytic water splitting was used and the influence of catalyst self-assembly on the catalytic activity was evaluated with cyclic voltammetry (CV). First studies were performed at concentrations distinctly below *cac* as the reference state at a threshold concentration of a 0.025 mM of (**4**) in aqueous solution (pH = 7) (**Figure 2)**. The pure organic compound (**3**) is, as expected, catalytically inactive. The redox behavior of the solution in the presence of the Co-containing surfactant (**4**) is significantly different. There are strongly increased currents at onset potentials of $\eta_{0.5}$ = +1940 mV for OER and $\eta_{0.5}$ = -740 mV for HER at j = 0.5 mA/cm^2, which are both accompanied by strong gas formation. The voltammogram of (**4**) displays a partially reversible reduction signal at a E_{max} = +20 mV, which is a feature belonging to the fullerene-based ligand. Furthermore, it contains an oxidation at E_{max} = +1600 mV which can be assigned to the Co(II) to Co(III) oxidation, which features indirect reversibility.

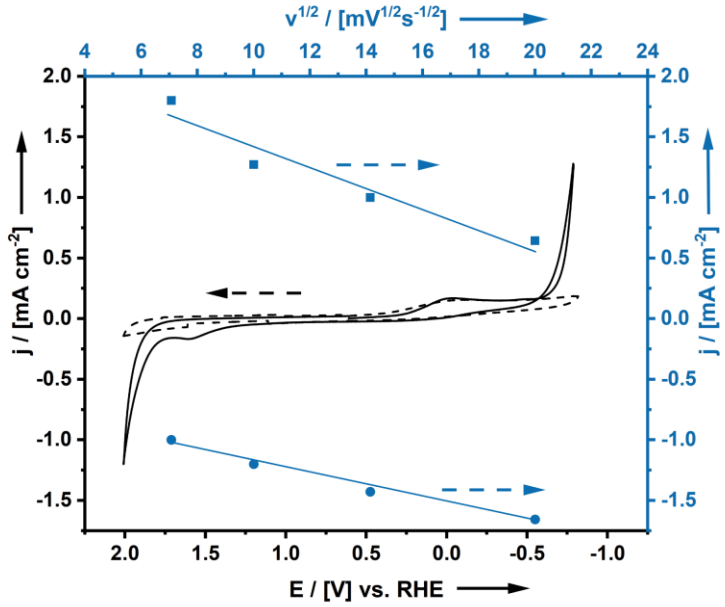

Figure 2. CV measurement (black) and Randles-Sevcik plot (blue; OER = circles; HER = squares of (**4**) at 0.025 mM compared to the CV of the organic ligand (**3**; dashed line).

Current densities remain unchanged on repetitive cycling, thus confirming that the homogeneous catalyst (**4**) is the catalytically active species and no decomposition product like colloidal cobalt. X-ray spectroscopy (EDX) coupled scanning electron microscopy (SEM) analysis revealed that no cobalt is precipitated on the electrode for (**4**) (**Figure S3**). The surface of the electrode is clean with absolutely no Co-containing residues caused by adsorption of the catalysis or decomposition. In particular, metallic Co nanoparticles cannot be found anywhere. As a reference experiment, analogous experiments using a $CoCl_2$ in solution have been perdormed (**Figure S3a**). Not only could we not see comparable electrocatalytic activity, but also the electrode is now covered by Co-nanoparticles. Furthermore, repetitive cycling of $CoCl_2$ shows several changes of the system over time. In essence, it can be excluded that any other compound than the metal-surfactant is responsible for the electrocatalytic activity. In order to quantify the catalyst´s properties in more detail, the turnover frequency was calculated, assuming a pseudo-first-order catalytic model (see Supporting Information **equation 1**, **Figure S4**).[233, 237-240] Evaluation of the data results in $TOF(OER)_{2000mV} = 57\pm10\ s^{-1}$ and $TOF(HER)_{800mV} = 25\pm10\ s^{-1}$, which indicates a medium activity compared to other electrocatalysts known to literature ranging from several to a maximum of several thousand per second.[229-235] The Randles-Sevcik plot depicted in **Figure 2** shows a linear increase of the current density with the square root of the scan rate *v* for OER, indicating a diffusion controlled process. However, the value of current density for HER decreases with increasing *v*, which indicates that the catalytic process is kinetically slow giving rise to the assumption that the fullerene ligand is involved in the reaction. As the cyclic voltammograms of (**4**) do not show a wave for cobalt(II) to cobalt(I) reduction, which would be expected at approximately -400 mV versus RHE, but solely a ligand reduction. This is consistent with the fullerene-DETA ligand acting as a non-innocent ligand similar to the work presented by Thompson *et al.* or Haddad *et al.*[232, 241, 242] Different from the mentioned literature the ligand is not likely to be protonated and is not catalytically active alone, excluding a metal-assisted ligand-centered as well as a only ligand-centered mechanism. It is more likely to be a metal-centered mechanism supported by the ligand. While the reaction takes place at the cobalt itself, the fullerene-DETA acts as electron reservoir for the reaction with the fullerene being an efficient electron mediator as reported for a nickel complex (**Figure S5a**).[243] The release of water from the initial complex results in the catalytically active species. The fullerene-DETA ligand is reduced in a one electron reduction, followed by the coordination of a proton to the metal center. A further reduction is followed by the reaction with a proton to release hydrogen. The detailed mechanism needs to be further evaluated with

calculations. The mechanism for OER follows another pathway. According to the presence of the cobalt oxidation wave the mechanism might feature a Co(IV) intermediate (**Figure S5b**).[124, 244]

The central issue of this work is unravelling the dependency of the catalytic properties on the level of aggregation. Consequently, we performed analogous electrochemical investigations at various concentrations, including c > *cac* and a threshold concentration of 0.8 mM aqueous solution of (**4**) at which the defined vesicular aggregates are present (**Figure 3a**).

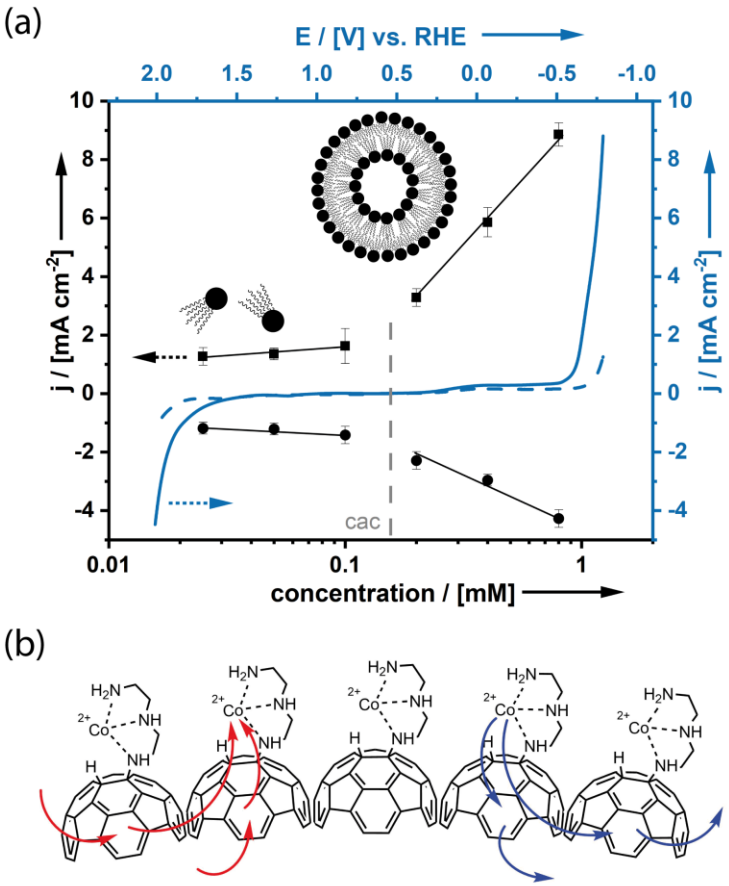

Figure 3. (a) Concentration-dependency of current density (black) for OER (circles) and HER (squares) below (left) and above (right) the *cac*. The grey dashed line marks the *cac*, when single surfactant molecules (left) assemble to vesicular aggregates (right). Linear sweep measurements (blue) of surfactant (**4**) below (0.025 mM) (dashed line) and above (0.8mM) (solid line) *cac*. (b) Scheme showing the molecular structure of the vesicle surface and the proposed intra- and intermolecular charge transfer processes; (red arrows: reduction process; blue arrows: oxidation process).

As long as the surfactant concentration remains below *cac*, there is only an insignificant change in OER and HER-related current density at 2000 mV and -800 mV, respectively (**Figure 3a blue**). However, **Figure 3a (black)** displays that the concentration dependent current density increases tremendously stronger above the c < *cac* than below. Whereas, the systems showed to be a medium

active catalyst at 0.025 mM concentration, the concentration increase does not improve the system's activity a lot. The catalytic process seems to be rather ineffective. But after eventually reaching the *cac*, the situation changes. The system's performance instantly showed a drastic increase which continues with further increasing concentration. Speaking in numbers, doubling the concentration below the *cac* only results in an increase in current density by factor 1.1 whereas, doubling the concentration above the *cac* increases the current density by almost factor 2. This leads also in a change in turnover frequency. For concentrations above the *cac* the turnover frequency at -800 mV increases from 25 ±10 s^{-1} to 346 ±10 s^{-1} (**Equation 1**, **Figure S6**). This observed increase of 1300 % compared to the turnover frequency determined for c < *cac* obviously correlates with the self-assembly of the surfactant into vesicles (**Figure 1d,e**). This result is very astonishing considering that, in general, the mobility and accessibility of the catalytic centers should be lower in the aggregates, and, accordingly, activity should rather decrease or at the most remain constant at c > *cac*. Aqueous solution of fullerene based vesicles do not behave like nanoparticle systems[245, 246] since a vesicle is a rather dynamic and permeable system. During the reaction, solvent molecules, reactant and product molecules can diffuse in and out the vesicular aggregate therefore, the number of accessible molecules for the reaction is not lowered but there is obviously an effect on the catalyst molecule upon aggregation. In addition to the turnover frequency, also the onset potential for OER decreases from $\eta_{0.5}$ = +1940 mV to $\eta_{0.5}$ = +1720 mV, while the onset potential for HER shifts from $\eta_{0.5}$ = -740 to $\eta_{0.5}$ = -540 mV (**Figure 3a**; **Figure S6**). The observed effect of enhanced catalytic activity can only be explained, if there is a cooperative effect between the individual surfactant molecules within the aggregate (**Figure 3b**). In fact, a change in the electronic situation upon aggregation can be observed. The emission of the single molecule diminishes completely upon reaching the *cac* when the system is excited at the fullerene core, but a new, heavily red shifted and broadened emission appears, that can be assigned to the aggregate state (**Figure S7**).

For the electron transfer reaction, our hypothesis (**Figure 3b**) is, that the vicinity and distinct orientation of the surfactant molecules with respect to each other in vesicle wall renders electron transfer from the ligand to the reactant more efficient and allows for intermolecular charge transfer processes in the aggregates. Intermolecular charge transfer is thus held responsible for improving electrocatalytic activity of the surfactant aggregates with respect that of dispersed surfactant molecules. If this hypothesis is correct, one would expect that a diminishing content of molecules

(**4**) in the vesicle walls should also decrease its catalytic activity. It is known that sodium dodecyl sulfate (SDS) can also form vesicular structures[247, 248] and it is totally inactive in the water splitting reaction. We therefore tried to use SDS as a co-surfactant in a mixture with surfactant (**4**); see **Figure 4 insert**. According to DLS, no SDS micelles are present in such mixtures and the size of the vesicles (D_H = 143nm) changes only insignificantly with respect to pure (**4**) (**Figure S8a**). Upon adding SDS to the catalytic system, the current at +2000 mV and -800 mV is lowered by approximately 30% (see **Figure 4)**. This interpretation is also in line with the observed anodic shift of the onset potential of 45 mV for OER and a cathodic shift of 40 mV for HER (**Figure S8b**). In the mixed aggregates fewer molecules (**4**) are adjacent to each other and, therefore, intermolecular electronic communication as initiated by aggregation is rendered less efficient.

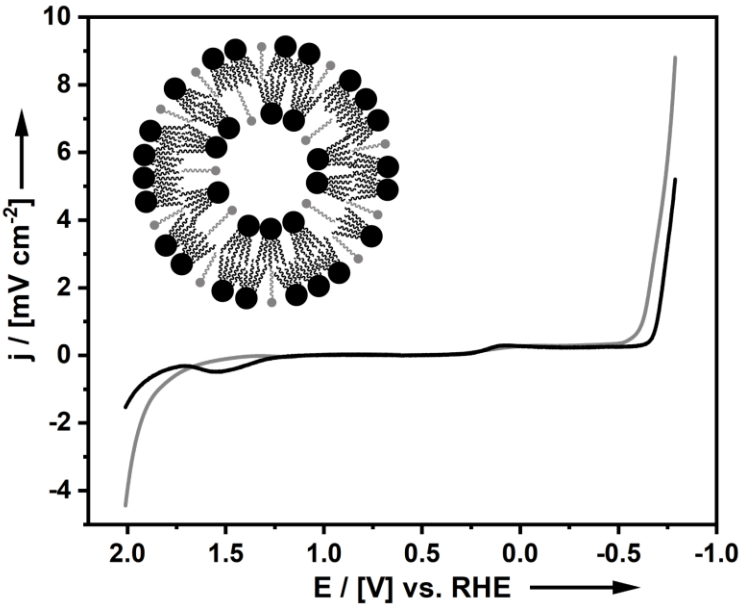

Figure 4. CV of (**4**) at c = 0.8 mM (grey) as a reference compare to the (**4**)/SDS mixed aggreagtes (black). Insert shows schematic illustration of a vesicle of (**4**; black) diluted with SDS (grey).

8.4.4 Conclusion

Supramolecular catalysis give rise to new catalytic systems. In this work, we were able to show that aggregation of a surfactant based catalyst leads to a beneficial feature for electron transfer reactions like water splitting reaction as a model system and increase system's performance. We present an amphiphilic cobalt-fullerene catalyst, which at concentrations below its *cac* shows an

only medium catalytic activity in OER and HER at neutral pH in aqueous solution. The compound´s catalytic activity, especially for HER increases tremendously at concentrations above *cac*, at which vesicular aggregates form. The onset potentials and current densities are improved and the turnover frequency increases by up to 1300 %. Aggregation allows for intermolecular electron transfer and improves electronic communication within the system, leading to more efficient water splitting.

8.4.5 Supporting Information

Synthesis and characterization

Synthesis of $C_{60}Cl_6$

C_{60} (0.28 mmol) was dissolved in chlorobenzene (11 mL) and sonicated for 5 min. Iodine monochloride (6.95 mmol) was added in one shot, and the solvent was evaporated as fast as possible. The crude product was further purified by column chromatography (silica gel, eluent: toluene). $C_{60}Cl_6$ is obtained as a red solid (0.2 mmol, 70%) and used without further characterization.

Synthesis of $C_{60}H(NC_{12}H_{26})_5$

$C_{60}Cl_6$ (0.2 mmol) was dissolved in chloroform (50 mL) and vigorously stirred. Dodecylamine (2 mmol) and NEt3 (0.2 mL) were added. The mixture was stirred for 12 h. The crude product was precipitated with cold methanol, filtrated and washed several times with methanol. The crude product was then dissolved in ethyl acetate. The solvent was evaporated, and the crude product was further purified by column chromatography (silica gel, eluent: toluene/EE). The title compound is obtained as a red solid (0.17 mmol, 60%).

IR (powder): 3285, 2920, 2851, 1770, 1658, 1570, 1466, 1316, 1115 cm^{-1}; ^1H NMR (400 MHz, $CDCl_3$): δ 0.89 (t, ^3J = 7.2 Hz, 15H), 1.27 (m, 90H), 1.45 (m, 10H), 1.67 (m, 10H), 3.22 (m, 5H) ^{13}C NMR (100 MHz, $CDCl_3$): δ 14.2, 22.56, 27.57, 27.67, 29.56, 29.58, 29.91, 29.93, 30.95, 31.02, 32.11, 47.36, 47.87, 47.88, 66.02, 68.21, 69.35, 143.24, 143.31, 143.71, 143.81, 143.83, 143.84, 143.84, 143.88, 144.02, 144.08, 144.31, 144.47, 144.51, 144.53, 144.91, 145.43, 147.16,

147.21, 147.23, 147.29, 147.62, 148.02, 148.21, 148.33, 148.57, 148.71, 149.12, 150.81, 153.88, 155.31; MS (MALDI): 1641.1 $[M - H^+]^-$ (1641.03)

Synthesis of $(H_{12}N_3C_4)_2C_{60}H(NC_{12}H_{26})_5$

$C_{60}H(NC_{12}H_{26})_5$ (0.12 mmol) was suspended in diethylenetriamine and stirred at 65 °C for 3 days. The crude product was precipitated with cold ethyl acetate and filtrated. The filtrate was washed several times with acetone to remove remaining diethylenetriamine. The product was extracted from the filter with methanol. Solvent was evaporated to obtain (H12N3C4)3C60H(NC12H26)5 as a brown solid (0.036 mmol, 30 %)

IR (powder): 3296, 2923, 2846, 1646, 1588, 1447, 1351, 1274, 1113 cm^{-1}; ^1H NMR (400 MHz, MeOD): δ 0.92 (t, ^3J = 7.2 Hz, 15H), 1.31 (m, 100H), 1.67 (m, 10H), 2.90 (m, 12H). 3.03 (m, 10H), 3.22 (m, 5H), 6.99 (s, 1H), 7.20 (s, 1H), 7.25 (s, 1H); ^{13}C NMR (200 MHz, MeOD): δ 14.5, 23.8, 25.25, 25.8, 30.5, 30.8, 31.7, 33.1, 38.1, 38.9, 39.4, 39.5, 39.6, 40.8, 41.2, 41.9, 42.7, 43.6, 43.7, 44.7, 46.5, 49.2, 50.4, 51.2, 51.5, 63.4, 65.7, 78.1, 127.7, 127.8, 128.5, 129.4, 129.5, 130.5, 144.9, 154.7, 156.9, 159.3, 162.5, 162.6, 162.8, 162.9,163,164.3,164.5, 164.7; MS (ESI): 1866.23 $[M - H^+ + H_2O]^-$ (1866.37)

Synthesis of $(H_{12}N_3C_4\text{-}CoCl_2)_2C_{60}H(NC_{12}H_{26})_5$

$(H_{12}N_3C_4)_2C_{60}H(NC_{12}H_{26})_5$ (0.1 mmol) was dissolved in methanol and $CoCl_2$ (0.4 mmol) was added. The mixture was stirred overnight. The product was precipitated with acetone, filtrated and washed with acetone to remove remaining $CoCl_2$. The product was extracted from the filtrate by dissolving in water. The solvent was evaporated to obtain a green-brown solid (80%).

IR (powder):3368, 3227, 2923, 2853, 2052,1608, 1447 1348, 1290, 1017; MS: (ESI): 2161.99 $[M + Cl^- + H_2O]^-$ (2161.98)

Methods

The synthesis that acquired inert gas atmosphere was performed using general Schlenk techniques under argon atmosphere. The solvents were dried according to the standard literature and stored under argon. Water was deionized with Millipore Milli-Q. All starting materials used for the synthesis were purchased from commercial sources unless stated differently. The fullerene C_{60} (pur. 99.5 %) was purchased from Research & Production Company "Modern Synthesis Technology".

Analytical Methods

Attenuated total reflection–infrared (ATR–IR) spectra were measured with a Perkin Elmer 100 Spectrum spectrometer including an ATR unit.

NMR measurements (1H, 13C) were performed on a Bruker Avance III 400 MHz spectrometer or on Bruker AVANCE Neo 800 MHz.

MALDI-MS measurements were performed using a Bruker Microflex MALDI-TOF. The samples were prepared in a cyano-4-hydroxycinnamic acid matrix or a trans-2-[3-(4-tert-butylphenyl)-2-methyl-2-propenylidene]malononitrile matrix.

ESI mass spectra were recorded on a Bruker microTOF focus II mass spectrometer in negative mode with water as solvent.

UV/Vis absorption spectra were acquired using an Agilent Cary 60 spectrometer.

Dynamic light scattering measurements were performed by using a Malvern Zen5600.

The surface tension measurements were performed using Krüss K100 with a manual dilution series. Additionally, surface tension measurements were performed with capillary method.

Transmission electron microscopy observations were carried out using Zeiss Libra120.

Cyclic voltammetry measurements

CV measurements were conducted using a three-neck electrochemical cell. Electrochemical data were acquired with a computer-controlled BASi CV50 potentiostat.

Cyclic voltammetry measurements were performed in aqueous solution at pH 7 with 0.1 M potassium nitrate as electrolyte. As working electrode a glassy carbon electrode with 0.07 cm^2 was

used, as counter electrode a platinum wire electrode and as reference electrode, saturated Ag/AgCl was used. The reference electrode was regenerated after every measuring segment. The pH value was controlled after every measurement segment and adjusted if needed. Every measurement was at least performed 3 times to ensure reproducibility. The used data represent an average value of the data. The working electrode was rinsed with distillated water after every measurement segment.

In the manuscript. the measured potentials vs. Ag/AgCl were converted to the reversible hydrogen electrode (RHE) scale according to the Nernst equation:

$E_{RHE} = E_{Ag/AgCl} + 0.059*pH + E^0_{Ag/AgCl}$

with E_{RHE} ist he converted potential vs. RHE, $E^0_{Ag/AgCl}$ = 0.1976 at 25°C and $E_{Ag/AgCl}$ is the experimentally measured potential against Ag/AgCl reference.

Preparation of mixed aggregates

For the preparation of mixed aggregates of the catalyst and SDS 1 eq of SDS was added to a solution of the catalyst in water. The mixture was stirred for 2 h.

Calculation of K_{obs}

K_{obs} was calculated from equation 1. J_c is the catalytic current density at 1400/-1400 mV, j_p is the non-catalytic peak current taken from the cobalt(II) to cobalt(III) oxidation respectively from the ligand reduction. N values the number of electrons in the reaction. R is the ideal gas constant. T is taken at 298.15 K. F is Faraday's constant and v is the scan rate. For the calculation the slope of j_c/j_p versus $v^{-1/2}$ was used.

Equation 1

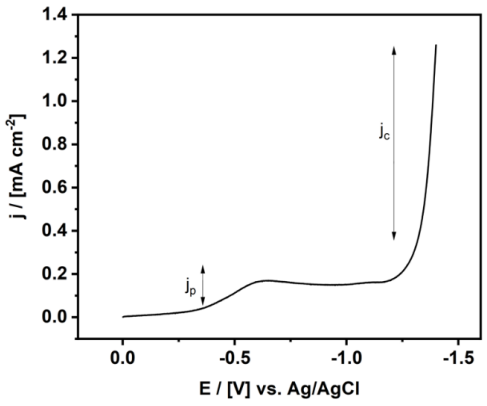

$$\frac{j_c}{j_p} = \frac{n}{0.446}\sqrt{\frac{RTk_{obs}}{Fv}}$$

Supporting figures

Figure S1 Molecular characterization of compound (**4**).

(a) Infrared spectrum of the catalyst (**4**).

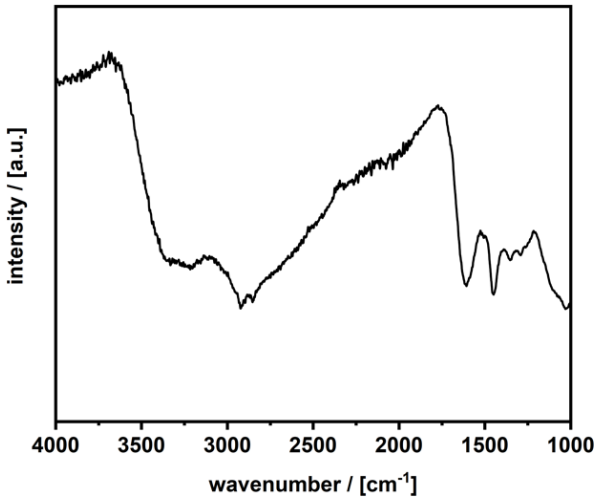

(b) UV/Vis spectrum of the catalyst (**4**) (grey) and (**3**) (black).

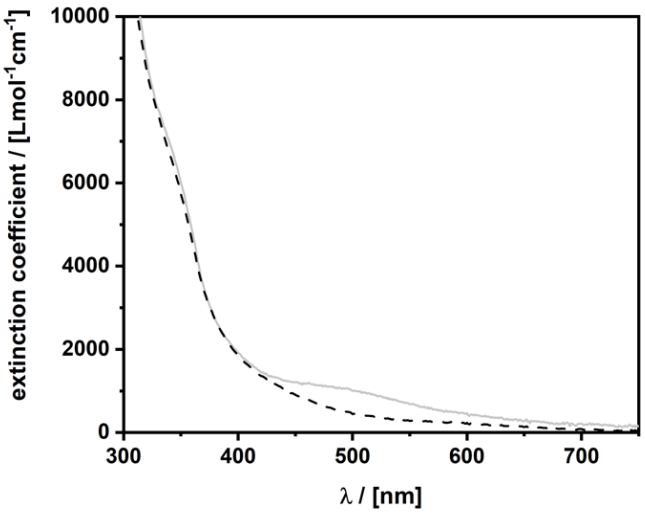

(c) Photograph of a 0.8 mM solution of (**4**).

(d) ESI-MS spectrum of (**4**) in negative mode.

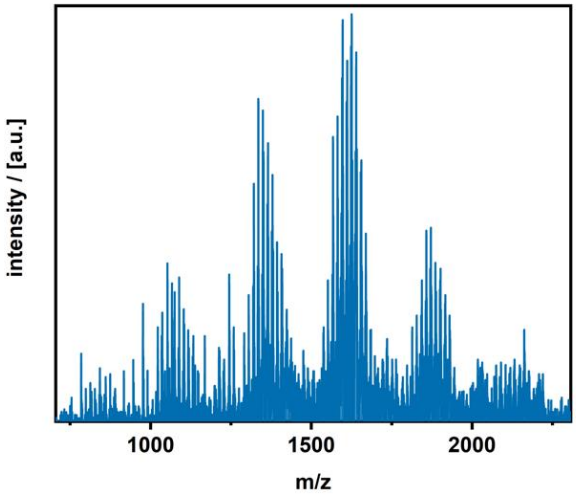

(e) Zoom-in version of ESI-MS spectrum of (**4**) in negative mode.

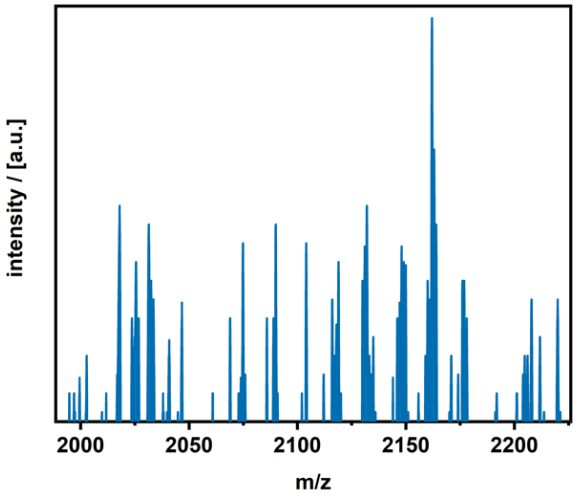

Figure S2 Characterization of surfactant properties of compound (**4**).

(a) Aggregate size distribution derived from DLS-data at a surfactant concentration of 0.8 mM.

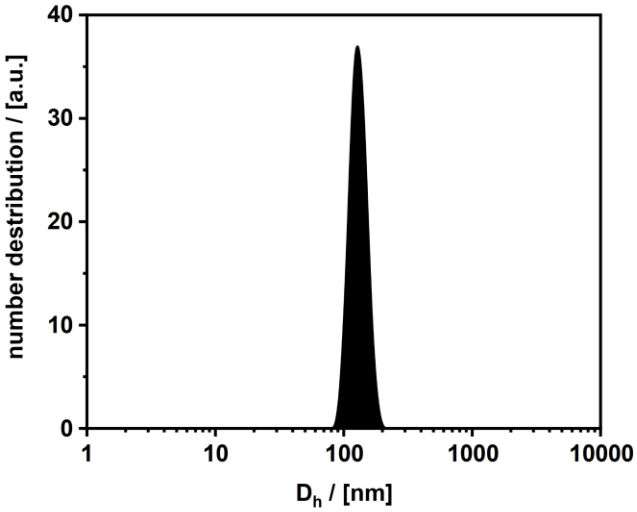

Figure S3 Stability studies for catalyst system (**4**) and $CoCl_2$ as comparison at 0.8 mM, 1.6 mM respectively.

(a) Cyclic voltammogram after repetitive cycling of (4) with 100 cycles with 100 mV/s.

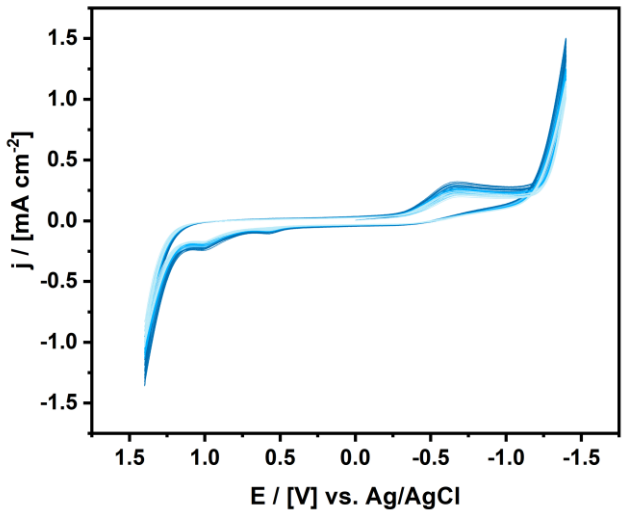

(b) Cyclic voltammogram after repetitive cycling of a $CoCl_2$ solution with 100 cycles with 100 mV/s.

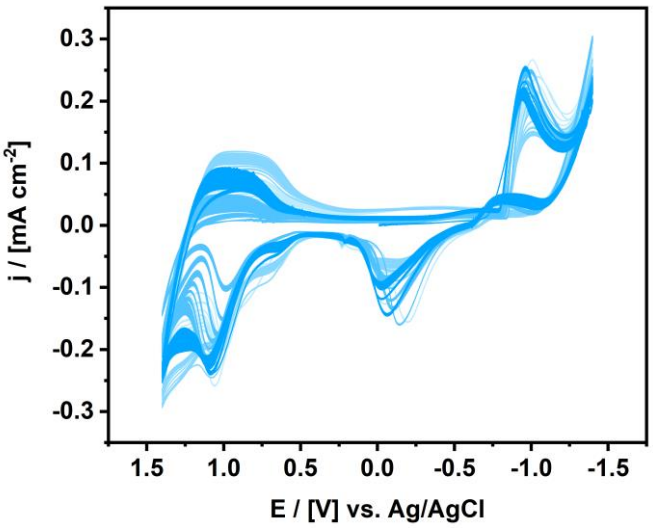

SEM micrographs of electrodes after repetitive cycling (grey: carbon, green: fluorine, yellow: chlorine, blue: cobalt)

(c) Micrograph of electrode tip after repetitive cycling with CoCl2 1.6 mM as reference. The electrode was rinsed with water. Scalebar 500 µm.

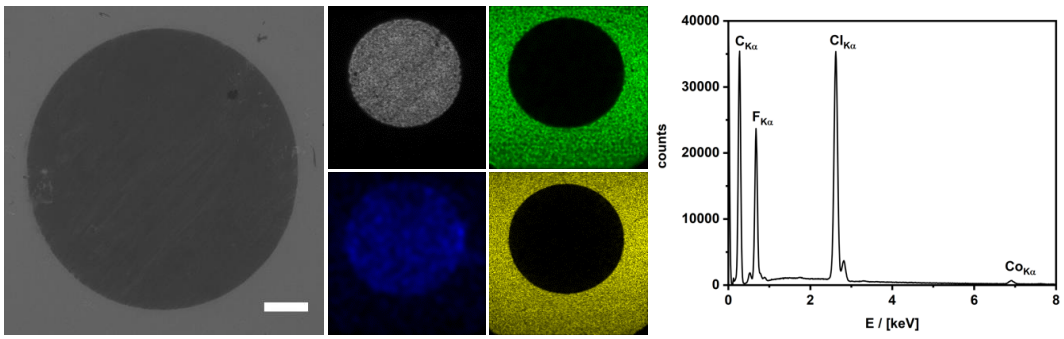

(d) Micrograph of electrode tip after repetitive cycling with compound (4) 0.8 mM. The electrode was rinsed with water. Scalebar 500 µm.

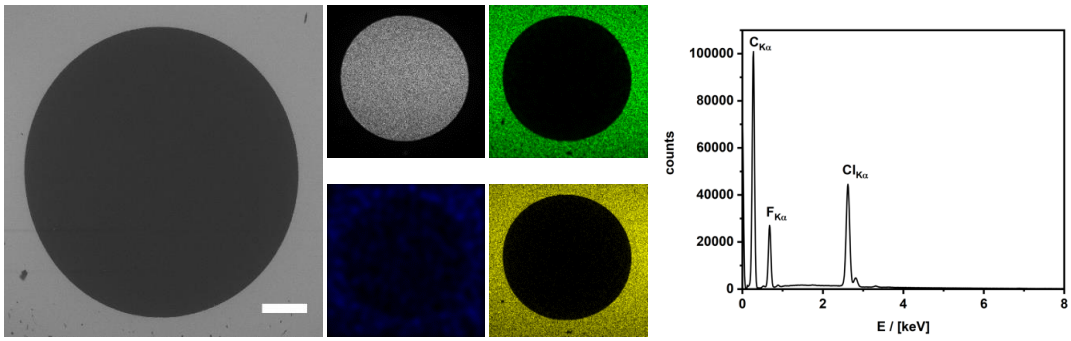

Figure S4. Electrochemical studies performed for compound (**4**) as an electrocatalyst below the cac. J_c is the catalytic current density at 1400/-1400 mV vs Ag/AgCl, j_p is the non-catalytic peak current taken from the cobalt(II) to cobalt(III) oxidation respectively from the ligand reduction.

(a) Plot j_c/j_p versus $v^{-1/2}$ for OER (0.025 mM).

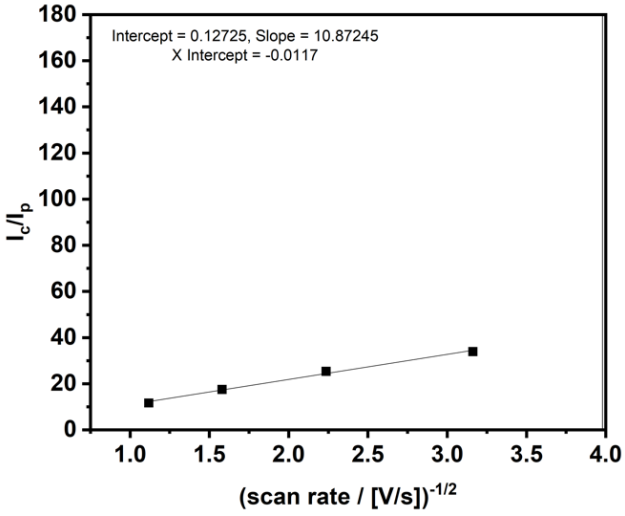

(b) Plot j_c/j_p versus $v^{-1/2}$ for HER (0.025 mM).

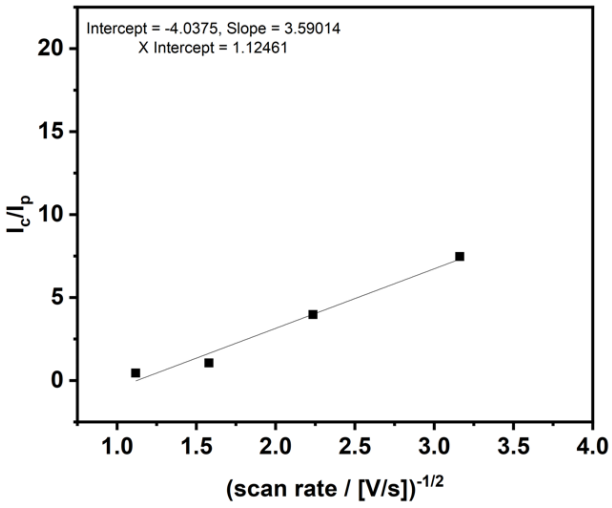

(c) Cyclic voltammograms of the catalyst below the CAC at 0.025 mM at different scan rates with absolute current versus potential (vs Ag/AgCl).

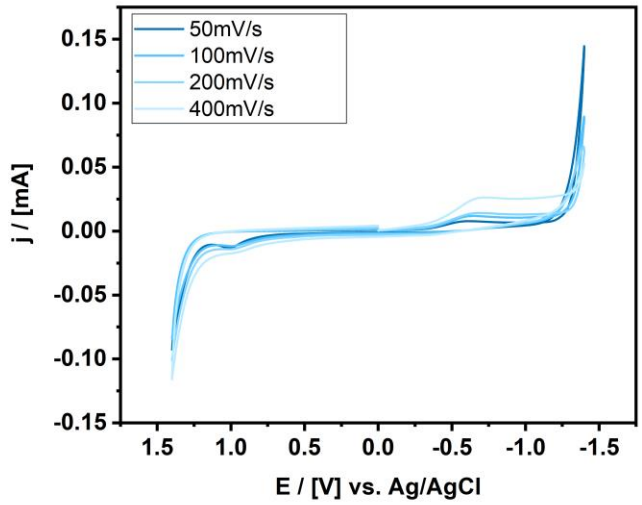

Figure S5. Proposed mechanism for HER and OER.

(a) Proposed mechanism for HER.

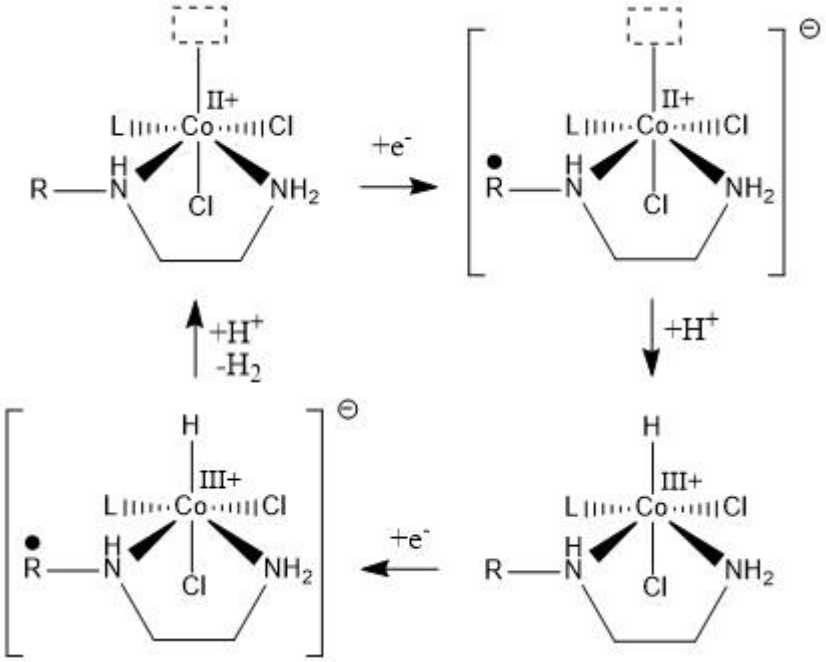

(b) Proposed mechanism for OER

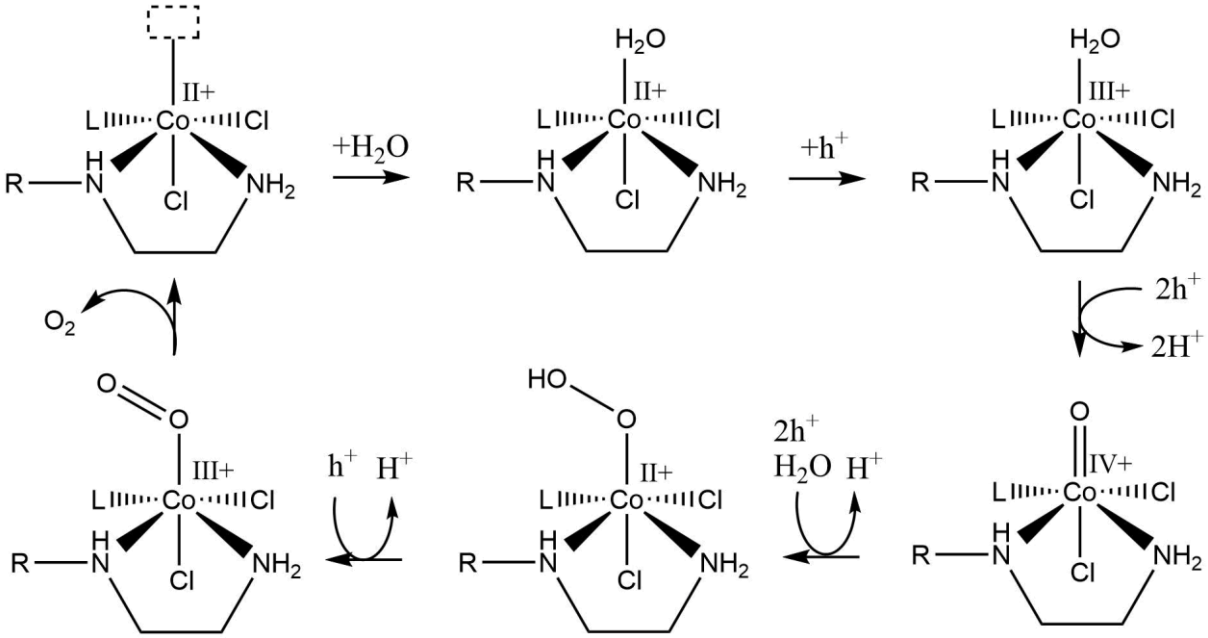

Figure S6. Electrochemical studies performed for compound (**4**) as an electrocatalyst above the cac (0.8mM and 0.4 mM). J_c is the catalytic current density at 1400/-1400 mV vs Ag/AgCl, j_p is the non-catalytic peak current taken from the cobalt(II) to cobalt(III) oxidation respectively from the ligand reduction.

(a) j_c/j_p versus $v^{-1/2}$ for HER (0.8mM).

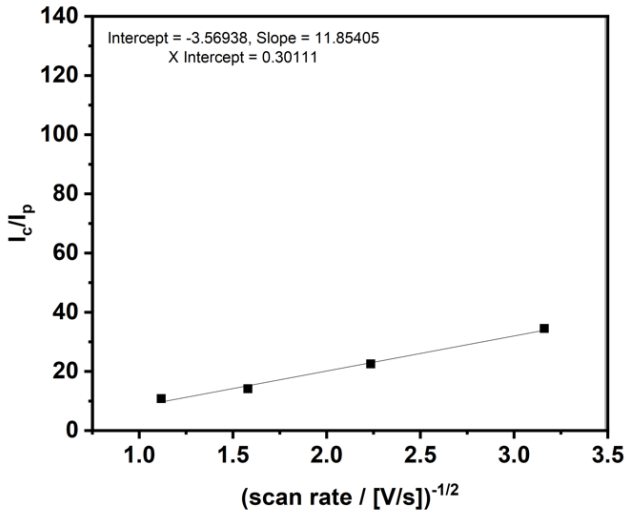

(b) j_c/j_p versus $v^{-1/2}$ for OER (0.8mM).

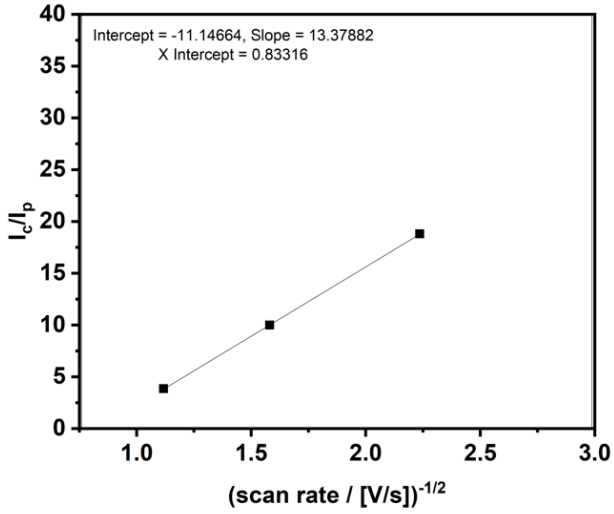

(c) Cyclic voltammograms of the catalyst above the cac at different scan rates (0.8mM) with absolute current versus potential (vs Ag/AgCl).

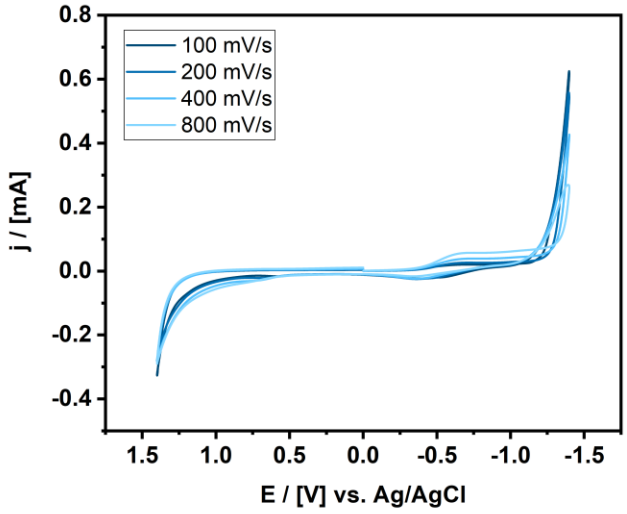

(d) j_c/j_p versus $v^{-1/2}$ for HER (0.4mM).

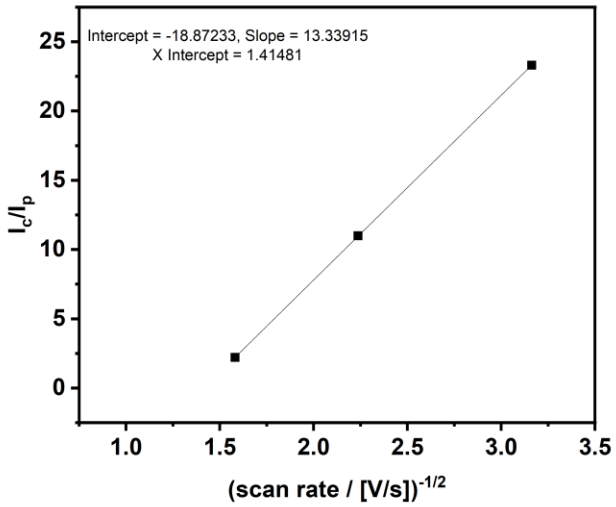

(e) Cyclic voltammograms of the catalyst above the cac at different scan rates (0.4mM) with absolute current versus potential (vs Ag/AgCl).

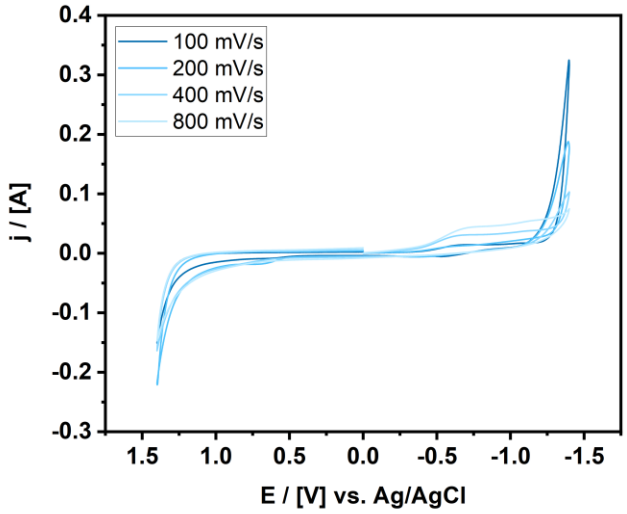

Figure S7. Change in electronic situation of the system in dependence of concentration.

Emission spectra of (**4**) below (line) and above (dashed) the cac with an excitation wavelength of 300 nm.

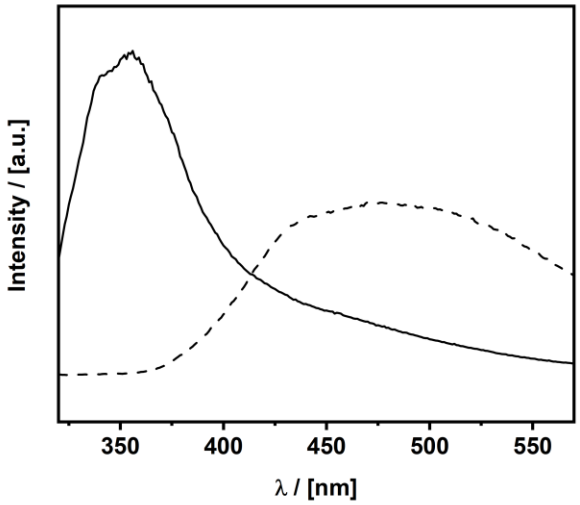

Figure S8. SDS - surfactant (**4**) co-aggregates.

(a) Aggregate size distribution derived from DLS data.

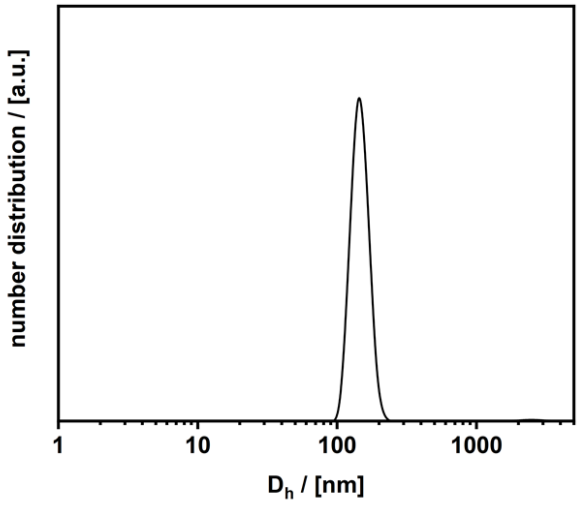

(b) Cyclic voltammograms of the catalyst at 0.8 mM with SDS as additive.

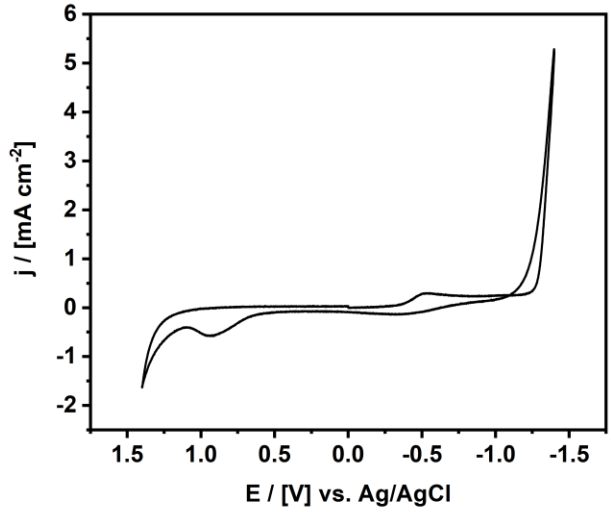

9 Conclusion and Outlook

Amphiphilic molecules are not only part of our everyday life but also play a crucial role in biological and material science. With their versatility in properties and application they proved to be a high tech nano material. Research is going on to improve the properties of amphiphiles and to find new fields of application. One rare aspect of these efforts is the focus of this thesis - the combination of amphiphilic features with intrinsic properties of its building blocks. The building block of choice was the fullerene. Fullerenes possess unique electronic and optoelectronic properties and have been subject of research for around 40 years. Nevertheless, using the fullerenes properties in aqueous solution still remains challenging. Facing this challenge leads to new fields of research and expands the horizon of fullerene chemistry.

The presented thesis focused on the development of amphiphilic fullerenes that obtain a beneficial effect by forming superstructures. For this purpose, new fullerene derivatives have been established that controllably form defined aggregates in solution and that are equipped with an intrinsic functionality. The published results of this work can be distinguished into three main aspects. In the first part, a new structural motif for fullerene-based surfactants was developed. The resulting compounds were evaluated for the beneficial effect of amphiphilicity in direct comparison with non-amphiphilic fullerenol. The second part deals with the advancement of the previously established system regarding intrinsic properties and self-assembly. In addition to the fullerene as electron mediator, electron donor units were added to the surfactant resulting in a supramolecular semiconductor which was evaluated as photocatalytic reducing agent. The third part deals with the direct effect of self-assembly on electron transfer reactions evaluated with a prototype metal-fullerene surfactant in electrocatalytic water splitting as model system.

In the first publication (Chapter 8.1) we presented biocompatible, fullerene based, surfactants that could be incorporated into living cells to be used as antioxidative agent. Inside the cells it could function as membrane guard.[99] The fullerene-based surfactants have a newly developed structural motif. The fullerene is substituted in a janus-like fashion. One hemisphere bears five alkyl chains as hydrophobic unit of the surfactant, whereas the other hemisphere bears hydroxyl moieties. The compounds form stable vesicular aggregates in aqueous solution with a monodisperse size distribution and they are medium surface active. Interestingly,

their extremely low critical aggregation concentration in the milimolar range does not correlate with the surface tension as it would be expected for a common surfactant. Aggregates are formed before the surface is saturated due to the unfavored formation of a Gibbs monolayer. In *ex vivo* experiments the fullerenol head group showed great activity as antioxidative agent against the biologically relevant reactive oxygen species superoxide. It was outperforming its' non-amphiphilic equivalent and reference antioxidants. Furthermore, the use of these compounds in biological systems was evaluated. The surfactants proofed their biocompatibility with eukaryotic and prokaryotic cells, being harmless towards the cells, even at high concentrations. In cellular systems the surfactants showed potent antioxidative properties for superoxide, hydroxyl radicals, hydrogen peroxide and oxonitrite. Incorporated into the cells, where it is expected that the surfactants arrange in the cell membrane due to their amphiphilic nature, it could be demonstrated that the compounds are able to protect the cell against internally produced radical cell stress. **Within this publication we could not only present a new structural motif for fullerene based surfactants but we could also show that the intrinsic antioxidative properties of fullerenols is enhanced by a janus-like amphiphilic structure. Additionally, the amphiphilic structure enabled the distribution into and in the cells as well as the incorporation into cell membranes.**

Based on this system more complex derivatives with further focus on transferring intrinsic properties to the aggregate state should be generated. To achieve this, a new synthesis strategy needed to be developed. **This new synthetic route was presented in the second publication (Chapter 8.2) with various example compounds.**[149] A versatile one-pot synthesis strategy via phase transfer reaction enables the simultaneous janus-like modification of the fullerene. One hemisphere is polyhydroxylized and the other hemisphere is modified with selectively five substituents. The scope of the reaction is so far limited to primary amines but is applicable from aliphatic to aromatic amines. Additionally, it was shown that it is possible to use primary amines with further functionalities like carbonic acids or ethylenes. Furthermore, several analytical methods were presented to characterize these compounds, ranging from solid state magic angle nuclear magnetic resonance to thermogravimetric measurements and infrared spectroscopy. **It could be shown that this easy to perform one-pot synthesis enables the synthesis of a broad variety of janus-like fullerenol surfactants.**

This new synthetic procedure was eventually used to generate a more complex fullerenol surfactant possessing linear dye molecules instead of alkyl chains. **The resulting molecular semiconductor**

system was presented in publication 3 (Chapter 8.3).[176] Being a molecular semiconductor the compounds produced a charge separated state upon irradiation with visible light. The resulting chemical energy of the charge separated state could be used for catalytic reduction reactions in solution. This feature was evaluated by reducing molecular oxygen to superoxide. It was observed that the intrinsic property of the molecules, being a molecular semiconductor, was transferred to the aggregates. An inter- and inner-aggregate electron transfers could be observed. This phenomenon was further tested with carbon dioxide which could be reduced to acetate in aqueous solution. **We presented a new kind of artificial leaf which consists of an arrangement of molecular semiconductors forming strong electronic communication within the aggregates. Chemical energy, produced by irradiating the system could selectively be harvested.**

The effect of inter- and inner-aggregate electron transfers was further evaluated in publication 4 (Chapter 8.4). A prototype based on the previously established systems was developed to show the direct beneficial effect of self-assembly on catalytic electron transfer reactions.[249] As a model system the electrocatalytic water splitting reaction was chosen. A closer look has been taken on the comparison between properties below the critical aggregation concentration, at which no aggregates are present, and concentrations above this concentration. It could be shown that aggregates lead to a drastically enhanced electronic communication within the aggregates influencing the properties as catalyst. The catalytic performance could be enhanced reaching the critical aggregation concentration. **We could present a new kind of supramolecular catalyst that improves its intrinsic properties upon aggregation. Self-assembly was identified as potent tool to improve electron mediated reactions.**

In summary, this thesis presented for the first time the self-assembly related properties of janus-like fullerene surfactants. It could be shown that the fullerene as head group of the surfactant could be adapted to diverse electron transfer reactions like as antioxidant, oxidant or electro catalyst, by varying the attached moieties. This fullerene surfactant acted as electron mediator in catalytic reactions whereas, this property is heavily related to the compounds self-assembly. The defined and controllable self-assembly leads not only to new areas of application but also enhances the electronic communication within the system. This has a direct impact on the compound's performance in catalytic reactions in which the performance can be improved. With this work it could be shown that the two worlds, electron transfer reactions and aggregation, can be combined

in a beneficial way. **Fullerenes proofed to be suitable model system due to their modifiability and their electronic properties.**

Future perspectives of this project are discussed under two different aspects, the evaluation of self-assembly and evaluation of the self-assembly related enhancements. As a key feature, the unconventional self-assembly of fullerene-based surfactants should be evaluated in further detail. It is proven that fullerene surfactants of various structures, like the conical fullerene amphiphiles presented by Nakamura, as well as the fullerene surfactants presented in this thesis form spherical aggregates in aqueous solution at extremely low concentrations and that their surface activity behaves differently compared to normal surfactants. Nevertheless, the stability and the forming behavior of the aggregates is not well understood yet. As shown in this thesis, the aggregates play a crucial role in the usage of self-assembly related enhancements, it is desired to further tune the aggregates to their purpose. In a first step, the variation of the standard fullerenol surfactant presented in publication 1 would be useful to understand the influence of the chain number and length, as well as the head groups size and polarity on the self-assembly. First results of changing the head groups polarity have been already presented in this publication with interesting results. This approach could be further followed by adapting the fullerenol as head group. As presented in Chapter 4, there are various structures and substitution patterns that exist for fullerenols with different moieties. Adapting these moieties changes the polarity of the head group as well as the interaction in between the head groups in the aggregate. This will tune not only the aggregate size and the aggregation concentration, but also the stability of the aggregates. On the other hand, changing the length of the attached alkyl chains is expected to only have a medium influence on the self-assembly using chains with 6 to 16 carbon atoms. The fact that five chains are attached will yield a conical structure for any chain length with a suitable hydrophobicity. A greater influence is expected when changing the number of chains to one, two or eight (easy substitution patterns to achieve) in total. This will drastically change the packing parameter, as well as the HLB value. Therefore, it is expected that the appearance of the aggregates is changed. Especially, lowering the number of chains could be interesting since this should also reduce the general size of the aggregates and it could even be possible to obtain micellar structures. This leads to the second aspect that needs to be discussed - the phenomenon of self-assembly related enhancement of catalytic reactions. In publication 3 and 4 it could be shown that aggregation of fullerene surfactants leads to an enhanced electronic communication within the system related to the spatial closeness of the fullerene head groups. It is expected that size and nature of the aggregates influences this

aspect, but this needs to be further evaluated. So far, this phenomenon was evaluated regarding the reaction type with two different types, a photocatalytic and an electrocatalytic reaction. There are plenty of further possibilities. This is a more than promising playground for future research projects and some inspiration shall be presented here. Due to the versatility of the system, which was established in this thesis, it can easily be adapted to various reaction types. A fullerenol head group for fullerene surfactants was presented that combines the electronic properties of the fullerene with water solubility. It could be shown that this system is capable of undergoing catalytic electron transfer reactions with oxygen as well as the reduction of carbon dioxide. An important feature of this head group is the ability to coordinate various compounds to its surface due to the adaptable fullerenol moieties via e.g. multiple hydrogen bonds. The spatial closeness to the reaction center enables and facilitates catalytic reactions. This system has not yet reached its limits regarding electron transfer reactions in aqueous solution but especially regarding its modifiability. Publication 2 presented an easy synthesis to obtain manifold derivatives by changing the hydrophobic chains. In publication 3 it was shown that also more complex molecules than alkylchains can be combined with this system. Dye molecules were added as visible light antennas and electron donors. This concept can be further advanced. Molecules with different intrinsic properties could be added e.g. further reactive centers for catalytic reactions. This would give the possibility to catalyze several reactions with one compound. Besides the fullerenol head group a metal fullerene head group was established to evaluate the direct effect of self-assembly on its catalytic properties. Since the results were very promising, further effort should be taken into this research aspect. It could be shown that this system is a new supramolecular catalyst changing its properties upon aggregation. Although the concept was evaluated, further experiment should be conducted to evaluate the underlying mechanism in detail. This includes theoretical calculations for the change in electronic situation. With this knowledge, the properties can be further tuned and the system can be improved to compete with established catalytic systems. This concept should also be tested for different catalytic reactions also in the field of micellar catalysis. The versatility of the presented system enables easy variation of the used ligands and metals. Having a building kit in hand derivatives can be synthesized that can easily be adapted to common cross coupling or polymerization reactions, in which it is expected to have influence on the catalytic cycle. The current metal fullerene surfactant contains two amine ligands chelating cobalt ions. The ligand itself is suggested to be an electronic bridge between the metal and the fullerene. This ligand can be exchanged by ligand further changing the electronic situation with electron rich or electron poor

ligands. The metal ion can be chosen freely in respect of the ligand. This system gives rise to a new kind of supramolecular catalysts with manifold possibilities.

10 Zusammenfassung und Ausblick

Amphiphile Moleküle sind nicht nur Bestandteil unseres Alltags, sondern spielen auch eine entscheidende Rolle in den Bio- und Materialwissenschaften. Mit ihren vielen verschiedenen Eigenschaften und Anwendungsgebieten haben sie sich als hightech Nanomaterial etabliert. Es wird viel geforscht, um die Eigenschaften dieser Amphiphile zu verbessern und neue Anwendungsgebiete zu erschließen. Ein eher seltener Aspekt dieser Anstrengungen ist Bestandteil dieser Arbeit – die Kombination aus amphiphilem Charakter und intrinsischen Eigenschaften der Moleküle selbst. Das Molekül, um das es in dieser Arbeit geht, ist das Fulleren. Fullerene besitzen einzigartige elektronische und optoelektronische Eigenschaften und sind fester Bestandteil der Forschung der letzten 40 Jahre. Trotzdem ist es immer noch eine Herausforderung sich die besonderen Eigenschaften der Fullerene in wässriger Lösung zu Nutzen zu machen. Diese Herausforderung anzugehen führt in das Gebiet der amphiphilen Fullerene.

Diese Arbeit ist fokussiert auf die Entwicklung amphiphiler Fullerene deren intrinsische Eigenschaften durch die Bildung von Überstrukturen verstärkt oder verändert werden. Neue Fullerene Derivate wurden etabliert, die in Lösung kontrollierbar definierte Aggregate bilden. Die Hauptaufgabe bestand darin den Effekt der Selbstanordnung auf intrinsische Eigenschaften der Moleküle zu identifizieren und zu untersuchen. Die veröffentlichten Ergebnisse dieser Arbeit können in drei Teile unterteilt werden. Der erste Teil befasst sich mit der Nutzbarmachung lipidartiger Selbstanordnung von Fulleren Tensiden. Ein Strukturmotiv wurde entwickelt, welches durch die supramolekularen Eigenschaften die intrinsischen antioxidativen Eigenschaften in biologischen System nutzbar macht. Der zweite Teil stellt eine Weiterentwicklung des etablierten Systems dar, indem eine weitere intrinsische Eigenschaft hinzugefügt wurde. Zusätzlich zum Fulleren, das als Elektronenmediator fungiert, wurden Farbstoffmoleküle als Elektronendonoren hinzugefügt. Daraus resultierte ein supramolekularer Halbleiter. Dessen Eigenschaften als photokatalytischer Elektronentransferierer wurden anschließend getestet. Der dritte Teil handelt von der Untersuchung des unmittelbaren Effekts der Selbstanordnung auf Elektrontransfer Reaktionen, was an Hand eines Prototyp Metall-Fulleren-Tensids in einem Modell System untersucht wurde.

In der ersten Publikation (Kapitel 8.1) wurde ein biokompatibles fulleren-basiertes Tensid präsentiert, welches als Antioxidant in lebende Zellen transferiert werden konnte, um als Membranschutz zu fungieren. Das Fulleren Tensid besitzt ein neu entwickeltes Strukturmotiv bei dem das Fulleren janusartig modifiziert wurde. Auf einer Hemisphäre befinden sich fünf Alkylketten als hydrophobe Einheit und auf der anderen Hemisphäre finden sich Hydroxyl Gruppen. Die Verbindungen bilden stabile vesikuläre Aggregate in wässriger Lösung, die eine monodisperse Größenverteilung besitzen. Zusätzlich sind die Verbindungen moderat oberflächenaktiv. Interessanter Weise hängt die sehr niedrige Kritische Aggregationskonzentration, bei Milimolaren Konzentrationen, nicht direkt mit der Oberflächenspannung zusammen, wie es bei einem gewöhnlichen Tensid der Fall ist. Aggregate werden bereits ausgebildet, bevor die Oberfläche mit Tensidmolekülen besetzt ist. In *ex vivo* Experimenten konnte gezeigt werden, dass die Fullerenol Kopfgruppe des Tensids ein effektives Antioxidant gegen biologisch relevante reaktive Sauerstoffspezies ist. Die Tenside bewiesen ihre Biokompatibilität mit eukaryotischen und prokarytischen Zellen, unabhängig von der Konzentration. Es konnte eine effiziente antioxidative Wirkung gegen Superoxid, Hydroxylradikale, Wasserstoffperoxid und Oxonitrit nachgewiesen werden. In die Zellen eingebracht, in denen es sich vorzugsweise in die Zellmembran integriert, konnte gezeigt werden, dass die Verbindungen Zellen effektiv vor intern produzierten reaktiven Sauerstoffspezies schützt. **In dieser Publikation wurde nicht nur ein neues Strukturmotiv für ein fullerenbasiertes Tensid aufgezeigt, sondern es konnte auch demonstriert werden, dass die antioxidativen Eigenschaften der Kopfgruppe durch die janusartige Struktur und die Selbstanordnung verstärkt wurden. Zusätzlich konnte gezeigt werden, dass die amphiphile Struktur es ermöglicht die Verbindung in die Zellmembran einzubringen.**

Aufbauend auf diesem neuen System wurden komplexere Derivate entwickelt. Dabei lag der Fokus weiter darauf, die intrinsischen Eigenschaften des Moleküls auf die supramolekularen Strukturen zu übertragen. Um diese Verbindungen herzustellen wurde eine neue Synthesestrategie benötigt. Die neue Synthese wurde in der zweiten Publikation (Kapitel 8.2) präsentiert und anhand verschiedener Beispiele demonstriert. Es handelt sich bei dieser Syntheseroute um eine vielseitige Ein-Topf Synthese Strategie, die es ermöglichte mittels Phasentransfer die janusartige Substitution des Fullerens parallel durchzuführen. Dabei wurden auf einer Hemisphäre selektiv fünf Substituenten angebracht und die andere Hemisphäre wurde polyhydroxiliert. Die Variation der Substituenten ist zunächst auf primäre Amine beschränkt, aber reicht von aliphatischen zu

aromatischen Aminen. Außerdem konnte gezeigt werden, dass auch Amine mit weiteren funktionellen Gruppen wie Carbonsäuren oder Ethyleneinheiten genutzt werden können. Zusätzlich wurden diverse, simple Analytikmethoden präsentiert, um die erhaltenen Verbindungen genau zu charakterisieren**. In dieser Publikation konnte gezeigt werden, dass es mit einer einfachen, vielseitigen Ein-Topf Synthese möglich ist, eine große Bandbreite an Fullerenol Tensiden herzustellen.**

Schließlich wurde diese neue Synthesestrategie dazu verwendet komplexere Fullerenol Tenside zu synthetisieren, die anstelle von Alkylketten, als hydrophobe Einheit, lineare Farbstoffmoleküle besitzen. Diese Verbindungen und deren Eigenschaften wurden in Publikation 3 (Kapitel 8.3) präsentiert. Diese neuen Verbindungen sind molekulare Halbleiter die sich in wässriger Lösung zu definierten vesikulären Aggregaten anordnen. Unter Anregung mit sichtbarem Licht produzieren molekulare Halbleiter einen ladungsgetrennten Zustand. Die resultierende chemische Energie dieses Zustands kann für weitere Reaktionen genutzt werden. Dies wurde mit der Reaktion mit molekularem Sauerstoff demonstriert. Weiterhin wurde beobachtet, dass sich die intrinsische Eigenschaft eines molekularen Halbleiters auf die supramolekularen Strukturen übertragen lässt, die einen Elektronentransfer zwischen und innerhalb der Aggregate aufweisen. Dieses Phänomen wurde weiter an der Reaktion mit Kohlenstoffdioxid in wässriger Lösung gezeigt. **Hierbei wurde eine neue Art eines sogenannten Künstlichen Blattes präsentiert, dass aus der supramolekularen Struktur von molekularen Halbleitern besteht.**

Der Effekt eines Elektronentransfers zwischen und innerhalb der Aggregate wurde in Publikation 4 (Kapitel 8.4) näher beleuchtet. Eine Prototyp-Verbindung, basierend auf den vorher etablierten Systemen, wurde entwickelt, um den verbessernden Effekt der Selbstanordnung auf katalytische Elektrontransfer Reaktionen zu untersuchen. Als Modelsystem wurde die elektrokatalytische Wasserspaltung gewählt. Dabei lag der Fokus auf konzentrationsabhängigen Messungen, unterhalb und oberhalb der kritischen Aggregationskonzentration. Es konnte gezeigt werden, dass die Bildung von Aggregaten starken Einfluss auf die elektronische Kommunikation des Systems hat und damit die Eigenschaften als Katalysator beeinflusst. Sobald die Konzentration erreicht wurde bei der sich Aggregate bilden, wurde die katalytische Effektivität drastisch verbessert. **Es konnte ein neuer Typ von supramolekularem Katalysator präsentiert werden der seine intrinsischen Eigenschaften durch Aggregation verbessert, was zu einem besseren katalytischen System**

führt. Selbstanordnung wurde als Möglichkeit identifiziert Elektronentransfer Reaktionen zu verbessern.

Zusammenfassend präsentiert diese Arbeit die selbstanordnungs-abhängigen Eigenschaften von janusartigen Fulleren Tensiden. Es konnte gezeigt werden, dass das Fulleren als Kopfgruppe des Tensides für verschiedene Elektrontransfer Reaktionen modifiziert werden kann und dabei als katalytischer Antioxidant oder Oxidant sowie als Elektronenmediator dienen kann. Das Fulleren Tensid ist dabei in katalytischen Reaktionen aktiv, wobei diese Eigenschaft sehr von der Selbstanordnung des Systems abhängt. Die kontrollierbare und definierte Selbstanordnung des Systems führte zu neuen Einsatzmöglichkeiten und zu einer erhöhten elektronischen Kommunikation innerhalb des Systems. Diese verbesserte elektronische Kommunikation hat direkten Einfluss auf katalytische Elektronentransfer Reaktionen, in denen die Effektivität der Fulleren Tenside durch Aggregation verbessert wurde**. In dieser Arbeit konnte gezeigt werden, dass die Kombination zweier Welten, Elektronentransfer Reaktionen und Aggregation zu einem positiven Effekt führt. Fullerene eigneten sich durch ihre Modifizierbarkeit und ihre elektronischen Eigenschaften als Testsystem.**

Die Zukunftsperspektiven dieses Projekts werden unter zwei verschiedenen Aspekten diskutiert, nämlich der Untersuchung der Selbstanordnung und der Untersuchung der mit der Selbstanordnung verbundenen Verbesserungen. Als ein Schlüsselmerkmal sollte die unkonventionelle Selbstorganisation von Fulleren-Tensiden weiter evaluiert werden. Es wurde gezeigt, dass Fulleren-Tenside unterschiedlicher Struktur, in wässriger Lösung, bei extrem niedrigen Konzentrationen, kugelförmige Aggregate bilden und, dass sich ihre Oberflächenaktivität im Vergleich zu normalen Tensiden anders verhält. Dennoch sind die Stabilität und das Bildungsverhalten der Aggregate noch nicht gut verstanden. Wie in dieser Arbeit gezeigt wurde, spielen die Aggregate eine entscheidende Rolle bei der Verbesserung der intrinsischen Eigenschaften, wobei es wünschenswert ist, die Aggregate weiter auf diesen Zweck abzustimmen. In einem ersten Schritt wäre, die in Publikation 1 vorgestellte Variation des Standard-Fullerenol-Tensids nützlich, um den Einfluss der Kettenanzahl und -länge sowie der Größe und Polarität der Kopfgruppen auf die Selbstorganisation zu verstehen. Erste Ergebnisse der Änderung der Polarität der Kopfgruppen wurden in dieser Publikation bereits mit interessanten Ergebnissen vorgestellt. Dieser Ansatz könnte weiter verfolgt werden, indem das Fullerenol als Kopfgruppe angepasst wird. Wie in Kapitel 4 dargestellt, gibt es verschiedene Strukturen und Substitutionsmuster, die für

Fullerenole mit unterschiedlichen Molekülgruppen existieren. Die Anpassung dieser Komponenten verändert die Polarität der Kopfgruppe sowie die Interaktion zwischen den Kopfgruppen im Aggregat. Dadurch werden nicht nur die Aggregatgröße und die Aggregatkonzentration, sondern auch die Stabilität der Aggregate abgestimmt. Andererseits wird erwartet, dass eine Änderung der Länge der angehängten Alkylketten bei Ketten mit 6 bis 16 Kohlenstoffatomen nur einen mittleren Einfluss auf die Selbstorganisation haben wird. Die Tatsache, dass fünf Ketten angebracht sind, ergibt eine konische Struktur für jede Kettenlänge mit einer geeigneten Hydrophobie. Ein größerer Einfluss wird erwartet, wenn die Anzahl der Ketten auf insgesamt eine, zwei oder acht (leicht zu erreichende Substitutionsmuster) geändert wird. Dies wird sowohl den Packungsparameter als auch den HLB-Wert drastisch verändern. Es wird daher erwartet, dass sich das Aussehen der Aggregate verändert. Insbesondere die Verringerung der Anzahl der Ketten könnte interessant sein, da dadurch auch die allgemeine Größe der Aggregate reduziert werden sollte und es sogar möglich sein könnte, mizellare Strukturen zu erhalten. Dies führt direkt zum zweiten Aspekt, der Verstärkung intrinsischer Eigenschaften durch die Selbstanordnung. In den Publikationen 3 und 4 konnte gezeigt werden, dass die Aggregation von Fulleren-Tensiden zu einer verbesserten elektronischen Kommunikation innerhalb des Systems führt, die mit der räumlichen Nähe der Fulleren-Kopfgruppen zusammenhängt. Auch wenn dieses Phänomen mit zwei verschiedenen Reaktionstypen, einer photokatalytischen und einer elektrokatalytischen Reaktion, untersucht wurde, gibt es noch viele weitere Möglichkeiten, vor allem in Hinblick auf den Einfluss der Aggregatgröße. Dies ist eine mehr als vielversprechende Spielwiese für weitere Forschungsprojekte, und einige Inspirationen sollen hier vorgestellt werden. Aufgrund der Vielseitigkeit des in dieser Arbeit etablierten Systems, kann es leicht an verschiedene Reaktionstypen angepasst werden. Es wurde eine Fullerenol-Kopfgruppe für Fullerentenside vorgestellt, die die elektronischen Eigenschaften des Fullerens mit der Wasserlöslichkeit kombiniert. Es konnte gezeigt werden, dass dieses System in der Lage ist, verschiedene katalytische Elektronentransferreaktionen wie katalytische Oxidation, Reduktion von Sauerstoff sowie die Reduktion von Kohlendioxid durchzuführen. Ein wichtiges Merkmal dieser Kopfgruppe ist die Fähigkeit, verschiedene Verbindungen an seiner Oberfläche zu koordinieren, was durch die anpassungsfähigen Fullerenoleinheiten, z.B. über mehrfache Wasserstoffbrückenbindungen, erreicht wird. Diese räumliche Nähe ermöglicht und erleichtert katalytische Reaktionen. Dieses System ist noch nicht an seine Grenzen bezüglich der Elektronenübertragungsreaktionen in wässriger Lösung, insbesondere aber bezüglich seiner Modifizierbarkeit gestoßen. In Publikation

2 wurde eine einfache Synthese vorgestellt, um durch Veränderung der hydrophoben Ketten vielfältige Derivate zu erhalten. In Publikation 3 wurde gezeigt, dass auch komplexere Moleküle als Alkylketten mit diesem System kombiniert werden können. Farbstoffmoleküle wurden als Antennen für sichtbares Licht und als Elektronendonatoren hinzugefügt. Dieses Konzept kann weiter vorangetrieben werden. Es könnten Moleküle mit unterschiedlichen intrinsischen Eigenschaften hinzugefügt werden, z.B. weitere reaktive Zentren für katalytische Reaktionen. Neben der Fullerenol-Kopfgruppe für Fulleren-Tenside wurde eine Metall-Fulleren-Kopfgruppe gezeigt, um den direkten Einfluss der Selbstorganisation auf die katalytischen Eigenschaften zu untersuchen. Da die Ergebnisse sehr vielversprechend waren, sollten weitere Anstrengungen unter diesem Forschungsaspekt unternommen werden. Es konnte gezeigt werden, dass dieses System ein neuer supramolekularer Katalysator ist, der seine Eigenschaften bei der Aggregation verändert. Obwohl das Konzept untersucht wurde, sollten weitere Anstrengungen unternommen werden, um den zugrundeliegenden Mechanismus im Detail zu untersuchen. Dazu gehören auch theoretische Berechnungen für die Veränderung der elektronischen Situation. Mit diesem Wissen können die Eigenschaften weiter abgestimmt und das System verbessert werden, um mit den etablierten katalytischen Systemen zu konkurrieren. Dieses Konzept sollte auch für verschiedene katalytische Reaktionen, auch auf dem Gebiet der mizellaren Katalyse getestet werden. Die Vielseitigkeit des vorgestellten Systems ermöglicht eine einfache Variation der verwendeten Liganden und Metalle. Mit einem Baukastensystem in der Hand können Derivate synthetisiert werden, die leicht an gängige Kreuzkupplungs- oder Polymerisationsreaktionen angepasst werden können, bei denen ein Einfluss auf die katalytische Reaktion erwartet wird. Das derzeitige Metall-Fulleren-Tensid enthält zwei Aminliganden, die Kobaltionen chelatieren. Der Ligand selbst wird als eine elektronische Brücke zwischen dem Metall und dem Fulleren gesehen. Dieser Ligand kann durch einen Liganden ausgetauscht werden, der die elektronische Situation mit elektronenreichen oder elektronenarmen Gruppen weiter verändert. Das Metallion kann in Bezug auf den Liganden frei gewählt werden. Dieses System führte zu einer neuen Art von supramolekularen Katalysatoren mit vielfältigen Möglichkeiten, die weiter untersucht werden sollte.

11 Appendix

11.1 Abbreviations

Δ	delta
γ	surface tension
η	onset potential
λ	wavelength
μ	micro
τ	(fluorescence) lifetime
°C	degree Celsius
Å	angstrom
A	ampere
ATR	attenuated total reflection
a.u.	arbitrary unit
c	concentration
cac	critical aggregation concentration
cat	catalyst
CB	chlorobenzene
cm	centimeter
cmc	critical micellation concetrantion
cryo	cryogenic
CV	cyclic voltammetry
DETA	diethylenetriamine

DFT	density functional theory
D_H	hydrodynamic diameter
DLS	dynamic light scattering
E	energy
EE	ethyl acetate
EDX	energy dispersive X-ray
e.g.	exempli gratia / for example
ESI-TOF	electronspray ionization time of flight
et al.	et alii
eV	electronvolt
g	gram
GC	gaschromatography
h	hour
HER	hydrogen evolution reaction
HLB	hydrophilic-lipophilic balance
HOMO	highest occupied molecular orbital
IC_{50}	half maximal inhibitory concentration
IR	infrared
IV	current-voltage
j	current
K	degree Kelvin
LED	light emitting diode
LUMO	lowest unoccupied molecular orbital

M	molar
mA	milliampere
MALDI	matrix assisted laser desorption ionization
MAS	magic angle spinning
mg	milligram
MHz	megahertz
mL	milliliter
mM	millimolar
mV	millivolt
MS	mass spectrometry
NaOH	sodium hydroxide
NBT	nitrotetrazolium blue
NEt_3	triethylamine
nm	nanometer
NMR	nuclear magnetic resonance
ns	nanosecond
OER	hydrogen evolution reaction
PL	photoluminescence
POLMIC	polarized light microscope
ppm	parts per million
RHE	reversible hydrogen electrode
rt	room temperature
ROS	reactive oxygen species

s	second
SDS	sodium dodecyl sulfate
SEM	scanning electron microscopy
T	temperature
TBAH	tetrabutyl ammoniumhydroxide
TEM	transmission electron microscopy
TGA	thermogravimetric analysis
TOF	turnover frequencies
V	volt

11.2 Bibliography

1. Israelachvili, J. N., *Intermolecular and surface forces*. Academic press: **2011**.
2. Polarz, S.; Kunkel, M.; Donner, A.; Schlotter, M., *Chemistry–A European Journal* **2018**, *24*, 18842-18856.
3. Brown, P.; Butts, C. P.; Eastoe, J., *Soft Matter* **2013**, *9*, 2365-2374.
4. Donner, A.; Hagedorn, K.; Mattes, L.; Drechsler, M.; Polarz, S., *Chemistry–A European Journal* **2017**, *23*, 18129-18133.
5. Hermann, S.; Wessig, M.; Kollofrath, D.; Gerigk, M.; Hagedorn, K.; Odendal, J. A.; Hagner, M.; Drechsler, M.; Erler, P.; Fonin, M., *Angewandte Chemie International Edition* **2017**, *129*, 5567-5571.
6. Klaiber, A.; Kollek, T.; Cardinal, S.; Hug, N.; Drechsler, M.; Polarz, S., *Advanced Materials Interfaces* **2018**, *5*, 1701430.
7. Sutter, S.; Trepka, B.; Siroky, S.; Hagedorn, K.; Theiss, S.; Baum, P.; Polarz, S., *ACS Applied Material Interfaces* **2019**, *11*, 15936-15944.
8. Smalley, R. E.; Kroto, H.; Heath, J., *Nature* **1985**, *318*, 162-163.
9. Osawa, E. J. K., **1970**, *25*, 854-863.
10. Browne, M., The New York Times: **1991**.
11. Godly, E.; Taylor, R., *Fullerenes, Nanotubes, Carbon Nanostructures* **1997**, *5*, 1667-1708.
12. Powell, W.; Cozzi, F.; Moss, G.; Thilgen, C.; Hwu, R.-R.; Yerin, A., *Pure applied chemistry* **2002**, *74*, 629-695.
13. Krätschmer, W.; Lamb, L. D.; Fostiropoulos, K.; Huffman, D. R., *Nature* **1990**, *347*, 354.
14. Shanbogh, P. P.; Sundaram, N. G., *Resonance* **2015**, *20*, 123-135.
15. Boorum, M. M.; Vasil'ev, Y. V.; Drewello, T.; Scott, L. T., *Science* **2001**, *294*, 828-31.
16. Anderson, T.; Dyer, P.; Dykes, J.; Klavins, P.; Anderson, P.; Liu, J.; Shelton, R., *Review of scientific instruments* **1994**, *65*, 3820-3822.
17. Krestinin, A.; Moravsky, A., *Chemical physics letters* **1998**, *286*, 479-484.
18. Goroff, N. S., *Accounts of chemical research* **1996**, *29*, 77-83.
19. Churilov, G.; Novikov, P.; Tarabanko, V.; Lopatin, V.; Vnukova, N.; Bulina, N., *Carbon* **2002**, *40*, 891-896.
20. Pierson, H. O., *Handbook of carbon, graphite, diamonds and fullerenes: processing, properties and applications*. William Andrew: **2012**.
21. Schein, S.; Sands-Kidner, M.; Friedrich, T., *Biophysical journal* **2008**, *94*, 938-957.
22. Hirsch, A., *Synthesis* **1995**, *1995*, 895-913.
23. Prato, M., *Journal of Materials Chemistry* **1997**, *7*, 1097-1109.
24. Schulz, G. L.; Urdanpilleta, M.; Fitzner, R.; Brier, E.; Mena-Osteritz, E.; Reinold, E.; Bäuerle, P., *Beilstein journal of nanotechnology* **2013**, *4*, 680-689.
25. Campbell, E. E.; Rohmund, F., *Reports on Progress in Physics* **2000**, *63*, 1061.
26. Diederich, F.; Thilgen, C., *Science* **1996**, *271*, 317-324.
27. Tajima, Y.; Takeshi, K.; Shigemitsu, Y.; Numata, Y., *Molecules* **2012**, *17*, 6395-414.
28. Bingel, C., *Chemische Berichte* **1993**, *126*, 1957-1959.
29. Ball, G. E.; Burley, G. A.; Chaker, L.; Hawkins, B. C.; Williams, J. R.; Keller, P. A.; Pyne, S. G., *Journal of Organic Chemistry* **2005**, *70*, 8572-4.
30. Olah, G. A., *Friedel-crafts and Related Reactions: Alkylation and Related Reactions*. Interscience: **1964**.

31. Olah, G. A.; Bucsi, I.; Ha, D. S.; Aniszfeld, R.; Lee, C. S.; Prakash, G. S., *Fullerenes, Nanotubes, Carbon Nanostructures* **1997**, *5*, 389-405.
32. Śliwa, W., *Fullerenes, Nanotubes, Carbon Nanostructures* **1997**, *5*, 1133-1175.
33. Selig, H.; Lifshitz, C.; Peres, T.; Fischer, J.; McGhie, A.; Romanow, W.; McCauley Jr, J.; Smith III, A., *Journal of the American Chemical Society* **1991**, *113*, 5475-5476.
34. Ala'a, K., *Journal of the Chemical Society, Perkin Transactions 2* **1995**, 981-985.
35. Troshin, P. A.; Kolesnikov, D.; Burtsev, A. V.; Lubovskaya, R. N.; Denisenko, N. I.; Popov, A. A.; Troyanov, S. I.; Boltalina, O. V., *Fullerenes, Nanotubes Carbon Nanostructures* **2003**, *11*, 47-60.
36. Matsuo, Y.; Nakamura, E., *Chemical Reviews* **2008**, *108*, 3016-28.
37. Langa, F.; Nierengarten, J., Fullerenes Principles and Applications. 2007. Cambridge: The Royal Society of Chemistry.
38. Buhl, M.; Hirsch, A., *Chemical Reviews* **2001**, *101*, 1153-83.
39. Collavini, S.; Delgado, J. L.; *Sustainable Energy Fuels* **2018**, *2*, 2480-2493.
40. Ganesamoorthy, R.; Sathiyan, G.; Sakthivel, P., *Solar Energy Materials Solar Cells* **2017**, *161*, 102-148.
41. Castro, E.; Murillo, J.; Fernandez-Delgado, O.; Echegoyen, L., *Journal of Materials Chemistry C* **2018**, *6*, 2635-2651.
42. Xue, J., *Polymer Reviews* **2010**, *50*, 411-419.
43. Dennler, G.; Scharber, M. C.; Brabec, C. J., *Advanced Materials Interfaces* **2009**, *21*, 1323-1338.
44. Troshin, P. A.; Hoppe, H.; Renz, J.; Egginger, M.; Mayorova, J. Y.; Goryachev, A. E.; Peregudov, A. S.; Lyubovskaya, R. N.; Gobsch, G.; Sariciftci, N. S., *Advanced Functional Materials* **2009**, *19*, 779-788.
45. Yu, G.; Gao, J.; Hummelen, J. C.; Wudl, F.; Heeger, A. J., *Science* **1995**, *270*, 1789-1791.
46. Xu, Y.; Yao, H.; Hou, J., *Chinese Journal of Chemistry* **2019**, *37*, 207-215.
47. Ans, M.; Ayub, K.; Muhammad, S.; Iqbal, J., *Computational Theoretical Chemistry* **2019**, *1161*, 26-38.
48. Jeng, J. Y.; Chiang, Y. F.; Lee, M. H.; Peng, S. R.; Guo, T. F.; Chen, P.; Wen, T. C., *Advanced Materials* **2013**, *25*, 3727-32.
49. Wojciechowski, K.; Stranks, S. D.; Abate, A.; Sadoughi, G.; Sadhanala, A.; Kopidakis, N.; Rumbles, G.; Li, C. Z.; Friend, R. H.; Jen, A. K.; Snaith, H. J., *ACS Nano* **2014**, *8*, 12701-9.
50. Liu, X.; Lin, F.; Chueh, C.-C.; Chen, Q.; Zhao, T.; Liang, P.-W.; Zhu, Z.; Sun, Y.; Jen, A. K.-Y., *Nano energy* **2016**, *30*, 417-425.
51. Zhang, F.; Shi, W.; Luo, J.; Pellet, N.; Yi, C.; Li, X.; Zhao, X.; Dennis, T. J. S.; Li, X.; Wang, S.; Xiao, Y.; Zakeeruddin, S. M.; Bi, D.; Gratzel, M., *Advanced Materials* **2017**, *29*, 1606806.
52. Djordjevic, A.; Srdjenovic, B.; Seke, M.; Petrovic, D.; Injac, R.; Mrdjanovic, J., *Journal of Nanomaterials* **2015**, *2015*.
53. Thakral, S.; Mehta, R., *Indian journal of pharmaceutical sciences* **2006**, *68*, 13.
54. Jensen, A. W.; Wilson, S. R.; Schuster, D. I., *Bioorganic & Medicinal Chemistry* **1996**, *4*, 767-79.
55. Bakry, R.; Vallant, R. M.; Najam-ul-Haq, M.; Rainer, M.; Szabo, Z.; Huck, C. W.; Bonn, G. K., *International Journal of Nanomedicine* **2007**, *2*, 639-49.
56. Semenov, K.; Charykov, N.; Postnov, V.; Sharoyko, V.; Vorotyntsev, I.; Galagudza, M.; Murin, I., *Progress in Solid State Chemistry* **2016**, *44*, 59-74.

57. Sergeeva, V.; Kraevaya, O.; Ershova, E.; Kameneva, L.; Malinovskaya, E.; Dolgikh, O.; Konkova, M.; Voronov, I.; Zhilenkov, A.; Veiko, N., *Oxidative medicine cellular longevity* **2019**, *2019*.
58. Goodarzi, S.; Da Ros, T.; Conde, J.; Sefat, F.; Mozafari, M., *Materials Today* **2017**, 20, 8, 460-480
59. Kazemzadeh, H.; Mozafari, M., *Drug Discovery Today* **2019**, *24*, 898-905.
60. Semenov, K. N.; Charykov, N. A.; Keskinov, V. A.; Piartman, A. K.; Blokhin, A. A.; Kopyrin, A. A., *Journal of Chemical Engineering Data* **2009**, *55*, 13-36.
61. Beck, M. T., *Pure applied chemistry* **1998**, *70*, 1881-1887.
62. Lyon, D. Y.; Adams, L. K.; Falkner, J. C.; Alvarezt, P. J., *Environ Sci Technol* **2006**, *40*, 4360-6.
63. Lyon, D. Y.; Brunet, L.; Hinkal, G. W.; Wiesner, M. R.; Alvarez, P. J., *Nano letters* **2008**, *8*, 1539-1543.
64. Fileti, E. E.; Rivelino, R.; Brito Mota, F.; Malaspina, T., *Nanotechnology* **2008**, *19*, 365703.
65. Piatek, A.; Dawid, A.; Gburski, Z., *Spectrochimica Acta A: Molecular and Biomolecular Spectroscopy* **2011**, *79*, 819-23.
66. Li, J.; Takeuchi, A.; Ozawa, M.; Li, X.; Saigo, K.; Kitazawa, K., *Chemical Communications* **1993**, 1784-1785.
67. Chiang, L. Y.; Upasani, R. B.; Swirczewski, J. W.; Soled, S., *Journal of the American Chemical Society* **1993**, *115*, 5453-5457.
68. Mirkov, S. M.; Djordjevic, A. N.; Andric, N. L.; Andric, S. A.; Kostic, T. S.; Bogdanovic, G. M.; Vojinovic-Miloradov, M. B.; Kovacevic, R. Z., *Nitric Oxide* **2004**, *11*, 201-7.
69. Chiang, L. Y.; Wang, L.-Y. Swirczewski, J. W.; Soled, S.; Cameron, S., *The Journal of Organic Chemistry* **1994**, *59*, 3960-3968.
70. Kokubo, K.; Shirakawa, S.; Kobayashi, N.; Aoshima, H.; Oshima, T., *Nano Research* **2011**, *4*, 204-215.
71. Wang, Z.; Chang, X.; Lu, Z.; Gu, M.; Zhao, Y.; Gao, X., *Chemical Science* **2014**, *5*, 2940-2948.
72. Rodriguez-Zavala, J. G.; Guirado-Lopez, R. A., *Journal Physical Chemistry A* **2006**, *110*, 9459-68.
73. Zhou, S.; Zhang, L.; Feng, Y.; Li, H.; Chen, M.; Pan, W.; Hao, J., *Chemistry–A European Journal* **2018**, *24*, 16609-16619.
74. Sun, X.; Zhang, Q.; Yin, K.; Zhou, S.; Li, H., *Chemical Communications* **2016**, *52*, 12024-12027.
75. Liu, Y.; Zhang, G.; Niu, L.; Gan, L.; Liang, D., *Journal of Materials Chemistry* **2011**, *21*, 14864-14868.
76. Harano, K.; Nakamura, E., *Account of Chemical Ressearch* **2019**, *52*, 2090-2100.
77. Sawamura, M.; Kawai, K.; Matsuo, Y.; Kanie, K.; Kato, T.; Nakamura, E., *Nature* **2002**, *419*, 702.
78. Nitta, H.; Harano, K.; Isomura, M.; Backus, E. H. G.; Bonn, M.; Nakamura, E., *Journal of American Chemical Society* **2017**, *139*, 7677-7680.
79. Zhou, S.; Burger, C.; Chu, B.; Sawamura, M.; Nagahama, N.; Toganoh, M.; Hackler, U. E.; Isobe, H.; Nakamura, E., *Science* **2001**, *291*, 1944-7.
80. Homma, T.; Harano, K.; Isobe, H.; Nakamura, E., *Angewewandte Chemie International Edition* **2010**, *49*, 1665-8.
81. Isobe, H.; Homma, T.; Nakamura, E., *Proceedings of the National Academy of Sciences* **2007**, *104*, 14895-14898.

82. Homma, T.; Harano, K.; Isobe, H.; Nakamura, E., *Journal of the American Chemical Society* **2011**, *133*, 6364-6370.
83. Burghardt, S.; Hirsch, A.; Schade, B.; Ludwig, K.; Bottcher, C., *Angewwandte Chemie International Edition* **2005**, *44*, 2976-9.
84. Maierhofer, A. P.; Brettreich, M.; Burghardt, S.; Vostrowsky, O.; Hirsch, A.; Langridge, S.; Bayerl, T. M., *Langmuir* **2000**, *16*, 8884-8891.
85. Brettreich, M.; Burghardt, S.; Böttcher, C.; Bayerl, T.; Bayerl, S.; Hirsch, A., *Angewandte Chemie International Edition* **2000**, *39*, 1845-1848.
86. Schade, B.; Ludwig, K.; Bottcher, C.; Hartnagel, U.; Hirsch, A., *Angewandte Chemie International Edition* **2007**, *46*, 4393-6.
87. Hirsch, A., *Pure Applied Chemistry* **2008**, *80*, 571-587.
88. Zhao, Y.; Chen, G., *Fullerenes and Other Carbon-rich Nanostructures*, Springer: **2013**; pp 23-53.
89. Gorgoll, R. M.; Harano, K.; Nakamura, E., *Journal of the American Chemical Society* **2016**, *138*, 9675-81.
90. Harano, K.; Gorgoll, R. M.; Nakamura, E., *Chemical Communications* **2013**, *49*, 7629-31.
91. Lin, M.-S.; Chen, R.-T.; Yu, N.-Y.; Sun, L.-C.; Liu, Y.; Cui, C.-H.; Xie, S.-Y.; Huang, R.-B.; Zheng, L.-S., *Colloids Surfaces B: Biointerfaces* **2017**, *159*, 613-619.
92. Donskyi, I.; Achazi, K.; Wycisk, V.; Böttcher, C.; Adeli, M., *Chemical Communications* **2016**, *52*, 4373-4376.
93. Partha, R.; Mitchell, L. R.; Lyon, J. L.; Joshi, P. P.; Conyers, J. L., *ACS Nano* **2008**, *2*, 1950-8.
94. Klaiber, A.; Polarz, S., *ACS nano* **2016**, *10*, 10041-10048.
95. Klaiber, A.; Landsmann, S.; Löffler, T.; Polarz, S., *New Journal of Chemistry* **2016**, *40*, 919-922.
96. Polarz, S.; Landsmann, S.; Klaiber, A., *Angewwandte Chemie International Edition* **2014**, *53*, 946-54.
97. Landsmann, S.; Luka, M.; Polarz, S., *Nature communications* **2012**, *3*, 1-6.
98. Donner, A.; Trepka, B.; Theiss, S.; Immler, F.; Traber, J.; Polarz, S., *Langmuir* **2019**, *35*, 16514-16520.
99. Kunkel, M.; Schildknecht, S.; Boldt, K.; Zeyffert, L.; Schleheck, D.; Leist, M.; Polarz, S., *ACS Applied Materials & Interfaces* **2018**, *10*, 23638-23646.
100. Prather, K. L.; Martin, C. H., *Current Opinion in Biotechnology* **2008**, *19*, 468-74.
101. Adkins, J.; Pugh, S.; McKenna, R.; Nielsen, D. R., *Frontiers in Microbiology* **2012**, *3*, 313.
102. Finkel, T.; Holbrook, N. J., *Nature* **2000**, *408*, 239-47.
103. Circu, M. L.; Aw, T. Y., *Free Radical Biology & Medicine* **2010**, *48*, 749-62.
104. Ott, M.; Gogvadze, V.; Orrenius, S.; Zhivotovsky, B., *Apoptosis* **2007**, *12*, 913-22.
105. Chiang, L. Y.; Lu, F.-J.; Lin, J.-T., *Chemical Communications* **1995**, 1283-1284.
106. Yin, J. J.; Lao, F.; Fu, P. P.; Wamer, W. G.; Zhao, Y.; Wang, P. C.; Qiu, Y.; Sun, B.; Xing, G.; Dong, J.; Liang, X. J.; Chen, C., *Biomaterials* **2009**, *30*, 611-21.
107. Chiang, L. Y.; Bhonsle, J. B.; Wang, L.; Shu, S. F.; Chang, T. M.; Hwu, J. R., *Tetrahedron Letters* **1996**, *52*, 4963-4972.
108. Markovic, Z.; Trajkovic, V., *Biomaterials* **2008**, *29*, 3561-73.
109. Partha, R.; Conyers, J. L., *International Journal of Nanomedicine* **2009**, *4*, 261-75.
110. Djordjevic, A.; Bogdanovic, G.; Dobric, S., *Journal of BUON* **2006**, *11*, 391-404.
111. Nakamura, H.; Nozaki, Y.; Koizumi, Y.; Watano, S., *Journal of the Taiwan Institute of Chemical Engineers* **2018**, *90*, 18-24.

112. Guldi, D. M.; Zerbetto, F.; Georgakilas, V.; Prato, M., *Accounts of Chemical Research* **2005**, *38*, 38-43.
113. Yu, X.; Li, Y.; Dong, X.-H.; Yue, K.; Lin, Z.; Feng, X.; Huang, M.; Zhang, W.-B.; Cheng, S. Z. D., *Journal of Polymer Science Part B: Polymer Physics* **2014**, *52*, 1309-1325.
114. Burger, C.; Hao, J.; Ying, Q.; Isobe, H.; Sawamura, M.; Nakamura, E.; Chu, B., *Journal of Colloid and Interface Science* **2004**, *275*, 632-41.
115. Sano, M.; Oishi, K.; Ishi-i, T.; Shinkai, S., *Langmuir* **2000**, *16*, 3773-3776.
116. Cassell, A. M.; Asplund, C. L.; Tour, J. M., *Angewandte Chemie International Edition* **1999**, *38*, 2403-2405.
117. Zhao, Y.; Chen, G., *Fullerenes and Other Carbon-Rich Nanostructures*, Nierengarten, J. F., Ed. Springer-Verlag Berlin: Berlin, **2013**; Vol. 159, pp 23-53.
118. Partha, R.; Lackey, M.; Hirsch, A.; Casscells, S. W.; Conyers, J. L., *Journal of Nanobiotechnology* **2007**, *5*, 6.
119. Lin, Z.; Lu, P.; Hsu, C. H.; Yue, K.; Dong, X. H.; Liu, H.; Guo, K.; Wesdemiotis, C.; Zhang, W. B.; Yu, X.; Cheng, S. Z., *Chemistry* **2014**, *20*, 11630-5.
120. Chen, M.; Zhu, H.; Zhou, S.; Xu, W.; Dong, S.; Li, H.; Hao, J., *Langmuir* **2016**, *32*, 2338-47.
121. Kuvychko, I. V.; Streletskii, A. V.; Popov, A. A.; Kotsiris, S. G.; Drewello, T.; Strauss, S. H.; Boltalina, O. V., *Chemistry-A European Journal* **2005**, *11*, 5426-5436.
122. Kornev, A. B.; Khakina, E. A.; Troyanov, S. I.; Kushch, A. A.; Peregudov, A.; Vasilchenko, A.; Deryabin, D. G.; Martynenko, V. M.; Troshin, P. A., *Chemical Communications* **2012**, *48*, 5461-5463.
123. Wang, S.; He, P.; Zhang, J. M.; Jiang, H.; Zhu, S. Z., *Synthetic Communications* **2005**, *35*, 1803-1808.
124. Wang, Z.; Wang, S.; Lu, Z.; Gao, X., *Journal of Cluster Science* **2015**, *26*, 375-388.
125. Xing, G.; Zhang, J.; Zhao, Y.; Tang, J.; Zhang, B.; Gao, X.; Yuan, H.; Qu, L.; Cao, W.; Chai, Z.; Ibrahim, K.; Su, R., *Journal of Physical Chemistry B* **2004**, *108*, 11473-11479.
126. Afreen, S.; Kokubo, K.; Muthoosamy, K.; Manickam, S., *RSC Advances* **2017**, *7*, 31930-31939.
127. Semenov, K.; Letenko, D.; Charykov, N.; Nikitin, V.; Matuzenko, M. Y.; Keskinov, V.; Postnov, V.; Kopyrin, A., *Russian Journal of Applied Chemistry* **2010**, *83*, 2076-2080.
128. Chao, T. C.; Song, G.; Hansmeier, N.; Westerhoff, P.; Herckes, P.; Halden, R. U., *Analytical Chemistry* **2011**, *83*, 1777-83.
129. Wang, Z.; Lu, Z.; Zhao, Y.; Gao, X., *Nanoscale* **2015**, *7*, 2914-2925.
130. McConnell, H., *Annual Review of Physical Chemistry* **1991**, *42*, 171-195.
131. Egberts, J.; Sloot, H.; Mazure, A., *Biochimca et Biophysica Acta* **1989**, *1002*, 109-13.
132. Lin, M.-S.; Chen, R.-T.; Yu, N.-Y.; Sun, L.-C.; Liu, Y.; Cui, C.-H.; Xie, S.-Y.; Huang, R.-B.; Zheng, L.-S., *Colloids and Surfaces B: Biointerfaces* **2017**, 159, 613-619
133. Guida, V., *Advances in Colloid and Interface Science* **2010**, *161*, 77-88.
134. Almgren, M.; Rangelov, S., *Langmuir* **2004**, *20*, 6611-6618.
135. Choi, H. S.; Kim, J. W.; Cha, Y. N.; Kim, C., *Journal of Immunoassay Immunochem* **2006**, *27*, 31-44.
136. Troshin, P. A.; Astakhova, A. S.; Lyubovskaya, R. N., *Fullerenes, Nanotubes and Carbon Nanostructures* **2005**, *13*, 331-343.
137. Jovanovic, S. V.; Steenken, S.; Tosic, M.; Marjanovic, B.; Simic, M. G., *Journal of the American Chemical Society* **1994**, *116*, 4846-4851.
138. Schildknecht, S.; Pape, R.; Muller, N.; Robotta, M.; Marquardt, A.; Burkle, A.; Drescher, M.; Leist, M., *Journal of Biological Chemistry* **2011**, *286*, 4991-5002.

139. Torchilin, V. P., *Journal of Controlled Release* **2001**, *73*, 137-72.
140. Hrenovic, J.; Ivankovic, T., *Open Life Sciences* **2007**, *2*, 405-414.
141. Alkilany, A. M.; Nagaria, P. K.; Hexel, C. R.; Shaw, T. J.; Murphy, C. J.; Wyatt, M. D., S*mall* **2009**, *5*, 701-708.
142. Schildknecht, S.; Poltl, D.; Nagel, D. M.; Matt, F.; Scholz, D.; Lotharius, J.; Schmieg, N.; Salvo-Vargas, A.; Leist, M., *Toxicology and Applied Pharmacology* **2009**, *241*, 23-35.
143. Nazari, M.; Kurdi, M.; Heerklotz, H., *Biophysical Journal* **2012**, *102*, 498-506.
144. Rabbel, H.; Werner, M.; Sommer, J.-U., *Macromolecules* **2015**, *48*, 4724-4732.
145. le Maire, M.; Champeil, P.; Moller, J. V., *Biochimica et Biophysica Acta* **2000**, *1508*, 86-111.
146. Farn, R. J., *Chemistry and Technology of Surfactants*. Blackwell Publishing Ltd.: **2006**; p 315 pp.
147. Demus, D.; Goodby, J.; Gray, G. W.; Spiess, H. W.; Vill, V., *Handbook of Liquid Crystals, Volume 2A: Low Molecular Weight Liquid Crystals I*. Wiley-VCH: 1998; p 490 pp.
148. Scholz, D.; Poltl, D.; Genewsky, A.; Weng, M.; Waldmann, T.; Schildknecht, S.; Leist, M., *Journal of Neurochemistry* **2011**, *119*, 957-71.
149. Kunkel, M.; Polarz, S., *Beilstein Journal of Organic Chemistry* **2019**, *15*, 901-905.
150. Roh, K. H.; Martin, D. C.; Lahann, J., *Nature Materials* **2005**, *4*, 759-63.
151. Walther, A.; Muller, A. H., *Chemical Reviews* **2013**, *113*, 5194-261.
152. Muller, A.; Sarkar, S.; Shah, S. Q.; Bogge, H.; Schmidtmann, M.; Kogerler, P.; Hauptfleisch, B.; Trautwein, A. X.; Schunemann, V. V., *Angewandte Chemie International Edition* **1999**, *38*, 3238-3241.
153. Bosi, S.; Da Ros, T.; Spalluto, G.; Prato, M., *European Jorunal of Medicinal Chemistry* **2003**, *38*, 913-23.
154. Coro, J.; Suárez, M.; Silva, L. S.; Eguiluz, K. I.; Salazar-Banda, G. R., *International Journal of Hydrogen Energy* **2016**, *41*, 17944-17959.
155. Thompson, B. C.; Frechet, J. M., *Angewandte Chemie International Edition* **2008**, *47*, 58-77.
156. Hirsch, A.; Brettreich, M., *Fullerenes: chemistry and reactions*. John Wiley & Sons: 2006.
157. Tzirakis, M. D.; Orfanopoulos, M., *Chemical Reviews* **2013**, *113*, 5262-321.
158. Lopez, A. M.; Mateo-Alonso, A.; Prato, M., *Journal of Materials Chemistry C* **2011**, *21*, 1305-1318.
159. Chiang, L. Y.; Bhonsle, J.; Wang, L.; Shu, S.; Chang, T.; Hwu, J. R., *Tetrahedron Letters* **1996**, *52*, 4963-4972.
160. Zhang, G.; Liu, Y.; Liang, D.; Gan, L.; Li, Y., *Angewandte Chemie International Edition* **2010**, *49*, 5293-5.
161. Semenov, K. N.; Charykov, N. A.; Keskinov, V. N., *Journal of Chemical & Engineering Data* **2011**, *56*, 230-239.
162. Kokubo, K.; Matsubayashi, K.; Tategaki, H.; Takada, H.; Oshima, T., *ACS Nano* **2008**, *2*, 327-333.
163. Singh, R.; Goswami, T., *Synthetic metals* **2007**, *157*, 951-955.
164. Goswami, T.; Nandan, B.; Alam, S.; Mathur, G., *Polymer* **2003**, *44*, 3209-3214.
165. Bahuguna, S.; Kumar, M.; Sharma, G.; Kumar, R.; Singh, B.; Raza, K., *AAPS PharmSciTech* **2018**, *19*, 1084-1092.
166. Huang, H.; Zhang, G.; Liang, S.; Xin, N.; Gan, L., *Journal of Organic Chemistry* **2012**, *77*, 2456-62.
167. Jiang, Z.; Zhang, Y.; Gan, L.; Wang, Z., *Tetrahedron Letters* **2008**, *64*, 11394-11403.

168. Kraevaya, O. A.; Peregudov, A. S.; Martynenko, V. M.; Troshin, P. A., *Tetrahedron Letters* **2018**, *59*, 605-607.
169. Liu, Y.; Zhang, G.; Niu, L.; Gan, L.; Liang, D., *Journal of Materials Chemistry C* **2011**, *21*, 14864-14868.
170. David, R., *Chemical Communications* **1993**, 1230-1232.
171. Khakina, E. A.; Ol'ga, A. K.; Popova, M. L.; Peregudov, A. S.; Troyanov, S. I.; Chernyak, A. V.; Martynenko, V. M.; Kulikov, A. V.; Schols, D.; Troshin, P. A., *Organic Biomolecular Chemistry* **2017**, *15*, 773-777.
172. Khakina, E. A.; Yurkova, A. A.; Peregudov, A. S.; Troyanov, S. I.; Trush, V. V.; Vovk, A. I.; Mumyatov, A. V.; Martynenko, V. M.; Balzarini, J.; Troshin, P. A., *Chemical Communications* **2012**, *48*, 7158-7160.
173. Silion, M.; Dascalu, A.; Pinteala, M.; Simionescu, B. C.; Ungurenasu, C., *Beilstein Journal of Organic Chemistry* **2013**, *9*, 1285-95.
174. Andreeva, D. V.; Ratnikova, O. V.; Melenevskaya, E. Y.; Gribanov, A. V., *International Journal of Polymer Analysis Characterization* **2007**, *12*, 105-113.
175. Silion, M.; Dascalu, A.; Pinteala, M.; Simionescu, B. C.; Ungurenasu, C., *Beilstein Journal of Organic Chemistry* **2013**, *9*, 1285-95.
176. Kunkel, M.; Sutter, S.; Polarz, S., *Angewandte Chemie International Edition* **2019**, *58*, 15620-15625.
177. Nocera, D. G., *Accounts of Chemical Research* **2012**, *45*, 767-76.
178. Sivula, K.; van de Krol, R., *Nature Reviews Materials* **2016**, 1, 15010
179. Chang, X.; Wang, T.; Gong, J., *Energy Environmental Science* **2016**, *9*, 2177-2196.
180. Li, X.; Yu, J.; Jaroniec, M.; Chen, X., *Chemical Reviews* **2019**, *119*, 3962-4179.
181. Morris, A. J.; Meyer, G. J.; Fujita, E., *Accounts of Chemical Research* **2009**, *42*, 1983-94.
182. Guo, Z.; Cheng, S.; Cometto, C.; Anxolabehere-Mallart, E.; Ng, S. M.; Ko, C. C.; Liu, G.; Chen, L.; Robert, M.; Lau, T. C., *Journal of American Chemical Society* **2016**, *138*, 9413-6.
183. Esswein, A. J.; Nocera, D. G., *Chemical Reviews* **2007**, *107*, 4022-47.
184. Mohajeri, A.; Omidvar, A., *Physical Chemistry Chemical Physics* **2015**, *17*, 22367-76.
185. Georgakilas, V.; Tiwari, J. N.; Kemp, K. C.; Perman, J. A.; Bourlinos, A. B.; Kim, K. S.; Zboril, R., *Chemical Reviews* **2016**, *116*, 5464-519.
186. Wang, D.-W.; Su, D., *Energy Environmental Science* **2014**, *7*, 576-591.
187. Leary, R.; Westwood, A., *Carbon* **2011**, *49*, 741-772.
188. D'Souza, F.; Chitta, R.; Ohkubo, K.; Tasior, M.; Subbaiyan, N. K.; Zandler, M. E.; Rogacki, M. K.; Gryko, D. T.; Fukuzumi, S., *Journal of American Chemical Society* **2008**, *130*, 14263-72.
189. Amin, A. N.; El-Khouly, M. E.; Subbaiyan, N. K.; Zandler, M. E.; Fukuzumi, S.; D'Souza, F., *Chemical Communications* **2012**, *48*, 206-208.
190. Lewandowska, K.; Barszcz, B.; Graja, A.; Bursa, B.; Biadasz, A.; Wróbel, D.; Bednarski, W.; Waplak, S.; Grzybowski, M.; Gryko, D. T., *Synthetic Metals* **2013**, *166*, 70-76.
191. Obondi, C. O.; Lim, G. N.; Jang, Y.; Patel, P.; Wilson, A. K.; Poddutoori, P. K.; D'Souza, F., *The Journal of Physical Chemistry C* **2018**, *122*, 13636-13647.
192. Bandi, V.; Das, S. K.; Awuah, S. G.; You, Y.; D'Souza, F., *Journal of American Chemical Society* **2014**, *136*, 7571-4.
193. Lebedeva, M. A.; Chamberlain, T. W.; Scattergood, P. A.; Delor, M.; Sazanovich, I. V.; Davies, E. S.; Suyetin, M.; Besley, E.; Schröder, M.; Weinstein, J. A., *Chemical Science* **2016**, *7*, 5908-5921.

194. Lin, Y.; Li, Y.; Zhan, X., *Chemical Society Reviews* **2012**, *41*, 4245-72.
195. Narayanaswamy, K.; Venkateswararao, A.; Nagarjuna, P.; Bishnoi, S.; Gupta, V.; Chand, S.; Singh, S. P., *Angewandte Chemical International Edition* **2016**, *55*, 12334-7.
196. Blanco, G. D.; Hiltunen, A. J.; Lim, G. N.; Kc, C. B.; Kaunisto, K. M.; Vuorinen, T. K.; Nesterov, V. N.; Lemmetyinen, H. J.; D'Souza, F., *ACS Applied Materials & Interfaces* **2016**, *8*, 8481-90.
197. Nguyen, T. L.; Lee, T. H.; Gautam, B.; Park, S. Y.; Gundogdu, K.; Kim, J. Y.; Woo, H. Y., *Advanced Functional Materials* **2017**, *27*, 1702474.
198. Ciammaichella, A.; Dral, P. O.; Clark, T.; Tagliatesta, P.; Sekita, M.; Guldi, D. M., *Chemistry–A European Journal* **2012**, *18*, 14008-14016.
199. Cowart Jr, J. S.; Liman, C.; Garnica, A.; Page, Z. A.; Lim, E.; Zope, R. R.; Baruah, T.; Hawker, C. J.; Chabinyc, M. L., *Inorganica Chimica Acta* **2017**, *468*, 192-202.
200. Youssef, Z.; Vanderesse, R.; Colombeau, L.; Baros, F.; Roques-Carmes, T.; Frochot, C.; Wahab, H.; Toufaily, J.; Hamieh, T.; Acherar, S.; Gazzali, A. M., *Cancer Nanotechnology* **2017**, *8*, 6.
201. Yamakoshi, Y.; Aroua, S.; Nguyen, T. M.; Iwamoto, Y.; Ohnishi, T., *Faraday Discussions* **2014**, *173*, 287-96.
202. Rybkin, A. Y.; Belik, A. Y.; Kraevaya, O.; Khakina, E.; Zhilenkov, A.; Goryachev, N.; Volyniuk, D.; Grazulevicius, J.; Troshin, P.; Kotelnikov, A., *Dyes Pigments* **2019**, *160*, 457-466.
203. Kotelnikov, A. I.; Rybkin, A. Y.; Khakina, E. A. Kornev, A. B.; Barinov, A. V.; Goryachev, N. S.; Ivanchikhina, A. V.; Peregudov, A. S.; Martynenko, V. M.; Troshin, P. A., *Organic & Biomolecular Chemistry* **2013**, *11*, 4397-404.
204. Hong, J.; Zhang, W.; Ren, J.; Xu, R., *Analytical methods* **2013**, *5*, 1086-1097.
205. Lim, J.; Kim, H.; Alvarez, P. J.; Lee, J.; Choi, W., *Environmental science technology* **2016**, *50*, 10545-10553.
206. Pickering, K. D.; Wiesner, M. R., *Environmental Science & Technology* **2005**, *39*, 1359-65.
207. Grebowski, J.; Kazmierska, P.; Krokosz, A., *BioMed Research International* **2013**, *2013*.
208. Yamakoshi, Y.; Umezawa, N.; Ryu, A.; Arakane, K.; Miyata, N.; Goda, Y.; Masumizu, T.; Nagano, T., *Journal of the American Chemical Society* **2003**, *125*, 12803-12809.
209. Hadgiivanova, R.; Diamant, H.; Andelman, D., *Journal of Physical Chemistry B* **2011**, *115*, 7268-80.
210. Ren, D.; Fong, J.; Yeo, B. S., *Nature Communications* **2018**, *9*, 925.
211. La Sorella, G.; Strukul, G.; Scarso, A., *Green Chemistry* **2015**, *17*, 644-683.
212. Meeuwissen, J.; Reek, J. N., *Nature Chemistry* **2010**, *2*, 615-21.
213. Brown, C. J.; Toste, F. D.; Bergman, R. G.; Raymond, K. N., *Chemical Reviews* **2015**, *115*, 3012-35.
214. Cram, D. J., *Angewandte Chemie International Edition* **1988**, *27*, 1009-1020.
215. Yoshizawa, M.; Tamura, M.; Fujita, M., *Science* **2006**, *312*, 251-4.
216. Sanders, J. K., *Chemistry–A European Journal* **1998**, *4*, 1378-1383.
217. Bijlard, A.-C.; Wald, S.; Crespy, D.; Taden, A.; Wurm, F. R.; Landfester, K., *Advanced Materials Interfaces* **2017**, 4, 1600443
218. Polarz, S.; Bahrle, C.; Landsmann, S.; Klaiber, A., *Angewandte Chemie International Edition* **2013**, *52*, 13665-70.
219. Lubitz, W.; Tumas, W., Hydrogen: an overview. ACS Publications: 2007, 107, 10, 3900-3903

220. Cook, T. R.; Dogutan, D. K.; Reece, S. Y.; Surendranath, Y.; Teets, T. S.; Nocera, D. G., *Chemical Reviews* **2010**, *110*, 6474-502.
221. DuBois, D. L., *Inorganic Chemistry* **2014**, *53*, 3935-60.
222. Li, P.; Zhao, R.; Chen, H.; Wang, H.; Wei, P.; Huang, H.; Liu, Q.; Li, T.; Shi, X.; Zhang, Y., *Small* **2019**, *15*, 1805103.
223. Wang, Y.; Zhang, J., *Frontiers of Chemical Science and Engineering* **2018**, *12*, 838-854.
224. You, B.; Sun, Y., *Accounts of Chemical Research* **2018**, *51*, 1571-1580.
225. Hu, C.; Zhang, L.; Gong, J., *Energy & Environmental Science* **2019**, 12, 2620-2645
226. McCrory, C. C.; Jung, S.; Ferrer, I. M.; Chatman, S. M.; Peters, J. C.; Jaramillo, T. F., *Journal of the American Chemical Society* **2015**, *137*, 4347-57.
227. Roger, I.; Shipman, M. A.; Symes, M. D., *Nature Reviews Chemistry* **2017**, *1*, 0003.
228. Lu, B.; Guo, L.; Wu, F.; Peng, Y.; Lu, J. E.; Smart, T. J.; Wang, N.; Finfrock, Y. Z.; Morris, D.; Zhang, P.; Li, N.; Gao, P.; Ping, Y.; Chen, S., *Nature Communications* **2019**, *10*, 631.
229. Du, P.; Eisenberg, R., *Energy & Environmental Science* **2012**, *5*, 6012-6021.
230. Queyriaux, N.; Jane, R. T.; Massin, J.; Artero, V.; Chavarot-Kerlidou, M., *Coordination Chemistry Reviews* **2015**, *304-305*, 3-19.
231. Fang, T.; Fu, L.-Z.; Zhou, L.-L.; Zhan, S.-Z.; Chen, S., *Electrochimica Acta* **2015**, *178*, 368-373.
232. Haddad, A. Z.; Garabato, B. D.; Kozlowski, P. M.; Buchanan, R. M.; Grapperhaus, C. A., *Journal of the American Chemical Society* **2016**, *138*, 7844-7.
233. Haddad, A. Z.; Kumar, D.; Ouch Sampson, K.; Matzner, A. M.; Mashuta, M. S.; Grapperhaus, C. A., *Journal of the American Chemical Society* **2015**, *137*, 9238-9241.
234. Najafpour, M. M.; Mehrabani, S.; Mousazade, Y.; Holynska, M., *Dalton Transactions* **2018**, *47*, 9021-9029.
235. Liu, Y.; Han, Y.; Zhang, Z.; Zhang, W.; Lai, W.; Wang, Y.; Cao, R., *Chemical Science* **2019**, *10*, 2613-2622.
236. Artero, V.; Chavarot-Kerlidou, M.; Fontecave, M., *Angewandte Chemie International Edition* **2011**, *50*, 7238-66.
237. Saveant, J.; Vianello, E., *Electrochimica Acta* **1965**, *10*, 905-920.
238. McCrory, C. C.; Uyeda, C.; Peters, J. C., *Journal of the American Chemical Society* **2012**, *134*, 3164-70.
239. Hu, X.; Brunschwig, B. S.; Peters, J. C., *Journal of the American Chemical Society* **2007**, *129*, 8988-8998.
240. Eckenhoff, W. T.; McNamara, W. R.; Du, P.; Eisenberg, R., *Biochimica et Biophysica Acta* **2013**, *1827*, 958-973.
241. Haddad, A. Z.; Cronin, S. P.; Mashuta, M. S.; Buchanan, R. M.; Grapperhaus, C. A., *Inorganic chemistry* **2017**, *56*, 11254-11265.
242. Thompson, E. J.; Berben, L. A., *Angewandte Chemie International Edition* **2015**, *54*, 11642-6.
243. Kankanamalage, P. H.; Mazumder, S.; Tiwari, V.; Kpogo, K. K.; Schlegel, H. B.; Verani, C. N., *Chemical Communications* **2016**, *52*, 13357-13360.
244. Wang, Z.-Q.; Tang, L.-Z.; Zhang, Y.-X.; Zhan, S.-Z.; Ye, J.-S., *Journal of Power Sources* **2015**, *287*, 50-57.
245. Zhang, Y.; Pang, S.; Wei, Z.; Jiao, H.; Dai, X.; Wang, H.; Shi, F., *Nature Communications* **2018**, *9*, 1465.
246. Kondrat, S. A.; van Bokhoven, J. A., *Topics in Catalysis* **2018**, 62, 1218-1227.
247. Almgren, M., *Biochimica et Biophysica Acta* **2000**, *1508*, 146-63.

248. Rupp, C.; Steckel, H.; Muller, B. W., *International Journal of Pharmaceutics* **2010**, *387*, 120-8.
249. Kunkel, M.; Bitter, S.; Sailer, F.; Winter, R. F.; Polarz, S., *ChemCatChem* **2020**, 12, 2726

12 Records of Contribution (Overview) and Original Paper Prints

Publication I

Kunkel, M., Schildknecht, S., Boldt, K., Zeyffert, L., Schleheck, D., Leist, M., & Polarz, S. (2018). Increasing the Resistance of Living Cells against Oxidative Stress by Nonnatural Surfactants as Membrane Guards. *ACS applied materials & interfaces*, *10*(28), 23638-23646.

DOI:10.1021/acsami.8b07032

Record of Contribution

Material synthesis, characterization, further chemical experiments and interpretation were performed by M. Kunkel if not stated differently. S. Schildknecht designed, performed and interpreted the experiments with eukaryotic cells. K. Boldt assisted M. Kunkel with the design of the experiments and the interpretation. L. Zeyffert performed preliminary experiments on ROS quenching under the supervision of M. Kunkel. D. Schleheck and M. Leist designed the biological experiments. M. Kunkel and S. Polarz designed the research and S. Polarz wrote the manuscript. All authors have given approval to the final version of the manuscript.

Publication II

Kunkel, M., & Polarz, S. (2019). Easy, efficient and versatile one-pot synthesis of Janus-type-substituted fullerenols. *Beilstein journal of organic chemistry*, *15*(1), 901-905.

DOI:10.3762/bjoc.15.87

Record of Contribution

Material Synthesis, characterization and data interpretation were performed by M. Kunkel. M. Kunkel and S. Polarz designed the research. M. Kunkel and S. Polarz wrote the manuscript. All authors have given approval to the final version of the manuscript.

Publication III

Kunkel, M., Sutter, S., & Polarz, S. (2019). Molecular Semiconductor Surfactants with Fullerenol Heads and Colored Tails for Carbon Dioxide Photoconversion. *Angewandte Chemie International Edition*, *58*(44), 15620-15625.

DOI:10.1002/anie.201905410

Record of Contribution

Material Synthesis, characterization and data interpretation were performed by M. Kunkel. S. Sutter performed the DFT calculations. M. Kunkel and S. Polarz designed the research and M. Kunkel and S. Polarz wrote the manuscript. All authors have given approval to the final version of the manuscript.

Publication IV

Kunkel, M., Bitter, S., Sailer, F., Winter, R. F., & Polarz, S. (2020). Aggregation-Induced Improvement of Catalytic Activity by Inner-Aggregate Electronic Communication of Metal-Fullerene-Based Surfactants. *ChemCatChem*.

DOI:10.1002/cctc.202000412

Record of Contribution

Material synthesis, characterization and data interpretation were performed by M. Kunkel. S. Bitter and R. F. Winter assisted M. Kunkel with the electrochemical measurements. F. Sailer developed the syntheses under the supervision of M. Kunkel. M. Kunkel designed the research and M. Kunkel and S. Polarz wrote the manuscript. All authors have given approval to the final version of the manuscript.

ACS APPLIED MATERIALS & INTERFACES

Research Article

Cite This: ACS Appl. Mater. Interfaces 2018, 10, 23638−23646

www.acsami.org

Increasing the Resistance of Living Cells against Oxidative Stress by Nonnatural Surfactants as Membrane Guards

Marius Kunkel, Stefan Schildknecht, Klaus Boldt, Lukas Zeyffert, David Schleheck, Marcel Leist, and Sebastian Polarz*

University of Konstanz, Universitätsstrasse 10, 78457 Konstanz, Germany

Supporting Information

ABSTRACT: The importation of construction principles or even constituents from biology into materials science is a prevailing concept. Vice versa, the cellular level modification of living systems with nonnatural components is much more difficult to achieve. It has been done for analytical purposes, for example, imaging, to learn something about intracellular processes. Cases describing the improvement of a biological function by the integration of a nonnatural (nano)constituent are extremely rare. Because biological membranes contain some kind of a surfactant, for example, phospholipids, our idea is to modify cells with a newly synthesized surfactant. However, this surfactant is intended to possess an additional functionality, which is the reduction of oxidative stress. We report the synthesis of a surfactant with Janus-type head group architecture, a fullerene C_{60} modified by five alkyl chains on one side and an average of 20 oxygen species on the other hemisphere. It is demonstrated that the amphiphilic properties of the fullerenol surfactant are similar to that of lipids. Not only quenching of reactive oxygen species (superoxide, hydroxyl radicals, peroxynitrite, and hydrogen peroxide) was successful, but also the fullerenol surfactant exceeds benchmark antioxidant agents such as quercetin. The surfactant was then brought into contact with different cell types, and the viability even of delicate cells such as human liver cells (HepG2) and human dopaminergic neurons (LUHMES) has proven to be extraordinarily high. We could show further that the cells take up the fullerenol surfactant, and as a consequence, they are protected much better against oxidative stress.

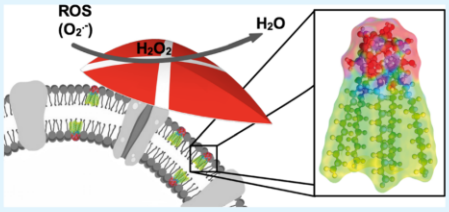

KEYWORDS: *surfactant, amphiphile, fullerenol, fullerene, ROS quenching, superoxide, membrane, living cells*

INTRODUCTION

Because of the exponentially growing global population, we will have to provide more commodities than have ever been produced before. In addition to the extension and improvement of the capacities of chemical industry as we know, a seminal approach is to use microbes in chemical factories.[1,2] One of the problems involved in realizing this goal is that many cells, prokaryotes as well as eukaryotes, are sensitive to oxidative stress.[3] Reactive oxygen species (ROS) are in any case major reasons for cellular damages and aging processes. Anaerobic microorganisms are of course even more sensitive to an oxygen-rich environment. In particular, in an aqueous dispersion and in contact to daylight, there is an inevitable level of ROS such as the superoxide anion, hydroxyl radicals, or singlet oxygen. Evolution has countered this problem by the development of cellular mechanisms for self-protection against those species by scavenging enzymes such as superoxide dismutase.[4] However, if the oxidative stress level becomes too high or occurs very fast, the biological protection alone is not sufficient anymore, which then results in damages and diseases associated with oxidative stress.[5] Therefore, it would be highly interesting to aid cells and to increase their resistance against ROS.

Fullerene derivatives have been evaluated for biomedical use for quite some time. Depending on their modification, they have shown promising results as antiviral, antibacterial, or antioxidative compounds. However, a huge disadvantage of most fullerene derivatives is their poor solubility in water, which is of course pivotal for most biomedical usage. One approach for making them more suitable for applications in biotechnology is the formation of hybrids with phospholipids, the so-called fullerene liposomes. The encapsulation of fullerene derivatives in liposomes or the direct interaction with cell membranes can lower the compound's toxicity and enhance its bioavailability. Another approach is the use of water-soluble derivatives such as polyhydroxylated fullerenes, the so-called fullerenols.[6,7] It has been reported that these compounds can reliably quench ROS in aqueous systems.[8−11] Fullerenols can even penetrate the cellular membranes and accumulate inside the cell, where they possibly aggregate. Unfortunately, it was found that the presence of fullerenols in the internal regions of the cell is harmful and can even lead to necrosis. Besides ill-defined accumulation, there are also other

Received: April 30, 2018
Accepted: June 27, 2018
Published: June 27, 2018

DOI: 10.1021/acsami.8b07032
ACS Appl. Mater. Interfaces 2018, 10, 23638−23646

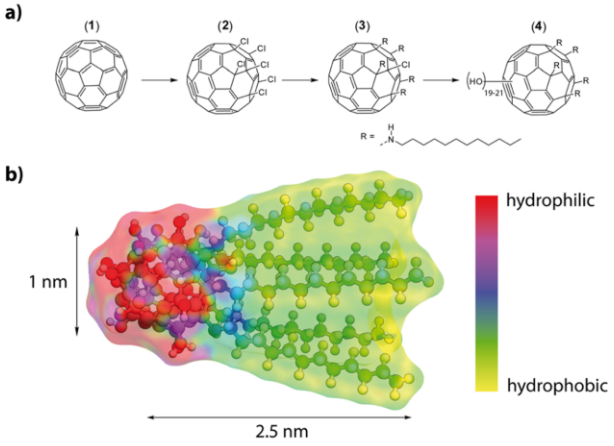

Figure 1. (a) Synthesis sequence to derive surfactants with a fullerenol head group. (b) Optimized molecular structure of surfactant (**4**) with dimensions and electrostatic potential map.

reasons for the toxicity of fullerene derivatives in cellular systems. The solubility of the compound, functional groups, and the degree of derivatization influence the compound's toxicity.[11,12]

Because of the argument given above, one has to effectively suppress the undesired aggregation of fullerenols. Further, they would ideally remain as guards against oxidative stress integrated in the cellular membrane instead of entering the cell. The importance of the exact positioning of the fullerenol entities was also discussed by Nakamura et al. in a theoretical study in 2017.[13] Because cellular membranes mainly consist of phospholipids, our idea is to generate a new surfactant showing lipid-like behavior and a fullerenol head group as the entity capable of protection against oxidative stress via catalytic conversion of ROS into less harmful compounds. A great body of work exists on amphiphiles containing fullerenes.[14,15] Amphiphilic fullerenes are known for forming bi- or multilayered vesicular aggregates in solution.[16−19] They have also been explored for biochemical applications.[14,20,21] The work of Hirsch et al. needs to be mentioned in this context, who synthesized membrane-forming hexa-adducts of C_{60}.[22] These compounds can, for example, be used as nanocarriers for drug delivery systems.[21,23] The vesicular self-assembly of amphiphilic fullerenes was also investigated by Nakamura et al. They showed that different kinds of fullerene amphiphiles aggregate in a membrane-like structure.[16,19,24] However, the fullerene is part of the hydrophobic moiety in most cases. True surfactants, in which the fullerene represents the hydrophilic head group, are rare.[25−28]

In this paper, we report the synthesis and characterization of a surfactant (see Figure 1) comprising a fullerenol head group. After characterization of its surfactant and self-assembly properties, we will test the ROS deactivation features. Finally, the biocompatibility of the surfactant will be explored, and the protection of cells against oxidative stress will be tested.

RESULTS AND DISCUSSION

Surfactant Preparation. We achieved the synthesis of the Janus-type target molecule (**4**) as follows (Figure 1a,b). The method published by Kuvychko et al. was applied to obtain hexa-chlorination selectively on only one side of C_{60} (**2**).[29] Penta-alkylation with dodecyl amine was achieved by adapting a protocol published by Kornev et al.[30] to obtain the precursor molecule (**3**). ^{1}H NMR, ^{13}C NMR, and matrix-assisted laser desorption ionization mass spectrometry (MALDI-MS) could confirm the penta-alkylation. This can clearly be seen in the ^{1}H NMR. Besides the signals for the alkyl chains, it shows the signals of the secondary amines bound to the fullerene core as five triplets centered at 3.22 ppm (see the Supporting Information, Figure S1). Also, the ^{13}C NMR shows distinct signals for the sp^3-hybridized carbons of the fullerene core at which the chains are attached at 66, 68.2, and 69.4 ppm. Three signals can be observed because of the 2:2:1 symmetry (see the Supporting Information, Figure S2). The MALDI-MS reveals the M − HCl peak at m/z = 1641.6 (1641.3). In the last step, the hydroxyl moieties are introduced to the precursor using NaOH and H_2O_2 (see also the experimental part). The fullerenol surfactant (**4**) was characterized by a combination of methods. Fourier transform infrared (FT-IR) spectroscopy confirms the polyhydroxylation of precursor (**3**). The observed spectrum is in agreement with the characteristics compared to fullerenols found in the literature.[31−33] Signals at 3365, 1410, and 1032 cm^{-1} can be assigned to the hydroxyl moieties. Weak signals at 2971 and 2942 cm^{-1} fit to the attached alkyl chains. Furthermore, a strong signal at 1645 cm^{-1} indicates the presence of hemiketal moieties which include the hydroxyl groups (shown in the Supporting Information, Figure S3).[34,35] The ^{13}C NMR spectrum (see the Supporting Information, Figure S4) is also in full agreement with the proposed structure and confirms that the scaffold of the precursor is still intact. The alkyl chains are located between 13 and 40 ppm. Signals at 52.4, 57.2, and 57.3 ppm fit the carbons of the fullerene at which the alkyl amines are attached to. Three signals are observed because they have a 2:2:1 symmetry. Because the hydroxyl groups are not introduced by substitution of, for example, halogens but directly to the fullerene core, one needs to determine the degree of poly-hydroxylation and the kind of the attached oxygen species. Therefore, thermogravimetric

DOI: 10.1021/acsami.8b07032
ACS Appl. Mater. Interfaces 2018, 10, 23638−23646

analysis (TGA) was performed among others (shown in the Supporting Information, Figure S5). We assign the mass loss below 200 °C to the removal of water loosely bound to the head group via hydrogen bonding. The mass loss at a higher temperature (Δm = −17.05%) fits to the elimination of hydroxyl groups and vinyl ethers (hemiketals).[36] The latter mass loss corresponds to an average number of ≈20 ± 1 oxygen species attached to C_{60} in (**4**). The penta-alkylated fullerene remains after the loss of the oxygen species. The successful synthesis and structure of the surfactant could be confirmed conclusively by MALDI-MS (shown in the Supporting Information, Figure S6). All signals of the complex fragmentation pattern could also be assigned by comparison with fullerenol compounds known in the literature.[37,38] Every signal belongs to a singly charged species and can be assigned with the following formula: $[M - (v - 1)H - w(OH) - xH_2O - yNH - zC_{12}H_{25}]^+$. Like for other fullerenols, the hydroxyl groups are released as water, generating an oxygen radical species or hydroxyl radicals. Furthermore, the chains can be released with or without the amine linker. A maximum of five chains can be detected, which fits the findings from the NMR. As a result of these decomposition mechanisms, no molecular ion peak can be observed. Though MALDI-MS reveals a mixture of different oxygen species, a maximum number of 21 oxygen species could be detected, which is in agreement with the results from the TGA. Further information about the degree of poly-hydroxylation and the kind of oxygen species can be obtained from the ^{13}C NMR spectrum of the compound. It reveals 11 signals between 61 and 77 ppm which correspond to the sp^3-hybridized carbons of the fullerene core, where the hydroxyl groups are attached to, and 5 signals between 110 and 130 ppm which correspond to the vinyl ether species. To ensure the identity and purity of the compound, liquid chromatography was performed. It shows three very narrow signals with a similar retention time (shown in the Supporting Information, Figure S7). These signals represent the different number of oxygen species and confirm that no broad distribution nor a mixture of other compounds but a narrow distribution of oxygen species is present. It is also confirmed that no species with different chain numbers exist. Conclusively, one can say that precursor (**3**) was successfully polyhydroxylated with about 10 hemiketal moieties (which consist of a hydroxyl group and a vinyl ether group), resulting in an average of 20 oxygen species in total. It can be concluded that because of the inevitable characteristics of the poly-hydroxylation chemistry of fullerenes (see, for instance, the overview given by Wang et al.),[39] we are not dealing with a monomolecular species but rather with a system. In addition, the occurrence of regioisomers cannot be excluded. However, from all we can say is that there is a narrow distribution among the compounds and that their behavior is very similar.

It is important to note one further twist in the chemistry of fullerenols. It has been shown in the literature that the addition of acids leads to the conversion of hemiketals to ketones and hydroxyl groups accompanied by partial ring opening.[34,35] These reactions can be transferred successfully to our fullerenol surfactant, leading to the open-cage (oc) compound (**4oc**) (see the schematic Schlegel diagram shown in the Supporting Information, Figure S8). The FT-IR of (**4oc**) no longer shows the hemiketal signal but a strong ketone signal at 1720 cm^{-1} and 10 new ^{13}C NMR signals between 170 and 175 ppm, which are also characteristic for the presence of carbonyl units (see the Supporting Information, Figures S9 and S10). The number of ketone moieties perfectly fits the results obtained for the number of hemiketals in (**4cc**). Also, because of the complexity of the ring-opening processes (see also Figure S8), it is important to note that (**4oc**) does not represent a single molecular species but rather a range of compounds. In agreement with the literature, we also observed that the process is entirely reversible. The reformation of the molecule with its closed cage head group (**4cc**) can be achieved by the addition of diluted sodium hydroxide solution to (**4oc**).

Interfacial Properties and Self-Assembly. A first indication for the surfactant properties of (**4**) is that it forms strong foams at the air/water interface even at a low concentration (Figure 2). Further information can be obtained from concentration-dependent surface tension (γ) measurements shown in Figure 2.

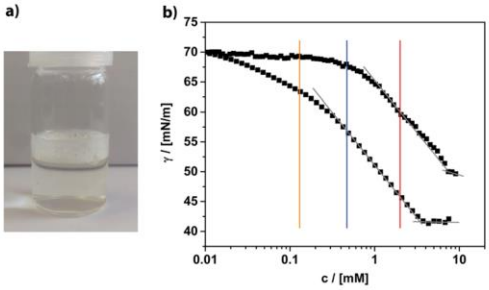

Figure 2. (a) Photograph of a diluted solution of the fullerenol surfactant indicating its foaming abilities. (b) Concentration-dependent surface tension measurements of (**4cc**) ≅ circles and (**4oc**) ≅ squares in water. The vertical bars indicate the concentrations whose particle size distribution curves are shown in Figure 3.

Compound (**4**) is obviously surface-active, but compared to classical nonionic surfactants such as Brij or Tween, there are differences. The behavior is more comparable to lipids.[40,41] The surface tension γ drops more slowly and does not reach such low values as for classical surfactants ($\gamma_{c=sat}$(Brij) ≈ 32 mN/m), and the concentration, at which γ begins to saturate, is roughly 1 magnitude higher [c_s(Brij 35) = 0.09 mM]. A possible explanation for the latter could be a less dense coverage of the air/water interface because of the large size of the head group in (**4**). This assumption can be confirmed by the calculation of the surface excess Γ and the minimum area per molecule at the air/water interface (A_m ≈ 60 Å^2), which represents a rather large value. The corresponding radius r_m = 0.44 nm fits very well to the cross section of the surfactant molecule (Figure 1b). One can also see that the chemical structure of the head has a marked influence on the surfactant properties. The overall performance of the (**4oc**) system seems to be better; the surfactant is more soluble and occupies the air/water interface at a lower concentration compared to (**4cc**).

Micelles are usually formed above the critical micelle concentration (cmc), which is reached as soon as the air/water interface is fully occupied. Therefore, at none of the three concentrations marked in Figure 2, one should expect to find aggregates in solution. We checked this by dynamic light scattering (DLS) shown in Figure 3a. However, already at c ≈

DOI: 10.1021/acsami.8b07032
ACS Appl. Mater. Interfaces 2018, 10, 23638−23646

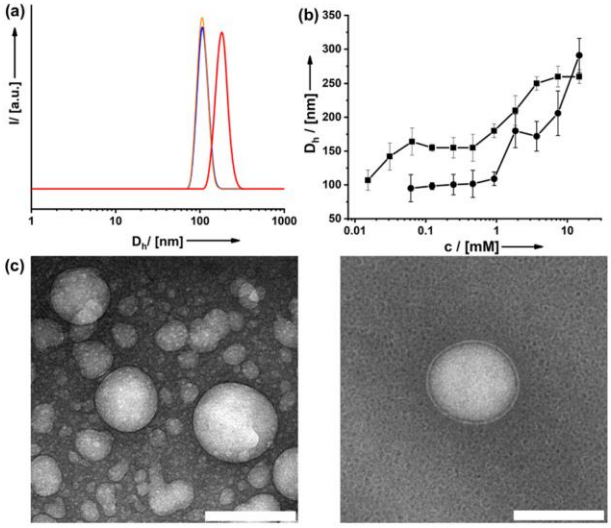

Figure 3. (a) Particle size distribution functions derived from DLS for the three concentrations of (**4cc**) given in Figure 2. (b) Aggregate size in water at different surfactant concentrations of (**4cc**) ≅ circles and (**4oc**) ≅ squares. (c) Cryo-TEM micrographs of aggregates in solution; scale bar = 100 nm.

0.1 mM, one observes large aggregates, although γ has just begun to drop, and thus, the air/water interface is covered only partially. The absence of a classic cmc was confirmed by independent methods (concentration-dependent viscosity and ionic conductivity measurements; see the Supporting Information, Figure S11). We suppose that the packing of (**4**) at the air/water interface is so ineffective that it is thermodynamically more favorable to form aggregates even at very low concentration. Interestingly, Nakamura and co-workers observed that for an alternative amphiphilic fullerene system, aggregate formation is possible without interaction with the air/water interface.[24] Even at much lower concentration, we never saw the formation of micelles but large aggregates with ($D_H \approx 100$ nm) even at ≈20 μM. The concentration of the aggregates becomes lower, until they vanish. The particle size ($D_H \approx 100/150$ nm) remains unchanged in the concentration range 0.1−2 mM and then raises until the solution is saturated (Figure 2b). As a consequence, the optical appearance of the dispersions has become turbid (see also the Supporting Information, Figure S12).

The mentioned aggregates are obviously much larger than the ordinary micelles, which are typically only twice the length of the surfactant. Because the packing parameter of (**4**) is close to 1, one can expect a tendency for the formation of bilayered or vesicle-like structures. Other researchers working on amphiphilic fullerenes could also observe vesicle-like structures.[19,23,42,43] Investigations using cryogenic transmission electron microscopy (cryo-TEM) confirm this (Figure 3c). The size of the hollow aggregates is in agreement with the DLS data. One has to bear in mind that DLS is an averaging technique, and one preferentially sees only the strongest light scatters, for example, the larger aggregates. Actually, the size of the vesicles is not monodisperse at all (Figure 3c). Additional TEM data are given in the Supporting Information (Figure S12). It can also be seen that with higher concentration, more and more vesicles form, and they seem to be fusing together, which is the reason for the increasing aggregate size observed in DLS. Similar processes have also been reported in the literature for other surfactant systems, for example, cetyltrimethylammonium bromide.[44,45] The TEM data reveal that the vesicles contain a single shell. The thickness of this shell (~4.8 nm) is compliant with the double dimension of the fullerenol surfactant (Figure 1b) and, thus, fits a double-layer structure. Although both surfactant types (**4cc**) and (**4oc**) form vesicles, one can see that the chemical conformation of the head groups has an influence on the average size of the aggregates (Figure 3b). At higher concentration, liquid-crystalline phases can be observed. Optical microscopy under crossed polarizers shows phases with intense birefringence and marked textures (see the Supporting Information, Figure S13). Depending on the surfactant concentration, one observes columnar droplets with the characteristic Maltese cross or smectic phases.

Ex Vivo ROS Quenching. The antioxidative properties and the influence of the amphiphilic character are investigated next. Quenching of superoxide monitored by a nitroblue tetrazolium assay (see the Supporting Information, Figure S14)[46] was used to evaluate the efficiency of the fullerenol surfactants at different concentrations (Figure 4). The results were compared to two reference systems: a nonamphiphilic fullerenol compound, synthesized by hydroxylation of $C_{60}Br_{24}$,[47] and the flavonoid quercetin which was employed as a benchmark because it is a commercially available and well-understood antioxidant.[9−11,32,48] The nonamphiphilic fullerenol is active in superoxide quenching, as described in the literature. The quenching efficiency depends almost linearly on the concentration of (**4cc**) (Figure 4). A substantial amount of superoxide (>60%) remains in solution even at a relatively high concentration of fullerenol. The 50% inhibitory concentration (IC_{50}) of this reference is not reached during our experiment.

DOI: 10.1021/acsami.8b07032
ACS Appl. Mater. Interfaces 2018, 10, 23638−23646

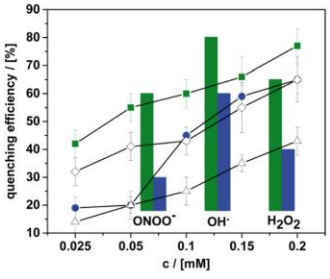

Figure 4. Concentration-dependent superoxide quenching efficiency of different compounds: (**4cc**) ≅ blue circles, (**4oc**) ≅ green squares, nonamphiphilic fullerenol (open triangles), and quercetin (open hashes). The bars give an overview over the ROS quenching capabilities of (**4cc**) (blue) and (**4oc**) (green) for $ONOO^-$, $OH^•$, and H_2O_2 as the alternative ROS (see the Supporting Information for method details).

The surfactant containing fullerenol as a head group (**4cc**) clearly shows an improved performance. The IC_{50} of (**4cc**) is 0.15 mM. One sees that there is a jump in the quenching efficiency between 0.05 and 0.1 mM surfactant concentration. Because this is the same region, where the (**4cc**) vesicles are formed (see Figure 3a), the step can be seen as an indication; the presence of the vesicles is very important. The fraction of the fullerenol entities exposed to the aqueous interface is obviously maximized for the vesicles, and therefore, the superoxide quenching ability is much better.

The vesicles containing (**4cc**) are just as efficient as the benchmark quercetin (Figure 4) but unfortunately not better. Because (**4oc**) forms vesicles at much lower concentration (Figure 3a), we hoped that it could exhibit higher quenching efficiency in particular at those low concentrations. This is indeed the case as can be seen from Figure 4. Compound (**4oc**) does outperform (**4cc**) and, more importantly, quercetin. Since this is also the case for higher concentrations, one can assume that more than the tendency to form vesicles is a relevant factor. Because the vesicles of (**4oc**) are larger than those formed by (**4cc**) (Figure 3), the explanation cannot be due to an improved surface-to-volume ratio, which could result in an increased catalytic conversion rate of superoxide. Therefore, the chemical structure of the head group in (**4oc**) must be relevant; in particular, the ketone moieties play a crucial role regarding the ROS deactivation mechanism (see the Supporting Information, Figure S15). Besides the superoxide ion ($O_2^{•-}$), other ROS were investigated as well, such as peroxynitrite ($ONOO^-$), hydroxyl radicals ($OH^•$), and hydrogen peroxide (H_2O_2).[49] For the other ROS, the surfactants also quenched the radical species reliably (Figure S16), and (**4oc**) was in all cases superior than (**4cc**). The activity regarding the catalytic conversion of H_2O_2 is a positive result. According to the literature, H_2O_2 is the main product of the deactivation process of superoxide.[32] Of course, H_2O_2 is still quite reactive and a strong oxidant. Because the surfactants (**4**) lead to a decrease in H_2O_2 concentration, we expect an even more significant improvement in the oxidative stress level.

Biocompatibility and in Vivo ROS Quenching. Before a beneficial biological function of (**4**) can be explored, it is pivotal to scrutinize any potential toxicity factors. Although nonnatural surfactants are in general not very toxic, they can be harmful, in particular, when they come in contact with more sensitive cells.[50−52] Therefore, we investigated the viability and morphology of a range of prokaryotic and eukaryotic cell types in contact to (**4**). *Pseudomonas aeruginosa* and *Escherichia coli* were chosen as prokaryotic model organisms. In comparison, the eukaryotic model systems human liver cells (HepG2) and human dopaminergic neurons (LUHMES) represent much more delicate systems. The intrinsic toxicity of the surfactants was tested in a range of 1−125 μM, according to standard procedures (see also the Supporting Information).

For *E. coli*, as well as for *P. aeruginosa* (not shown), the presence of the surfactant had no negative effects neither on their growth (see the Supporting Information, Figure S17) nor on their viability (Figure 5a). The viability of both, LUHMES

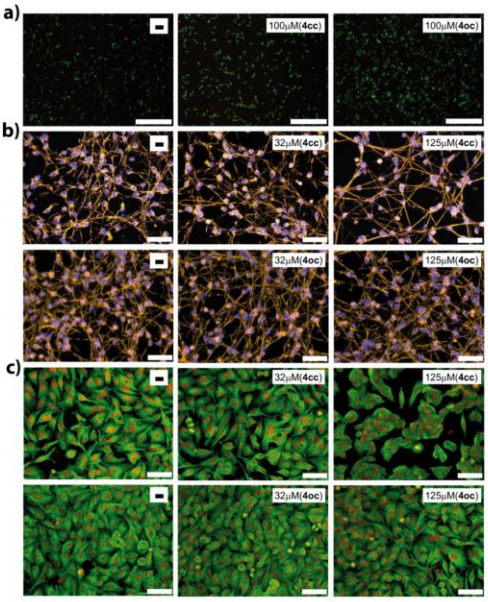

Figure 5. Live/dead stain images or morphology of different cells treated with (**4**). Blank experiments in the absence of any surfactant are always shown on the left. The concentration of the surfactant and the head group form is given in the white boxes. *E. coli* (a; scale bar = 20 μm), LUHMES neurons (b; scale bar = 100 μm), and HepG2 hepatoma cells (c; scale bar = 100 μm).

and HepG2, is also not influenced at a low concentration (32 μM) of the surfactant (Figure 5b,c). There is a minor effect at a higher concentration (125 μM), if compound (**4cc**) is used. Interestingly, the toxicity of (**4oc**) is so low; we cannot see any changes at the same concentration. The extraordinary biocompatibility of the surfactants was confirmed further by lactate dehydrogenase (LDH) release assay and resazurin metabolization assay (Figures S18−S21). Obviously, our fullerenol surfactants are harmless to both prokaryotic and eukaryotic cells in biologically relevant concentrations. Therefore, we can test now the possible antioxidative properties of the compounds in a cellular system (LUHMES). The cells were treated with the neurotoxicant 1-methyl-4-phenyl-

DOI: 10.1021/acsami.8b07032
ACS Appl. Mater. Interfaces 2018, 10, 23638−23646

pyridinium (MPP^+).[53] As expected, the viability of the cells is drastically reduced caused by MPP^+ (Figure 6). The situation changed when the surfactant was present. Even low concentrations of (**4**) had a positive effect, and at 25 μM, the viability of the cells has increased significantly. The viability of the cells was again confirmed by LDH release assay and resazurin metabolization assay (Supporting Information, Figure S22). There are only minor differences comparing (**4cc**) and (**4oc**).

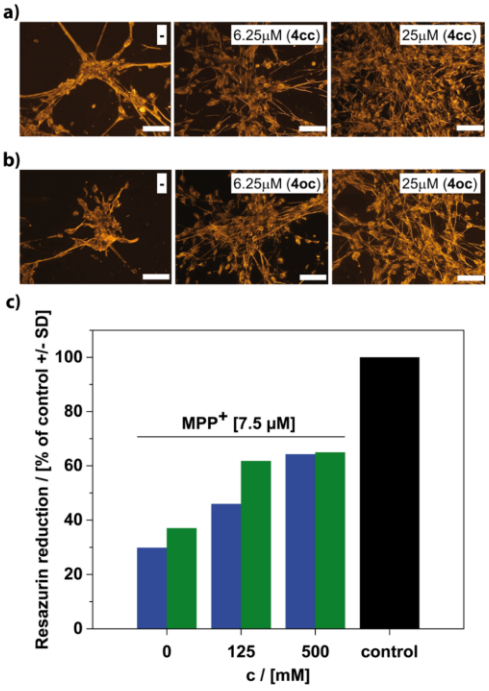

Figure 6. (a,b; scale bar = 100 μm) Morphology of eukaryotic LUHMES cell line treated with MPP^+ (7.5 μM) and surfactant (**4**). Blank experiments in the absence of any surfactant are always shown on the left. The concentration of the surfactant and the head group form is given in the white boxes. (c) Viability of LUHMES after the cells were loaded with the surfactant in the concentrations as indicated for a period of 3 h. Following the removal of the compounds in the supernatant by medium exchange, the toxicant MPP^+ (7.5 μM) was added for 60 h. Control cells received neither MPP^+ nor surfactant. Compound (**4cc**) blue bars and compound (**4oc**) green bars.

The final question remaining is that if the protection against oxidative stress is due to surfactants and their vesicle present in the outer medium or if the cells do actually include the surfactants into their cell membrane. The treatment of cells with the surfactant is a standard procedure in cell biology. We have followed similar protocols (see Methods section), but the surfactant concentration was low enough to avoid lysis. Furthermore, we have exposed LUHMES to a surfactant solution containing different concentrations of (**4**) only for 3 h. This short time was sufficient; a notable decrease of concentration in the mother liquor could be detected. The cells were then separated from the supernatant solvent and washed. It was made sure that there is no surfactant anymore in the external medium. Finally, the cells were then treated with MPP^+ for 60 h. If the surfactant had just been present in the external medium, we should not expect any protection anymore and in particular no concentration dependence. Figure 6c shows the results of the assessment of resazurin reduction assay; there still remains significant protection, which scales with the concentration of the surfactant used in the original solution. This allows only one conclusion. LUHMES cells have integrated with the fullerenol surfactant, and this way, they could decrease the stress level significantly. It is important to mention that the interaction of the surfactants with cells has already been studied multiple times by others in the past.[54−56] It could be proven that certain amphiphiles do interact with cellular membranes and become incorporated. Therefore, we have followed similar protocols. Therefore, it is not surprising that the fullerenol surfactant behaves similar.

■ CONCLUSIONS

On the basis of the encouraging findings about potential biotechnological applications of fullerene derivatives in the literature, we prepared a defined surfactant species containing a polyhydroxylated C_{60}, a fullerenol, as the hydrophilic head group. The necessary Janus-type modification of the fullerene was accomplished by attaching five alkyl chains on one side of C_{60} first, followed by modification with an average of 20 oxygen species consisting of hemiketals for compound **4cc** and ketones and hydroxyl groups for compound **4oc** on the other side. Caused by the packing parameter close to 1, the surfactant showed features similar to natural surfactants (lipids). There is a high tendency for the formation of vesicle-like structures in water, and at higher concentration lyotropic liquid crystals with lamellar characteristics have been observed.

Because of the fullerenol head group, the surfactant obtained an added functionality, the catalytic deactivation of ROS-like superoxide, peroxynitrite, hydroxyl radicals, and even hydrogen peroxide. Because the surfactants are fully biocompatible and benign even against delicate cells such as human liver cells (HepG2) and human dopaminergic neurons (LUHMES), we could explore the in vivo application for the reduction of oxidative stress. It was shown that the cells do actually integrate the surfactants. The lipid-like character and the high activity in ROS quenching in the cells indicate that the cells implement the fullerenol surfactants into their cellular membranes.

We have also seen that the fullerenol head group can exist in two alternative forms, which can be reversibly converted into each other by acid/base treatment. The form of the head group had a marked effect on all surfactant properties, including self-assembly and ROS quenching behavior. The surfactant containing the open-cluster form (**4oc**) seems to be superior overall.

■ METHODS

General Information. The synthesis that acquired inert gas atmosphere was performed using general Schlenk techniques under argon atmosphere. The solvents were dried according to the standard literature and stored under argon. Water was deionized with Millipore Milli-Q. All starting materials used for the synthesis were purchased

DOI: 10.1021/acsami.8b07032
ACS Appl. Mater. Interfaces 2018, 10, 23638−23646

from commercial sources unless stated differently. The fullerene C_{60} (pur. 99.9%) was purchased from SES research.

Synthesis of Hexachlorofullerene ($C_{60}Cl_6$) (2). C_{60} (0.28 mmol) was dissolved in chlorobenzene (11 mL) and sonicated for 5 min. Iodine monochloride (6.95 mmol) was added in one shot, and the solvent was evaporated at 35 °C. The crude product was further purified by column chromatography (silica gel, eluent: toluene). $C_{60}Cl_6$ is obtained as a red solid (0.2 mmol, 70%).

Synthesis of Penta-Alkylated Fullerene ($C_{60}R_5Cl$) (3). $C_{60}Cl_6$ (0.28 mmol) was dissolved in dry toluene (30 mL) and vigorously stirred. Dodecylamine (2.52 mmol) and potassium carbonate (1 g) were added. The mixture was stirred for 12 h. The solvent was evaporated under reduced pressure. The obtained solid was suspended in methanol, filtrated, and washed three times with methanol. The crude product was obtained by washing with ethyl acetate. The solvent was evaporated, and the crude product was further purified by column chromatography (silica gel, eluent: toluene/EE). The title compound is obtained as a red solid (0.17 mmol, 60%).

IR (powder): 3285, 2920, 2851, 1770, 1658, 1570, 1466, 1316, 1115 cm^{-1}; ^1H NMR (400 MHz, $CDCl_3$): δ 0.89 (t, ^3J = 7.2 Hz, 15H), 1.27 (m, 90H), 1.45 (m, 10H), 1.67 (m, 10H), 3.22 (m, 5H); ^{13}C NMR (100 MHz, $CDCl_3$): δ 22.56, 27.57, 27.67, 29.56, 29.58, 29.91, 29.93, 30.95, 31.02, 32.11, 47.36, 47.87, 47.88, 66.02, 68.21, 69.35, 143.24, 143.31, 143.71, 143.81, 143.83, 143.84, 143.84, 143.88, 144.02, 144.08, 144.31, 144.47, 144.51, 144.53, 144.91, 145.43, 147.16, 147.21, 147.23, 147.29, 147.62, 148.02, 148.21, 148.33, 148.57, 148.71, 149.12, 150.81, 153.88, 155.31; MS (MALDI): 1641.6 $[M - HCl]^-$, 1506.2 $[M - C_{12}H_{26}]^-$, 1457.1 $[M - C_{12}H_{25} - Cl]^-$, 1337.9 $[M - C_{24}H_{51}]^-$, 1307.0 $[M - N_2C_{24}H_{54}]^-$, 1272.8, 1307.0 $[M - N_2C_{24}H_{54} - Cl]^-$, 1167.6 $[M - C_{36}H_{76}]^-$, 1152.5 $[M - NC_{36}H_{77}]^-$, 1137.5 $[M - N_2C_{36}H_{78}]^-$, 1122.5 $[M - N_3C_{36}H_{79}]^-$, 1087.3 $[M - N_3C_{36}H_{79} - Cl]^-$.

Synthesis of the Polyhydroxylated Penta-Alkylated Fullerene Surfactant (4cc). $C_{60}Cl(HNC_{12}H_{25})_5$ (0.15 mmol) was dissolved in tetrahydrofuran (THF) (8 mL) and sonicated for 10 min. Solid NaOH (0.3 g) was added, and H_2O_2 (15 mL) was added under vigorous stirring. The mixture was heated to reflux for 4 h until a yellow solution is formed. THF was evaporated under reduced pressure, and the mixture was filtrated to remove nonwater-soluble compounds. Afterward, the volume of the solution was reduced to about 3 mL, and the reaction was cooled to room temperature. Methanol was added, and the product was precipitated. The precipitate was stirred in diluted NaOH for 5 min, and the solvent was evaporated. The crude product was washed five times with methanol to remove the remaining NaOH. The product is obtained as a light yellow-brown solid with an average number of 20 oxygen species (0.075 mmol, 50%). For characterization data, see the Supporting Information.

Conversion to the Open-Cage Compound (4oc). Compound (**4**) was dissolved in diluted hydrochloric acid and stirred for 10 min. The solvent was evaporated, and the product was obtained as a yellow oily solid. For characterization data, see the Supporting Information.

Biological Experiments. *Treatment of Cells with the Surfactant.* In a first step, the cells were grown under standard conditions as described in Figure S18. The cell culture plates were coated with 50 poly-L-ornithine and fibronectin overnight at 37 °C and washed two times with water. Cells were propagated in advanced Dulbecco's modified Eagle's medium (DMEM)/F12, 1× N_2 supplement, 2 mM L-glutamine (Gibco), and 40 ng/mL recombinant bFGF (R + D Systems; Minneapolis, MN). The differentiation process was initiated by the addition of differentiation medium consisting of advanced DMEM/F12, 1× N_2 supplement, 2 mM L-glutamine, 1 mM dibutyryl-cAMP, 1 μg/mL tetracycline, and 2 ng/mL recombinant human GDNF (R + D Systems). After 2 days, cells were trypsinized and collected in advanced DMEM/F12 medium. Cells were seeded onto 96-well plates at a density of 35 000 cells/well. The differentiation process was continued for additional 3 days. After the growing and differentiation process, the cells were treated with different surfactant concentrations for 3 h. During this time, the surfactant molecules could interact with the cell membranes. After that process, the medium was changed and washed several times, so all remaining surfactant molecules that are not incorporated into the cell wall are removed from the system. With these prepared cells, the experiments were performed. These cells were then treated with MPP^+. After an incubation time of 60 h, resazurin metabolization assay and LDH release assay have been performed.

Live/Dead Stain E. coli Treated with the Surfactant. Live/dead staining is performed by following the manufacturer's instructions (LIVE/DEAD BacLight Bacterial Viability Kit, Thermofisher); it stains cells with membrane damage in red, against viable cells stained in green. The stained cells were placed on agar-coated microscopic slides and observed under a fluorescence microscope at 400-fold magnification.

Morphology of LUHMES Treated with the Surfactant. For visualization of cell morphology, the cells were fixed with 4% paraformaldehyde for 20 min at room temperature (RT), permeabilized with 0.2% Triton X-100, washed, and blocked with 1% bovine serum albumin (BSA; Calbiochem, San Diego, CA) in phosphate-buffered saline (PBS) for 1 h. LUHMES were stained with an anti-β-III-tubulin antibody (rabbit, Sigma, 1:1000) in 1% BSA/PBS at 4 °C overnight. After washing, the secondary antibodies were added for 1 h, and nuclei were stained by Hoechst H-33342 (1 μg/mL) for 20 min. For quantitative evaluation of the neurite area, live staining of LUHMES was conducted with calcein-AM (1 μM) and Hoechst H-33342 (1 μg/mL) for 30 min. Images were collected by an automated microplate-reading microscope (Array-Scan II HCS Reader, Cellomics, Pittsburgh, PA) equipped with a Hamamatsu ORCA-ER camera (resolution 1024 × 1024; run at 2 × 2 binning) in two different fluorescence channels. Nuclei were identified as objects according to their intensity, size, area, and shape. A virtual area corresponding to the cell soma was defined around each nucleus. The total calcein pixel area per field minus the soma areas in that field was defined as the neurite mass. In addition, viability was analyzed by the detection of the percentage of those cells positive for calcein and for H-33342.

Morphology of HepG2 Treated with the Surfactant. For visualization of cell morphology, the cells were fixed with 4% paraformaldehyde for 20 min at RT, permeabilized with 0.2% Triton X-100, washed, and blocked with 1% BSA (Calbiochem, San Diego, CA) in PBS for 1 h. HepG2 cells were stained with a monoclonal anti-α-tubulin antibody (Sigma; 1:1000).

Resazurin Metabolization Assay and LDH Release Assay. Resazurin metabolization assay: Resazurin (Sigma) was added to the cell culture medium in a final concentration of 5 μg/mL and fluorescence was measured after 60 min (λ_{ex} = 530 nm; λ_{em} = 590 nm). LDH release assay: The LDH activity was detected separately in the supernatant and cell lysate. Following the separation of the supernatants, the cells were lysed in PBS/0.5% Triton X-100 for >60 min. The percentage of LDH released was calculated as 100 × $LDH_{supernatant}/LDH_{supernatant+lysate}$. For the enzymatic assay, 20 μL of the sample was combined with 180 μL of the reaction buffer containing NADH (100 μM) and sodium pyruvate (600 μM) in sodium phosphate buffer adjusted to pH 7.4 by titration with K_2HPO_4 (40 mM) and KH_2PO_4 (10 mM). Absorption at 340 nm was detected at 37 °C in 1 min intervals over a period of 20 min, and the enzyme activity was calculated from the respective slopes.

Analytical Methods. NMR measurements (^1H, ^{13}C) were performed on a Varian INOVA 400 MHz spectrometer. MALDI-MS measurements were performed using a Bruker Microflex MALDI-TOF. The samples were prepared in a cyano-4-hydroxycinnamic acid matrix or a *trans*-2-[3-(4-*tert*-butylphenyl)-2-methyl-2-propenylidene]malononitrile matrix. Attenuated total reflection–infrared (ATR–IR) spectra were measured with a Perkin Elmer 100 Spectrum spectrometer including an ATR unit. TGA was measured at Netzsch Jupiter STA 449 F3. Liquid chromatography was measured with Thermo Fisher Scientific Dionex 3000. As the column, Agilent Poroshell 120 EC-C18 (2.1 × 100 mm, 2.7 μm) was used. MeCN (5%) as eluent A and 95% water as eluent B with 0.1% formic acid were used. A linear gradient of 5% A to 100% A was applied with

DOI: 10.1021/acsami.8b07032
ACS Appl. Mater. Interfaces 2018, 10, 23638–23646

a flow rate of 0.3 mL/min. The DLS measurements were done by using a Malvern Zen5600. Liquid-crystal pictures were taken with an Olympus CX41 light microscope. The high-resolution TEM observations were carried out using JEOL JEM-2200FS, and the TEM observations were carried out using Zeiss Libra120. The surface tension measurements were performed using Krüss K100.

■ ASSOCIATED CONTENT

Supporting Information

The Supporting Information is available free of charge on the ACS Publications website at DOI: 10.1021/acsami.8b07032.

Supporting molecular characterization and details regarding biological experiments (PDF)

■ AUTHOR INFORMATION

Corresponding Author

*E-mail: sebastian.polarz@uni-konstanz.de.

ORCID

Klaus Boldt: 0000-0002-0035-2490

Sebastian Polarz: 0000-0003-1651-4906

Author Contributions

The manuscript was written through contributions from all authors. All authors have given approval to the final version of the manuscript.

Notes

The authors declare no competing financial interest.

■ ACKNOWLEDGMENTS

The current research was funded by an ERC consolidator grant (I-SURF; project 614606). K.B. is thankful for the financial support from the Fonds der Chemischen Industrie through a Liebig Fellowship and by the Zukunftskolleg Konstanz through a 5-year Marie Curie ZIF Research Fellowship. European Research Council Fonds der Chemischen Industrie.

■ REFERENCES

(1) Prather, K. L. J.; Martin, C. H. De novo biosynthetic pathways: rational design of microbial chemical factories. *Curr. Opin. Biotechnol.* **2008**, *19*, 468−474.

(2) Adkins, J.; Pugh, S.; McKenna, R.; Nielsen, D. R. Engineering microbial chemical factories to produce renewable biomonomers. *Front. Microbiol.* **2012**, *3*, 313.

(3) Finkel, T.; Holbrook, N. J. Oxidants, oxidative stress and the biology of ageing. *Nature* **2000**, *408*, 239−247.

(4) Circu, M. L.; Aw, T. Y. Reactive oxygen species, cellular redox systems, and apoptosis. *Free Radical Biol. Med.* **2010**, *48*, 749−762.

(5) Ott, M.; Gogvadze, V.; Orrenius, S.; Zhivotovsky, B. Mitochondria, oxidative stress and cell death. *Apoptosis* **2007**, *12*, 913−922.

(6) Chiang, L. Y.; Lu, F.-J.; Lin, J.-T. Free radical scavenging activity of water-soluble fullerenols. *J. Chem. Soc., Chem. Commun.* **1995**, 1283−1284.

(7) Yin, J.-J.; Lao, F.; Fu, P. P.; Wamer, W. G.; Zhao, Y.; Wang, P. C.; Qiu, Y.; Sun, B.; Xing, G.; Dong, J.; Liang, X.-J.; Chen, C. The scavenging of reactive oxygen species and the potential for cell protection by functionalized fullerene materials. *Biomaterials* **2009**, *30*, 611−621.

(8) Chiang, L. Y.; Bhonsle, J. B.; Wang, L.; Shu, S. F.; Chang, T. M.; Hwu, J. R. Efficient one-flask synthesis of water-soluble [60]-fullerenols. *Tetrahedron* **1996**, *52*, 4963−4972.

(9) Yin, J.-J.; Lao, F.; Fu, P. P.; Wamer, W. G.; Zhao, Y.; Wang, P. C.; Qiu, Y.; Sun, B.; Xing, G.; Dong, J.; Liang, X.-J.; Chen, C. The scavenging of reactive oxygen species and the potential for cell protection by functionalized fullerene materials. *Biomaterials* **2009**, *30*, 611−621.

(10) Markovic, Z.; Trajkovic, V. Biomedical potential of the reactive oxygen species generation and quenching by fullerenes (C60). *Biomaterials* **2008**, *29*, 3561−3573.

(11) Partha, R.; Conyers, J. L. Biomedical applications of functionalized fullerene-based nanomaterials. *Int. J. Nanomed.* **2009**, *4*, 261−275.

(12) Djordjević, A.; Bogdanović, G.; Dobrić, S. Fullerenes in biomedicine. *J. BUON* **2006**, *11*, 391−404.

(13) Nakamura, H.; Nozaki, Y.; Koizumi, Y.; Watano, S. Effect of number of hydroxyl groups of fullerenol C60(OH)n on its interaction with cell membrane. *J. Taiwan Inst. Chem. Eng.* **2017**, DOI: 10.1016/j.jtice.2017.11.016.

(14) Guldi, D. M.; Zerbetto, F.; Georgakilas, V.; Prato, M. Ordering Fullerene Materials at Nanometer Dimensions. *Acc. Chem. Res.* **2005**, *38*, 38−43.

(15) Yu, X.; Li, Y.; Dong, X.-H.; Yue, K.; Lin, Z.; Feng, X.; Huang, M.; Zhang, W.-B.; Cheng, S. Z. D. Giant Surfactants Based on Molecular Nanoparticles: Precise Synthesis and Solution Self-assembly. *J. Polym. Sci., Part B: Polym. Phys.* **2014**, *52*, 1309−1325.

(16) Burger, C.; Hao, J.; Ying, Q.; Isobe, H.; Sawamura, M.; Nakamura, E.; Chu, B. Multilayer vesicles and vesicle clusters formed by the fullerene-based surfactant C60(CH3)5K. *J. Colloid Interface Sci.* **2004**, *275*, 632−641.

(17) Sano, M.; Oishi, K.; Ishi-i, T.; Shinkai, S. Vesicle Formation and Its Fractal Distribution by Bola-Amphiphilic [60]Fullerene. *Langmuir* **2000**, *16*, 3773−3776.

(18) Cassell, A. M.; Asplund, C. L.; Tour, J. M. Self-Assembling Supramolecular Nanostructures from a C60 Derivative: Nanorods and Vesicles. *Angew. Chem., Int. Ed.* **1999**, *38*, 2403−2405.

(19) Homma, T.; Harano, K.; Isobe, H.; Nakamura, E. Preparation and properties of vesicles made of nonpolar/polar/nonpolar fullerene amphiphiles. *J. Am. Chem. Soc.* **2011**, *133*, 6364−6370.

(20) Zhao, Y. M.; Chen, G. C-60 Fullerene Amphiphiles as Supramolecular Building Blocks for Organized and Well-Defined Nanoscale Objects. In *Fullerenes and Other Carbon-rich Nanostructures*; Nierengarten, J. F., Ed.; Springer-Verlag Berlin: Berlin, 2014; Vol. *159*, pp 23−53.

(21) Partha, R.; Mitchell, L. R.; Lyon, J. L.; Joshi, P. P.; Conyers, J. L. Buckysomes: fullerene-based nanocarriers for hydrophobic molecule delivery. *ACS Nano* **2008**, *2*, 1950−1958.

(22) Brettreich, M.; Burghardt, S.; Böttcher, C.; Bayerl, T.; Bayerl, S.; Hirsch, A. Globular Amphiphiles: Membrane-Forming Hexaadducts of C60. *Angew. Chem., Int. Ed.* **2000**, *39*, 1845−1848.

(23) Partha, R.; Lackey, M.; Hirsch, A.; Casscells, S. W.; Conyers, J. L. Self assembly of amphiphilic C60 fullerene derivatives into nanoscale supramolecular structures. *J. Nanobiotechnol.* **2007**, *5*, 6.

(24) Nitta, H.; Harano, K.; Isomura, M.; Backus, E. H. G.; Bonn, M.; Nakamura, E. Conical Ionic Amphiphiles Endowed with Micellization Ability but Lacking Air-Water and Oil-Water Interfacial Activity. *J. Am. Chem. Soc.* **2017**, *139*, 7677−7680.

(25) Lin, Z.; Lu, P.; Hsu, C.-H.; Yue, K.; Dong, X.-H.; Liu, H.; Guo, K.; Wesdemiotis, C.; Zhang, W.-B.; Yu, X.; Cheng, S. Z. D. Self-Assembly of Fullerene-Based Janus Particles in Solution: Effects of Molecular Architecture and Solvent. *Chem.—Eur. J.* **2014**, *20*, 11630−11635.

(26) Chen, M.; Zhu, H.; Zhou, S.; Xu, W.; Dong, S.; Li, H.; Hao, J. Self-Organization and Vesicle Formation of Amphiphilic Fullerenomonodendrons Bearing Oligo(poly(ethylene oxide)) Chains. *Langmuir* **2016**, *32*, 2338−2347.

(27) Burghardt, S.; Hirsch, A.; Schade, B.; Ludwig, K.; Böttcher, C. Switchable supramolecular organization of structurally defined micelles based on an amphiphilic fullerene. *Angew. Chem., Int. Ed.* **2005**, *44*, 2976−2979.

(28) Donskyi, I.; Achazi, K.; Wycisk, V.; Böttcher, C.; Adeli, M. Synthesis, self-assembly, and photocrosslinking of fullerene-polyglycerol amphiphiles as nanocarriers with controlled transport properties. *Chem. Commun.* **2016**, *52*, 4373−4376.

(29) Kuvychko, I. V.; Streletskii, A. V.; Popov, A. A.; Kotsiris, S. G.; Drewello, T.; Strauss, S. H.; Boltalina, O. V. Seven-Minute Synthesis of Pure Cs-C60Cl6 from [60] Fullerene and Iodine Monochloride: First IR, Raman, and Mass Spectra of 99 mol% C60Cl6. *Chem.—Eur. J.* **2005**, *11*, 5426−5436.
(30) Kornev, A. B.; Khakina, E. A.; Troyanov, S. I.; Kushch, A. A.; Peregudov, A.; Vasilchenko, A.; Deryabin, D. G.; Martynenko, V. M.; Troshin, P. A. Facile preparation of amine and amino acid adducts of [60]fullerene using chlorofullerene C60Cl6 as a precursor. *Chem. Commun.* **2012**, *48*, 5461−5463.
(31) Wang, S.; He, P.; Zhang, J.-M.; Jiang, H.; Zhu, S.-Z. Novel and Efficient Synthesis of Water-Soluble [60]Fullerenol by Solvent-Free Reaction. *Synth. Commun.* **2005**, *35*, 1803−1808.
(32) Wang, Z.; Wang, S.; Lu, Z.; Gao, X. Syntheses, structures and antioxidant activities of fullerenols: knowledge learned at the atomistic level. *J. Cluster Sci.* **2015**, *26*, 375−388.
(33) Kokubo, K.; Shirakawa, S.; Kobayashi, N.; Aoshima, H.; Oshima, T. Facile and scalable synthesis of a highly hydroxylated water-soluble fullerenol as a single nanoparticle. *Nano Res.* **2011**, *4*, 204−215.
(34) Xing, G.; Zhang, J.; Zhao, Y.; Tang, J.; Zhang, B.; Gao, X.; Yuan, H.; Qu, L.; Cao, W.; Chai, Z.; Ibrahim, K.; Su, R. Influences of structural properties on stability of fullerenols. *J. Phys. Chem. B* **2004**, *108*, 11473−11479.
(35) Chiang, L. Y.; Upasani, R. B.; Swirczewski, J. W.; Soled, S. Evidence of hemiketals incorporated in the structure of fullerols derived from aqueous acid chemistry. *J. Am. Chem. Soc.* **1993**, *115*, 5453−5457.
(36) Afreen, S.; Kokubo, K.; Muthoosamy, K.; Manickam, S. Hydration or hydroxylation: direct synthesis of fullerenol from pristine fullerene [C60] via acoustic cavitation in the presence of hydrogen peroxide. *RSC Adv.* **2017**, *7*, 31930−31939.
(37) Semenov, K. N.; Letenko, D. G.; Charykov, N. A.; Nikitin, V. A.; Matuzenko, M. Y.; Keskinov, V. A.; Postnov, V. N.; Kopyrin, A. A. Synthesis and identification of fullerenol prepared by the direct oxidation route. *Russ. J. Appl. Chem.* **2010**, *83*, 2076−2080.
(38) Chao, T.-C.; Song, G.; Hansmeier, N.; Westerhoff, P.; Herckes, P.; Halden, R. U. Characterization and liquid chromatography-MS/MS based quantification of hydroxylated fullerenes. *Anal. Chem.* **2011**, *83*, 1777−1783.
(39) Wang, Z.; Lu, Z.; Zhao, Y.; Gao, X. Oxidation-induced water-solubilization and chemical functionalization of fullerenes C60, Gd@C60and Gd@C82: atomistic insights into the formation mechanisms and structures of fullerenols synthesized by different methods. *Nanoscale* **2015**, *7*, 2914−2925.
(40) McConnell, H. M. Structures And Transitions In Lipid Monolayers At The Air-Water Interface. *Annu. Rev. Phys. Chem.* **1991**, *42*, 171−195.
(41) Egberts, J.; Sloot, H.; Mazure, A. Minimal surface tension, squeeze-out and transition temperatures of binary mixtures of dipalmitoylphosphatidylcholine and unsaturated phospholipids. *Biochim. Biophys. Acta* **1989**, *1002*, 109−113.
(42) Lin, M.-S.; Chen, R.-T.; Yu, N.-Y.; Sun, L.-C.; Liu, Y.; Cui, C.-H.; Xie, S.-Y.; Huang, R.-B.; Zheng, L.-S. Fullerene-based amino acid ester chlorides self-assembled as spherical nano-vesicles for drug delayed release. *Colloids Surf., B* **2017**, *159*, 613.
(43) Burger, C.; Hao, J.; Ying, Q.; Isobe, H.; Sawamura, M.; Nakamura, E.; Chu, B. Multilayer vesicles and vesicle clusters formed by the fullerene-based surfactant C60(CH3)5K. *J. Colloid Interface Sci.* **2004**, *275*, 632−641.
(44) Guida, V. Thermodynamics and kinetics of vesicles formation processes. *Adv. Colloid Interface Sci.* **2010**, *161*, 77−88.
(45) Almgren, M.; Rangelov, S. Spontaneously Formed Non-equilibrium Vesicles of Cetyltrimethylammonium Bromide and Sodium Octyl Sulfate in Aqueous Dispersions. *Langmuir* **2004**, *20*, 6611−6618.
(46) Choi, H. S.; Kim, J. W.; Cha, Y.-N.; Kim, C. A quantitative nitroblue tetrazolium assay for determining intracellular superoxide anion production in phagocytic cells. *J. Immunoassay Immunochem.* **2006**, *27*, 31−44.
(47) Troshin, P. A.; Astakhova, A. S.; Lyubovskaya, R. N. Synthesis of fullerenols from halofullerenes. *Fullerenes, Nanotubes, Carbon Nanostruct.* **2005**, *13*, 331−343.
(48) Jovanovic, S. V.; Steenken, S.; Tosic, M.; Marjanovic, B.; Simic, M. G. Flavonoids as Antioxidants. *J. Am. Chem. Soc.* **1994**, *116*, 4846−4851.
(49) Schildknecht, S.; Pape, R.; Müller, N.; Robotta, M.; Marquardt, A.; Bürkle, A.; Drescher, M.; Leist, M. Neuroprotection by minocycline caused by direct and specific scavenging of peroxynitrite. *J. Biol. Chem.* **2011**, *286*, 4991−5002.
(50) Torchilin, V. P. Structure and design of polymeric surfactant-based drug delivery systems. *J. Controlled Release* **2001**, *73*, 137−172.
(51) Hrenovic, J.; Ivankovic, T. Toxicity of anionic and cationic surfactant to Acinetobacter junii in pure culture. *Cent. Eur. J. Biol.* **2007**, *2*, 405−414.
(52) Alkilany, A. M.; Nagaria, P. K.; Hexel, C. R.; Shaw, T. J.; Murphy, C. J.; Wyatt, M. D. Cellular Uptake and Cytotoxicity of Gold Nanorods: Molecular Origin of Cytotoxicity and Surface Effects. *Small* **2009**, *5*, 701−708.
(53) Schildknecht, S.; Pöltl, D.; Nagel, D. M.; Matt, F.; Scholz, D.; Lotharius, J.; Schmieg, N.; Salvo-Vargas, A.; Leist, M. Requirement of a dopaminergic neuronal phenotype for toxicity of low concentrations of 1-methyl-4-phenylpyridinium to human cells. *Toxicol. Appl. Pharmacol.* **2009**, *241*, 23−35.
(54) Nazari, M.; Kurdi, M.; Heerklotz, H. Classifying surfactants with respect to their effect on lipid membrane order. *Biophys. J.* **2012**, *102*, 498−506.
(55) Rabbel, H.; Werner, M.; Sommer, J.-U. Interactions of amphiphilic triblock copolymers with lipid membranes: modes of interaction and effect on permeability examined by generic Monte Carlo simulations. *Macromolecules* **2015**, *48*, 4724−4732.
(56) le Maire, M.; Champeil, P.; Møller, J. V. Interaction of membrane proteins and lipids with solubilizing detergents. *Biochim. Biophys. Acta, Biomembr.* **2000**, *1508*, 86−111.

DOI: 10.1021/acsami.8b07032
ACS Appl. Mater. Interfaces 2018, 10, 23638−23646

SUPPORTING INFORMATION

Increasing the Resistance of Living Cells Against Oxidative Stress by Non-Natural Surfactants as Membrane Guards

*Marius Kunkel, Stefan Schildknecht, Klaus Boldt, Lukas Zeyffert, David Schleheck, Marcel Leist and Sebastian Polarz**

University of Konstanz, Universitätsstrasse 10, 78457 Konstanz, Germany

Corresponding Author

*E-mail: sebastian.polarz@uni-konstanz.de.

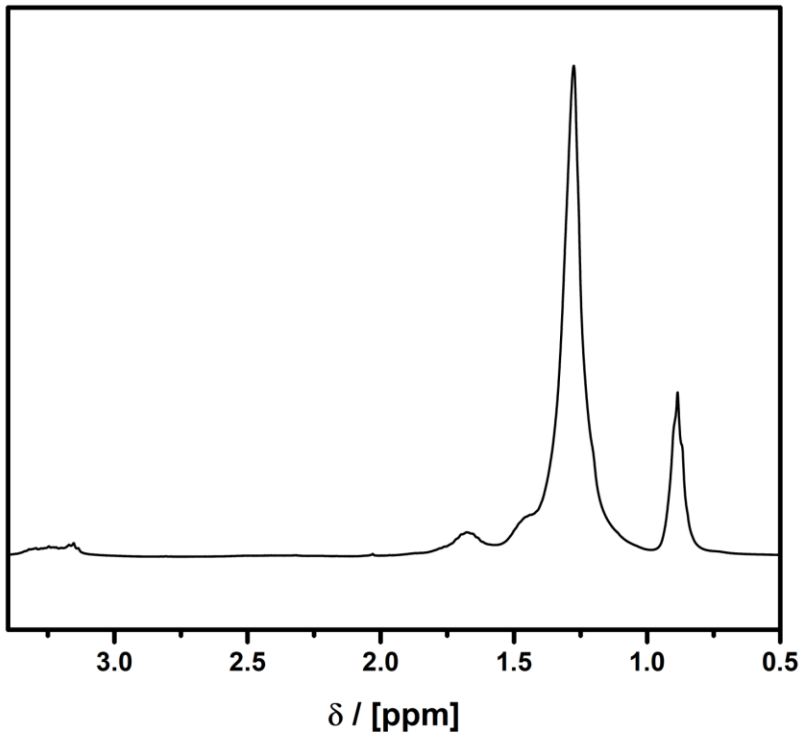

Fig. S1. ^{1}H-NMR for compound (**3**) in $CDCl_3$. **^{1}H-NMR** (400 MHz, $CDCl_3$): δ(ppm) = 0.89 (t, 3J = 7.2 Hz, 15 H), 1.27 (m, 90 H), 1.45 (m, 10 H), 1.67 (m, 10 H), 3.22 (m, 5 H)

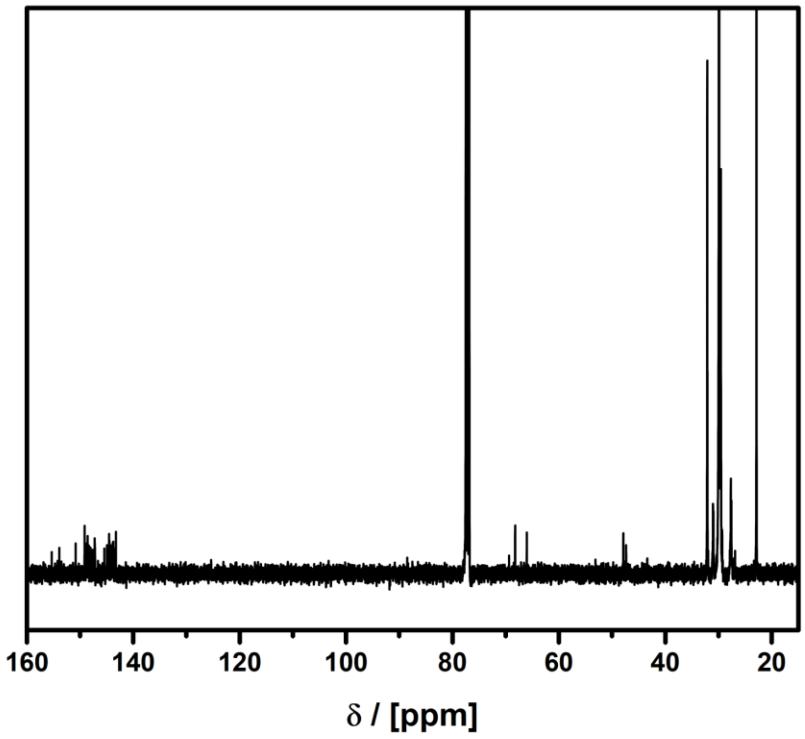

Fig. S2. ^{13}C-NMR for compound (**3**) in $CDCl_3$. **^{13}C-NMR** (100 MHz, $CDCl_3$): δ(ppm) = 22.56, 27.57, 27.67, 29.56, 29.58, 29.91, 29.93, 30.95, 31.02, 32.11, 47.36, 47.87, 47.88, 66.02, 68.21, 69.35, 143.24, 143.31, 143.71, 143.81, 143.83, 143.84, 143.84, 143.88, 144.02, 144.08, 144.31, 144.47, 144.51, 144.53, 144.91, 145.43, 147.16, 147.21, 147.23, 147.29, 147.62, 148.02, 148.21, 148.33, 148.57, 148.71, 149.12, 150.81, 153.88, 155.31

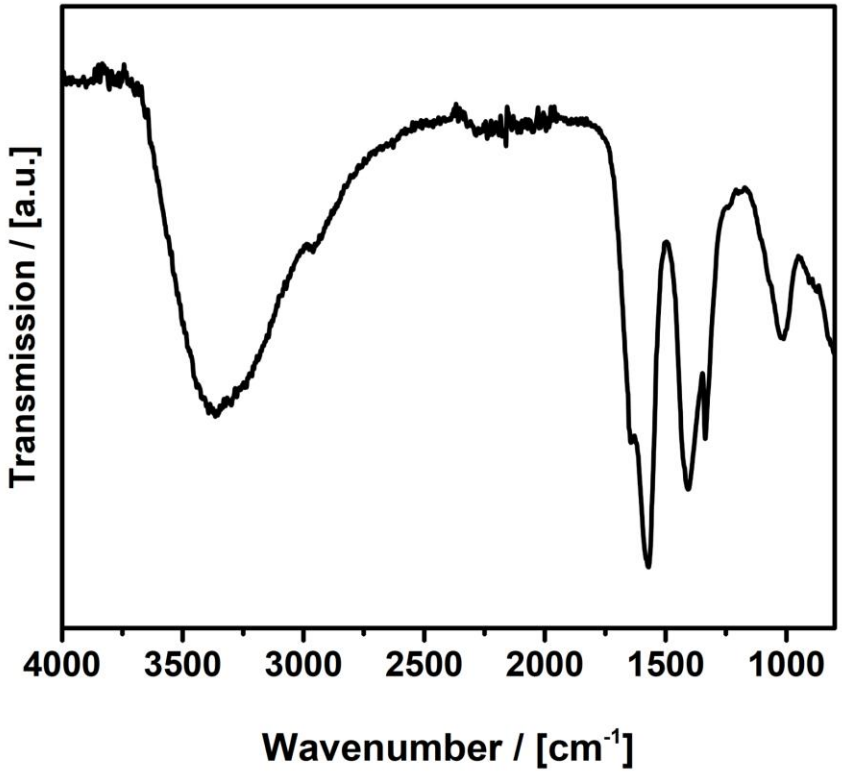

Fig. S3. FT-IR for compound (**4cc**). ATR-IR: ν (cm^{-1}) = 3365, 2942, 2971, 1645, 1574, 1409, 1325, 1032.

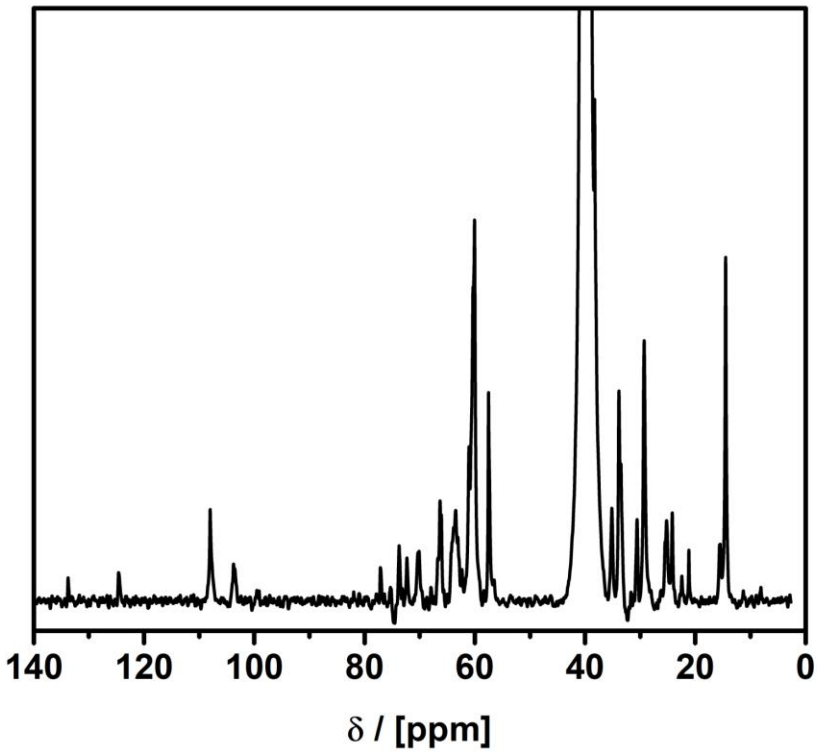

Fig. S4. ^{13}C-NMR for compound (**4cc**) in D_2O.^{13}C-NMR (100 MHz, D2O): δ(ppm) = 13.26, 16.81, 20.39, 20.53, 23.23, 23.34, 27.93, 28.77, 30.35, 30.65, 33.24, 33.33, 36.722, 36.84. 36.85, 52.42, 57.26, 57.28, 60.52, 60.59, 60.76, 60.84, 61.73, 64.45, 174.16, 174.48.

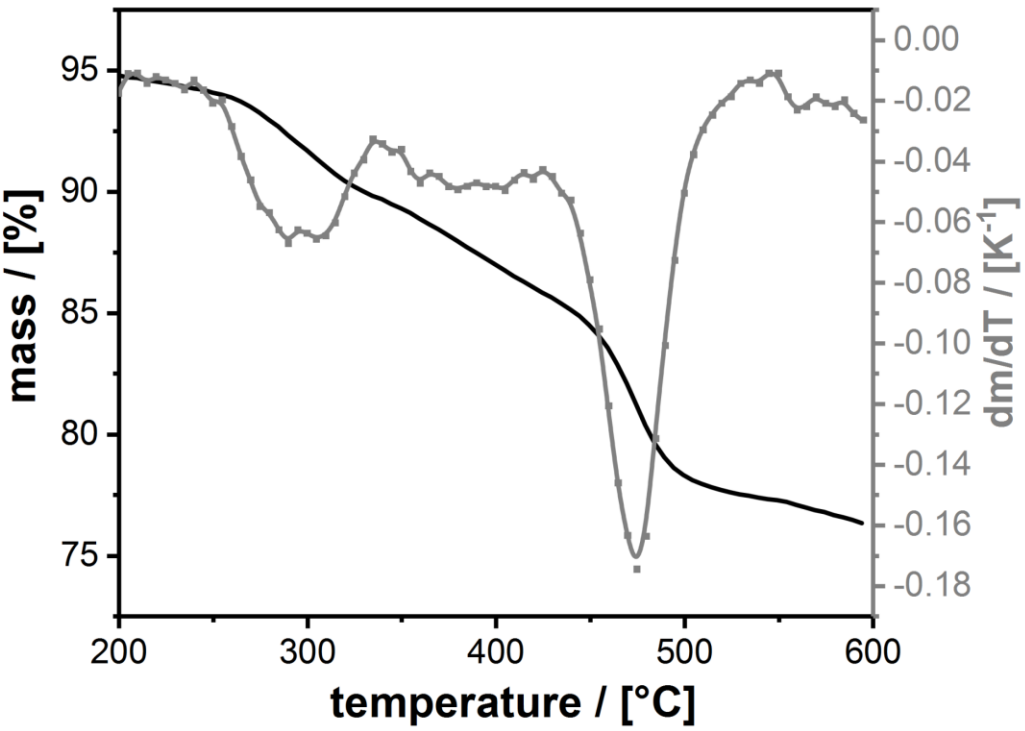

Fig. S5. TGA for compound (**4cc**) under inert conditions (N_2 atmosphere). step: 5.91 %, 2. step: 17.05 %. The number of OH-groups was among others determined by TGA (N_2, 1 K/min).

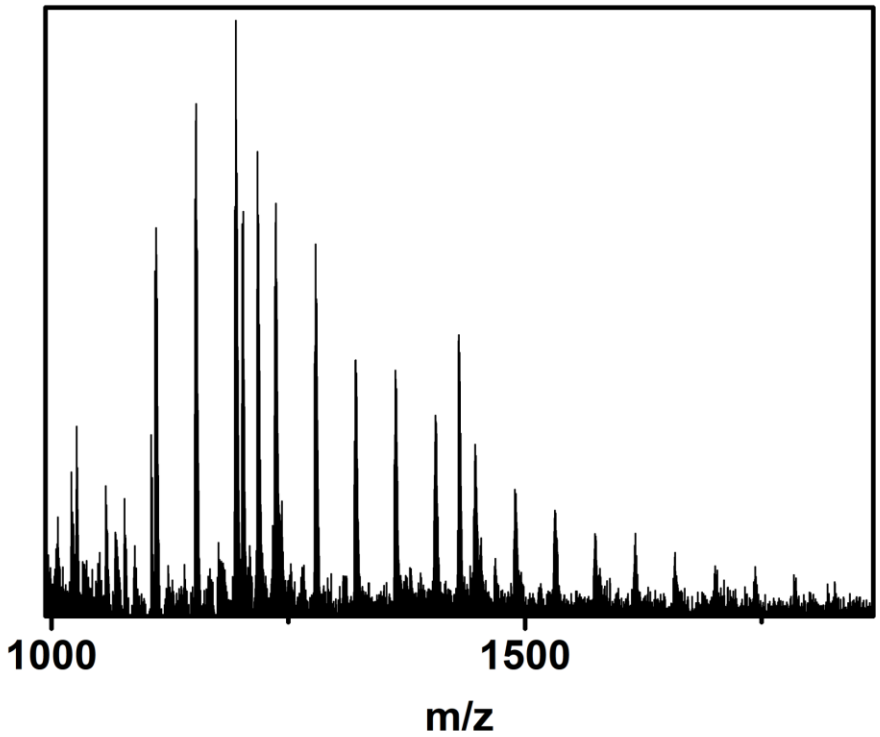

Fig. S6. MALDI-MS for compound (**4cc**). 1615 $[HC_{60}(HNC_{12}H_{25})_3(OH)_{20}]^+$,1827.1 $[HC_{60}(HNC_{12}H_{25})_5(OH)_8(O)_3]^+$, 1741,7 $[HC_{60}(HNC_{12}H_{25})_4(OH)_{12}(O)_4(NH)]^+$, 1656.8 $[HC_{60}(HNC_{12}H_{25})_4(OH)_7(O)_4NH]^+$, 1615 $[HC_{60}(HNC_{12}H_{25})_3(OH)_{20}]^+$, 1573.6 $[HC_{60}(HNC_{12}H_{25})_3(HN)_2(OH)_{13}(O)_3]^+$, 1529.6 $[HC_{60}(HNC_{12}H_{25})_3(OH)_{15}]^+$, 1488.6 $[HC_{60}(HNC_{12}H_{25})_3(NH)(OH)_7(O)_5]^+$, 1446.9 $[HC_{60}(HNC_{12}H_{25})_2(OH)_{21}]^+$, 1429.8 $[HC_{60}(HNC12H25)_2(OH)_{20}]^+$, 1404.2 $[HC_{60}(HNC_{12}H_{25})_2(HN)_2(OH)_{13}(O)_4]^+$, 1361.5 $[HC_{60}(HNC12H25)_2(OH)_{16}]^+$, 1319.9 $[HC_{60}(HNC12H25)_2(HN)_3(OH)_9(O)_2]^+$, 1277.8 $[HC_{60}(HNC_{12}H_{25})_2(OH)_{11}]^+$, 1235.8 $[HC_{60}(HNC_{12}H_{25})_1(HN)_3(OH)_{13}O_4]^+$, 1217.3 $[HC_{60}(HNC_{12}H_{25})_1(HN)_3(OH)_{11}O_5]^+$, 1201.3 $[HC_{60}(HNC_{12}H_{25})_1(HN)_3(OH)_{11}O_4]^+$, 1193.7 $[HC_{60}(HNC_{12}H_{25})_1(OH)_{16}O]^+$, 1151.5 $[HC_{60}(HNC_{12}H_{25})_1(HN)_2(OH)_8(O)_5]^+$, 1109.4 $[HC_{60}(HNC_{12}H_{25})_1(OH)_{12}]^+$**,** 1026.3 $[HC_{60}(OH)_{17}(O)]^+$

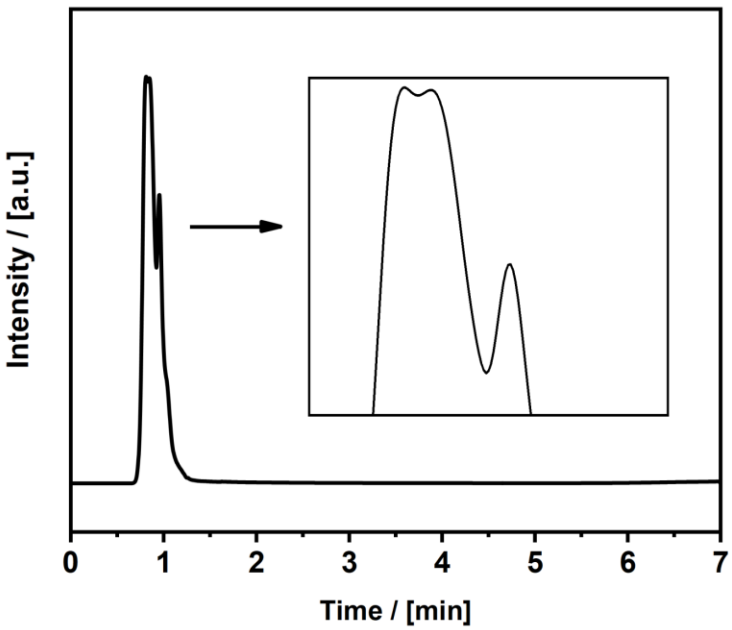

Fig. S7. Chromatogram of (**4cc**). 5% MeCN as eluent A and 95% water as eluent B with 0.1 % formic acid. A linear gradient of 5% A to 100% A was applied with a flow rate of 0.3 mL/min.

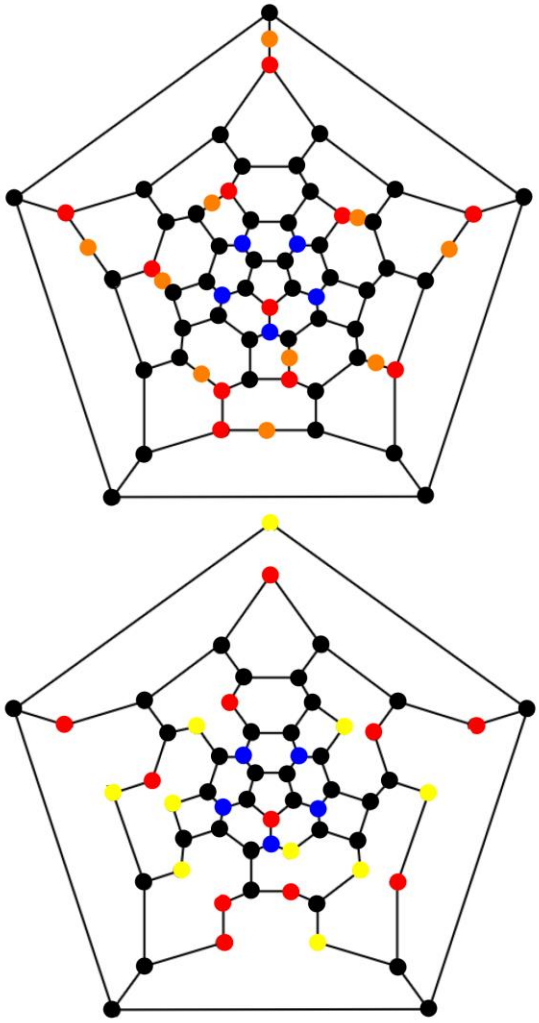

Fig. S8. Schematic Schlegel diagrams of one possible structure for the fullerenol surfactant systems. Top hemiketal structure (**4cc**), bottom ketone enriched structure (**4oc**). Red: C-OH, orange: -O-, yellow: C=O, blue: C-NHR.

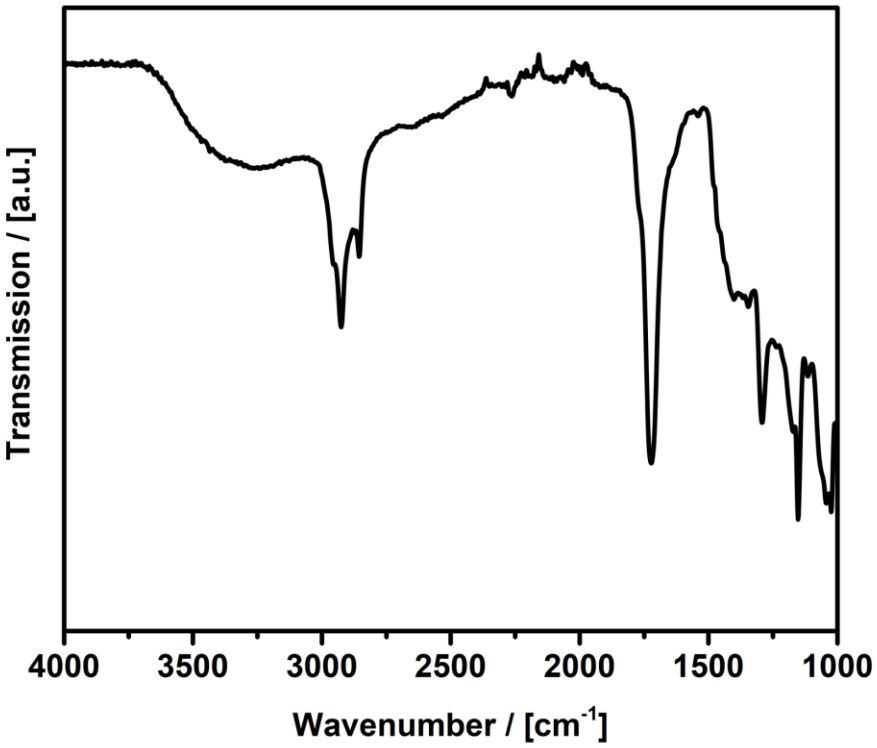

Fig. S9. Conversion of (**4cc**) to (**4oc**). ATR-IR: ν (cm^{-1}) = 3600-2364, 2971, 2942, 1720, 1623, 1396, 1155, 1023.

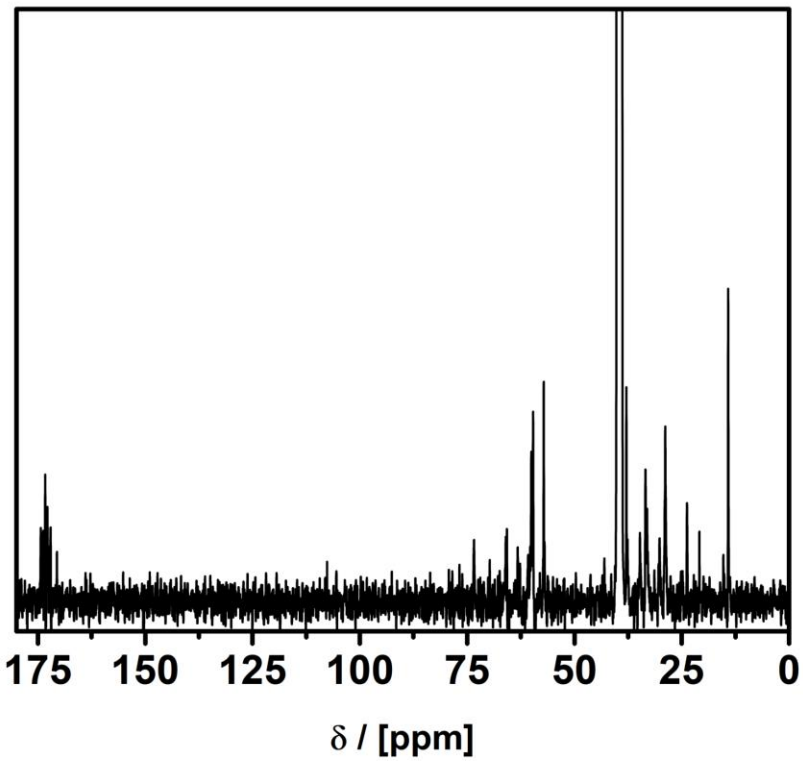

Fig. S10. ^{13}C-NMR compound open cage (**4oc**) in DMSO-d_6. ^{13}C-NMR (100 MHz, DMSO): δ(ppm) = 14.18, 20.89, 23.78, 28.84, 28.89, 30.18, 32.88, 33.07, 33.45, 34.74, 37.63, 37.89. 37.91, 60.31, 60.78, 62.65, 63.21, 65.72, 65.77, 65.98, 69.73, 73.39, 114.32, 170.54, 172.02, 172.27, 172.62, 172.76, 173.27, 173.52, 173.73, 174.29, 174.33.

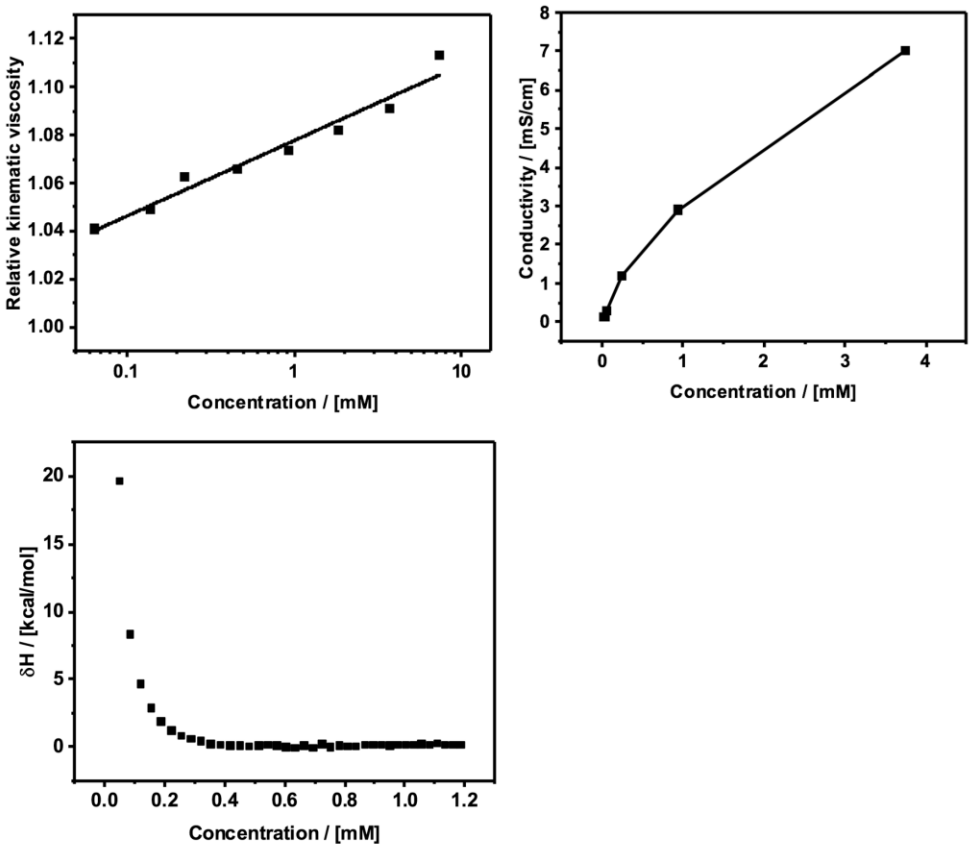

Fig. S11. Top left: Relative viscosity measurement of (**4cc**) in Milli-Q at rt. Top right: Conductivity (ionic) of (4) in Milli-Q at rt. Bottom: Isothermal titration calorimetry (ITC) of (4) in Milli-Q. A discontinuous relation between concentration and the observable parameter (viscosity, conductivity, or ITC signal) would indicate a change in the aggregation state of the system, respectively the occurrence of aggregation/ micellization. Obviously, all curves are continuous. A classic cmc cannot be identified.

Fig. S12. Additional data for aggregate dispersions in water.

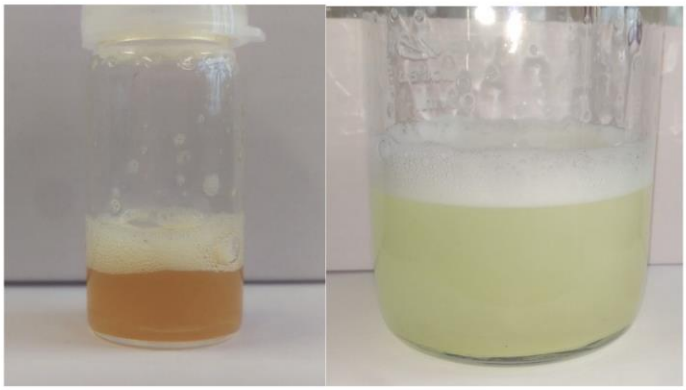

(a) Dispersions of (**4cc**; left) and (**4oc**; right) in water at oversaturated concentration.

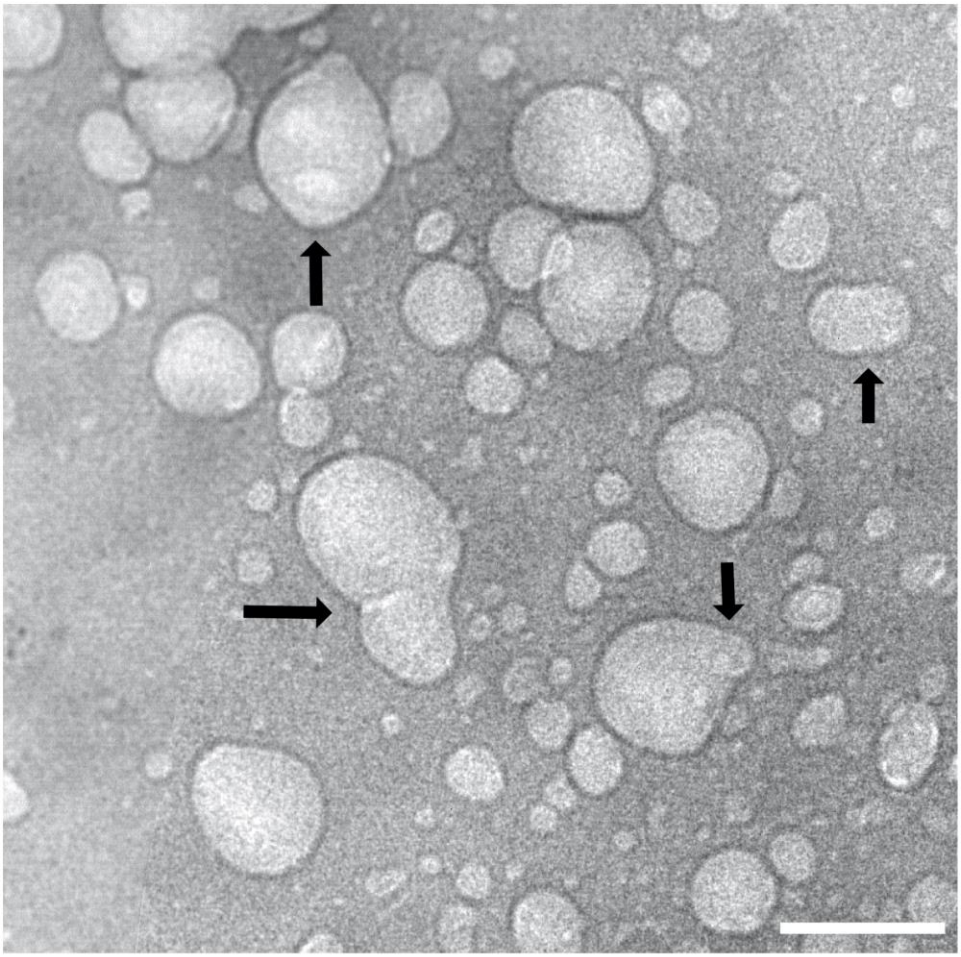

(b) Additional TEM micrograph, scalebar = 100 nm. Arrows indicate positions, where vesicles have started to fuse.

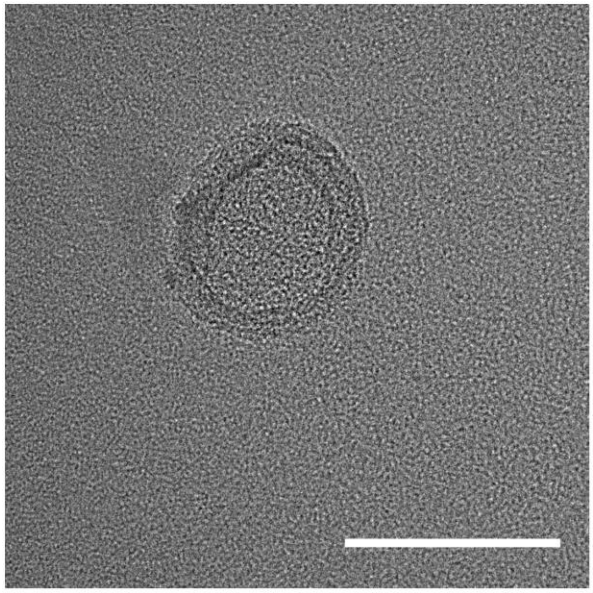

(c) Additional TEM micrograph, scalebar = 50 nm.

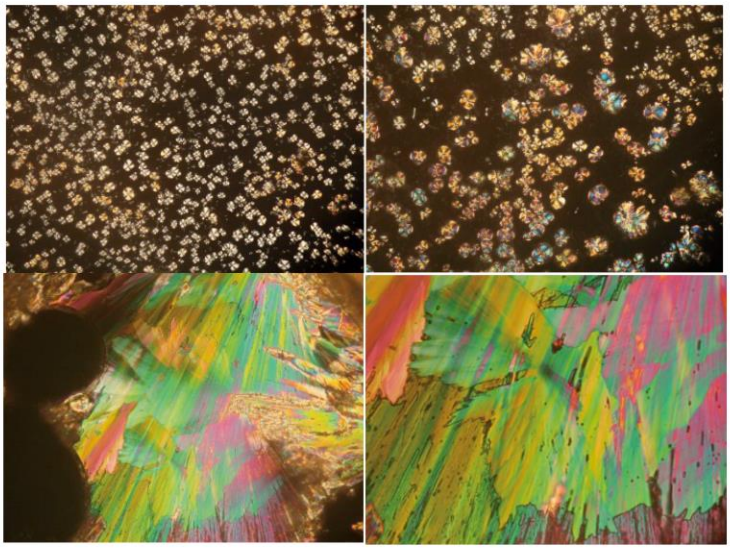

Fig. S13. Optical polarization microscopy image of columnar super structures of (**4cc**) with characteristic Maltese crosses (top) and smectic phase of (**4cc**) (bottom). In dependence of the surfactant concentration and grow time, one observes columnar droplets and extended birefringent areas. The columnar droplets show the classic Maltese cross pattern indicating a 360 ° rotation in optic axis orientation. The extended birefringent areas imply lamellar packing.[1-2]

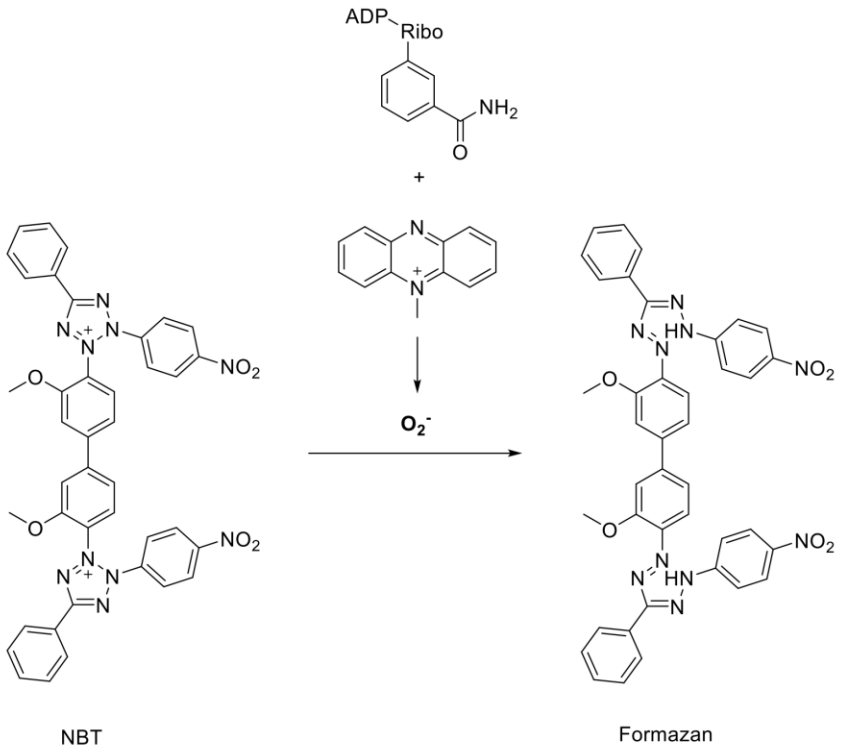

Fig. S14. Nitroblue tetrazolium assay.[3] The NBT-assay was performed after a standard procedure. 1 mL reaction mixture contained phosphate buffer (20 mM, pH 7.4), NADH (146 μM), NBT (100 μM), PMS (30 μM) and various concentrations of sample solution. After incubation for 5 min at ambient temperature, the absorbance was taken at 560 nm against an appropriate blank solution. All tests were performed at least 3 times. For the quercetin experiment methanolic solutions were used.

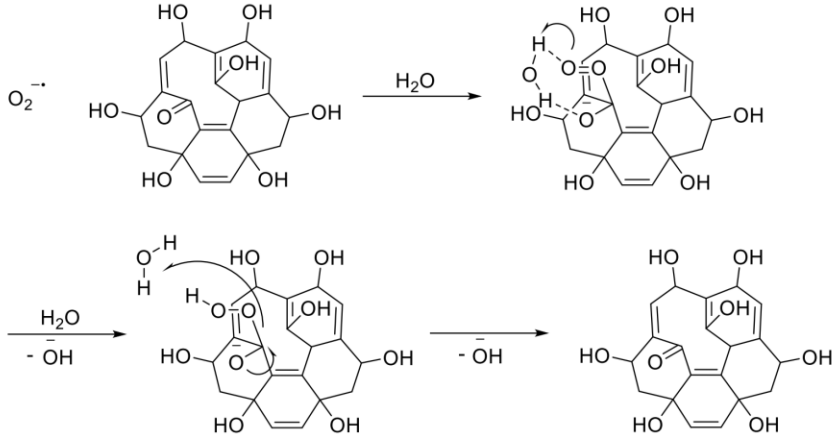

Fig. S15. Molecular mechanism for the improved ROS quenching activity of the open form. Additionally, to the classic superoxide quenching mechanism of fullerenol, in which the superoxide coordinates to the remaining double bonds, one can assume a mechanism in which the superoxide directly reacts with a ketone moiety. This mechanism might be reversible.

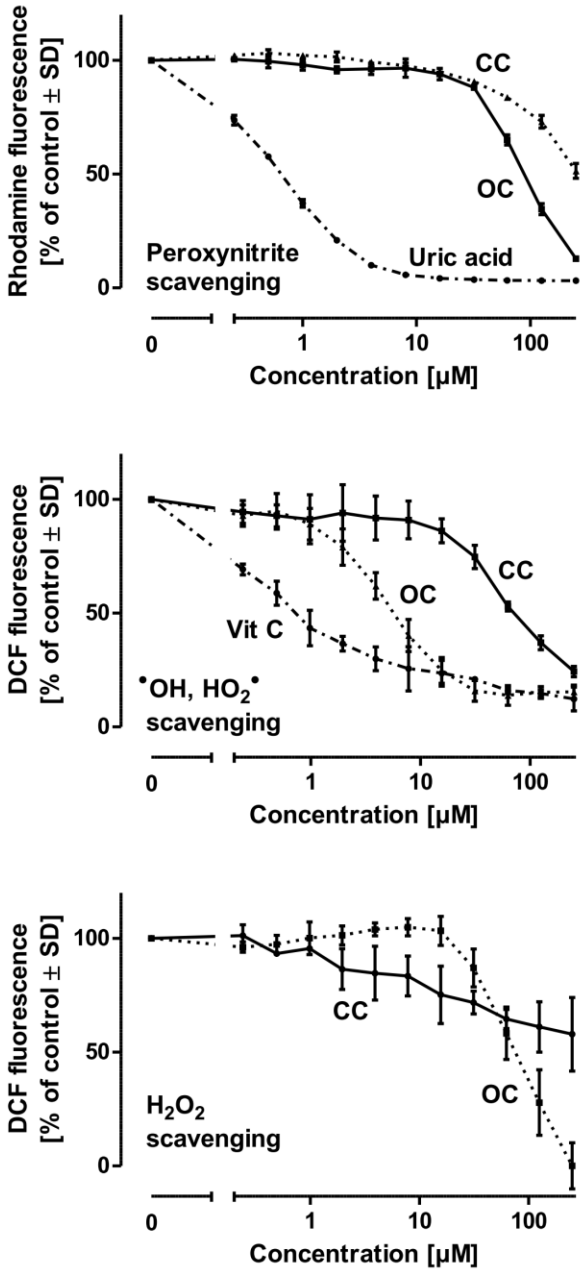

Fig. S16. ROS quenching assays for peroxynitrite, hydroxyl radicals and hydrogen peroxide[4]

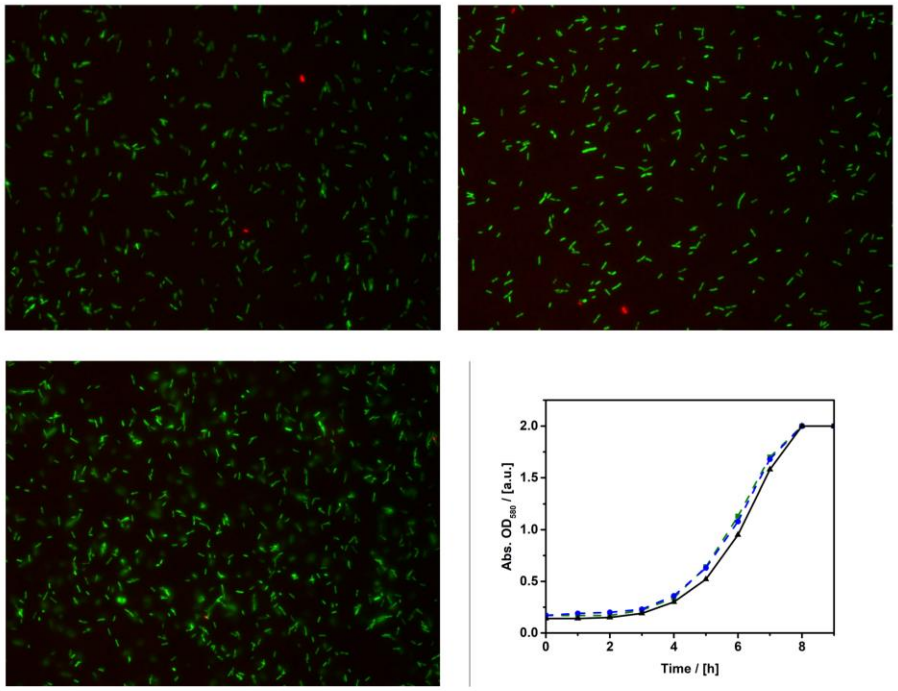

Fig. S17. Live-Dead stain and growth for *E.coli* treated with surfactant . Top left control, top right, in the presence of 100 μM of (**4cc**), bottom left, in the presence of 100 μM of (**4oc**), bottom right growth curves with the control culture indicated in blue, the culture with (**4**) green, and the culture with the open cage isomer of (**4**) in black.
E.coli K-12 as well as *P. aeruginosa* PAO1 (data not shown) was inoculated from precultures into 3 mL LB-medium (10 g tryptone, 5 g yeast extract, 5 g NaCl per liter) and incubated at 30 °C. The surfactant was tested from 1 μM up to 100 μM. The growth of the cultures was followed by measuring the optical density (OD 580 nm), and during the growth and in the stationary phase, samples were taken. For live-dead staining when following the manufacturer's instructions (LIVE/DEAD BacLight Bacterial Viability Kit, Thermofisher), it stains cells with membrane damage in red, against viable cells stained in green. The stained cells were placed on agar-coated microscope slides and observed under a fluorescence microscope at 400-fold magnification.

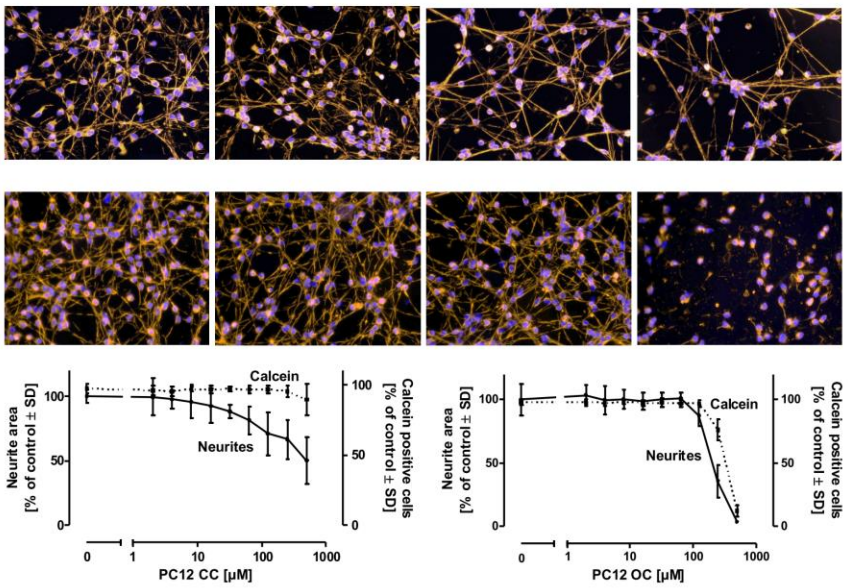

Fig. S18. Morphology of LUHMES treated with (**4cc**) (top), with (**4oc**) (mid) and quantification of the assay (bot) (0 µM, 32 µM, 125 µM, 500 µM). ***Cell culture:*** LUHMES cells are conditionally immortalized human fetal ventral mesencephalic neuronal precursor cells with a distinct dopaminergic phenotype, described in detail previously.[5-6] Cell culture plates (Sarstedt) were coated with 50 µg/ml poly-L-ornithine (PLO) and 1 µg/ml fibronectin over night at 37°C and washed 2 times with water. Cells were propagated in Advanced DMEM/F12 (Gibco/Invitrogen, Darmstadt, Germany), 1x N2 supplement (Invitrogen), 2 mM L-glutamine (Gibco), and 40 ng/ml recombinant bFGF (R+D Systems; Minneapolis, MN). The differentiation process was initiated by addition of differentiation medium consisting of advanced DMEM/F12, 1x N2 supplement, 2 mM L-glutamine, 1 mM dibutyryl-cAMP (Sigma), 1 µg/ml tetracycline (Sigma), and 2 ng/ml recombinant human GDNF (R+D Systems). After 2 days, cells were trypsinized and collected in Advanced DMEM/F12 medium. Cells were seeded onto 96-well plates at a density of 35.000 cells/well. The differentiation process was continued for additional 3 days, the cells were then treated with the respective compounds for an additional period of 48 h. For visualization of cell morphology, cells were fixed with 4% paraformaldehyde for 20 min at RT, permeabilized with 0.2% Triton X-100, washed, and blocked with 1% BSA (Calbiochem, San Diego, CA) in PBS for 1 h. LUHMES were stained with an anti-β-III-tubulin antibody (rabbit, Sigma, 1:1000) in 1% BSA/PBS at 4°C over night. After washing, the secondary antibodies were added for 1 h, nuclei were stained by Hoechst H-33342 (1 µg/ml) for 20 min. For quantitative evaluation of the neurite area, live staining of LUHMES was conducted with Calcein-AM (1 µM) and Hoechst H-33342 (1 µg/ml) for 30 min. Images were collected by an automated microplate-reading microscope (Array-Scan II® HCS Reader, Cellomics, Pittsburgh, PA) equipped with a Hamamatsu ORCA-ER camera (resolutuion 1024 x 1024; run at 2 x 2 binning) in two different fluorescence channels. Nuclei were identified as objects according to their intensity, size, area and shape. A virtual area corresponding to the cell soma was defined around each nucleus. The total Calcein pixel area per field minus the soma areas in that field was defined as neurite mass. In addition, viability was analyzed by the detection of the percentage of those cells positive for Calcein and for H-33342.

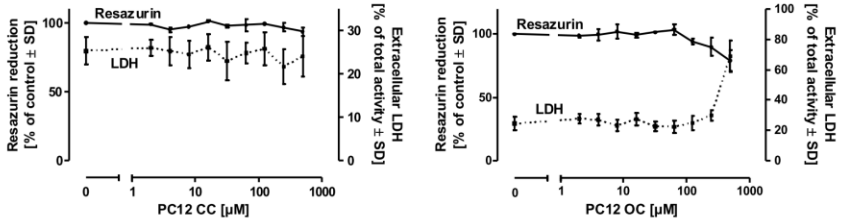

Fig. S19. Resazurin metabolization assay and Lactate dehydrogenase (LDH) release assay for the treatment of LUHMES with (**4cc**) (left) and (**4oc**) (right).

Resazurin metabolization assay: Resazurin (Sigma) was added to the cell culture medium in a final concentration of 5 µg/ml, fluorescence was measured after 60 min (λ_{ex}=530 nm; λ_{em}=590 nm). Lactate dehydrogenase (LDH) release assay: LDH activity was detected separately in the supernatant and cell lysate. Following separation of the supernatants, cells were lysed in PBS / 0.5% Triton X-100 for > 60 min. The percentage of LDH released was calculated as 100 x LDH $_{supernatant}$ / LDH $_{supernat + lysate}$. For the enzymatic assay, 20 µl of sample was combined with 180 µl of reaction buffer containing NADH (100 µM) and sodium pyruvate (600 µM) in sodium phosphate buffer adjusted to pH 7.4 by titration with K_2HPO_4 (40 mM) and KH_2PO_4 (10 mM). Absorption at 340 nm was detected at 37°C in 1 min intervals over a period of 20 min, enzyme activity was calculated from the respective slopes.

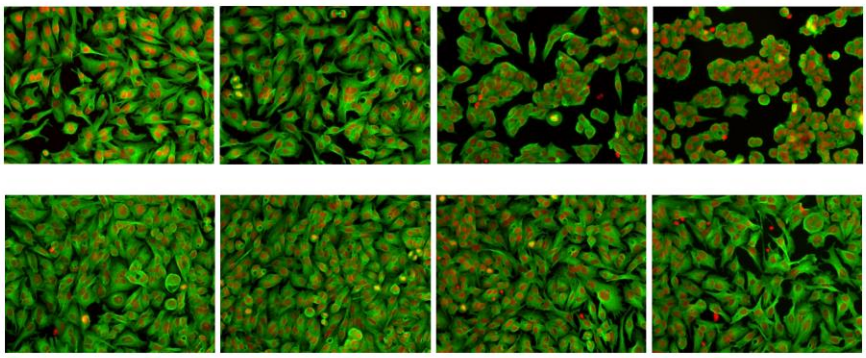

Fig. S20. Morphology of HepG2 treated with (**4cc**) (top), with (**4oc**) (mid) and quantification of the assay (bot) (0 µM, 32 µM, 125 µM, 500 µM). Human hepatoma HepG2 cells were propagated and maintained in DMEM (high glucose), supplemented with 10 % FBS, 25 U/ml penicillin and 25 µg/ml streptomycin. 96-well plates were coated with 50 µg/ml poly-L-ornithine (PLO) and 1 µg/ml fibronectin over night at 37°C. Following a washing step of the coated plates with water, 30.000 cells/well were seeded and grown for 1 day. Then, the cells were treated with the respective compounds for additional 48 h. For visualization of cell morphology, cells were fixed with 4% paraformaldehyde for 20 min at RT, permeabilized with 0.2% Triton X-100, washed, and blocked with 1% BSA (Calbiochem, San Diego, CA) in PBS for 1 h. HepG2 were stained with a monoclonal anti-α-tubulin antibody (Sigma; 1:1000)

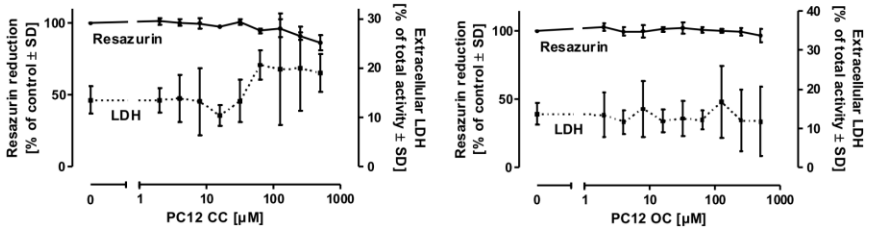

Fig. S21. Resazurin metabolization assay and Lactate dehydrogenase (LDH) release assay for the treatment of HepG2 with (**4cc**) (left) and (**4oc**) (right).
Resazurin metabolization assay: Resazurin (Sigma) was added to the cell culture medium in a final concentration of 5 µg/ml, fluorescence was measured after 60 min (λ_{ex}=530 nm; λ_{em}=590 nm). Lactate dehydrogenase (LDH) release assay: LDH activity was detected separately in the supernatant and cell lysate. Following separation of the supernatants, cells were lysed in PBS / 0.5% Triton X-100 for > 60 min. The percentage of LDH released was calculated as 100 x $LDH_{supernatant}$ / $LDH_{supernat + lysate}$. For the enzymatic assay, 20 µl of sample was combined with 180 µl of reaction buffer containing NADH (100 µM) and sodium pyruvate (600 µM) in sodium phosphate buffer adjusted to pH 7.4 by titration with K_2HPO_4 (40 mM) and KH_2PO_4 (10 mM). Absorption at 340 nm was detected at 37°C in 1 min intervals over a period of 20 min, enzyme activity was calculated from the respective slopes.

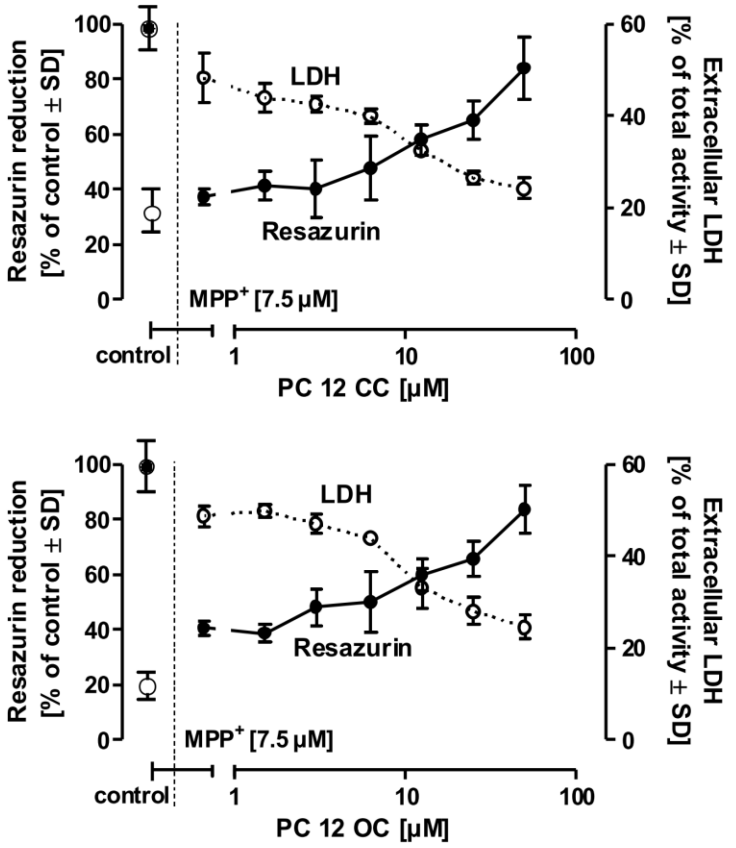

Fig. S22. Resazurin metabolization assay and Lactate dehydrogenase (LDH) release assay for the treatment of LUHMES with (**4cc**) and partially open cage compound (**4oc**) and MPP+.[5-6]

References.

1. Farn, R. J.; Editor, *Chemistry and Technology of Surfactants*. Blackwell Publishing Ltd.: 2006; p 315 pp.

2. Demus, D.; Goodby, J.; Gray, G. W.; Spiess, H. W.; Vill, V., *Handbook of Liquid Crystals, Volume 2A: Low Molecular Weight Liquid Crystals I*. Wiley-VCH: 1998; p 490 pp.

3. Choi, H. S.; Kim, J. W.; Cha, Y. N.; Kim, C., A Quantitative Nitroblue Tetrazolium Assay for Determining Intracellular Superoxide Anion Production in Phagocytic Cells. *J. Immunoass. Immunoch.* **2006,** *27* (1), 31-44.

4. Schildknecht, S.; Pape, R.; Müller, N.; Robotta, M.; Marquardt, A.; Bürkle, A.; Drescher, M.; Leist, M., Neuroprotection by Minocycline Caused by Direct and Specific Scavenging of Peroxynitrite. *Journal of Biological Chemistry* **2011,** *286* (7), 4991-5002.

5. Schildknecht, S.; Pöltl, D.; Nagel, D. M.; Matt, F.; Scholz, D.; Lotharius, J.; Schmieg, N.; Salvo-Vargas, A.; Leist, M., Requirement of a Dopaminergic Neuronal Phenotype for Toxicity of Low Concentrations of 1-methyl-4-phenylpyridinium to Human Cells. *Toxicology and applied pharmacology* **2009,** *241* (1), 23-35.

6. Scholz, D.; Pöltl, D.; Genewsky, A.; Weng, M.; Waldmann, T.; Schildknecht, S.; Leist, M., Rapid, Complete and Large-scale Generation of Post-mitotic Neurons from the Human LUHMES Cell Line. *Journal of neurochemistry* **2011,** *119* (5), 957-971.

BEILSTEIN JOURNAL OF ORGANIC CHEMISTRY

Easy, efficient and versatile one-pot synthesis of Janus-type-substituted fullerenols

Marius Kunkel and Sebastian Polarz*

Letter

Open Access

Address:
University of Konstanz, Universitätsstrasse 10, 78467 Konstanz, Germany

Email:
Sebastian Polarz* - sebastian.polarz@uni-konstanz.de

* Corresponding author

Keywords:
amphiphile; $C_{60}Cl_6$; fullerene; fullerenol; one-pot

Beilstein J. Org. Chem. **2019,** *15,* 901–905.
doi:10.3762/bjoc.15.87

Received: 14 February 2019
Accepted: 25 March 2019
Published: 12 April 2019

Associate Editor: K. Itami

Abstract

An efficient one-pot synthesis for Janus-type fullerenol derivatives and how to characterize them is reported. This synthesis provides access to asymmetrically substituted fullerenol with five substituents on one pole of the fullerene and polyhydroxylation moieties, mostly ether and hydroxy groups, on the rest of the fullerene core. As substituents a broad variety of primary amines can be used to obtain Janus-type amphiphilic fullerenols in good to excellent yield. These fullerenol amphiphiles can serve as suitable precursors for further reactions resulting in new applications for fullerenols.

Introduction

The roman god Janus, who is typically depicted with two faces, metaphorically stands for duality in one person or object. Consequently, nanoparticles characterized by two different hemispheres have been named Janus-type nanoparticles as well, and have attracted major attention due to their special properties [1,2]. The term 'Janus' is much less used in molecular chemistry, presumably because there are not many spherical molecules known. Examples are the giant polyoxometalates reported by Müller et al. [3] and, more importantly for the current paper, fullerene C_{60}. Because of the high symmetry of those compounds asymmetric modification is tedious with multiple synthesis and purification steps involved.

Fullerene derivatives are of great interest in numerous research areas such as biological sciences and materials sciences [4-9]. A vast amount of synthetic protocols have been developed over the years to modify fullerenes [10-13]. A particular task was to provide fullerenes with solubility in water. Thus, one important class of fullerene derivatives are the hydroxylated and polyhydroxylated compounds, so called fullerenols ($C_{60}(OH)_n$) [14]. The degree of hydroxylation and with that the solubility of these compounds can be tuned by using different synthetic approaches making it possible to obtain water soluble fullerenols as well as fullerenols that are still soluble in organic solvents [15-19]. The maximum number of OH groups, which could be attached to C_{60} is $n = 44$ [17]. Further derivatizations, where all hydroxy moieties of the compound have been modified, are well known in the literature. These reactions can be achieved by esterification or etherification [20-22]. However, partial modifications are rare, especially when it comes to asymmetric substi-

tutions [23,24]. Although, janus-type fullerenols at which only a part of the fullerene core is hydroxylated are known [25,26], literature lacks fullerenol compounds with Janus-type substitution. The advantage of those special molecular species, e.g., amphiphilic behaviour, was demonstrated in a paper published by our group in 2018 [27]. A fullerenol derivative with a maximum of 21 OH groups on one hemisphere and 5 alkyl chains on the other was reported. The synthesis of this species was elaborate and tedious with relatively low yield, we also failed to introduce more complex substituents than alkyl chains, for instance. The success of the used, multistep synthetic pathway drastically depends on the reactants that are used. One may obtain insoluble or unreactive intermediates, which then prevent the synthesis of the final compound in good yield or to obtain the final compound at all.

For future exploration of the potential of Janus-type fullerenols it is pivotal to establish new synthetic pathways, which allow to introduce a broader variety of substituents and better yield. We report an easy and efficient one-pot approach using $C_{60}Cl_6$ as a precursor. The attachment of substituents, in our case primary amines, and the polyhydroxylation of the fullerene core are performed simultaneously by using a common phase transfer reaction which enables even the combination of water-soluble substituents with the precursor $C_{60}Cl_6$. High yields of Janus-fullerenol derivatives bearing five defined substituents on one pole of the C_{60} core combined with in average 19 (+/−3) oxygen containing moieties on the other pole are obtained.

Results and Discussion

The general procedure for the one-pot preparation of asymmetrically substituted fullerenols is depicted in Scheme 1, and experimental details are presented in the following.

The starting material for all syntheses is $C_{60}Cl_6$ which was synthesized according to procedure reported by Kuvychko et al. and adapted by our group [27-29]. Though, several compounds are known to undergo the penta-substitution reaction with $C_{60}Cl_6$, like amines, thiols or alcohols [30-32], it has been observed that primary amines show a high reactivity under these conditions and form stable intermediates during this reaction that can further react. In a general procedure, $C_{60}Cl_6$ (200 mg, 0.21 mmol) and the primary amine of choice (8 equiv) are dissolved in a chlorobenzene/water mixture (8 mL/40 mL). The mixture is combined with the phase transfer agent tetrabutylammonium hydroxide (0.5 mL of a 30% solution in H_2O). The reactants for the polyhydroxylation are added, H_2O_2 (1.5 mL of a 30% solution) and NaOH (0.7 g). The mixture is heated to reflux until the chlorobenzene phase decolorizes. The reaction is completed after 2 h of reflux. The aqueous phase is separated and poured in methanol to precipitate the crude product. The obtained brown solid is washed with methanol to remove remaining TBAH and NaOH to obtain the sodium salt of the compound. The sodium salt compound can be ion exchanged (amberlite 120) prior to hydrophilic interaction liquid chromatography (silica gel 60, gradient acetonitrile/water 90:10 to 70:30) for purification.

In a first attempt a methyl-protected aminocatechol, namely dimethoxyaniline, was reacted under these conditions. After purification the product was obtained in a good yield of 88%. The compound was characterized as follows.

For the characterization of Janus-type fullerenol amphiphiles more than one method is needed to perfectly identify the compounds. Polyhydroxylation reaction of the fullerene can lead to a mixture of several oxygen moieties like hydroxy groups, diols, ketones, hemiketals, epoxides and ethers. The general formula of the compound is identified by electrospray ionization mass spectrometry (ESIMS). The degree of polyhydroxylation and the number of substituents is determined and confirmed with thermogravimetric analysis (TGA) and the nature of oxygen moieties as well as the substituents attached are evaluated via a ^{13}C magic angle spinning nuclear magnetic resonance spectroscopy (MAS NMR) ^1H-^{13}C-CP experiment. An overall information of the compound is obtained by attenuated total reflection infrared spectroscopy (ATR-IR). Figure 1 shows the results of the characterization exemplarily for the fullerenol

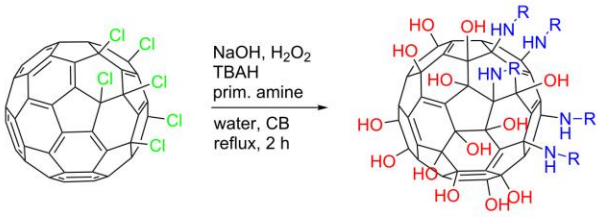

Scheme 1: Reaction scheme for the one-pot reaction of $C_{60}Cl_6$ to produce Janus-type fullerenols $(OH)_{19+/-3}C_{60}(HNR)_5$.

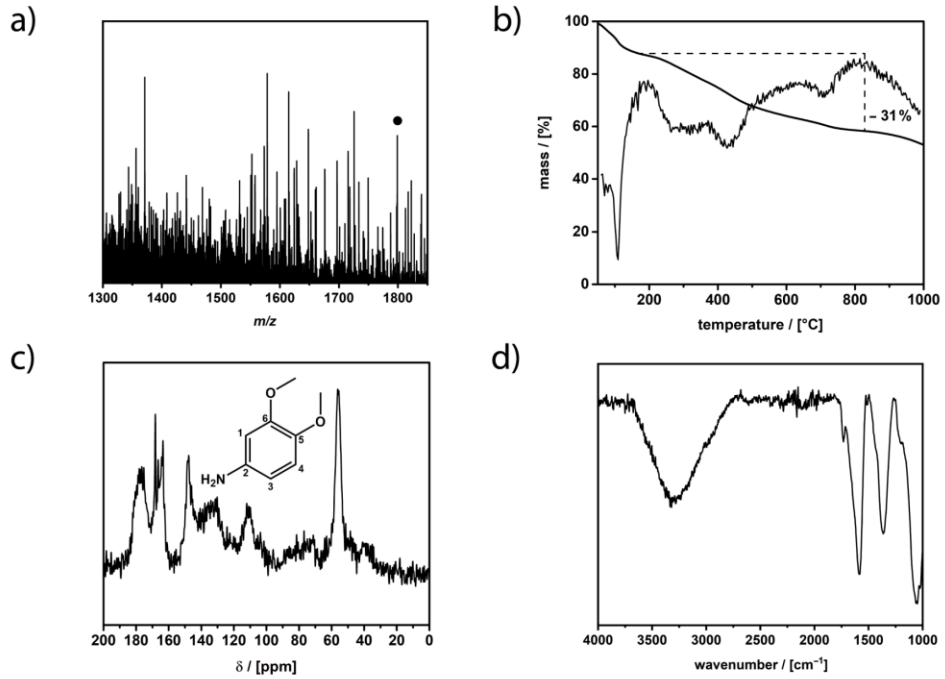

Figure 1: Characterization of fullerenol amphiphile with substituent **1**. a) ESIMS in positive mode, molecular ion peak marked with circle, b) TGA under nitrogen with 5 K/min, c) MAS-NMR (^{1}H-^{13}C-CP) with structure of substituent, d) ATR–IR.

amphiphile with dimethoxyaniline as substituent (all characterization data can be found in Supporting Information File 1).

ESIMS (Figure 1a) shows a rather complex fragmentation pattern similar to unsubstituted fullerenol compounds known in the literature [33]. The general complexity of the spectrum derives from the isomerization and fragmentation of the oxygen species in addition to the fragmentation of the substituents. The signals can be assigned with a general formula $[M - xH_2O - yH - zO - v(HNR)]^{a-/+}$. The molecular ion peak of the janus-fullerenol with **1** as substituent can be identified at *m*/*z* 1798.6 (1798.6) which corresponds to $(H)_{13}(O)_{19}C_{60}(HNR)_5^+$ and with that fits 19 oxygen species. As already mentioned there are several oxygen species present in the compound which are further identified later on with MAS NMR. The formula of the compound indicates that there are 12 hydroxy groups present and 7 other oxygen species. The TGA (Figure 1b) is another method to confirm the number of attached oxygen species and substituents. The first step up to 180 °C fits the release of secondary and tertiary bond water. The measurement shows that 12 H_2O molecules are bound to the fullerene. The second step up to around 800 °C can be assigned to the release of the different oxygen species, which also explains the little steps which correspond to different oxygen types. In addition to the oxygen species attached to the fullerene core, the methoxy moieties of the substituent are also released. The average number of oxygen species can be calculated to 19.5, which fits the data obtained from ESIMS. Above 800 °C the decomposition of the core structure and the substituents starts. After that step only amorphous carbon remains and the compound is completely decomposed. Finally, the MAS-NMR (Figure 1c) confirms the attachment of the substituents and that the structure of substituents is unchanged. Furthermore, it provides evidence to determine the kind of the oxygen species [34,35]. At 175 ppm the signals of C=C–O groups are located. These signals are rather intense which gives evidence that the most prominent oxygen structure motive besides hydroxy groups are ethers. This may result from the reaction conditions since it was already shown that the reaction conditions influence the obtained oxygen moieties. The signal at 163 ppm can be assigned to carbon atoms 5 and 6 of the substituent. Carbon atom 2 of the substituent is located at 148 ppm. Remaining sp^2-hybridized carbons of the fullerene

core are located between 142 and 120 ppm. At 110 ppm the remaining carbons of the substituent are located. The sp^3-hybridized carbons of the fullerene core at which the hydroxy groups are attached are located between 80 and 60 ppm. Finally, the carbon atoms of the methoxy moieties can be found at 55 ppm. Figure 1d displays the ATR–IR spectrum of the compound which confirms the results from the other analytical methods. Most prominent in the spectrum are the signals of the polyhydroxylation moieties. Signals at 3293, 1579, 1358, 1200 and 1049 cm^{-1} can be assigned to the O–H, C–O–C, C–O and C–OH vibrations.

The scope of the reaction was further tested with other primary amines, aliphatic as well as aromatic (Table 1). The aliphatic amines **2** and **3** react in good yields over 70%. For these compounds the reaction needs about 2 h to be finished. The reaction with compound **2** leads to a little amount of insoluble byproduct which might be double reacted amine although an excess of amine was used. The loss of yield for the reaction with **3** results mainly from byproducts that are not penta-substituted. The aromatic compound **4** reacts the fastest and the reaction was completed after 20 min. Strong foaming indicates the completion of the reaction. Almost no byproduct could be isolated here.

Table 1: Scope of the reaction and isolated yields.

Entry	Reactant	Yield[a]
1	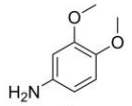 **1**	88%
2	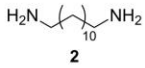 **2**	70%
3	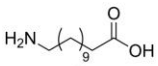 **3**	75%
4	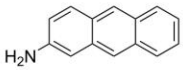 **4**	90%
5	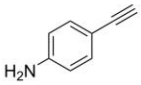 **5**	82%
6	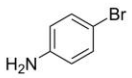 **6**	80%

[a]Yield after purification.

Of special interest for this reaction are compounds with additional functional groups like alkynes or bromides that can be reacted with other compounds in further reactions, e.g., click reactions or Sonogashira coupling. Systems for such reactions are tested with compounds **5** and **6**. These compounds react in high yields up to 90%. The additional functional groups, which must of course be not base-labile survive the reaction conditions with no harm. The attached moieties, no matter if electron withdrawing or donating, do not seem to influence the reaction. Moreover, neither the degree of polyhydroxylation nor the kind of attached oxygen species seem to be influenced by the attached substituents. For all compounds the average degree of polyhydroxylation is 19(+/−3). Noteworthy, neither the degree of polyhydroxylation could be increased nor the nature of oxygen species could be varied by extending the reaction time.

Conclusion

In summary, we have established a new and easy one-pot method for the synthesis of Janus-type fullerenol amphiphiles. The reaction includes a wide range of primary amines reaching from aliphatic amines over aromatic amines to further functionalized amines. All resulting compounds have the general formula $(OH)_{19+/-3}C_{60}(HNR)_5$, whereas, mainly hydroxy and ether moieties are included. They have been characterized with ESIMS, TGA and MAS NMR. These compounds can serve as precursors for further modified fullerenols or as true surfactants.

Supporting Information

Supporting Information File 1

General methods and characterization data.
[https://www.beilstein-journals.org/bjoc/content/supplementary/1860-5397-15-87-S1.pdf]

Acknowledgements

The current research was funded by an ERC consolidator grant (I-SURF; project 614606).

ORCID® iDs

Marius Kunkel - https://orcid.org/0000-0002-7531-6419
Sebastian Polarz - https://orcid.org/0000-0003-1651-4906

References

1. Roh, K.-H.; Martin, D. C.; Lahann, J. *Nat. Mater.* **2005,** *4,* 759–763. doi:10.1038/nmat1486
2. Walther, A.; Müller, A. H. E. *Chem. Rev.* **2013,** *113,* 5194–5261. doi:10.1021/cr300089t

3. Müller, A.; Sarkar, S.; Shah, S. Q. N.; Bögge, H.; Schmidtmann, M.; Sarkar, S.; Kögerler, P.; Hauptfleisch, B.; Trautwein, A. X.; Schünemann, V. *Angew. Chem., Int. Ed.* **1999,** *38,* 3238–3241. doi:10.1002/(sici)1521-3773(19991102)38:21<3238::aid-anie3238>3.0.co;2-6
4. Prato, M. *J. Mater. Chem.* **1997,** *7,* 1097–1109. doi:10.1039/a700080d
5. Bosi, S.; Da Ros, T.; Spalluto, G.; Prato, M. *Eur. J. Med. Chem.* **2003,** *38,* 913–923. doi:10.1016/j.ejmech.2003.09.005
6. Coro, J.; Suárez, M.; Silva, L. S. R.; Eguiluz, K. I. B.; Salazar-Banda, G. R. *Int. J. Hydrogen Energy* **2016,** *41,* 17944–17959. doi:10.1016/j.ijhydene.2016.08.043
7. Partha, R.; Conyers, J. L. *Int. J. Nanomed.* **2009,** *4,* 261–275. doi:10.2147/ijn.s5964
8. Thompson, B. C.; Fréchet, J. M. J. *Angew. Chem., Int. Ed.* **2008,** *47,* 58–77. doi:10.1002/anie.200702506
9. Goodarzi, S.; Da Ros, T.; Conde, J.; Sefat, F.; Mozafari, M. *Mater. Today* **2017,** *20,* 460–480. doi:10.1016/j.mattod.2017.03.017
10. Hirsch, A.; Brettreich, M. *Fullerenes: chemistry and reactions;* Wiley-VCH: Weinheim, Germany, 2005.
11. Diederich, F.; Thilgen, C. *Science* **1996,** *271,* 317–324. doi:10.1126/science.271.5247.317
12. Tzirakis, M. D.; Orfanopoulos, M. *Chem. Rev.* **2013,** *113,* 5262–5321. doi:10.1021/cr300475r
13. Montellano López, A.; Mateo-Alonso, A.; Prato, M. *J. Mater. Chem.* **2011,** *21,* 1305–1318. doi:10.1039/c0jm02386h
14. Chiang, L. Y.; Bhonsle, J. B.; Wang, L.; Shu, S. F.; Chang, T. M.; Hwu, J. R. *Tetrahedron* **1996,** *52,* 4963–4972. doi:10.1016/0040-4020(96)00104-4
15. Zhang, G.; Liu, Y.; Liang, D.; Gan, L.; Li, Y. *Angew. Chem., Int. Ed.* **2010,** *49,* 5293–5295. doi:10.1002/anie.201001280
16. Semenov, K. N.; Charykov, N. A.; Keskinov, V. N. *J. Chem. Eng. Data* **2011,** *56,* 230–239. doi:10.1021/je100755v
17. Kokubo, K.; Shirakawa, S.; Kobayashi, N.; Aoshima, H.; Oshima, T. *Nano Res.* **2011,** *4,* 204–215. doi:10.1007/s12274-010-0071-z
18. Chiang, L. Y.; Wang, L.-Y.; Swirczewski, J. W.; Soled, S.; Cameron, S. *J. Org. Chem.* **1994,** *59,* 3960–3968. doi:10.1021/jo00093a030
19. Kokubo, K.; Matsubayashi, K.; Tategaki, H.; Takada, H.; Oshima, T. *ACS Nano* **2008,** *2,* 327–333. doi:10.1021/nn700151z
20. Singh, R.; Goswami, T. *Synth. Met.* **2007,** *157,* 951–955. doi:10.1016/j.synthmet.2007.09.006
21. Goswami, T. H.; Nandan, B.; Alam, S.; Mathur, G. N. *Polymer* **2003,** *44,* 3209–3214. doi:10.1016/s0032-3861(03)00241-6
22. Bahuguna, S.; Kumar, M.; Sharma, G.; Kumar, R.; Singh, B.; Raza, K. *AAPS PharmSciTech* **2018,** *19,* 1084–1092. doi:10.1208/s12249-017-0920-0
23. Huang, H.; Zhang, G.; Liang, S.; Xin, N.; Gan, L. *J. Org. Chem.* **2012,** *77,* 2456–2462. doi:10.1021/jo300118h
24. Jiang, Z.; Zhang, Y.; Gan, L.; Wang, Z. *Tetrahedron* **2008,** *64,* 11394–11403. doi:10.1016/j.tet.2008.08.053
25. Kraevaya, O. A.; Peregudov, A. S.; Martynenko, V. M.; Troshin, P. A. *Tetrahedron Lett.* **2018,** *59,* 605–607. doi:10.1016/j.tetlet.2017.10.054
26. Liu, Y.; Zhang, G.; Niu, L.; Gan, L.; Liang, D. *J. Mater. Chem.* **2011,** *21,* 14864–14868. doi:10.1039/c1jm12964c
27. Kunkel, M.; Schildknecht, S.; Boldt, K.; Zeyffert, L.; Schleheck, D.; Leist, M.; Polarz, S. *ACS Appl. Mater. Interfaces* **2018,** *10,* 23638–23646. doi:10.1021/acsami.8b07032
28. Kuvychko, I. V.; Streletskii, A. V.; Popov, A. A.; Kotsiris, S. G.; Drewello, T.; Strauss, S. H.; Boltalina, O. V. *Chem. – Eur. J.* **2005,** *11,* 5426–5436. doi:10.1002/chem.200500185
29. Birkett, P. R.; Avent, A. G.; Darwish, A. D.; Kroto, H. W.; Taylor, R.; Walton, D. R. M. *J. Chem. Soc., Chem. Commun.* **1993,** 1230–1232. doi:10.1039/c39930001230
30. Khakina, E. A.; Kraevaya, O. A.; Popova, M. L.; Peregudov, A. S.; Troyanov, S. I.; Chernyak, A. V.; Martynenko, V. M.; Kulikov, A. V.; Schols, D.; Troshin, P. A. *Org. Biomol. Chem.* **2017,** *15,* 773–777. doi:10.1039/c6ob02251k
31. Khakina, E. A.; Yurkova, A. A.; Peregudov, A. S.; Troyanov, S. I.; Trush, V. V.; Vovk, A. I.; Mumyatov, A. V.; Martynenko, V. M.; Balzarini, J.; Troshin, P. A. *Chem. Commun.* **2012,** *48,* 7158–7160. doi:10.1039/c2cc32517a
32. Kornev, A. B.; Khakina, E. A.; Troyanov, S. I.; Kushch, A. A.; Peregudov, A.; Vasilchenko, A.; Deryabin, D. G.; Martynenko, V. M.; Troshin, P. A. *Chem. Commun.* **2012,** *48,* 5461–5463. doi:10.1039/c2cc00071g
33. Silion, M.; Dascalu, A.; Pinteala, M.; Simionescu, B. C.; Ungurenasu, C. *Beilstein J. Org. Chem.* **2013,** *9,* 1285–1295. doi:10.3762/bjoc.9.145
34. Wang, Z.; Chang, X.; Lu, Z.; Gu, M.; Zhao, Y.; Gao, X. *Chem. Sci.* **2014,** *5,* 2940–2948. doi:10.1039/c4sc00584h
35. Andreeva, D. V.; Ratnikova, O. V.; Melenevskaya, E. Y.; Gribanov, A. V. *Int. J. Polym. Anal. Charact.* **2007,** *12,* 105–113. doi:10.1080/10236660601137439

License and Terms

BEILSTEIN JOURNAL OF ORGANIC CHEMISTRY

Supporting Information

for

Easy, efficient and versatile one-pot synthesis of Janus-type-substituted fullerenols

Marius Kunkel and Sebastian Polarz

Beilstein J. Org. Chem. **2019,** *15,* 901–905. doi:10.3762/bjoc.15.87

General methods and characterization data

General methods

Synthesis that acquired inert gas atmosphere were performed using general Schlenk techniques under argon atmosphere. The solvents were dried according to standard literature and stored under argon. Water was deionized with Millipore Milli-Q. All starting materials used for the syntheses were purchased from commercial sources unless stated differently. The fullerene C_{60} (pur. 99.9%) was purchased from Research & Production Company “Modern Synthesis Technology”.

Analytical methods

Mass spectra were measured on Bruker amazon SL in pos. or neg. mode via direct inject from a methanolic solution. For assignment of signals work of Silion, Mihaela, et al. was used as reference.[1] Assignment was done as follows: $[M - xH_2O - yH - zO - v(HNR)]^{a-/+}$. The molecular ion peak was identified in combination with results from TGA and NMR. TGA was measured on Netzsch Jupiter STA 449 F3. All measurements were performed under nitrogen atmosphere with 80 mL/min flowrate and with a heating rate of 5 K/min. NMR measurements were performed on Bruker Avance II 400 solid-state NMR at 295 or 350 K and with 10 kHz rotational speed. Number of scans 5k–10k with D1 = 10 to 100 sec. Attenuated total reflection−infrared (ATR−IR) spectra were measured with a Perkin Elmer100 Spectrum spectrometer including an ATR unit.

Characterization data

Entry 1

Substituent

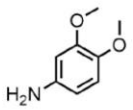

ESIMS

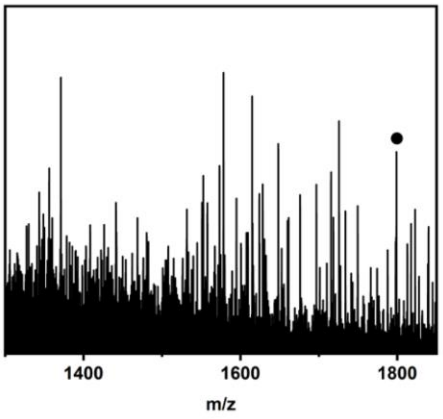

$[H_{13}O_{19}C_{60}(NC_8H_{10}O_2)]^+$ *m*/*z* = 1798.7 (1798.6).

MAS NMR

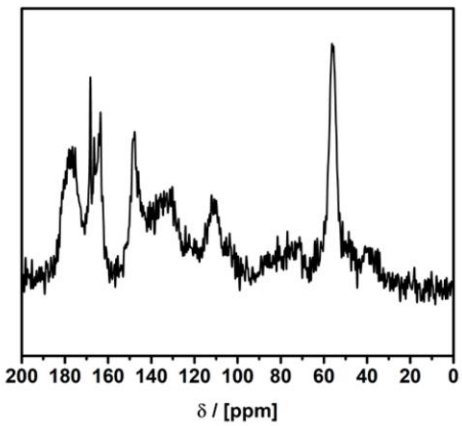

^{1}H-^{13}C-CP MAS-NMR (100 MHz): δ (ppm): 175 C=C–O, 163 160 C(sp^2)-N, 148 ppm C sp^2, 142–120 ppm C sp^2, 110 ppm C sp^2, 80–60 ppm C-OH, 55 ppm O–CH_3.

TGA

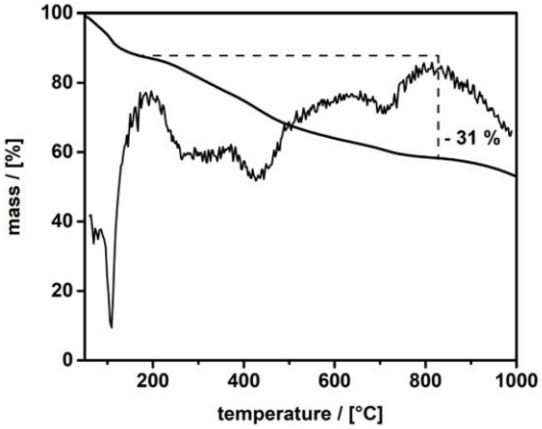

1. Step 50 °C – 180 °C 13%
2. 180 °C – 800 °C 31% → 19.5 oxygen species
3. >800 °C 56%

ATR-IR

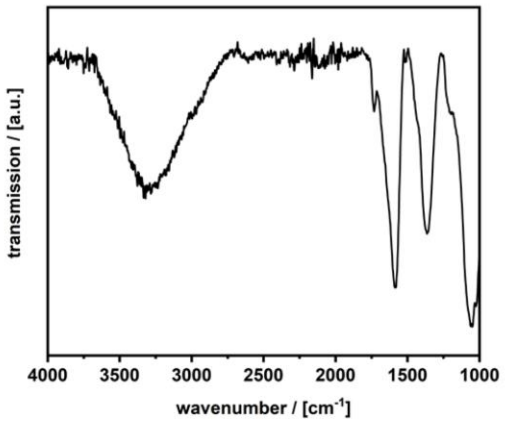

IR (powder): 3293, 3000, 2971, 1579, 1440, 1358, 1200, 1049 cm^{-1}.

Entry 2

Substituent

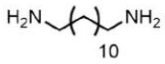

ESIMS

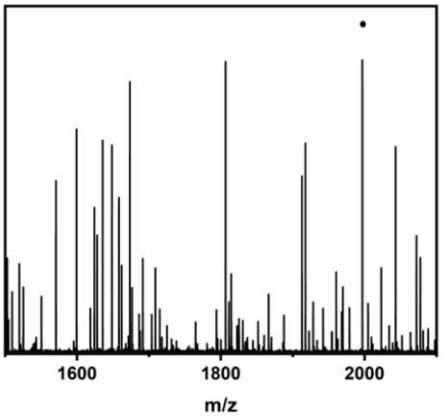

$[H_7O_{17}C_{60}(N_2C_{12}H_{27})]^-$ *m*/*z* = 1996.9 (1996.5).

MAS-NMR

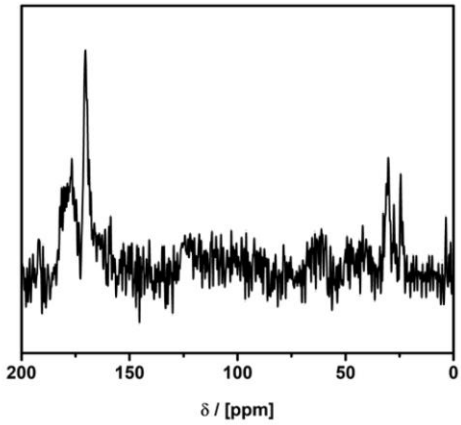

^{1}H-^{13}C-CP MAS-NMR (100 MHz): δ (ppm) 177 C=C–O, 150 C sp^2 (fullerene), 60–40 C–OH, 42 C–N-, 29 C sp^3 (chain).

TGA

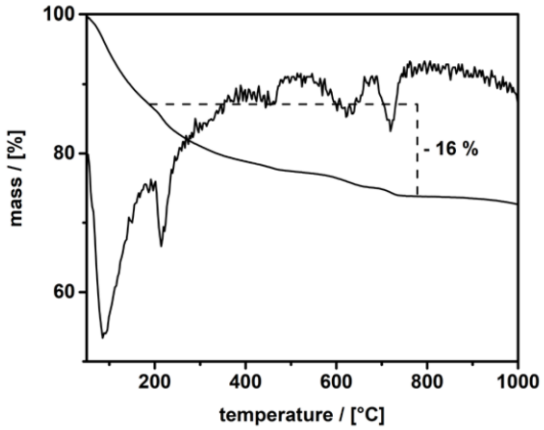

1. Step 50 °C – 190 °C 13%
2. 190 °C – 775 °C 16% → 18 oxygen species + amine endgroups
3. >775 °C 71%

ATR-IR

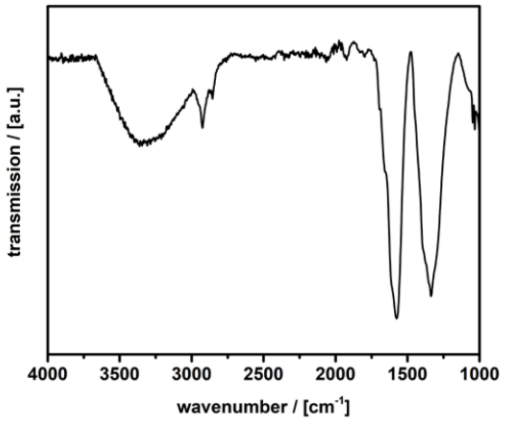

IR (powder): 3320, 2923, 2852, 1655, 1574, 1393, 1327 cm^{-1}.

Entry 3

Substituent

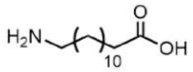

ESIMS

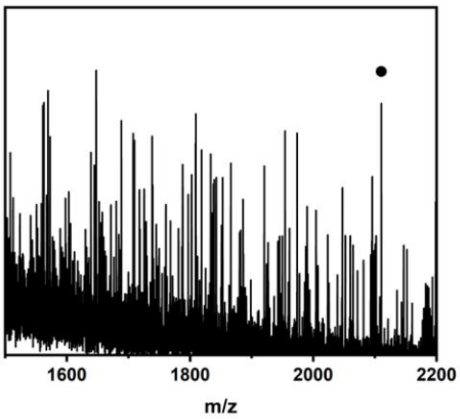

$[H_{14}O_{19}C_{60}(NO_2C_{12}H_{24})]^+$ *m*/*z* = 2110.2 (2110.4).

MAS-NMR

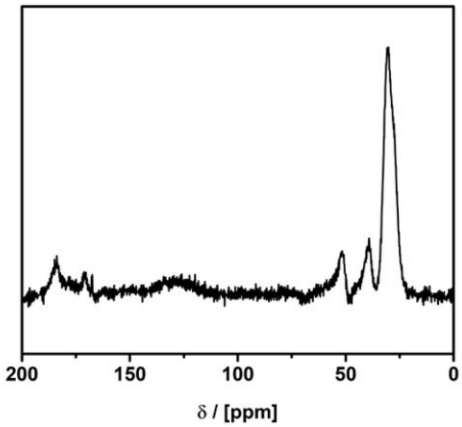

^{1}H-^{13}C-CP MAS-NMR (100 MHz): δ (ppm) 184 COOH, 170 C=C-O, 160 C sp^2 (fullerene), 75–50 C–OH, 51 C–N, 39 C–COOH, 29 C sp^3 (chain).

TGA

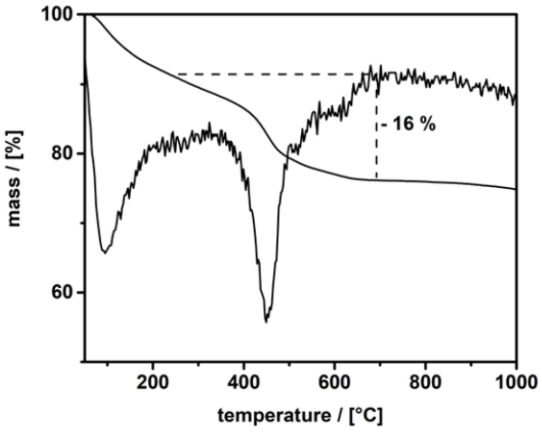

1. Step 50 °C – 190 °C 9%
2. 190 °C – 775 °C 16% → 21 oxygen species
3. >775 °C 75%

ATR-IR

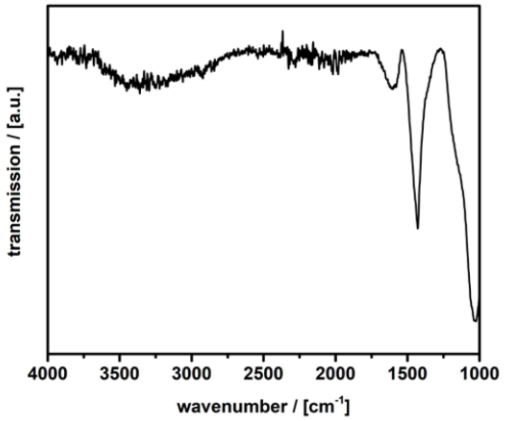

IR (powder): 3340, 2923, 2841, 2300, 1599, 1431, 1158, 1028 cm^{-1}.

Entry 4

Substituent

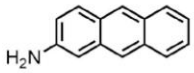

ESIMS

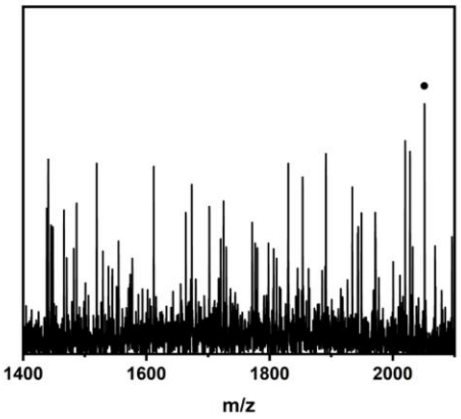

$[H_{17}O_{21}C_{60}(NC_{14}H_{10})]^-$ *m*/*z* = 2051.1 (2051.0).

MAS NMR

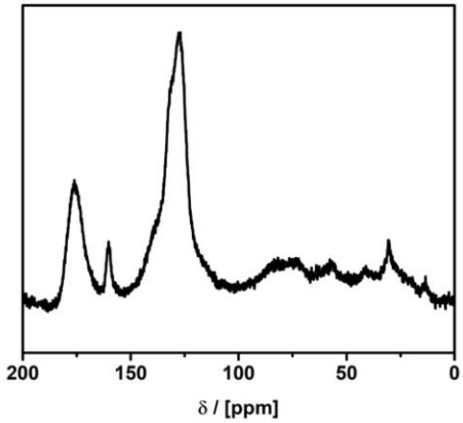

^{1}H-^{13}C-CP MAS-NMR (100 MHz): δ (ppm) 175 C=C-O, 160 C(sp^2)-N, 127 C sp^2, 75–50 C–OH, 29 SSB.

TGA

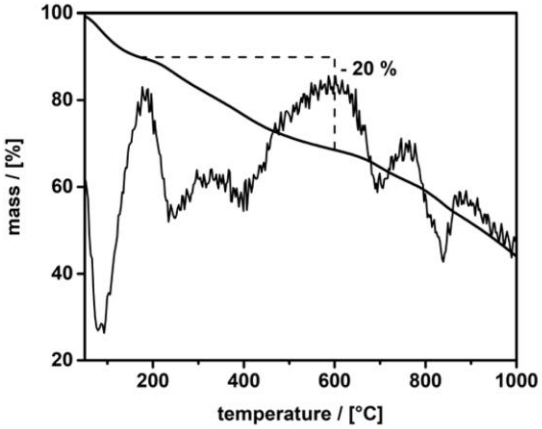

1. Step 50 °C – 180 °C 12%
2. 180 °C – 600 °C 20% → 22 oxygen species
3. >600 °C 68%

ATR-IR

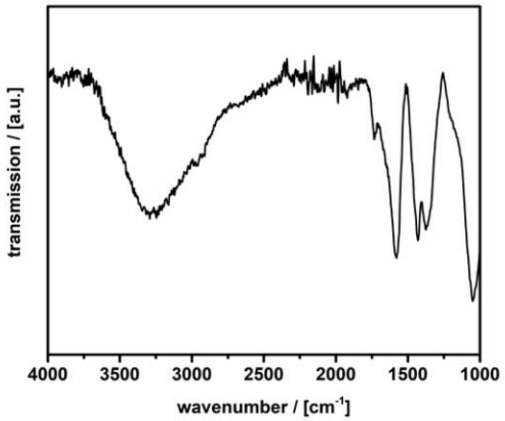

IR (powder): 3270, 2970, 2910, 1732, 1577, 1433, 1361, 1058 cm^{-1}.

Entry 5

Substituent

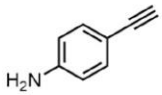

ESIMS

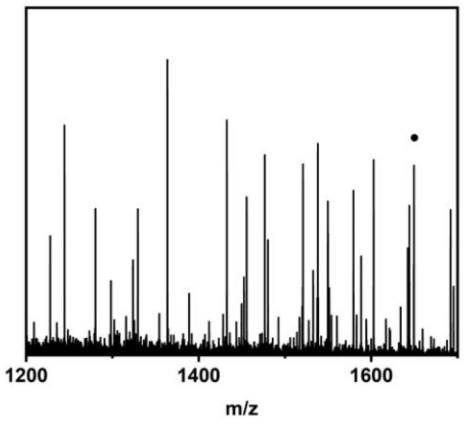

$[H_{12}O_{21}C_{60}(NC_8H_6)]^-$ *m*/*z* = 1649.5 (1649.5).

MAS-NMR

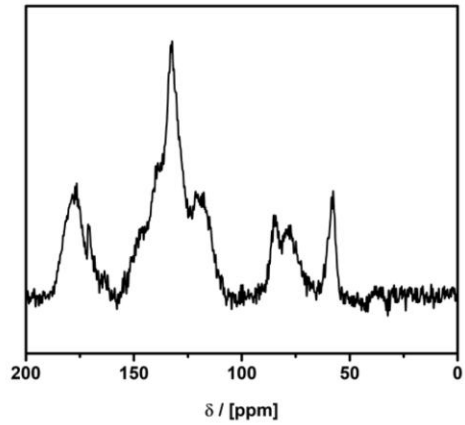

^{1}H-^{13}C-CP MAS-NMR (100 MHz): δ (ppm) 175 C=C-O, 132 C sp^2, 120 C sp^2, 84 C sp, 77 C sp, 60–40 C–OH.

TGA

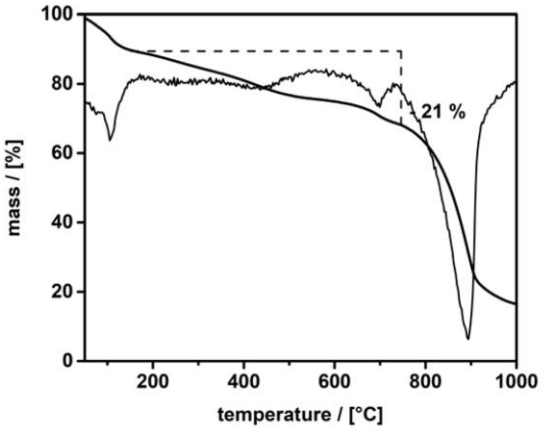

1. Step 50 °C – 150 °C 11%
2. 190 °C – 750 °C 21% → 22 oxygen species
3. >750 °C 68%

ATR-IR

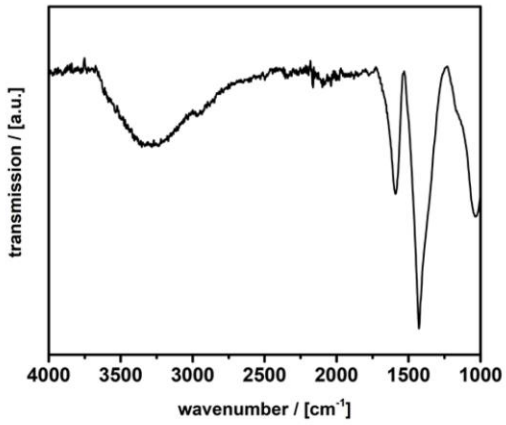

IR (powder): 3280, 2983, 2926, 1593, 1422, 1166, 1033 cm^{-1}.

Entry 6

Substituent

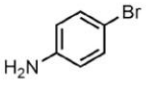

ESIMS

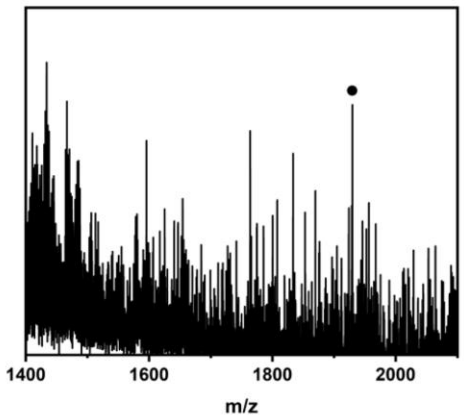

$[H_{18}O_{21}C_{60}(NC_8H_5Br)_5]^+$ *m*/*z* = 1929.7 (1929.9)

MAS-NMR

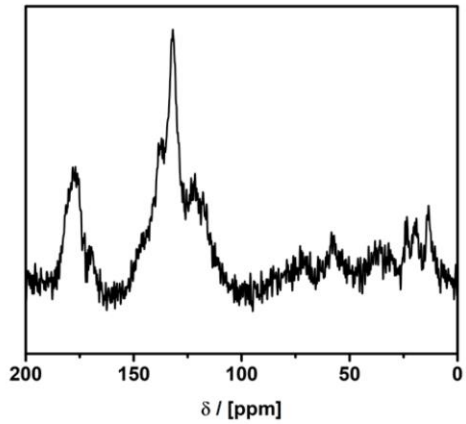

^{1}H-^{13}C-CP MAS-NMR (100 MHz): δ (ppm) 175 C=C–O, 140 C(sp^2)-N, 130 C sp^2, 118 C sp^2, 65–40 C-OH, 17 SSB.

TGA

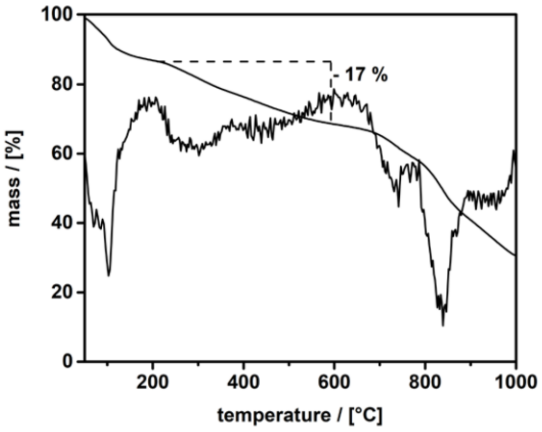

1. Step 50 °C – 200 °C 15%
2. 200 °C – 600 °C 17% → 21.5 oxygen species
3. >600 °C 68%

ATR-IR

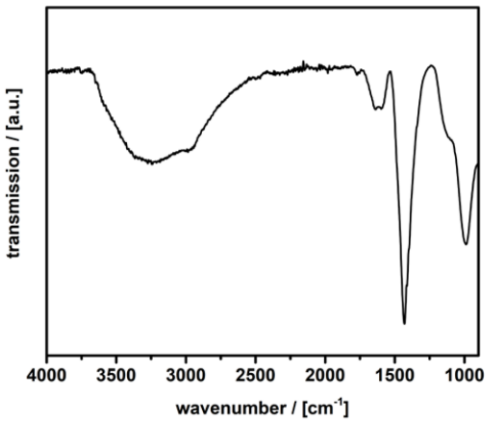

IR (powder): 3240, 2982, 2942, 1639, 1588, 1429, 1117 cm^{-1}.

References

1. Silion, M.; Dascalu, A.; Pinteala, M.; Simionescu, B. C.; Ungurenasu, C., A study on electrospray mass spectrometry of fullerenol C60 (OH) 24. *Beilstein J. Org. Chem.* **2013,** *9*, 1285.

Artificial Photosynthesis

International Edition: DOI: 10.1002/anie.201905410
German Edition: DOI: 10.1002/ange.201905410

Molecular Semiconductor Surfactants with Fullerenol Heads and Colored Tails for Carbon Dioxide Photoconversion

*Marius Kunkel, Sebastian Sutter, and Sebastian Polarz**

Abstract: *The leaf is a prime example of a material converting waste (CO_2) into value with maximum sustainability. As the most important constituent, it contains the coupled photosystems II and I, which are imbedded in the cellular membrane of the chloroplasts. Can key functions of the leaf be packed into soap? We present next-generation surfactants that self-assemble into bilayer vesicles (similar to the cellular membrane), are able to absorb photons of two different visible wavelengths, and exchange excited charge carriers (similar to the photosystems), followed by conversion of CO_2 (in analogy to the leaf). The amphiphiles contain five dye molecules as the hydrophobic entity attached exclusively to one hemisphere of a polyhydroxylated fullerene (Janus-type). We herein report on their surfactant, optical, electronic, and catalytic properties. Photons absorbed by the dyes are transferred to the fullerenol head, where they can react with different species such as CO_2 to give formic acid.*

Nature has found a unique way to exploit sunlight for driving biological processes: photosynthesis. The most important constituents of chloroplasts are the photosystems II and I, which convert light into chemical energy. As photosynthesis consumes the greenhouse gas CO_2, major research efforts have been devoted to the identification of synthetic mimics. The "artificial leaf" is an illustrative expression for this field of research.[1] Impressive success has been achieved for photocatalytic water splitting using semiconductor nanoparticles.[2] The absorption of light leads to the formation of electron–hole pairs, which are separated and, in an ideal case, induce photo-reduction and -oxidation in one system. Numerous systems have been evaluated for the photoreduction of CO_2, which are mostly based on inorganic semiconductors combined with suitable photosensitizers.[3]

However, as the customizability of inorganic semiconductors is restricted, it has also been considered to let molecular systems do the job.[3c,4] Fullerene derivatives have proven to be valuable compounds in optoelectronic or photocatalytic applications.[5] Fullerenes in general have a high electron affinity, which makes them suitable for donor–acceptor systems. A common example are fullerene dyads.[6] Fullerene dyads belong to the fascinating class of so-called small-molecule semiconductors,[7] which became of interest in bulk heterojunction solar cells as strong optical absorbents and electron mediators.[8] A donor unit is attached to the fullerene, which can be excited by absorbing light and then transfers an electron in a process accompanied by charge separation. During this process, a fullerene radical anion is produced, which can further transfer the electron.[6f,9] Studies have also shown that fullerene dyads can produce significant amounts of reactive oxygen species (ROS).[10]

Unfortunately, the use of fullerene dyads in aqueous systems is difficult because of their hydrophobic character. This problem could be addressed by a small-molecule, fullerene-based semiconductor with surfactant properties. Surfactants are functional molecules composed of a hydrophobic chain (typically alkyl groups) and a hydrophilic head group that are attached to each other in a dipolar fashion. The two important features of surfactants are their abilities to stabilize interfaces and to self-assemble into higher organized structures such as micelles, vesicles, or lyotropic phases depending on concentration, temperature, and, last but not least, molecular shape. The advantage of a self-organized superstructure formed by a molecular semiconductor surfactant is that it could come close to a new type of an artificial leaf (see Figure 1). It undergoes multi-wavelength light triggered charge generation and separation to compartments at the two sides of an interface, followed by coupling to chemical conversion of reagents such as CO_2 or others into different, more valuable products.[3a,11]

To realize such surfactant properties, we chose a so-called fullerenol as the head group as they are known to show similar electronic behavior as unmodified fullerenes and to be water-soluble.[12] We have recently presented surfactants with fullerenol head groups and alkyl tails and tested their biocompatibility.[13] In Ref. [14], we presented a new and efficient one-pot approach for the preparation of arbitrary Janus-type substituted fullerenols.[14] Whereas Ref. [14] focussed on synthetic details and molecular characterization of the compounds, any special, functional properties of those fascinating compounds have been omitted, and are the subject of the current paper.

We focused on compounds with one hemisphere of the fullerenol modified by five dye molecules (see Figure 1a,b and Figure S1 in the Supporting Information). These dyes are acridine yellow-G ($\lambda_{max} = 445$ nm; **FuDy-Y**), neutral red ($\lambda_{max} = 530$ nm; **FuDy-R**), and toluidine blue O ($\lambda_{max} = 629$ nm; **FuDy-B**). The dyes were selected to cover almost the entire visible range (Figure 1b). Because of their amphiphilic structure, the presented compounds are designated for possessing amphiphilic properties. Surface activity was probed by concentration-dependent surface-tension γ measurements (Figure 2a). The curves show a shape characteristic for surfactants. Above a certain concentration, aggregates form. The size of those aggregates is around 100 nm for **FuDy-Y** according to dynamic light scattering (DLS; Figure 2b). Considering the fact that the diameter of a single surfactant molecule is only about 1.5 nm, the aggregate size cannot correspond to spherical micelles, which are expected to have double the surfactant length.

The latter could be confirmed by transmission electron microscopy (TEM), also under cryogenic conditions, as shown in Figure 2d (see also Figure S2). Spherical objects with diameters corresponding well to the DLS results were observed. Thus we concluded that vesicles rather than micelles had been formed with a critical aggregation concentration of $c_{cac} \approx 0.4$ mM. Because of the relatively large

[*] M. Kunkel, S. Sutter, Prof. Dr. S. Polarz
Department of Chemistry, University of Konstanz
Universitätsstrasse 10, 78457 Konstanz (Germany)
E-mail: sebastian.polarz@uni-konstanz.de

Supporting information and the ORCID identification number(s) for the author(s) of this article can be found under: https://doi.org/10.1002/anie.201905410.

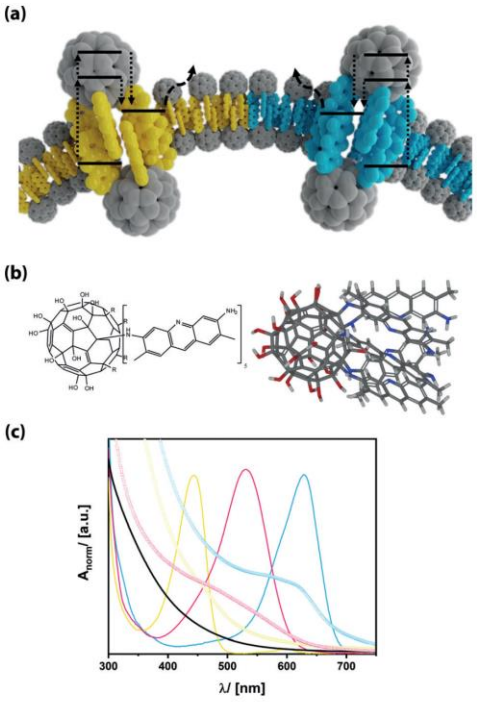

Figure 1. a) Fullerenol dyads as surfactant semiconductors with lipid-like properties and associated photochemical processes. b) Schematic structure (left) and calculated structure of **FuDy-Y**. C gray, H white, N blue, O red. c) UV/Vis absorption spectra of the dyes (lines) and the fullerenol dyads (symbols) according to the color of the dye. yellow-G: yellow, neutral red: red, toluidine blue: blue, reference fullerenol: black.

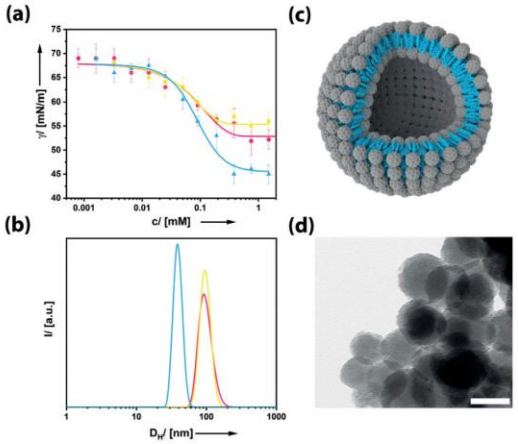

Figure 2. a) Concentration-dependent surface tension measurements and b) aggregate size distribution functions derived from DLS at $c = 0.4$ mM for the three different FuDy surfactants. **FuDy-B**: blue, **FuDy-Y**: yellow, **FuDy-R**: red. c) Schematic structure of the vesicular aggregates formed in solution. d) TEM image of a dried sample of a colloidal solution of **FuDy-Y** aggregates; scale bar: 100 nm.

packing parameter of the surfactants (see Figure S1), they behave rather similar to lipids and prefer structures of lower curvature. This observation is in line with our previous findings for fullerenol surfactants with simple alkyl chains as hydrophobic tails.[13] Although the sizes, shapes, and polarities of the three compounds are similar according to molecular geometry optimization (Figure S1), **FuDy-B** gave a lower γ value at saturation of the interface ($c > 0.5$ mM) than **FuDy-Y** and **FuDy-R**. The aggregates of the latter two compounds are also larger with a hydrodynamic diameter D_H of about 90–100 nm. The different substituents in the hydrophobic, conjugated π-system obviously have an effect on the so-called hydrophilic–lipophilic balance (HLB).

Having shown that the **FuDys** motifs have surfactant properties, we investigated whether they are molecular semiconductors. Therefore, a thorough photophysical characterization was necessary. Optical absorption spectra of reference compounds (the unmodified dyes and $C_{60}(OH)_{24}$)[15] are compared to each other in Figure 1b (see also Figure S3). The absorption spectra of the different **FuDy** compounds are not simple superpositions of the spectra of their constituents.[6f,9a] Instead of distinct absorption bands, an absorption edge has emerged, which is rather typical for semiconductors. The shift of the energy of the absorption edge compared to λ_{max} of the dyes indicates that there is electronic communication between the surfactant's head and tail. The fact that the dyes are not electronically isolated was confirmed by DFT calculations (Figure 3a). The highest occupied molecular orbital (HOMO) is located exclusively on the dye molecules. The absolute energy of the HOMO of **FuDy-Y**, for instance, is −5.8 eV according to photoelectron spectroscopy on air (PESA; Figure S3). The first unoccupied orbital with sufficient orbital overlap between head and tail is located at ca. −2.8 eV, and corresponds well to the optical transition (Figure 3a). However, the DFT calculations show that the lowest unoccupied molecular orbital (LUMO) is located at −3.4 eV and consists only of fullerenol orbitals. Therefore, after electronic excitation, the charge carriers are quickly transferred to the LUMO. This was confirmed by photoluminescence (PL) measurements (Figure S3). The red-shift in the PL maximum points to an extended conjugation length of the π-system. However, the PL intensity is reduced by almost 90%. Considering that fullerenols exhibit no fluorescence in the relevant spectral region (Figure S2), the decrease in the PL intensity can be interpreted as a sign for the transfer of photogenerated charges to the head group. These findings are in agreement with literature on standard fullerene dyads.[6] Our conclusions were further confirmed by fluorescence lifetime τ_{PL} measurements (Figure S3). The τ_{PL} of **FuDy** (1.7 ns) is tremendously reduced compared to that of the free dye ($\tau_{PL} = 6$ ns) in solution. Furthermore, the fluorescence decay of **FuDy** is not mono-exponential anymore, which indicates that relaxation processes have become more complex upon attachment to the fullerenol residue. Further confirmation of a true semiconductor nature was obtained by

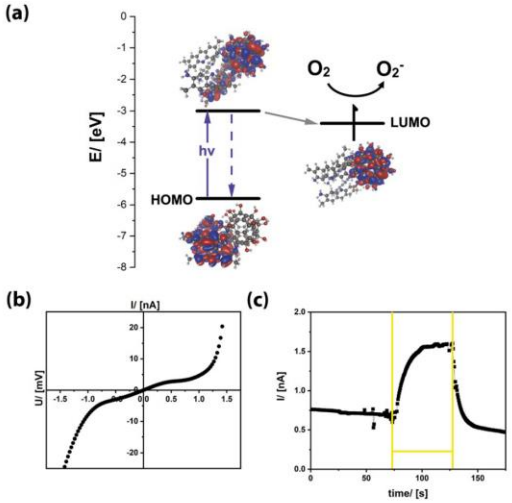

Figure 3. a) Frontier orbitals of **FuDy-Y** deduced from DFT calculations and PESA measurements (HOMO: combined HOMO to HOMO−4). b) *I*/*V* measurement (measurement in the dark with 20 $mV s^{-1}$) and c) photocurrent measurement of **FuDy-Y** (the yellow lines mark the irradiation time with white light; 1 mV was applied).

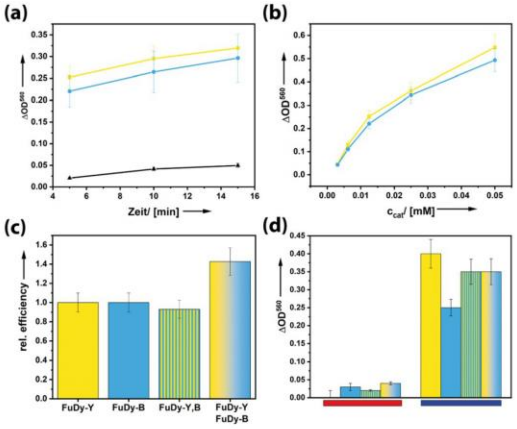

Figure 4. a–c) Results of the NBT essay for investigating the superoxide formation efficiency of different **FuDy** systems; $C_{60}(OH)_{24}$ (reference system): black; **FuDy-Y**: yellow; **FuDy-B**: blue, under white light irradiation. a) Superoxide formation over time for $c_{cat} = 0.0125$ mM. b) Concentration dependence; $t = 5$ min. c) Comparison of the relative photocatalytic efficiencies of systems comprising only one type of dye with a mixture of **FuDy-B,Y** (gradient color) and a **FuDy** compound containing two dyes in one molecule, $c_{cat} = 0.05$ mM. d) Wavelength-dependent superoxide efficiency for irradiation with monochromatic light (red: 630 nm, blue: 450 nm) for $c_{cat} = 0.05$ mM.

current–voltage (IV) measurements of **FuDy-Y** (Figure 3b). The material obviously shows macroscopic charge transport, but the behavior is non-ohmic, which is consistent with a semiconducting electronic system. Light absorption should increase the number of mobile charge carriers in a semiconductor material, and accordingly, also **FuDy-Y** displays a signal when used as a photoconductor (Figure 3c). After the light is switched off, the photocurrent decreases again, as expected.

We now expected that the charge-separated state with the high-energy electron depicted in Figure 3 can act as a donor state for initialization of further reactions. Thus we selected a reagent with high electronegativity, and thus energetically low-lying acceptor orbitals, first: molecular oxygen O_2. For quantification of the resulting superoxide, a nitrotetrazolium blue essay (NBT) was applied.[10d,16] To exclude unintentional and direct excitation of the fullerenol head group (by absorption in the UV range), tests were performed with light-emitting diodes (LEDs) as the light source with wavelengths strictly above 400 nm (Figure S4). As only the absorption edges of **FuDy-Y** and **FuDy-B** correlate well with the LED, **FuDy-R** will not be considered in the following. As a reference and for further confirmation, a non-substituted fullerenol $C_{60}(OH)_{24}$[15] was used. All systems containing fullerenols produced superoxide over time (Figure 4a), but at the same concentration of the photocatalyst (c_{cat}), both **FuDy** species produce up to 700% more than the reference system. This result clearly demonstrates the importance of the dye entities attached to the fullerene head and the charge separation process depicted in Figure 3. Higher superoxide production can, of course, be managed by increasing the concentration of the photocatalyst (Figure 4b). An interesting question is how a system behaves that contains two different photosystems/dyes like a leaf. Therefore, we combined **FuDy-B** and **FuDy-Y** under otherwise constant conditions. It does not make a difference if one uses a mixture of **FuDy-B** and **FuDy-Y** directly or combines aggregates of the two prepared in two separate vials. This can be understood by realizing that surfactant aggregates are highly dynamic systems in which molecules are rapidly exchanged.[17]

If the two photosystems act independently from each other, one would not expect a significant change in superoxide production efficiency because the previous experiments have shown **FuDy-B** and **FuDy-Y** are almost equally effective (Figure 4a,b). However, we measured an efficiency increase of 40% (Figure 4c). To make sure that this increase is really due to an intermolecular, cooperative effect (as in the natural leaf), we prepared a new **FuDy** with two types of dye (yellow-G and toluidine blue) attached to the fullerenol head group in one molecule (**FuDy-B,Y**). The efficiency of this system is slightly lower than that of the pure **FuDy** (Figure 4c), but within the measurement error. We interpret our findings as follows. The fullerenol head group can only host one electron transferred from one of the dye molecules attached to it, followed by superoxide formation. Therefore, attaching different types of dyes to one fullerenol head does not provide any advantages. However, it seems that the **FuDy** molecules can, in their self-assembled structures, transfer the photoexcited electron to neighboring surfactants, which then

leads to an overall increase in efficiency. Furthermore, the efficiency of superoxide production at different wavelengths was evaluated. Figure 4d shows that the **FuDy** systems, the combined as well as the mixed dyes, only produce little superoxide under irradiation at longer wavelengths whereas the efficiency tremendously increased under irradiation with blue light. As it was ensured that the fullerenol head group does not absorb in this region, this effect only derives from the absorption of the attached dyes into higher LUMOs, which then populate the charge-separated state. These findings indicate that all absorbed wavelengths take part in the generation of superoxide whereby especially the absorption of higher-energy photons leads to the charge-separated state. Again, the effect of an intermolecular electron transfer can be observed.

The final, exciting question is whether the acceptor orbitals of CO_2 are also low enough in energy for undergoing the described photoreduction process. Thus the experiments were repeated with CO_2 instead of O_2. The results were evaluated by ^{1}H NMR spectroscopy (Figure 5a) and GC-MS.

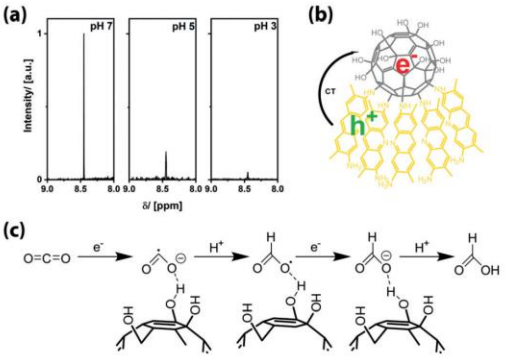

Figure 5. Photoreduction of carbon dioxide with a mixture of **FuDy-Y** and **FuDy-B** in aqueous solution. a) Excerpts of ^{1}H NMR spectra for formic acid production from CO_2 at different pH values. b) Overall scheme for the **FuDy**-catalyzed reaction. c) Proposed mechanism for the photoreduction of CO_2 by the **FuDy** system (water molecules not shown).

We clearly observed the generation of formic acid when **FuDy-B/FuDy-Y** was used as the photocatalyst. Formic acid can be formed by a two-electron two-proton reaction, which is likely to happen directly at the **FuDy**'s head groups. Figure 5b,c shows a proposed mechanism for this process.[18] We assume that the general mechanism is similar to that of photocatalyzed superoxide production of fullerenes and fullerenols, in which the fullerenol is likely to transfer electrons.[10b,d,12a,19] The reducibility of the fullerenol compound strongly depends on the degree of polyhydroxylation and the type of polyhydroxylation moieties and can vary between a slightly negative or a slightly positive potential, whereas a stronger reducibility derives from a larger π-electron stabilization.[20] An intramolecular charge transfer results in a reduction of the head group, whereas the charge is located at the C_{60} core as oxygen has a weak ability to accommodate radical electrons.[20] This fullerenol anion, according to the known literature mentioned above, can reduce, for example, carbon dioxide in a fast process to again enable the reduction of the fullerenol. The fullerenol head group is predestined for the coordination of, for example, carbon dioxide because of the multiple hydrogen binding sites. In a first step, carbon dioxide is reduced to yield the carbon dioxide radical anion. After protonation at the carbon atom, a fast second electron transfer has to take place, which emphasizes the importance of the intermolecular exciton transfer described before. Final protonation yields formic acid. No further reduction occurs according to GC-MS. Performing the reaction at different pH values shows that the highest yield of formic acid was achieved at pH 7, with decreasing efficiency with decreasing pH value. The yield of formic acid at pH 5 is only about 18% of the value at pH 7, whereas at more acidic pH values, almost no formic acid is produced. At pH 7, the predominant species is HCO_3^-, which can obviously interact very well with the fullerenol surfactants.

The leaf is an unparalleled example for the "green" conversion of energy in the form of light into valuable products. Therefore, numerous attempts have been made in materials science to create systems with similar functionality. We have presented a new approach based on multifunctional surfactants. Inspired by literature on fullerene dyads and our own work on amphiphiles with fullerenol head groups, we have discussed surfactants with semiconductor properties. The compounds self-assemble into bilayer vesicle structures in solution and exhibit properties such as charge separation of photogenerated excitons. Intermolecular electron transfer takes place between surfactant fullerenol dyads covering different regions of the electromagnetic spectrum, thus fulfilling one key criterium of an artificial leaf. The chemical energy of the charge-separated states could be exploited to produce superoxide from oxygen and formic acid from carbon dioxide by irradiation with visible light in aqueous solution. The dependence of the efficiency on different parameters was evaluated, and a mechanism was proposed. Therefore, also the second criterion of an artificial leaf, the conversion of less valuable compounds (CO_2) into better products, has been realized. The current work extends not only the horizon of functional fullerene-based materials but also that of surfactant chemistry in general.

Acknowledgements

The current research was funded by an ERC consolidator grant (I-SURF; project 614606). We thank Stephan Siroky for 3D graphics. We acknowledge support by the State of Baden-Württemberg through bwHPC.

Conflict of interest

The authors declare no conflict of interest.

Keywords: artificial leaves · CO_2 utilization · fullerenes · photocatalysis · surfactants

How to cite: *Angew. Chem. Int. Ed.* **2019**, *58*, 15620–15625
Angew. Chem. **2019**, *131*, 15766–15771

[1] D. G. Nocera, *Acc. Chem. Res.* **2012**, *45*, 767.
[2] K. Sivula, R. Van De Krol, *Nat. Rev. Mater.* **2016**, *1*, 15010.
[3] a) X. Chang, T. Wang, J. Gong, *Energy Environ. Sci.* **2016**, *9*, 2177–2196; b) X. Li, J. Yu, M. Jaroniec, X. Chen, *Chem. Rev.* **2018**; c) A. J. Morris, G. J. Meyer, E. Fujita, *Acc. Chem. Res.* **2009**, *42*, 1983; d) Z. Guo, S. Cheng, C. Cometto, E. Anxolabéhère-Mallart, S.-M. Ng, C.-C. Ko, G. Liu, L. Chen, M. Robert, T.-C. Lau, *J. Am. Chem. Soc.* **2016**, *138*, 9413.
[4] A. J. Esswein, D. G. Nocera, *Chem. Rev.* **2007**, *107*, 4022.
[5] a) A. Mohajeri, A. Omidvar, *Phys. Chem. Chem. Phys.* **2015**, *17*, 22367; b) R. Ganesamoorthy, G. Sathiyan, P. Sakthivel, *Solar Energy Mater. Solar Cells* **2017**, *161*, 102; c) G. Dennler, M. C. Scharber, C. J. Brabec, *Adv. Mater.* **2009**, *21*, 1323; d) V. Georgakilas, J. N. Tiwari, K. C. Kemp, J. A. Perman, A. B. Bourlinos, K. S. Kim, R. Zboril, *Chem. Rev.* **2016**, *116*, 5464; e) D. W. Wang, D. S. Su, *Energy Environ. Sci.* **2014**, *7*, 576; f) R. Leary, A. Westwood, *Carbon* **2011**, *49*, 741.
[6] a) F. D'Souza, R. Chitta, K. Ohkubo, M. Tasior, N. K. Subbaiyan, M. E. Zandler, M. K. Rogacki, D. T. Gryko, S. Fukuzumi, *J. Am. Chem. Soc.* **2008**, *130*, 14263; b) A. N. Amin, M. E. El-Khouly, N. K. Subbaiyan, M. E. Zandler, S. Fukuzumi, F. D'Souza, *Chem. Commun.* **2012**, *48*, 206; c) K. Lewandowska, B. Barszcz, A. Graja, B. Bursa, A. Biadasz, D. Wróbel, W. Bednarski, S. Waplak, M. Grzybowski, D. T. Gryko, *Synth. Met.* **2013**, *166*, 70; d) C. O. Obondi, G. N. Lim, Y. Jang, P. Patel, A. K. Wilson, P. K. Poddutoori, F. D'Souza, *J. Phys. Chem. C* **2018**, *122*, 13636; e) V. Bandi, S. K. Das, S. G. Awuah, Y. You, F. D'Souza, *J. Am. Chem. Soc.* **2014**, *136*, 7571; f) M. A. Lebedeva, T. W. Chamberlain, P. A. Scattergood, M. Delor, I. V. Sazanovich, E. S. Davies, M. Suyetin, E. Besley, M. Schröder, J. A. Weinstein, *Chem. Sci.* **2016**, *7*, 5908.
[7] Y. Z. Lin, Y. F. Li, X. W. Zhan, *Chem. Soc. Rev.* **2012**, *41*, 4245.
[8] a) K. Narayanaswamy, A. Venkateswararao, P. Nagarjuna, S. Bishnoi, V. Gupta, S. Chand, S. P. Singh, *Angew. Chem. Int. Ed.* **2016**, *55*, 12334; *Angew. Chem.* **2016**, *128*, 12522; b) G. D. Blanco, A. J. Hiltunen, G. N. Lim, C. B. Kc, K. M. Kaunisto, T. K. Vuorinen, V. N. Nesterov, H. J. Lemmetyinen, F. D'Souza, *ACS Appl. Mater. Interfaces* **2016**, *8*, 8481; c) T. L. Nguyen, T. H. Lee, B. Gautam, S. Y. Park, K. Gundogdu, J. Y. Kim, H. Y. Woo, *Adv. Funct. Mater.* **2017**, *27*, 1702474.
[9] a) A. Ciammaichella, P. O. Dral, T. Clark, P. Tagliatesta, M. Sekita, D. M. Guldi, *Chem. Eur. J.* **2012**, *18*, 14008; b) J. S. Cowart, Jr, C. Liman, A. Garnica, Z. A. Page, E. Lim, R. R. Zope, T. Baruah, C. J. Hawker, M. L. Chabinyc, *Inorg. Chim. Acta* **2017**, *468*, 192.
[10] a) Z. Youssef, R. Vanderesse, L. Colombeau, F. Baros, T. Roques-Carmes, C. Frochot, H. Wahab, J. Toufaily, T. Hamieh, S. Acherar, *Cancer Nanotechnol.* **2017**, *8*, 6; b) Y. Yamakoshi, S. Aroua, T.-M. D. Nguyen, Y. Iwamoto, T. Ohnishi, *Faraday Discuss.* **2014**, *173*, 287; c) A. Y. Rybkin, A. Y. Belik, O. Kraevaya, E. Khakina, A. Zhilenkov, N. Goryachev, D. Volyniuk, J. Grazulevicius, P. Troshin, A. Kotelnikov, *Dyes Pigm.* **2019**, *160*, 457; d) A. I. Kotelnikov, A. Y. Rybkin, E. A. Khakina, A. B. Kornev, A. V. Barinov, N. S. Goryachev, A. V. Ivanchikhina, A. S. Peregudov, V. M. Martynenko, P. A. Troshin, *Org. Biomol. Chem.* **2013**, *11*, 4397.
[11] J. Hong, W. Zhang, J. Ren, R. Xu, *Anal. Methods* **2013**, *5*, 1086.
[12] a) J. Lim, H. Kim, P. J. Alvarez, J. Lee, W. Choi, *Environ. Sci. Technol.* **2016**, *50*, 10545; b) K. Pickering, M. Wiesner, *Environ. Sci. Technol.* **2005**, *39*, 1359; c) J. Grebowski, P. Kazmierska, A. Krokosz, *BioMed Res. Int.* **2013**, 751913.
[13] M. Kunkel, S. Schildknecht, K. Boldt, L. Zeyffert, D. Schleheck, M. Leist, S. Polarz, *ACS Appl. Mater. Interfaces* **2018**, *10*, 23638.
[14] M. Kunkel, S. Polarz, *Beilstein J. Org. Chem.* **2019**, *15*, 901.
[15] P. A. Troshin, A. S. Astakhova, R. N. Lyubovskaya, *Fullerenes Nanotubes Carbon Nanostruct.* **2005**, *13*, 331.
[16] Y. Yamakoshi, N. Umezawa, A. Ryu, K. Arakane, N. Miyata, Y. Goda, T. Masumizu, T. Nagano, *J. Am. Chem. Soc.* **2003**, *125*, 12803.
[17] R. Hadgiivanova, H. Diamant, D. Andelman, *J. Phys. Chem. B* **2011**, *115*, 7268.
[18] D. Ren, J. Fong, B. S. Yeo, *Nat. Commun.* **2018**, *9*, 925.
[19] Z. Markovic, V. Trajkovic, *Biomaterials* **2008**, *29*, 3561.
[20] Z. Wang, X. Chang, Z. Lu, M. Gu, Y. Zhao, X. Gao, *Chem. Sci.* **2014**, *5*, 2940.

Manuscript received: May 1, 2019
Revised manuscript received: July 5, 2019
Accepted manuscript online: July 16, 2019
Version of record online: August 12, 2019

Angewandte
Eine Zeitschrift der Gesellschaft Deutscher Chemiker Chemie

Supporting Information

Molecular Semiconductor Surfactants with Fullerenol Heads and Colored Tails for Carbon Dioxide Photoconversion

*Marius Kunkel, Sebastian Sutter, and Sebastian Polarz**

anie_201905410_sm_miscellaneous_information.pdf

SUPPORTING INFORMATION

Experimental part.
The synthesis was performed according to a protocol by Kunkel et al.[1] For the synthesis of **FuDy-Y,B** a mixture of acridine yellow and toluidine blue was used instead of only one dye. This result is a statistic mixture. Additionally, to the protocol the compounds have been purified by HPLC (see Analytical methods).
The yield of the compounds is: FuDy-Y 60 %, FuDy-R 69 %, FuDy-B 45 %, FuDy-Y,B 38 %.

Characterization
FuDy-Y
^{1}H-^{13}C- CP MAS-NMR (100 MHz): δ (ppm) 176, 160, 133, 77, 56, 39, 15
ATR-IR: ν (cm^{-1}) = 3200, 2927, 2874, 2607, 1564, 1372, 1244, 989, 818
TGA: 40-192 °C 11 %; 192-550 °C 17 %; 550 °C+ 72 % → 20 +/- 2 OH
ESIMS: $[(OH)_8O_{12}C_{60}(C_{15}H_{14}N_3)_5]^+$ m/z = 2230.2 (2230.2); $[(OH)_4O_{17}C_{60}(C_{15}H_{14}N_3)_5]^-$ m/z = 2242.2 (2242.2)

FuDy-R
^{1}H-^{13}C- CP MAS-NMR (100 MHz): δ (ppm) 177, 160, 150, 137, 129, 101, 74, 57, 39, 18
ATR-IR: ν (cm^{-1}) = 3177, 2957, 2858, 1580, 1443, 1359, 1002
TGA: 40-180 °C 11 %; 180-575 °C 22 %; 575 °C+ 67 % → 21 +/-3 OH
ESIMS: $[(OH)_{17}O_4C_{60}(C_{15}H_{15}N_4)_5]^+$ m/z = 2330.3 (2330.3); $[(OH)_{17}O_3C_{60}(C_{15}H_{15}N_4)_5]^-$ m/z = 2314.3 (2314.3)

FuDy-B
^{1}H-^{13}C- CP MAS-NMR (100 MHz): δ (ppm) 176, 160, 133, 79, 57, 39, 15
ATR-IR: ν (cm^{-1}) = 3200, 2927, 2874, 1564, 1361, 1010
TGA: 40 – 200 °C 10%; 200-570 °C 21 %; 570 °C+ 69% → 20+/-3 OH
ESIMS: $[(OH)_{10}O_{11}C_{60}(C_{15}H_{16}N_3S)_5]^+$ m/z = 2418.6 (2418.6); $[(OH)_{16}O_4C_{60}(C_{15}H_{16}N_3S)_5]^-$ m/z = 2408.6 (2408.6)

FuDy-Y,B
ATR-IR: ν (cm^{-1}) = 3231, 2943, 2893, 1560, 1342, 1169, 1011
ESIMS: $[(OH)_{14}O_8C_{60}(C_{15}H_{14}N_4)_2(C_{15}H_{16}N_3S)_3]^+$ m/z = 2370.5 (2370.5)

Methods

General Methods

Synthesis that acquired inert gas atmosphere were performed using general Schlenk techniques under argon atmosphere. The solvents were dried according to standard literature and stored under argon. Water was deionized with Millipore Milli-Q. All starting materials used for synthesis were purchased from commercial sources unless stated differently. The fullerene C_{60} (pur. 99.9 %) was purchased from Research & Production Company “Modern Synthesis Technology”.

Analytical Methods

Liquid chromatography was measured with Thermo Fisher Scientific Dionex 3000. As the column, Agilent Poroshell 120 EC-C18 (2.1×100 mm, 2.7µm) was used. MeCN (5%) as eluent A and 95% water as eluent B with 0.1% formic acid were used. A linear gradient of 5% A to 100% A was applied a flow rate of 0.3 mL/min. Mass spectra were measured on Bruker amazon SL respectively on Bruker microtof II system in pos. or neg. mode via direct inject from a methanolic solution. Assignment of peaks was done as follows: $[M - xH_2O - yH - zO - v(HNR)]^{a-/+}$. Molecular ion peak is identified in combination with results from TGA and NMR. TGA was measured on Netzsch Jupiter STA 449 F3. All measurements were performed under nitrogen atmosphere with 80 mL/min flowrate and with heating rate of 5 K/min. MAS-NMR measurements were performed on Bruker Avance II 400 solid-state NMR at 295 or 350 K and with 10k Hz rotational speed. Number of scans 5k – 10k with D1 = 10 to 100 sec. NMR measurements (^{1}H, ^{13}C) were performed on a Varian INOVA 400 MHz spectrometer. Attenuated total reflection−infrared (ATR−IR) spectra were measured with a Perkin Elmer100 Spectrum spectrometer including an ATR unit. DLS measurements were done by using a Malvern Zen5600. Transmission electron microscopy (TEM) observations were carried out using Zeiss Libra120. For cryo transmission electron microscopy studies, a sample droplet of 2ul was put on a lacey carbon filmed copper grid (Science Services, Muenchen), which was hydrophilized by air plasma glow discharge unit (30s with 50W, Solarus 950, Gatan, Muenchen, Germany). Subsequently, most of the liquid was removed with blotting paper in a Leica EM GP (Wetzlar, Germany) grid plunge device, leaving a thin film stretched over the lace holes in the saturated water atmosphere of the environmental chamber. The specimens were instantly shock frozen by rapid immersion into liquid ethane cooled to approximately 97K by liquid nitrogen in the temperature-controlled freezing unit of the Leica EM GP. The temperature was monitored and kept constant in the chamber during all the sample preparation steps. The specimen was inserted into a cryotransfer holder (CT3500, Gatan, Muenchen, Germany) and transferred. Surface tension measurements were performed at Krüss K100. Photosensor measurements were performed on 3 mm×3 mm sensor substrates from Umweltsensortechnik and measured with a Zahner IM6 potentiostat. Measurements in solution were performed in a folded capillary cell. UV/Vis absorption spectra were acquired using an Agilent Cary 60 spectrometer. PL spectra were obtained from a PicoQuant FluoTime-300 spectrometer. Geometry optimization and frontier orbital calculation was performed using Density-Functional Theory (DFT) with the TURBOMOLE Program Package for ab initio Electronic Structure Calculations using B3LYP/def2-TZVP level of theory. TURBOMOLE V7.1, a development of University of Karlsruhe and Forschungszentrum Karlsruhe GmbH, 1989-2007, TURBOMOLE GmbH, since 2007; available from http://www.turbomole.com.

NBT assay

0.5 mM NBT and 0.05/0.025/0.0125/0.0061 mM FuDy in Milli-Q were irradiated for 5/10/15 min with 100 W white LED (see Fig. S3). The difference in absorbance was measured at 560 nm versus blank sample.

CO_2 conversion

5mM aqueous solution (pH 7, pH 5 and pH 3) of FuDy-Y,B has been saturated with 100% CO_2 gas. The vessel was sealed and irradiated with 100 W white LED (see Fig. S3). Formic acid was detected with ^{1}H-NMR. 0.1 M solution of ascorbate was added as electron donor.

Figure S1. Molecular structure of FuDy-compounds.
(a) Lewis-structures.

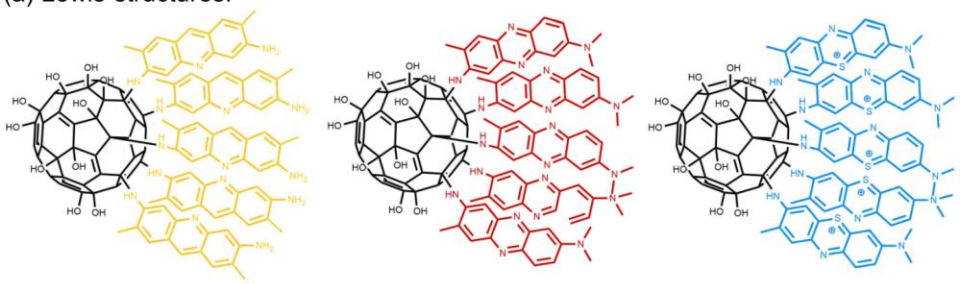

FuDy-Y **FuDy-R** **FuDy-B**

(b) Calculated molecular geometry and electrostatic potential maps.

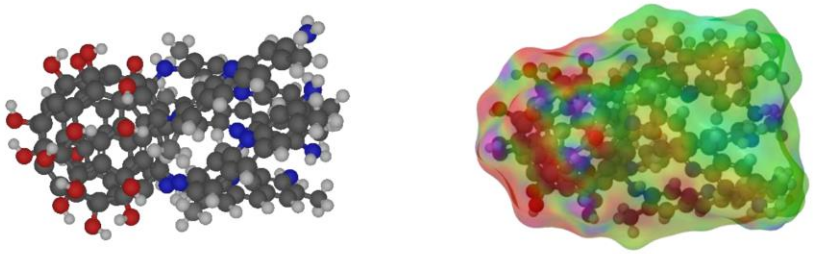

FuDy-Y

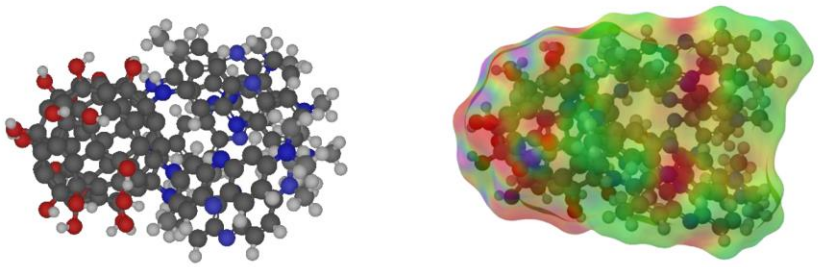

FuDy-R

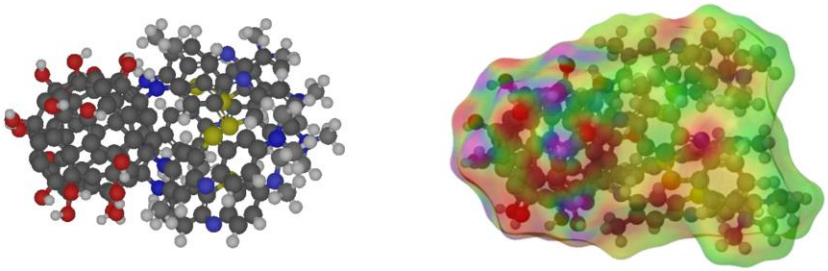

FUDY-B

Figure S2. Cryo-TEM investigation of FuDy-Y aggregates in solution.

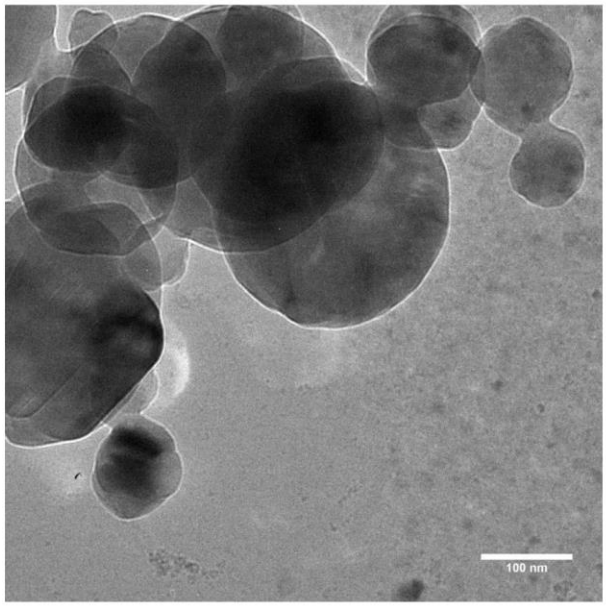

Figure S3. Photophysical characterization of **FuDy** compounds.

(a) Quantitative adsorption spectra.

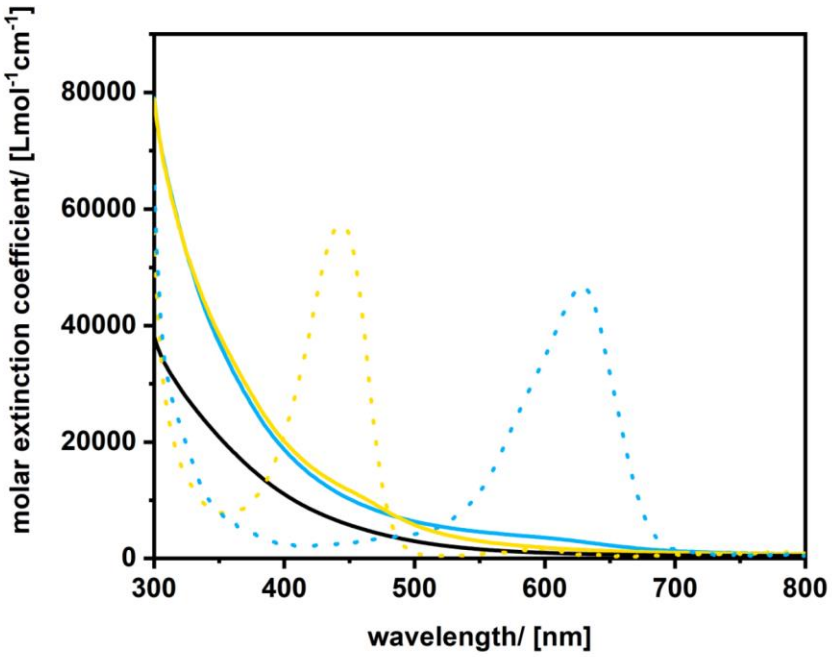

yellow dotted = yellow-G, blue dotted = toluidine blue, black = $C_{60}(OH)_{24}$, yellow line = **FuDy-Y**, blue line = **FuDy-B**.

(b) PL spectra.

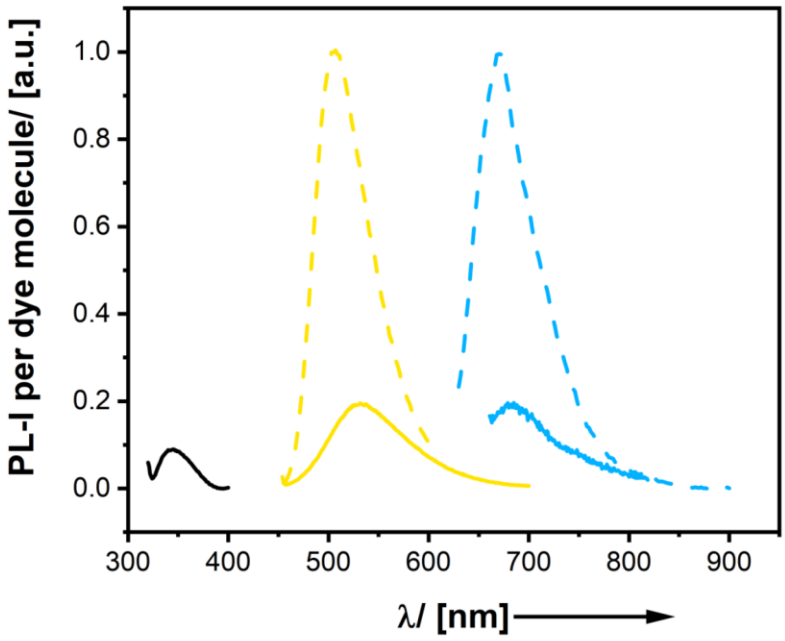

blue dashed = yellow-G, red dashed = toluidine blue, black = $C_{60}(OH)_{24}$, blue line = **FuDy-Y**, red line = **FuDy-B**.

(c) PESA

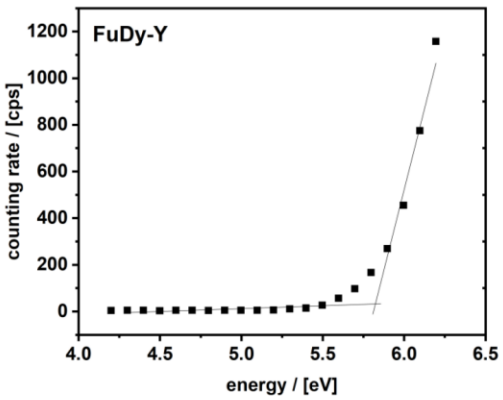
FuDy-Y
counting rate / [cps]
energy / [eV]
1200
1000
800
600
400
200
0
4.0
4.5
5.0
5.5
6.0
6.5

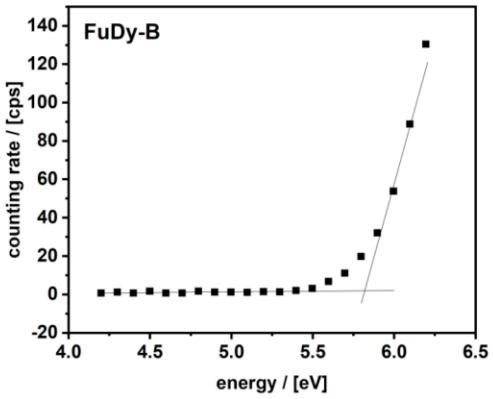
FuDy-B
counting rate / [cps]
energy / [eV]
140
120
100
80
60
40
20
0
-20
4.0
4.5
5.0
5.5
6.0
6.5

(d) fluorescence lifetime

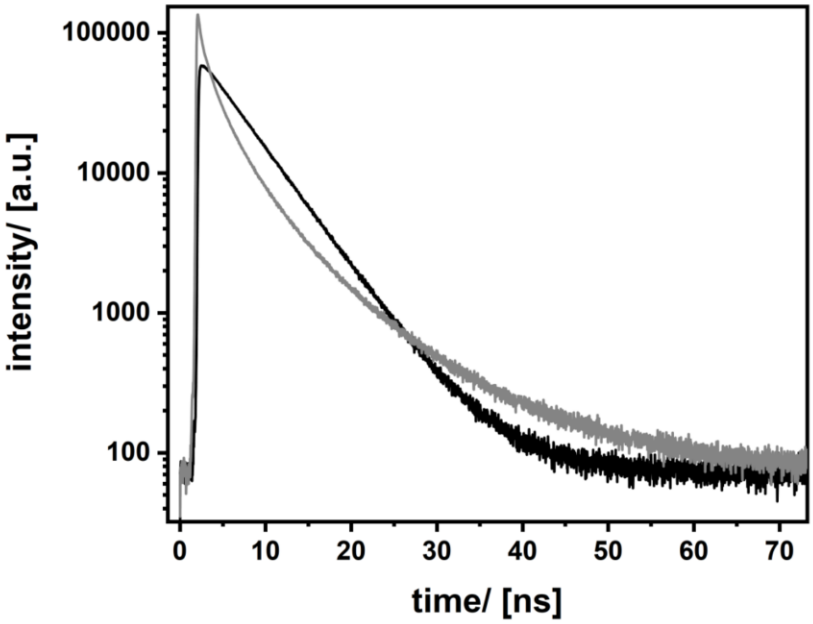

Figure S4. Spectrum of the white LED used for the photochemical reactions.

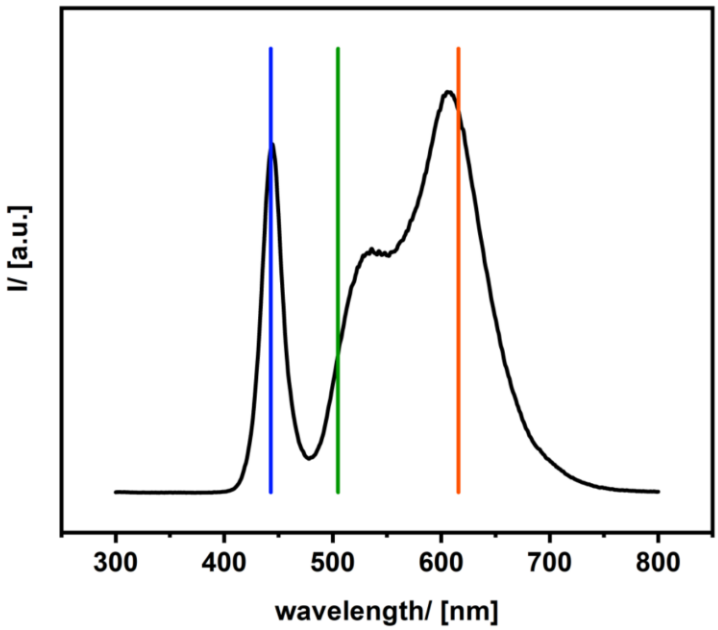

The vertical bars show the position of the absorption maxima of the dyes used in the current study.

References

1. Kunkel, M.; Polarz, S., Easy, efficient and versatile one-pot synthesis of Janus-type-substituted fullerenols. *Beilstein Journal of Organic Chemistry* **2019,** *15*, 901-905.

ChemCatChem

Communications
doi.org/10.1002/cctc.202000412

Aggregation-Induced Improvement of Catalytic Activity by Inner-Aggregate Electronic Communication of Metal-Fullerene-Based Surfactants

Marius Kunkel,[a] Stefan Bitter,[a] Frank Sailer,[a] Rainer F. Winter,[a] and Sebastian Polarz*[a, b]

A paradigm for active constituents in (homogeneous) catalysis is that optimum performance requires maximum dispersion. Generally, aggregation results in a decline. This is a different case in supramolecular catalysis. A new concept based on surfactants equipped with functional heads is presented, which becomes a more active catalyst itself upon aggregation. The head group of the surfactants is composed of a diethylenetriamine-functionalized fullerene capable of coordinating to catalytically active metals like Co^{II}. The improvement of catalytic properties upon aggregation is demonstrated via electrocatalytic water-splitting reaction as a model system. Detailed electrochemistry studies were performed at concentrations below and above the critical aggregation concentration (*cac*). While isolated surfactant molecules represent only moderately active catalysts, drastic improvement of efficiency in the hydrogen evolution (HER) as well as in the oxygen evolution reactions (OER) were detected, once vesicular structures have formed. Self-organization of the surfactants leads to an increase in turnover frequencies of up to 1300% (HER). The strongly beneficial effect of aggregation arises from the favorable alignment of individual molecules, thus, facilitating intermolecular charge transfer processes in the vesicles.

In many cases, aggregation is seen as a major drawback for catalytic reactions since upon aggregation the number of accessible reactive centers is reduced and a maximum of dispersion, especially for heterogeneous systems was the goal to achieve. Research perspective changed and systems have been developed in which aggregation comes hand in hand with beneficial effects. The field of self-assembled compounds, the supramolecular chemistry gives rise to supramolecular catalysis. In micellar catalysis, the formation of aggregates is used to perform reactions at their interface with compounds that would otherwise not be combinable. It is also possible to use solvents that would normally not be suitable for such reaction. These aggregates can be formed by supporting compounds that do not take place in the reaction themselves or by the catalyst molecule.[1–3] The phrase supramolecular catalysis is manly known from reactions with enzymatic systems which can catalyze reaction via weak interactions within their structural motif. Furthermore, this field describes the assembly of small-molecule organic catalysts.[4–5] This very assembly of the catalyst influences the reactants in a way that reactive moieties are exposed and activated, intermediates or transition states are stabilized or that the reactivity is enhanced by increasing the local concentration of the reactants.[6–8] In this work, we present a new concept of supramolecular catalysis that does not influence the reactant's properties but the catalyst itself. This is achieved by a catalytically active surfactant. Surfactants are molecular compounds with amphiphilic properties, which form well-defined aggregates. Depending on concentration, individual surfactant molecules self-assemble into micelles, vesicles or liquid crystals. Recently, more and more papers describe advanced surfactants with properties beyond simple amphiphilic properties.[9–10] Our group has specialized in the synthesis of surfactants equipped with functional, metal-containing head groups,[11–14] and several examples of catalytically active surfactants have already been published by us.[2–3] Important preliminary work of relevance to the current work is centered on fullerene-based surfactants that evaluated their self-assembly behavior and the related beneficial effect of self-assembly on their properties.[15–17]

For our supramolecular catalyst system electrocatalytic water splitting was chosen as a model system as a rather simple electron transfer reaction regarding intermediates and transition state species that is well observable. For water splitting, huge efforts during the last decades were taken in exploring and developing different realizations of the water splitting reaction, resulting in H_2 (hydrogen evolution reaction; HER) and O_2 (oxygen evolution reaction; OER).[18–20] A lot of heterogeneous and homogeneous systems have been evaluated. In the field of homogeneous systems mostly rare earth and transition metal complexes are used and groups have developed and tailored the systems to achieve low over potentials and high turnover frequencies (TOF).[21–27] The turnover frequency, one factor that defines the efficiency of a catalytic system ranges from several to several thousand per second for reported

[a] M. Kunkel, S. Bitter, F. Sailer, R. F. Winter, Prof. S. Polarz
Department of Chemistry
University of Konstanz
Universitätsstrasse 10
78457 Konstanz (Germany)
E-mail: sebastian.polarz@uni-konstanz.de
[b] Prof. S. Polarz
Institute of Inorganic Chemistry
Leibniz-University Hannover
Callinstrasse 9
30167 Hannover (Germany)

Supporting information for this article is available on the WWW under https://doi.org/10.1002/cctc.202000412

systems. A special challenge for such systems is the performance in pure aqueous system being stable as well as active. Catalytic systems of different facets with nickel, cobalt, copper and more are known to literature.[28–34] Although we do not want to compete with established systems we chose to combine a water soluble surfactant system with controlled self-assembly to enhance its catalytically activity via aggregation presenting a new way of improving such systems.

In the current work, we aim at developing a system, which is equipped with moieties that are capable of effecting electrocatalytic water splitting,[28,35] but with a fullerene-based surfactant design. Particular focus is on the role of self-assembly on catalytic activity.

The major synthesis steps leading to our target system are depicted in Figure 1a. The asymmetrical, pentachlorinated C_{60} (**1**)[36] is reacted with dodecylamine to obtain the penta-alkylated compound (**2**). Diethylenetriamine is then attached to the remaining hemisphere to obtain the ligand modified species (**3**). It is used as a ligand for complexation of cobalt(II) chloride to obtain the final product (**4**) (see Supporting Information for detailed synthesis procedure and characterization, Figure S1). Figure 1b,**c** shows the characteristic signals for the organic ligand before (**3**) and after coordination to cobalt (**4**) in electrospray ionization time of flight mass spectrometry (ESI-TOF MS). Successful coordination of Co^{II} ions was also proven by UV/Vis spectroscopy, which, in addition to the absorption of the fullerene core, showed the d-d transition band of a Co(II) triamine chelate with a maximum at 480 nm (Figure S1).

The amphiphilic properties of (**4**) were investigated by recording concentration dependent surface tension γ(c). The corresponding plot shows a shape, (see Figure 1d), which is typical for surfactants. The minimal surface tension reached is about 39 mN/m. The position of the kink in the γ(c) curve indicates that aggregation commences at a concentration *cac* of approximately 0.2 mM. Aggregation has also been confirmed

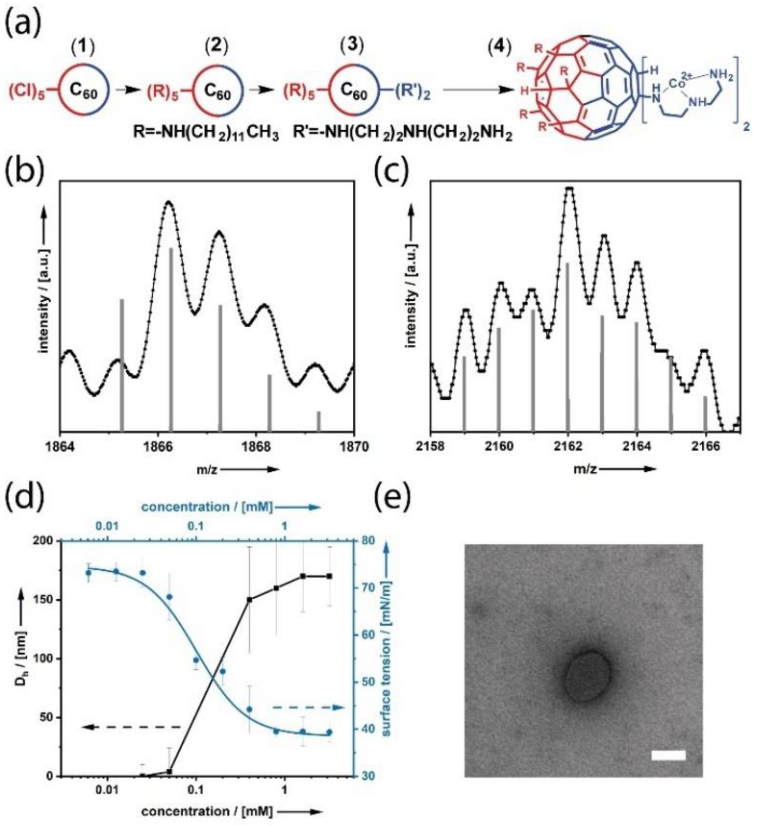

Figure 1. (a) Synthesis scheme for amphiphilic metal-fullerene-based catalyst (**4**). (b) ESI-TOF MS data of the organic ligand (**3**; black dots) and simulation of the molecular ion peak $[M]-(H^+)+(H_2O)=1866.23$ g/mol (grey bars) and (c) of the surfactant (**4**; black dots) and simulation of the molecular ion peak $[M]+(Cl^-)+(H_2O)=2161.98$ g/mol (grey bars). (d) Concentration-dependent aggregate size (black) and surface tension (blue). (e) TEM micrograph of a vesicle formed by (**4**) above the *cac*; scalebar = 100 nm.

by dynamic light scattering (DLS). The aggregate sizes determined from DLS are shown in Figure 1d. There were no aggregates found at low concentration, and above *cac* aggregates with a hydrodynamic diameter $D_H = 150$ nm (Figure S2) appear. Analysis of these aggregates using transmission electron microscopy (TEM; Figure 1e) confirms that surfactant (**4**) forms hollow, bilayer vesicular structures rather than micelles. In these aggregates the polar metal-fullerene complex, which serves as head group to the surfactant, align side by side at the outside of the bilayer. This general structuration was reported before for fullerene-based surfactants.[15,17] That this alignment is indeed the case a zetapotential measurement was performed. The measurement shows a high positive potential of +60 mV confirming this circumstance.

As a prototype reaction, electrocatalytic water splitting was used and the influence of catalyst self-assembly on the catalytic activity was evaluated with cyclic voltammetry (CV). First studies were performed at concentrations distinctly below the *cac* as the reference state at a threshold concentration of 0.025 mM of (**4**) in aqueous solution (pH = 7) (Figure 2).

The pure organic compound (**3**) is, as expected, catalytically inactive. The redox behavior of the solution in the presence of the Co-containing surfactant (**4**) is significantly different. There are strongly increased currents at onset potentials of $\eta_{0.5} = +1940$ mV for OER and $\eta_{0.5} = -740$ mV for HER at $j = 0.5$ mA/cm^2, which are both accompanied by strong gas formation. The voltammogram of (**4**) displays a partially reversible reduction signal at a $E_{max} = +20$ mV, which is a feature belonging to the fullerene-based ligand. Furthermore, it contains an oxidation at $E_{max} = +1600$ mV which can be assigned to the Co(II) to Co(III) oxidation, which features indirect reversibility.

Current densities remain unchanged on repetitive cycling, thus confirming that the homogeneous catalyst (**4**) is the catalytically active species and no decomposition product like colloidal cobalt. X-ray spectroscopy (EDX) coupled scanning electron microscopy (SEM) analysis revealed that no cobalt is precipitated on the electrode for (**4**) (Figure S3). The surface of the electrode is clean with absolutely no Co-containing residues caused by adsorption of the catalyst or decomposition. In particular, metallic Co nanoparticles cannot be found anywhere. As a reference experiment, analogous experiments using a $CoCl_2$ solution have been performed (Figure S3a). Not only could we not see comparable electrocatalytic activity, but also the electrode is now covered by Co-nanoparticles. Furthermore, repetitive cycling of $CoCl_2$ shows several changes of the system over time. In essence, it can be excluded that any other compound than the metal-surfactant is responsible for the electrocatalytic activity. In order to quantify the catalyst's properties in more detail, the turnover frequency was calculated, assuming a pseudo-first-order catalytic model (see Supporting Information equation 1, Figure S4).[32,37–40] Evaluation of the data results in $TOF(OER)_{2000mV} = 57 \pm 10$ s^{-1} and $TOF(HER)_{800mV} = 25 \pm 10$ s^{-1}, which indicates a medium activity compared to other electrocatalysts known to literature ranging from several to a maximum of several thousand per second.[28–34] The Randles-Sevcik plot depicted in Figure 2 shows a linear increase of the current density with the square root of the scan rate *v* for OER, indicating a diffusion controlled process. However, the value of current density for HER decreases with increasing *v*, which indicates that the catalytic process is kinetically slow giving rise to the assumption that the fullerene ligand is involved in the reaction. As the cyclic voltammograms of (**4**) do not show a wave for cobalt(II) to

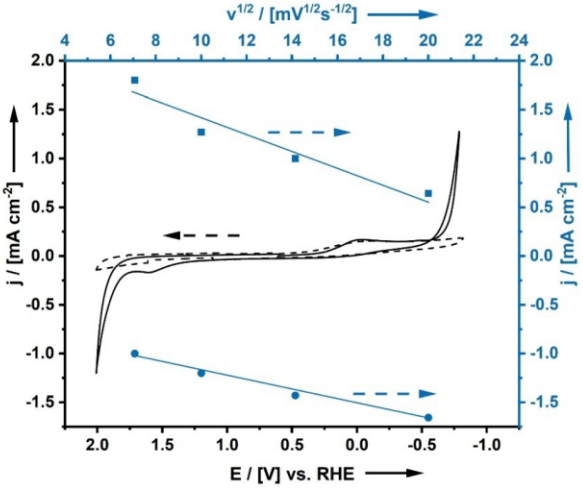

Figure 2. CV measurement (black) and Randles-Sevcik plot (blue; OER = circles; HER = squares of (**4**) at 0.025 mM compared to the CV of the organic ligand (**3**; dashed line).

cobalt(I) reduction, which would be expected at approximately −400 mV versus RHE, but solely a ligand reduction. This is consistent with the fullerene-DETA ligand acting as a non-innocent ligand similar to the work presented by Thompson *et al.* or Haddad *et al.*[31,41–42] Different from the mentioned literature the ligand is not likely to be protonated and is not catalytically active alone, excluding a metal-assisted ligand-centered as well as a only ligand-centered mechanism. It is more likely to be a metal-centered mechanism supported by the ligand. While the reaction takes place at the cobalt itself, the fullerene-DETA acts as electron reservoir for the reaction with the fullerene being an efficient electron mediator as reported for a nickel complex (Figure S5a).[43] The release of water from the initial complex results in the catalytically active species. The fullerene-DETA ligand is reduced in a one electron reduction, followed by the coordination of a proton to the metal center. A further reduction is followed by the reaction with a proton to release hydrogen. The detailed mechanism needs to be further evaluated with calculations. The mechanism for OER follows another pathway. According to the presence of the cobalt oxidation wave the mechanism might feature a Co (IV) intermediate (Figure S5b).[44–45]

The central issue of this work is unravelling the dependency of the catalytic properties on the level of aggregation. Consequently, we performed analogous electrochemical investigations at various concentrations, including $c > cac$ and a threshold concentration of 0.8 mM of an aqueous solution of (**4**) at which the defined vesicular aggregates are present (Figure 3a).

As long as the surfactant concentration remains below *cac*, there is only an insignificant change in OER and HER-related current density at 2000 mV and −800 mV, respectively (Figure 3a blue). However, Figure 3a (black) displays that the concentration dependent current density increases tremendously stronger above the $c > cac$ than below. Whereas, the systems showed to be a medium active catalyst at 0.025 mM

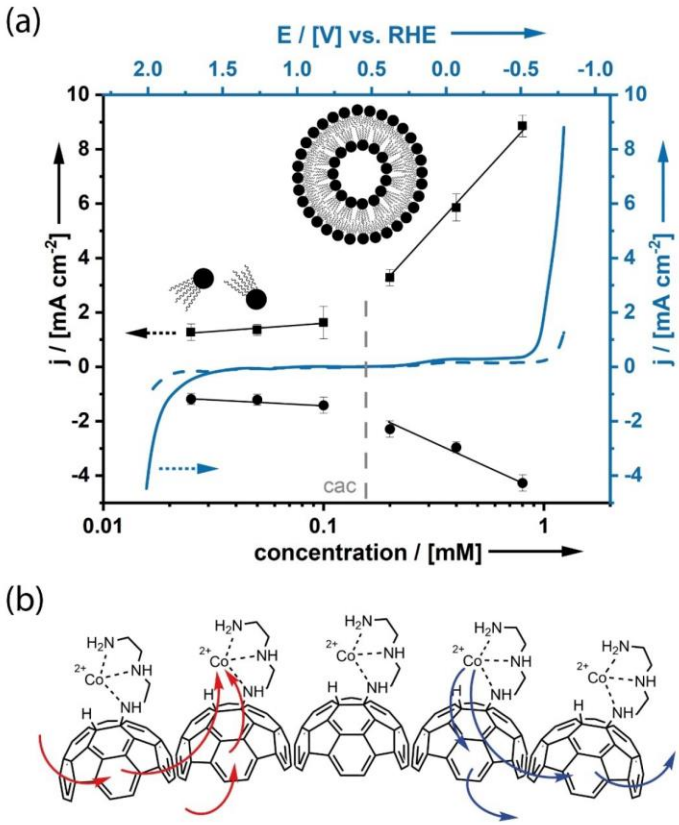

Figure 3. (a) Concentration-dependency of current density (black) for OER (circles) and HER (squares) below (left) and above (right) the *cac*. The grey dashed line marks the *cac*, when single surfactant molecules (left) assemble to vesicular aggregates (right). Linear sweep measurements (blue) of surfactant (**4**) below (0.025 mM) (dashed line) and above (0.8 mM) (solid line) *cac*. (b) Scheme showing the molecular structure of the vesicle surface and the proposed intra- and intermolecular charge transfer processes; (red arrows: reduction process; blue arrows: oxidation process).

concentration, the concentration increase does not improve the system's activity a lot. The catalytic process seems to be rather ineffective. But after eventually reaching the *cac*, the situation changes. The system's performance instantly showed a drastic increase which continues with further increasing concentration. Speaking in numbers, doubling the concentration below the *cac* only results in an increase in current density by factor 1.1 whereas, doubling the concentration above the *cac* increases the current density by almost factor 2. This leads also in a change in turnover frequency. For concentrations above the *cac* the turnover frequency at −800 mV increases from 25 ± 10 s^{-1} to 346 ± 10 s^{-1} (Equation 1, Figure S6). This observed increase of 1300% compared to the turnover frequency determined for c < *cac* obviously correlates with the self-assembly of the surfactant into vesicles (Figure 1d,e). This result is very astonishing considering that, in general, the mobility and accessibility of the catalytic centers should be lower in the aggregates, and, accordingly, activity should rather decrease or at the most remain constant at c > *cac*. Aqueous solution of fullerene based vesicles do not behave like nanoparticle systems[46–47] since a vesicle is a rather dynamic and permeable system. During the reaction, solvent molecules, reactant and product molecules can diffuse in and out the vesicular aggregate therefore, the number of accessible molecules for the reaction is not lowered but there is obviously an effect on the catalyst molecule upon aggregation. In addition to the turnover frequency, also the onset potential for OER decreases from $\eta_{0.5} = +1940$ mV to $\eta_{0.5} = +1720$ mV, while the onset potential for HER shifts from $\eta_{0.5} = -740$ to $\eta_{0.5} = -540$ mV (Figure 3a; Figure S6). The observed effect of enhanced catalytic activity can only be explained, if there is a cooperative effect between the individual surfactant molecules within the aggregate (Figure 3b). In fact, a change in the electronic situation upon aggregation can be observed. The emission of the single molecule diminishes completely upon reaching the *cac* when the system is excited at the fullerene core, but a new, heavily red shifted and broadened emission appears, that can be assigned to the aggregate state (Figure S7).

For the electron transfer reaction, our hypothesis (Figure 3b) is, that the vicinity and distinct orientation of the surfactant molecules with respect to each other in vesicle wall renders electron transfer from the ligand to the reactant more efficient and allows for intermolecular charge transfer processes in the aggregates.

Intermolecular charge transfer is thus held responsible for improving electrocatalytic activity of the surfactant aggregates with respect that of dispersed surfactant molecules. If this hypothesis is correct, one would expect that a diminishing content of molecules (**4**) in the vesicle walls should also decrease its catalytic activity. It is known that sodium dodecyl sulfate (SDS) can also form vesicular structures[48–49] and it is totally inactive in the water splitting reaction. We therefore tried to use SDS as a co-surfactant in a mixture with surfactant (**4**); see Figure 4 insert. According to DLS, no SDS micelles are present in such mixtures and the size of the vesicles (D_H = 143 nm) changes only insignificantly with respect to pure (**4**) (Figure S8a). Upon adding SDS to the catalytic system, the current at +2000 mV and −800 mV is lowered by approximately 30% (see Figure 4). This interpretation is also in line with the observed anodic shift of the onset potential of 45 mV for OER and a cathodic shift of 40 mV for HER (Figure S8b). In the mixed aggregates fewer molecules (**4**) are adjacent to each other and, therefore, intermolecular electronic communication as initiated by aggregation is rendered less efficient.

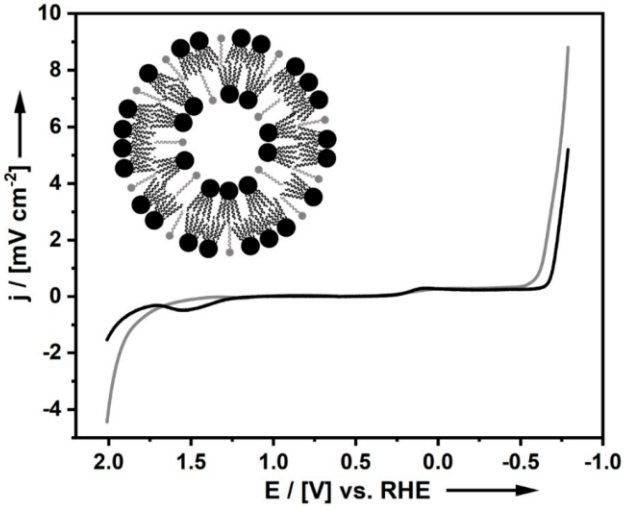

Figure 4. CV of (**4**) at c = 0.8 mM (grey) as a reference compare to the (**4**)/SDS mixed aggregates (black). Insert shows schematic illustration of a vesicle of (**4**; black) diluted with SDS (grey).

Supramolecular catalysis give rise to new catalytic systems. In this work, we were able to show that aggregation of a surfactant based catalyst leads to a beneficial feature for electron transfer reactions like water splitting reaction as a model system and increases the system's performance. We present an amphiphilic cobalt-fullerene catalyst, which at concentrations below its *cac* shows an only medium catalytic activity in OER and HER at neutral pH in aqueous solution. The compound's catalytic activity, especially for HER increases tremendously at concentrations above *cac*, at which vesicular aggregates form. The onset potentials and current densities are improved and the turnover frequency increases by up to 1300%. Aggregation allows for intermolecular electron transfer and improves electronic communication within the system, leading to more efficient water splitting.

Supporting Information

Supporting Information is available from the Wiley Online Library or from the author.

Acknowledgements

The current research was funded by an ERC consolidator grant (I-SURF; project 614606). We further thank Stephan Siroky for his support.

Conflict of Interest

The authors declare no conflict of interest.

Keywords: Fullerene · surfactant · self-assembly · catalysis · supramolecular chemistry · water splitting

[1] G. La Sorella, G. Strukul, A. Scarso, *Green Chem.* **2015**, *17*, 644.
[2] A. Donner, K. Hagedorn, L. Mattes, M. Drechsler, S. Polarz, *Chem. Eur. J.* **2017**, *23*, 18129.
[3] A. Donner, B. Trepka, S. Theiss, F. Immler, J. Traber, S. Polarz, *Langmuir* **2019**.
[4] J. Meeuwissen, J. N. Reek, *Nat. Chem.* **2010**, *2*, 615.
[5] C. J. Brown, F. D. Toste, R. G. Bergman, K. N. Raymond, *Chem. Rev.* **2015**, *115*, 3012.
[6] D. J.. Cram, *Angew. Chem. Int. Ed.* **1988**, *27*, 1009.
[7] M. Yoshizawa, M. Tamura, M. J. S. Fujita, *Science* **2006**, *312*, 251.
[8] J. K. Sanders, *Chem. Eur. J.* **1998**, *4*, 1378.
[9] S. Polarz, M. Kunkel, A. Donner, M. Schlötter, *Chem. Eur. J.* **2018**, *24*, 18842.
[10] A. C. Bijlard, S. Wald, D. Crespy, A. Taden, F. R. Wurm, K. Landfester, *Adv. Mater. Interfaces* **2017**, *4*.
[11] S. Landsmann, M. Wessig, M. Schmid, H. Colfen, S. Polarz, *Angew. Chem. Int. Ed.* **2012**, *51*, 5995.
[12] A. Klaiber, S. Polarz, *ACS Nano* **2016**, *10*, 10041.
[13] S. Polarz, C. Bahrle, S. Landsmann, A. Klaiber, *Angew. Chem. Int. Ed.* **2013**, *52*, 13665.
[14] S. Hermann, M. Wessig, D. Kollofrath, M. Gerigk, K. Hagedorn, J. A. Odendal, M. Hagner, M. Drechsler, P. Erler, M. Fonin, G. Maret, S. Polarz, *Angew. Chem. Int. Ed.* **2017**, *56*, 5475.
[15] M. Kunkel, S. Schildknecht, K. Boldt, L. Zeyffert, D. Schleheck, M. Leist, S. Polarz, *ACS Appl. Mater. Interfaces* **2018**, *10*, 23638.
[16] M. Kunkel, S. Polarz, *Beilstein J. Org. Chem.* **2019**, *15*, 901.
[17] M. Kunkel, S. Sutter, S. Polarz, *Angew. Chem. Int. Ed.* **2019**.
[18] W. Lubitz, W. Tumas, *Chem. Rev.* **2007**, 107, 10, 3900-3903.
[19] T. R. Cook, D. K. Dogutan, S. Y. Reece, Y. Surendranath, T. S. Teets, D. G. Nocera, *Chem. Rev.* **2010**, *110*, 6474.
[20] D. L. DuBois, *Inorg. Chem.* **2014**, *53*, 3935.
[21] P. Li, R. Zhao, H. Chen, H. Wang, P. Wei, H. Huang, Q. Liu, T. Li, X. Shi, Y. Zhang, *Small* **2019**, *15*, 1805103.
[22] Y. Wang, J. Zhang, *Front. Chem.* **2018**, *12*, 838.
[23] B. You, Y. Sun, *Acc. Chem. Res.* **2018**, *51*, 1571.
[24] C. Hu, L. Zhang, J. Gong, *Energy Environ. Sci.* **2019**.
[25] C. C. McCrory, S. Jung, I. M. Ferrer, S. M. Chatman, J. C. Peters, T. F. Jaramillo, *J. Am. Chem. Soc.* **2015**, *137*, 4347.
[26] I. Roger, M. A. Shipman, M. D. Symes, *Nat. Chem. Rev.* **2017**, *1*, 0003.
[27] B. Lu, L. Guo, F. Wu, Y. Peng, J. E. Lu, T. J. Smart, N. Wang, Y. Z. Finfrock, D. Morris, P. Zhang, *Nat. Commun.* **2019**, *10*, 631.
[28] P. W. Du, R. Eisenberg, *Energy Environ. Sci.* **2012**, *5*, 6012.
[29] N. Queyriaux, R. T. Jane, J. Massin, V. Artero, M. J. C. c. r. Chavarot-Kerlidou, *Coord. Chem. Rev.* **2015**, *304*, 3.
[30] T. Fang, L.-Z. Fu, L.-L. Zhou, S.-Z. Zhan, S. Chen, *Electrochim. Acta* **2015**, *178*, 368.
[31] A. Z. Haddad, B. D. Garabato, P. M. Kozlowski, R. M. Buchanan, C. A. Grapperhaus, *J. Am. Chem. Soc.* **2016**, *138*, 7844.
[32] A. Z. Haddad, D. Kumar, K. Ouch Sampson, A. M. Matzner, M. S. Mashuta, C. A. Grapperhaus, *J. Am. Chem. Soc* **2015**, *137*, 9238.
[33] M. M. Najafpour, S. Mehrabani, Y. Mousazade, M. Hołyńska, *Dalton Trans.* **2018**, *47*, 9021.
[34] Y. Liu, Y. Han, Z. Zhang, W. Zhang, W. Lai, Y. Wang, R. Cao, *Chem. Sci.* **2019**, *10*, 2613.
[35] V. Artero, M. Chavarot-Kerlidou, M. Fontecave, *Angew. Chem. Int. Ed.* **2011**, *50*, 7238.
[36] I. V. Kuvychko, A. V. Streletskii, A. A. Popov, S. G. Kotsiris, T. Drewello, S. H. Strauss, O. V. Boltalina, *Chem. Eur. J.* **2005**, *11*, 5426.
[37] J. Saveant, E. Vianello, *Electrochim. Acta* **1965**, *10*, 905.
[38] C. C. McCrory, C. Uyeda, J. C. Peters, *J. Am. Chem. Soc.* **2012**, *134*, 3164.
[39] X. Hu, B. S. Brunschwig, J. C. Peters, *J. Am. Chem. Soc.* **2007**, *129*, 8988.
[40] W. T. Eckenhoff, W. R. McNamara, P. Du, R. Eisenberg, *Biochim. Biophys. Acta* **2013**, *1827*, 958.
[41] A. Z. Haddad, S. P. Cronin, M. S. Mashuta, R. M. Buchanan, C. A. Grapperhaus, *Inorg. Chem.* **2017**, *56*, 11254.
[42] E. J. Thompson, L. A.. Berben, *Angew. Chem. Int. Ed.* **2015**, *54*, 11642.
[43] P. H. Kankanamalage, S. Mazumder, V. Tiwari, K. K. Kpogo, H. B. Schlegel, C. N. Verani, *Chem. Commun.* **2016**, *52*, 13357.
[44] Z.-Q. Wang, L.-Z. Tang, Y.-X. Zhang, S.-Z. Zhan, J.-S. Ye, *J. Power Sources* **2015**, *287*, 50.
[45] M. Zhang, H. Frei, *Catal. Lett.* **2015**, *145*, 420.
[46] Y. Zhang, S. Pang, Z. Wei, H. Jiao, X. Dai, H. Wang, F. Shi, *Nat. Commun.* **2018**, *9*, 1.
[47] S. A. Kondrat, J. A. van Bokhoven, *Top. Catal.* **2018**, 62, 1218.
[48] M. Almgren, *Biochim. Biophys. Acta Biomembr.* **2000**, *1508*, 146.
[49] C. Rupp, H. Steckel, B. W. Müller, *Int. J. Pharm.* **2010**, *387*, 120.

Manuscript received: March 9, 2020
Accepted manuscript online: March 16, 2020
Version of record online: ■■, ■■

COMMUNICATIONS

ChemCatChem

Supporting Information

Aggregation-Induced Improvement of Catalytic Activity by Inner-Aggregate Electronic Communication of Metal-Fullerene-Based Surfactants

Marius Kunkel, Stefan Bitter, Frank Sailer, Rainer F. Winter, and Sebastian Polarz*

WILEY-VCH

Supporting Information

Aggregation-Induced Improvement of Catalytic Activity by Inner-Aggregate Electronic Communication of Metal-Fullerene-Based Surfactants

*Marius Kunkel, Stefan Bitter, Frank Sailer, Rainer F. Winter and Sebastian Polarz**

Synthesis and characterization

Synthesis of $C_{60}Cl_6$

C_{60} (0.28 mmol) was dissolved in chlorobenzene (11 mL) and sonicated for 5 min. Iodine monochloride (6.95 mmol) was added in one shot, and the solvent was evaporated as fast as possible. The crude product was further purified by column chromatography (silica gel, eluent: toluene). $C_{60}Cl_6$ is obtained as a red solid (0.2 mmol, 70%) and used without further characterization.

Synthesis of $C_{60}H(NC_{12}H_{26})_5$

$C_{60}Cl_6$ (0.2 mmol) was dissolved in chloroform (50 mL) and vigorously stirred. Dodecylamine (2 mmol) and NEt3 (0.2 mL) were added. The mixture was stirred for 12 h. The crude product was precipitated with cold methanol, filtrated and washed several times with methanol. The crude product was then dissolved in ethyl acetate. The solvent was evaporated, and the crude product was further purified by column chromatography (silica gel, eluent: toluene/EE). The title compound is obtained as a red solid (0.17 mmol, 60%).

IR (powder): 3285, 2920, 2851, 1770, 1658, 1570, 1466, 1316, 1115 cm^{-1}; ^1H NMR (400 MHz, $CDCl_3$): δ 0.89 (t, ^3J = 7.2 Hz, 15H), 1.27 (m, 90H), 1.45 (m, 10H), 1.67 (m, 10H), 3.22 (m, 5H) ^{13}C NMR (100 MHz, $CDCl_3$): δ 14.2, 22.56, 27.57, 27.67, 29.56, 29.58, 29.91, 29.93,

30.95, 31.02, 32.11, 47.36, 47.87, 47.88, 66.02, 68.21, 69.35, 143.24, 143.31, 143.71, 143.81, 143.83, 143.84, 143.84, 143.88, 144.02, 144.08, 144.31, 144.47, 144.51, 144.53, 144.91, 145.43, 147.16, 147.21, 147.23, 147.29, 147.62, 148.02, 148.21, 148.33, 148.57, 148.71, 149.12, 150.81, 153.88, 155.31; MS (MALDI): 1641.1 $[M - H^+]^-$ (1641.03)

Synthesis of $(H_{12}N_3C_4)_2C_{60}H(NC_{12}H_{26})_5$

$C_{60}H(NC_{12}H_{26})_5$ (0.12 mmol) was suspended in diethylenetriamine and stirred at 65 °C for 3 days. The crude product was precipitated with cold ethyl acetate and filtrated. The filtrate was washed several times with acetone to remove remaining diethylenetriamine. The product was extracted from the filter with methanol. Solvent was evaporated to obtain (H12N3C4)3C60H(NC12H26)5 as a brown solid (0.036 mmol, 30 %)

IR (powder): 3296, 2923, 2846, 1646, 1588, 1447, 1351, 1274, 1113 cm^{-1}; ^1H NMR (400 MHz, MeOD): δ 0.92 (t, ^3J = 7.2 Hz, 15H), 1.31 (m, 100H), 1.67 (m, 10H), 2.90 (m, 12H). 3.03 (m, 10H), 3.22 (m, 5H), 6.99 (s, 1H), 7.20 (s, 1H), 7.25 (s, 1H); ^{13}C NMR (200 MHz, MeOD): δ 14.5, 23.8, 25.25, 25.8, 30.5, 30.8, 31.7, 33.1, 38.1, 38.9, 39.4, 39.5, 39.6, 40.8, 41.2, 41.9, 42.7, 43.6, 43.7, 44.7, 46.5, 49.2, 50.4, 51.2, 51.5, 63.4, 65.7, 78.1, 127.7, 127.8, 128.5, 129.4, 129.5, 130.5, 144.9, 154.7, 156.9, 159.3, 162.5, 162.6, 162.8, 162.9,163,164.3,164.5, 164.7; MS (ESI): 1866.23 $[M - H^+ + H_2O]^-$ (1866.37)

Synthesis of $(H_{12}N_3C_4\text{-}CoCl_2)_2C_{60}H(NC_{12}H_{26})_5$

$(H_{12}N_3C_4)_2C_{60}H(NC_{12}H_{26})_5$ (0.1 mmol) was dissolved in methanol and $CoCl_2$ (0.4 mmol) was added. The mixture was stirred overnight. The product was precipitated with acetone, filtrated and washed with acetone to remove remaining $CoCl_2$. The product was extracted from the filtrate by dissolving in water. The solvent was evaporated to obtain a green-brown solid (80%).

IR (powder):3368, 3227, 2923, 2853, 2052,1608, 1447 1348, 1290, 1017; MS: (ESI): 2161.99 $[M + Cl^- + H_2O]^-$ (2161.98)

Methods

The synthesis that acquired inert gas atmosphere was performed using general Schlenk techniques under argon atmosphere. The solvents were dried according to the standard literature and stored under argon. Water was deionized with Millipore Milli-Q. All starting materials used for the synthesis were purchased from commercial sources unless stated differently. The fullerene C_{60} (pur. 99.5 %) was purchased from Research & Production Company "Modern Synthesis Technology".

Analytical Methods

Attenuated total reflection–infrared (ATR–IR) spectra were measured with a Perkin Elmer 100 Spectrum spectrometer including an ATR unit.

NMR measurements (1H, 13C) were performed on a Bruker Avance III 400 MHz spectrometer or on Bruker AVANCE Neo 800 MHz.

MALDI-MS measurements were performed using a Bruker Microflex MALDI-TOF. The samples were prepared in a cyano-4-hydroxycinnamic acid matrix or a trans-2-[3-(4-tert-butylphenyl)-2-methyl-2-propenylidene]malononitrile matrix.

ESI mass spectra were recorded on a Bruker microTOF focus II mass spectrometer in negative mode with water as solvent.

UV/Vis absorption spectra were acquired using an Agilent Cary 60 spectrometer.

Dynamic light scattering measurements were performed by using a Malvern Zen5600.

The surface tension measurements were performed using Krüss K100 with a manual dilution series. Additionally, surface tension measurements were performed with capillary method.

Transmission electron microscopy observations were carried out using Zeiss Libra120.

Cyclic voltammetry measurements

CV measurements were conducted using a three-neck electrochemical cell. Electrochemical data were acquired with a computer-controlled BASi CV50 potentiostat.

Cyclic voltammetry measurements were performed in aqueous solution at pH 7 with 0.1 M potassium nitrate as electrolyte. As working electrode a glassy carbon electrode with 0.07 cm^2 was used, as counter electrode a platinum wire electrode and as reference electrode, saturated Ag/AgCl was used. The reference electrode was regenerated after every measuring segment. The pH value was controlled after every measurement segment and adjusted if needed. Every measurement was at least performed 3 times to ensure reproducibility. The used data represent an average value of the data. The working electrode was rinsed with distillated water after every measurement segment.

In the manuscript. the measured potentials vs. Ag/AgCl were converted to the reversible hydrogen electrode (RHE) scale according to the Nernst equation:

$E_{RHE} = E_{Ag/AgCl} + 0.059*pH + E^0_{Ag/AgCl}$

with E_{RHE} ist he converted potential vs. RHE, $E^0_{Ag/AgCl} = 0.1976$ at 25°C and $E_{Ag/AgCl}$ is the experimentally measured potential against Ag/AgCl reference.

Preparation of mixed aggregates

For the preparation of mixed aggregates of the catalyst and SDS 1 eq of SDS was added to a solution of the catalyst in water. The mixture was stirred for 2 h.

Calculation of K_{obs}

K_{obs} was calculated from equation 1. J_c is the catalytic current density at 1400/-1400 mV, j_p is the non-catalytic peak current taken from the cobalt(II) to cobalt(III) oxidation respectively from the ligand reduction. N values the number of electrons in the reaction. R is the ideal gas constant. T is taken at 298.15 K. F is Faraday's constant and v is the scan rate. For the calculation the slope of j_c/j_p versus $v^{-1/2}$ was used.

Equation 1

$$\frac{j_c}{j_p} = \frac{n}{0.446}\sqrt{\frac{RTk_{obs}}{Fv}}$$

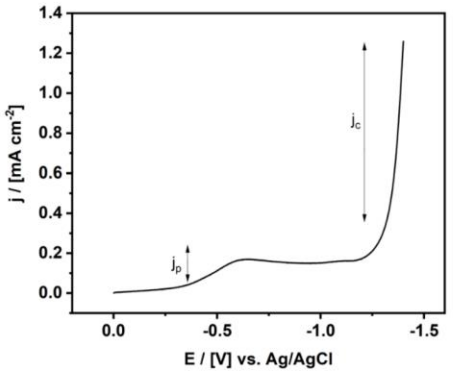

Supporting figures

Figure S1 Molecular characterization of compound (**4**).

(a) Infrared spectrum of the catalyst (**4**).

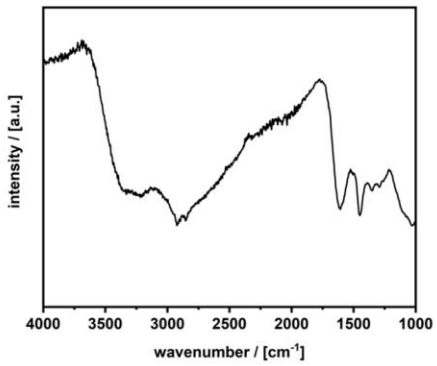

(b) UV/Vis spectrum of the catalyst (**4**) (grey) and (**3**) (black).

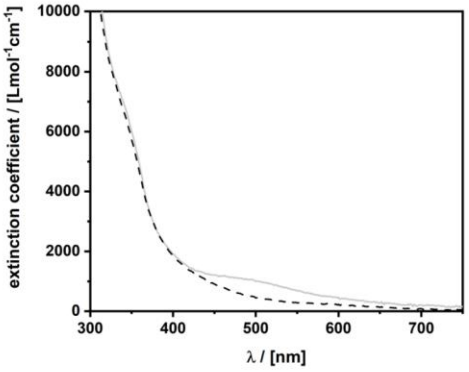

(c) Photograph of a 0.8 mM solution of (**4**).

(d) ESI-MS spectrum of (**4**) in negative mode.

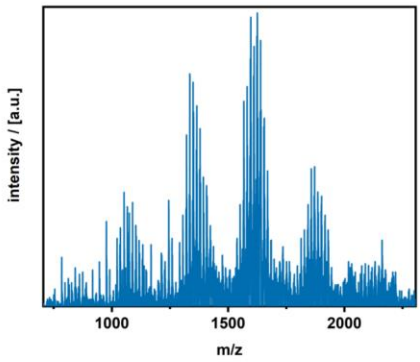

(e) Zoom-in version of ESI-MS spectrum of (**4**) in negative mode.

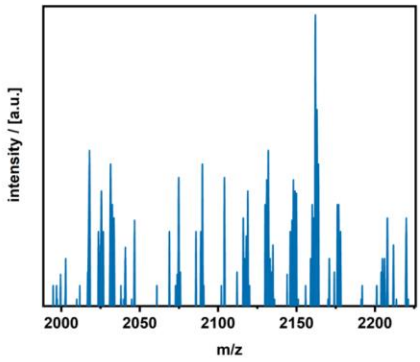

Figure S2 Characterization of surfactant properties of compound (**4**).

(a) Aggregate size distribution derived from DLS-data at a surfactant concentration of 0.8mM.

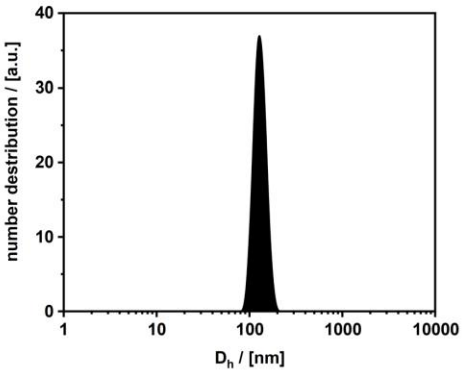

Figure S3 Stability studies for catalyst system (**4**) and $CoCl_2$ as comparison at 0.8 mM, 1.6 mM respectively.

(a) Cyclic voltammogram after repetitive cycling of (4) with 100 cycles with 100 mV/s.

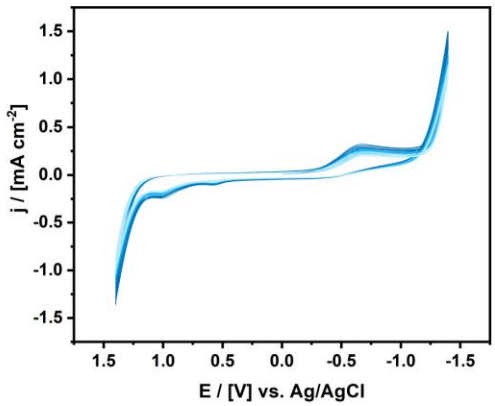

(b) Cyclic voltammogram after repetitive cycling of a $CoCl_2$ solution with 100 cycles with 100 mV/s.

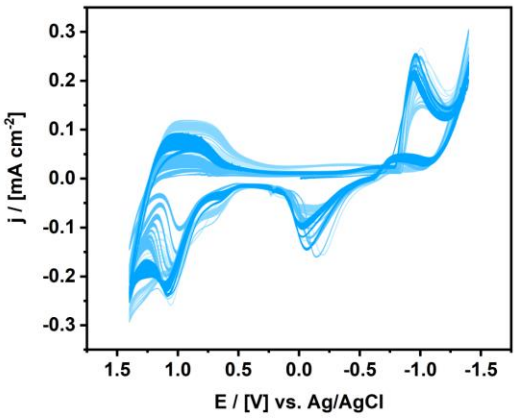

SEM micrographs of electrodes after repetitive cycling (grey: carbon, green: fluorine, yellow: chlorine, blue: cobalt)

(c) Micrograph of electrode tip after repetitive cycling with CoCl2 1.6 mM as reference. The electrode was rinsed with water. Scalebar 500 µm.

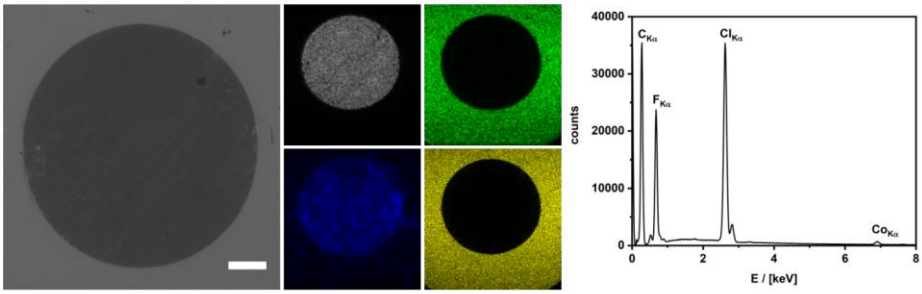

(d) Micrograph of electrode tip after repetitive cycling with compound (4) 0.8 mM. The electrode was rinsed with water. Scalebar 500 µm.

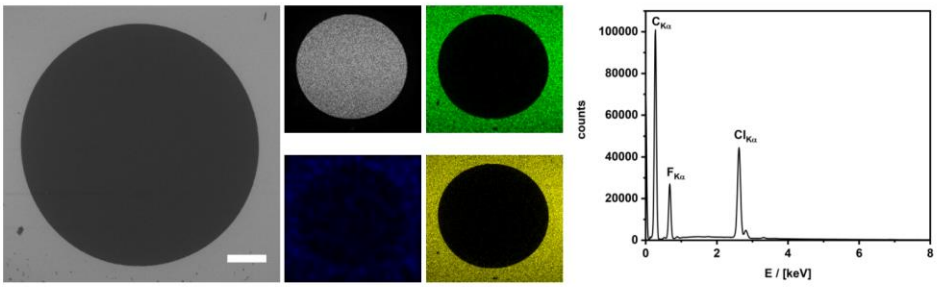

Figure S4. Electrochemical studies performed for compound (**4**) as an electrocatalyst below the cac. J_c is the catalytic current density at 1400/-1400 mV vs Ag/AgCl, j_p is the non-catalytic peak current taken from the cobalt(II) to cobalt(III) oxidation respectively from the ligand reduction.

(a) Plot j_c/j_p versus $v^{-1/2}$ for OER (0.025 mM).

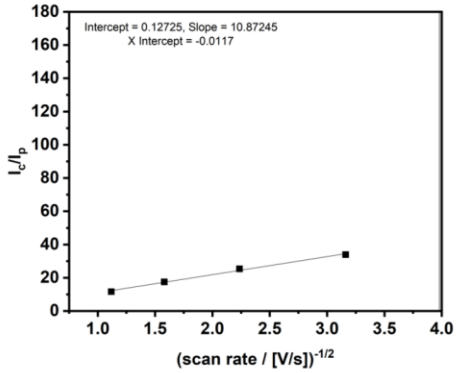

(b) Plot j_c/j_p versus $v^{-1/2}$ for HER (0.025 mM).

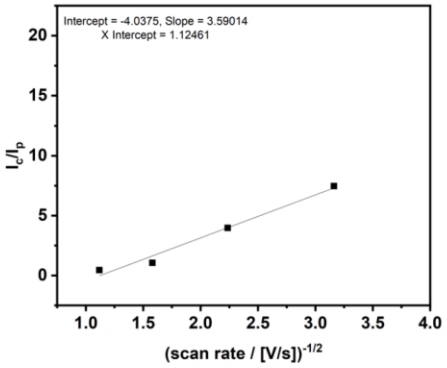

(c) Cyclic voltammograms of the catalyst below the CAC at 0.025 mM at different scan rates with absolute current versus potential (vs Ag/AgCl).

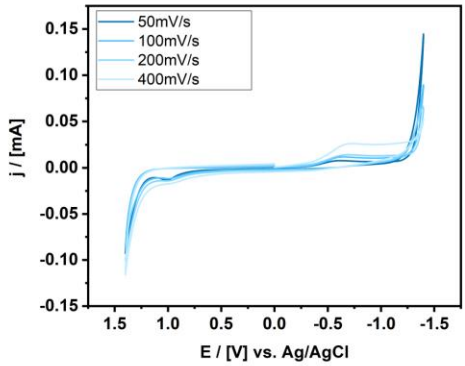

Figure S5. Proposed mechanism for HER and OER.

(a) Proposed mechanism for HER.

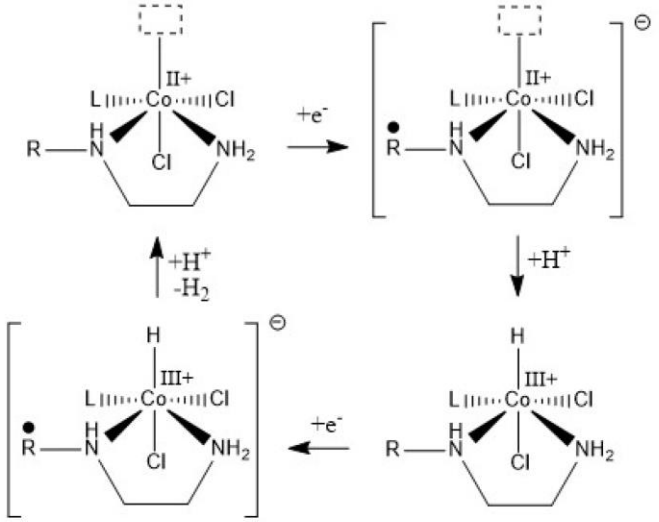

(b) Proposed mechanism for OER

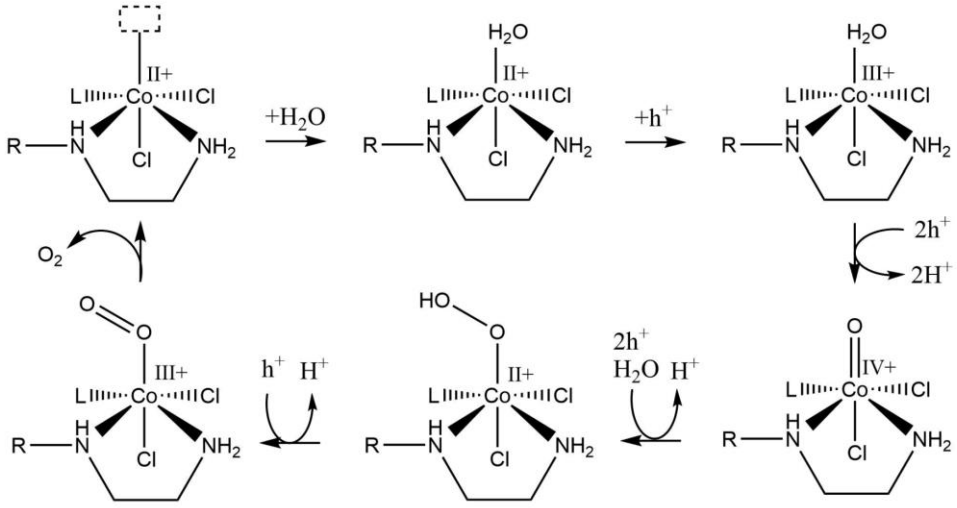

Figure S6. Electrochemical studies performed for compound (**4**) as an electrocatalyst above the cac (0.8mM and 0.4 mM). J_c is the catalytic current density at 1400/-1400 mV vs Ag/AgCl, j_p is the non-catalytic peak current taken from the cobalt(II) to cobalt(III) oxidation respectively from the ligand reduction.

(a) j_c/j_p versus $v^{-1/2}$ for HER (0.8mM).

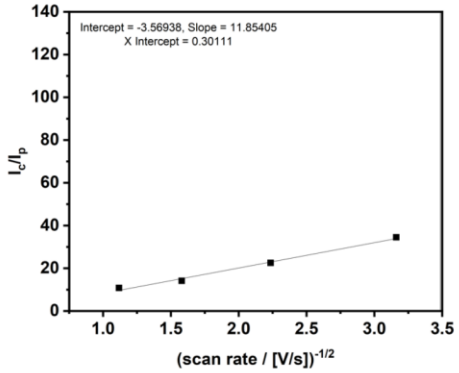

(b) j_c/j_p versus $v^{-1/2}$ for OER (0.8mM).

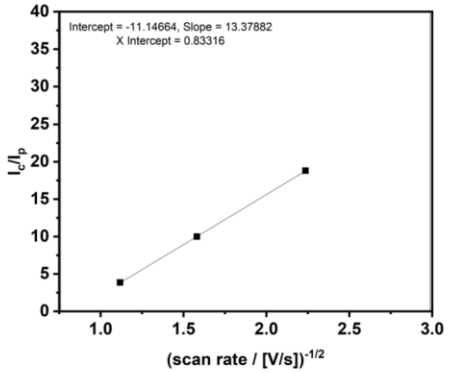

(c) Cyclic voltammograms of the catalyst above the cac at different scan rates (0.8mM) with absolute current versus potential (vs Ag/AgCl).

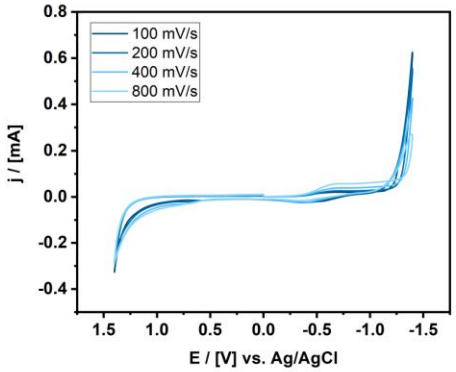

(d) j_c/j_p versus $v^{-1/2}$ for HER (0.4mM).

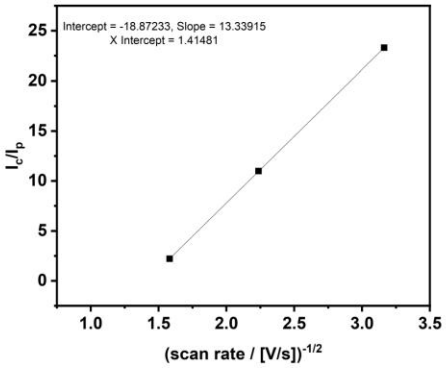

(e) Cyclic voltammograms of the catalyst above the cac at different scan rates (0.4mM) with absolute current versus potential (vs Ag/AgCl).

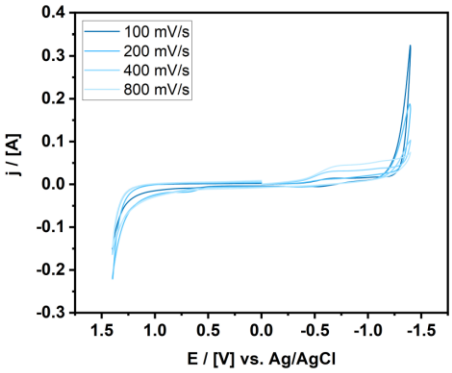
100 mV/s
200 mV/s
400 mV/s
800 mV/s
j / [A]
0.4
0.3
0.2
0.1
0.0
-0.1
-0.2
-0.3
1.5
1.0
0.5
0.0
-0.5
-1.0
-1.5
E / [V] vs. Ag/AgCl

Figure S7. Change in electronic situation of the system in dependence of concentration. Emission spectra of (**4**) below (line) and above (dashed) the cac with an excitation wavelength of 300 nm.

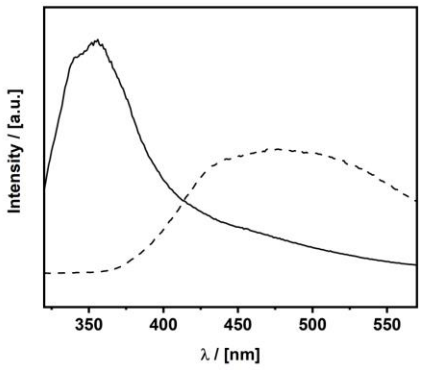

Figure S8. SDS - surfactant (**4**) co-aggregates.

(a) Aggregate size distribution derived from DLS data.

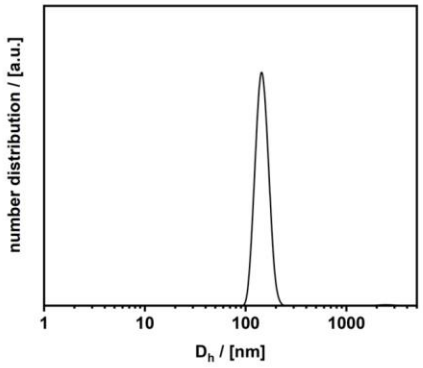

(b) Cyclic voltammograms of the catalyst at 0.8 mM with SDS as additive.